UNIVERSITA' DEGLI STUDI DI VERONA

Department of Biotechnology

Graduate School of Natural Science and Engineering

Doctoral Program in Nanoscience and Advanced Technology

Cycle XXXVI

Nanoparticles and ubiquitination as modulators of Tau aggregation and condensation.

S.S.D. CHIM/06

Coordinator: Prof. Adolfo Speghini

Tutor: Prof. Mariapina D'Onofrio

PhD Student: Dott.ssa Giovanna Viola

UNIVERSITA' DEGLI STUDI DI VERONA

Department of Biotechnology

Graduate School of Natural Science and Engineering

Doctoral Program in Nanoscience and Advanced Technology

Cycle XXXVI

Nanoparticles and ubiquitination as modulators of Tau aggregation and condensation.

S.S.D. CHIM/06

Coordinator: Prof. Adolfo Speghini

Firma_____

Tutor: Prof. Mariapina D'Onofrio

Firma_____

PhD Student: Dr.ssa Giovanna Viola

Firma_____

Nanoparticles and ubiquitination as modulators of Tau aggregation and condensation – Giovanna Viola
PhD thesis
Verona, 12 December 2023
ISBN

INDEX

ACRONYM

1D Mono-dimensional
2D Bi-dimensional
ACN Acetonitrile
AD Alzheimer's Disease
Aβ Amyloid-β
Amp Ampicillin
APP Amyloid precursor protein
BBB Blood-brain barrier
C-terminal carboxy-terminal
CD Circular Dichroism
Chl chloramphenicol
Cys cysteine
CNS Central Nervous System
Dha Dehydroalanine
DHLA Dihydrolipoic acid
DLS Dynamic Light Scattering
DTNB 5,5-dithio-bis-(2-nitrobenzoic acid)
DTT Dithiothreitol
EDTA Ethylenediaminetetraacetic acid
EGTA Ethylene glycol-bis (β-aminoethyl ether)-N,N,N′,N′-tetra acetic acid
HCCA α-Cyano-4-hydroxycinnamic acid
HSQC Heteronuclear single-quantum coherence
IDPs Intrinsically Disordered Proteins
IPTG Isopropyl-β-D-1-thiogalactopyranoside
KDa kiloDalton
L Liter
LB Luria broth
LLPS Liquid-liquid phase separation
M Molar
MALDI-TOF Matrix-assisted laser desorption/ionization-time of flight
MAPT Microtubule Associated Protein Tau (Human gene)
MD Molecular Dynamic
MDBP methyl 2,5-dibromopentanoate
MES 2-(N-morpholino) ethane sulfonic acid
MHz Megahertz
mL milliliter
MLOs Membraneless organelles
mM millimolar
MTBD Microtubule-binding domain
MTs Microtubules
N-terminal Amino-terminal
NAC Non-amyloid-β-component
NDDs Neurodegenerative Diseases
NFTs Neurofibrillary Tangles
NMR Nuclear Magnetic Resonance
NP Nanoparticle
PD Parkinson's Disease
PHFs Paired helical filaments.
PMSF Phenylmethylsulphonyl Fluoride
PP2A Protein phosphatase 2A
ppm Chemical shift in parts per million
PRD Proline-Rich Domain
PS phosphorylation site
PTMs Post-Translational Modifications
SDS-PAGE Sodium Dodecyl Sulfate Polyacrylamide Gel Electrophoresis
SFs Straight Filaments
TCEP tris(2-carboxyethyl) phosphine hydrochloride
TFA Trifluoroacetic acid
ThT Thioflavin-T
Ub Ubiquitin
UPS Ubiquitin-Proteasome System
α-syn α-Synuclein
µg microgram
µL microliter
µM micromolar
usGNPs ultrasmall Gold Nanoparticles

ABSTRACT

Neurodegenerative diseases (NDs) are a heterogeneous group of neurological disorders characterised by a progressive loss of neurons in central nervous system (CNS) or peripheral nervous system (PNS). NDs are caused by misfolded protein aggregates in specific areas of the brain. The collapse of the structure and function of neural networks, results in the breakdown of the core communicative circuitry, culminating in impaired memory, cognition, behaviour, sensory, and/or motoric functions. The prevalence of these diseases rises dramatically with age and is expected to surge with the increasing life expectancy in most countries, in the next decades.

Among neurogenerative disorders, Alzheimer's disease (AD) and Parkinson's disease are the most common forms of dementia in older adults and the two relevant related proteins are Tau and α-synuclein, respectively. Both are amyloidogenic and natively unfolded proteins, which convert from monomeric to aggregated states in pathological conditions. The formation of Neurofibrillary tangles (NFTs) of Tau underlies the onset of the AD, as well as the aggregation of α-synuclein is associated with PD.

The possibility to redirect aggregation pathway is essential to understand and prevent the doomed fate of these proteins.

In this thesis I focused my attention on Tau protein, I investigated the molecular mechanisms of aggregation, and I exploited different ways for preventing or targeting the aggregation pathway.

A body of evidence shows that post-translational modifications (PTMs) can play important role in both physiological and pathological behaviour of Tau protein. Therefore, I focused my attention on the investigation of the impact of ubiquitination of Tau on the conversion into toxic species. For this purpose, I optimized a novel method to insert ubiquitin protein onto a specific position of Tau, via dehydroalanine chemistry. After optimizing the synthetic step, I investigated the aggregation propensity of the ubiquitinated Tau and interestingly I observed that this modification interferes with the fibrils formation.

Moreover, I investigated the influence of nanomaterials, in particular gold nanoparticles, on Tau properties.

The application on nanomaterials in routine life is growing day by day, due to their unique physical properties. In this work, I used ultrasmall gold nanoparticles (usGNPs), because the core size gives them extraordinary properties like fluorescence and biocompatibility. So, I combined the nanomaterials with Tau studies, in two different directions. First of all, I tried to understand if nanomaterials can prevent or at least slow down Tau aggregation. As well as for ubiquitination studies, I monitored Tau aggregation in the presence of different usGNPs concentrations, and I discovered that usGNPs are able to reduce Tau aggregation, and, at a certain amount, they can even arrest the aggregates formation.

On the other hand, liquid-liquid phase separation of protein into condensed droplets, is a common mechanism for eukaryotic cells to carry out physiological reactions but mounting evidence suggest that this compartmentalization can be the spark that triggers amyloid protein aggregation. From this premise, I tried to characterize the system Tau-usGNPs, and actually I found that usGNPs are able to perturb Tau droplets formation, but more interestingly I realized that they are good markers candidates to monitor Tau aggregation event in LLPS formation.

Finally, I investigated the influence on Tau aggregation mediated by an Italian expresso coffee mixture of trigonelline, theobromine, genistein, and caffeine. In fact, it is well established that coffee and coffee derived phenolic compounds have a role in neuroprotection against oxidative-stress and neuro-inflammation thanks to the ability to cross the Blood Brain Barrier.

1 INTRODUCTION

1.1 Neurodegeneration: Alzheimer Disease

A large number of neurodegenerative diseases (NDDs) share the same abnormal accumulation of intracellular and/or extracellular protein aggregates that contribute to cellular proteostatic collapse. [1,2] The pathogenesis of neurodegenerative diseases is still poorly understood, however, it is coming from causal contributions of both genetic and environmental factors. [3]

Among NDDs, Alzheimer's disease (AD), first discovered by Alois Alzheimer in 1907, is the most prevalent and spread form of dementia. It is associated with aging and results in devastating disability and diminished quality of life; its occurrence will reach epidemic proportions by 2050, if not abated.

The pathological hallmarks of AD include amyloid plaques composed of amyloid β-protein (Aβ) [4,5] and neurofibrillary tangles of hyperphosphorylated Tau protein. [6,7] Although useful symptomatic therapies involving the use of acetylcholinesterase inhibitors and N-methyl-D-aspartate (NMDA) receptor antagonist are available, knowledge on the definitive pathophysiological cause of AD is limited, and no curative treatments are yet accessible. [8]

The limited knowledge of the origins and development of AD has prompted scientists to advance new techniques, in order to understand the mechanisms at molecular level that drive amyloidogenic proteins to disastrous fate.

1.1.1 Tauopathies

Tauopathies are morphologically heterogeneous neurodegenerative diseases, defined by the intracellular deposition and transcellular propagation of abnormal hyperphosphorylated Tau aggregates. Tauopathies can be classified, as primary or secondary, when a second protein, such as Aβ, is necessary for pathology, like in Alzheimer' disease. [9–12]

In adult human brain, Tau is expressed in six different isoforms, from a single gene, by alternative splicing of exons 2, 3 and 10.

Based on distinct isoform of Tau, several neuropathologic phenotypes are distinguished. The differences between phenotypes arise from the 3R\4R ratio and the number of phosphorylated sites. [13] A detailed classification is reported in Figure 1.

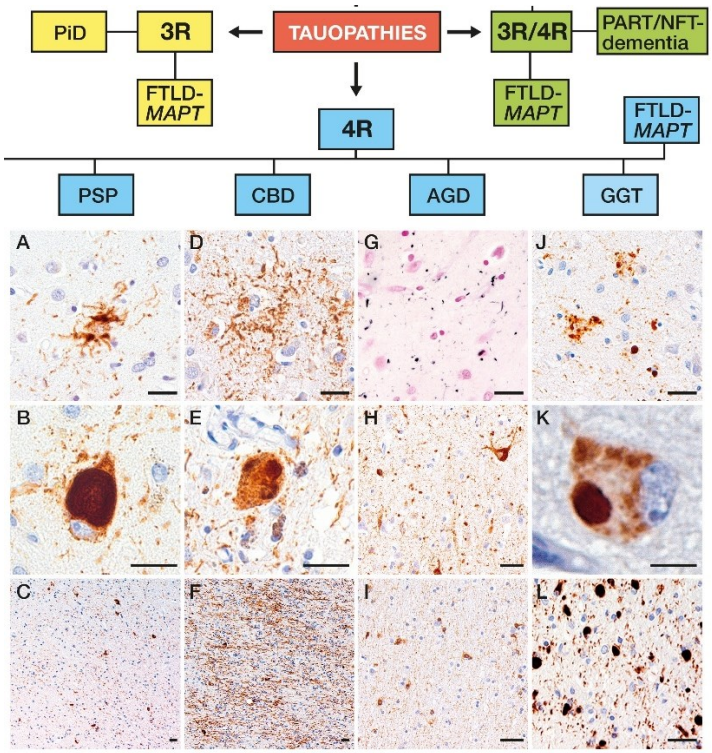

Figure 1. Tauopathies classification in presence of 3R(yellow),4R(green) or a mixed 3R/4R(blue) repeats. In order: PiD: Pick's disease; FTLD: frontotemporal lobar degeneration; NFT: neurofibrillary tangles; PSP: progressive supranuclear palsy; CBD: corticalbasal degeneration; AGD: argyrophilic grain disease; GGT: globular glial Tauopathy.[13]

1.2 Intrinsically Disordered Proteins (IDPs)

Intrinsically disordered proteins are a group of proteins which lack secondary structure. This unique property arises from amino acid sequences which include the presence of a great amount of negatively charged amino acid that lead to a high net charge at neutral pH, and a low content of hydrophobic amino acid residues. [14–17] The concept that protein, under native, functional conditions, [18,19] are disordered, emerged from the works of Jirgensons's and Arnone et all.

Although they lack a well-defined secondary structure, many IDPs undergo disorder-to order transition, upon binding to small and/or macromolecules [20–23] or after post-translational modifications. [24,25]

Since IDPs have no single, well-defined stable structure and exist as highly dynamic conformational ensembles, they do not undergo the dogma 'structure-function' paradigm. [17] Despite this property, many efforts have been done in structural biology to reveal the conformation dynamic of this class of proteins, through different techniques, like Nuclear Magnetic Resonance (NMR) [26], X-Ray crystallography [27], Circular Dichroism (CD) [28,29]spectroscopy and computational molecular dynamic (MD) simulations. [18,30]

1.2.1 Tau protein

Tau is a microtubule-associated protein, predominantly expressed in the neurons, which plays an important role in the assembly and stabilization of microtubules. Tau is a natively unfolded protein characterized by high solubility and structural flexibility. [31–35] The full-length protein Tau comprises 441 residues, and it is encoded by a gene located on chromosome 17 which consists of 16 exons [34,36]. Full-length Tau is organised in four domains: an N-terminal projection domain, a proline-rich domain (PRD), a microtubule-binding domain (MTBD), and a C-terminal domain. Human full-length Tau is presented in six isoforms, derived from alternative mRNA splicing of microtubule-associated protein Tau (MAPT) gene around exons 2,3 and 10, as reported in Figure 2.

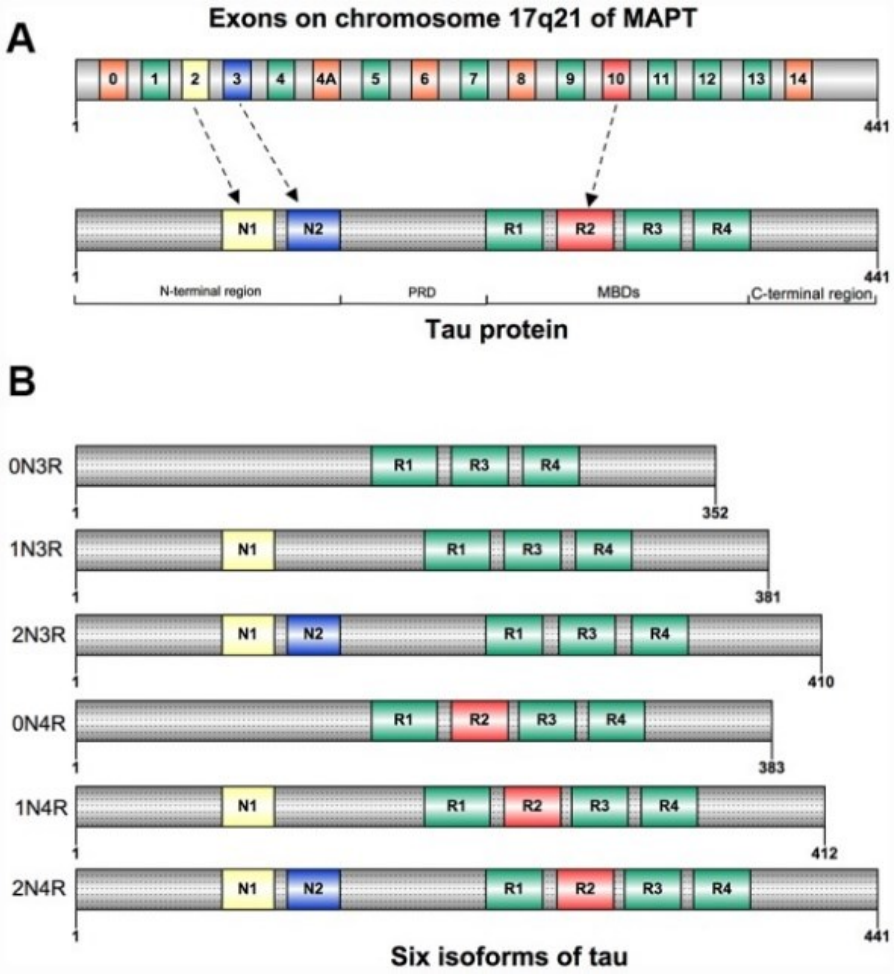

Figure 2. A) Full-length Tau protein B) Six different Tau isoforms derived from alternative splicing of exon 2(N1), exon 3(N2) and exon 10 (R1-R4).

Tau was first isolated in 1975 for its microtubules formation ability and, even though it is expressed in many tissues like heart, kidney, lung and testis, [35] it is mainly present in the brain neuronal axons. [37]

The N-terminal part and a short region at the C-terminus are acidic while the MTBD and the proline-rich region are both positively charged in order to ensure the binding with the microtubules that are mainly negatively charged.

In pathological conditions, Tau, is found hyperphosphorylated and this modification diminishes its ability to promote MTs assembly. [38] In particular, the reducing affinity to the MTs, leads to the release of soluble Tau proteins, targeted by post-translational modifications, that directly or indirectly alter Tau conformation, promoting Tau dimerization in an anti-parallel manner. [39]

From a histopathological point of view, AD is characterized by the presence of extracellular amyloid plaques, containing the aggregated amyloid precursor protein (APP) Aβ, and intracellular neurofibrillary tangles (NFTs) composed of hyperphosphorylated Tau protein in paired helical filaments (PHFs) or straight filaments (SFs). [40]

According to the amyloid cascade hypothesis, increased production and aggregation of Aβ lead to the accumulation of toxic species of this peptide, which further causes brain pathology and dementia; this hypothesis assumes that the presence of this started Aβ fibrils can induce Tau aggregation. [32,33,35,40]

A significant discovery for understanding Tau behaviour came when it was recognized that the protein contains isolated short peptide motifs, which have a high tendency for β-structure and aggregation, specifically, PHF6 (^{275}VQIINK^{280}) and PHF6* (^{306}VQIVYK^{311}), located at the beginning of R2 and R3 repeats. [41–43]

From recent Cryo Electron Microscopy (Cryo-EM) images was emerged that both PHF and SF of Tau aggregates, are composed of two C-shaped subunits which assemble in two protofilaments. The core structure of these filaments consists of residues 306 to 378, corresponding to R3 and R4 repeats of Tau. [42–45] The structure is an in-register parallel β-sheet formed by a β-bend and β-helix motif, linked by β-strands. [43] Notably, it was discovered that, in vitro, a longest construct, spanning residues 297-391, exhibits a potent ability to form filaments, without inducers, that is not observed with full-length Tau. [46]

Another important step in understanding Tau aggregation pathway, comes from the idea that MAPT, as intrinsically disordered protein, can assemble inside the neuronal cells into liquid droplets by phase separation (LLPS). [47] This process is thought to play a crucial role both in normal neuronal function and in neurodegeneration, however the underlying molecular mechanisms are still far from being fully clarified due to complicating factors like nonuniform charge patterning and sequence specificity.

1.2.2 α-Synuclein

Alpha-synuclein is an IDP, it comprises 140 amino acids and is mainly located in the presynaptic nerve terminal. The amino acidic sequence includes three regions, as depicted in Figure 3. [48]

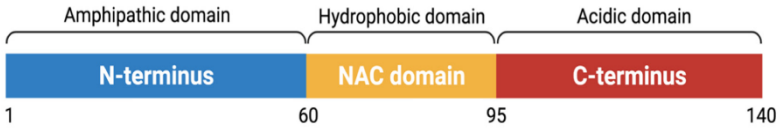

Figure 3. Schematic structure of α-synuclein. [48]

The N-terminal amphipathic lysin-rich motif (amino acids 1-60) plays a crucial role in modulating alpha-synuclein interaction with membranes, while the C-terminus domain is rich in acidic amino acids and prolines and it is involved in the interaction with small molecules, metals and other proteins. The central domain is the non-amyloid-β component, or NAC domain, it is highly amyloidogenic and is responsible for fibril formation and synuclein aggregation. The C-terminal region is able to decrease protein fibrillation due to the negative charge, by interacting with the NAC domain forming self-chaperone. Modifications in the C-terminus domain, coming from truncation or phosphorylation and other PTMs, lead to the formation of α-syn aggregates deposited in Lewy's body (Figure 4), associated with Parkinson's disease. [48–50]

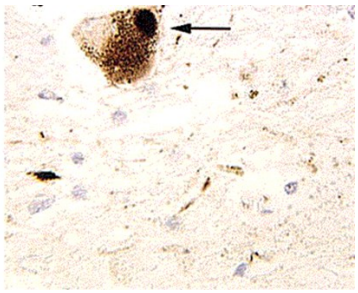

Figure 4. α-Synuclein-positive Lewy body (arrow) in pigmented nerve cell of the substantia nigra [51]

Parkinson's disease is the second most common form of dementia, after AD, it is a slowly progressive pathology that affects the neurons in the substantia nigra. Gradual degeneration of these cells causes a decrement in the dopamine content. PD is

characterized by different body impairments, like resting tremor of the body, bradykinesia and akinesia, rigidity of limbs and postural instability, gait or balance problems (postural instability).

1.3 Post-Translational Modifications

Protein regulation takes place predominantly through post-translational modifications (PTMs). Combinations of such PTMs are responsible for regulating and fine-tuning protein conformation and activity [52,53] however they can dramatically change the function driving to protein toxicity.

In the case of Tau protein, extensive reports have been published about hyperphosphorylation, as representing the starting point for aggregation of toxic species. [40,54]

Beside the abnormal phosphorylation of Tau, the synergic effect of others PTMs can result in a cooperative and anti-cooperative effect on Tau aggregation, as illustrated in Figure 5.

Among various PTMs, hereafter we will briefly discuss about phosphorylation and ubiquitination, with a particular focus on the latter.

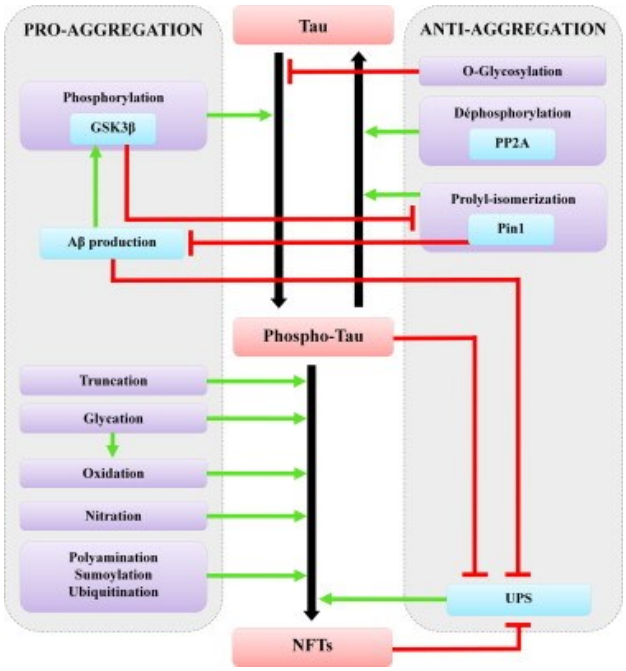

Figure 5. Tau aggregation related to PTMs scheme. On the right: anti-aggregation PTMs effect. On the left: pro-aggregation PTMs

1.3.1 Phosphorylation

Protein phosphorylation is the addition of a phosphate group by esterification at mainly three types of amino acids: serine, threonine, and tyrosine.

In physiological conditions it is very important to maintain a correct balance between Tau phosphorylation and dephosphorylation to guarantee the stability of cytoskeleton and microtubule binding.

Tau phosphorylation process is driven by different classes of protein kinases that are: proline-directed serine/threonine-protein kinases (GSK-3, Cdk5, MAPK, and ERK2), non-proline-directed serine/threonine-protein kinases (PKA, PKC, AMPK), tyrosine kinases (FYN), calmodulin-dependent protein kinases II (CaMKII). [46,55,56]

On the other hand, several phosphatases act in dephosphorylation of Tau protein, such as PP1, PP5, and PP2B, PP2A. [55]

Down-regulation of PP2A has been observed in AD which might intensify Tau hyperphosphorylation. To accelerate dephosphorylation process, Pin1 induces Tau prolyl-isomerization facilitating Tau dephosphorylation by PP2A. After a long period of time, Tau dephosphorylation cell machinery is overcome and Tau dephosphorylation becomes more difficult.

Moreover, down-regulation of Tau glycosylation, may cause conformation changes of Tau that expose the phosphorylation sites, normally buried within the protein. In fact, impairing brain glucose uptake/metabolism leads to down-regulation of O-GlcNAcylation (and over-activation of GSK3β), which in turn facilitates abnormal Tau hyperphosphorylation. [39,56]

The detailed Tau phosphorylation sites are illustrated in Figure 6.

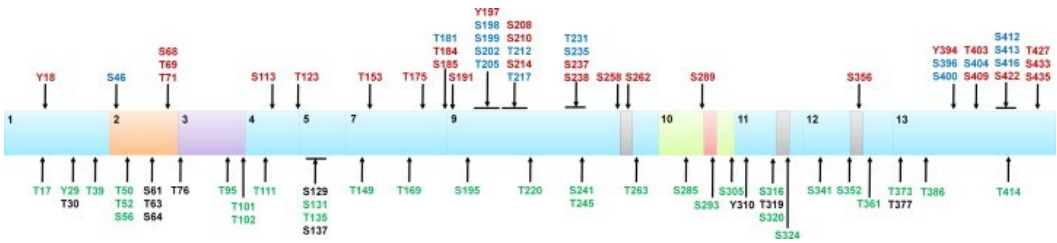

Figure 6. Tau Phosphorylation Sites (PSs). PSs found in AD brains (in brown), PSs found in normal brain (in green) and PSs present both in normal and AD brains (in blue). PSs unclear (in black). [57]

1.3.2 Ubiquitination

Ubiquitination is a post-translational modification that is involved in numerous cellular processes including protein degradation. It consists of the covalent attachment of a ubiquitin to target proteins. Ubiquitin is a folded protein which comprises 76 amino acids.

The ubiquitin proteasome system, together with the autophagy-lysosome system, are the main cell machinery for protein degradation.[58] Ubiquitin is not only involved in protein degradation but also in regulating gene transcription, cell cycle progression, DNA repair, apoptosis, virus budding, and receptor endocytosis. [59,60]

The ubiquitination of a substrate is biologically regulated by the coordinated action of a three enzyme-cascade. The E1 enzyme must first activate ubiquitin in an ATP-dependent reaction, upon binding the cysteine residue on the ubiquitin to its C-terminal through a covalent bond. At that point, the thioesterified ubiquitin passes from the E1 to E2 enzyme, the ubiquitin-conjugating enzyme. Finally, the E3 ubiquitin ligase binds to both the E2-bound ubiquitin and the protein substrate, promoting the transfer of ubiquitin onto the substrate that becomes attached to the ε-amine of a lysine residue through an isopeptide bond. [59,61]

The ubiquitinated substrate than moves to the 26S proteasome for degradation as illustrated in Figure 7.

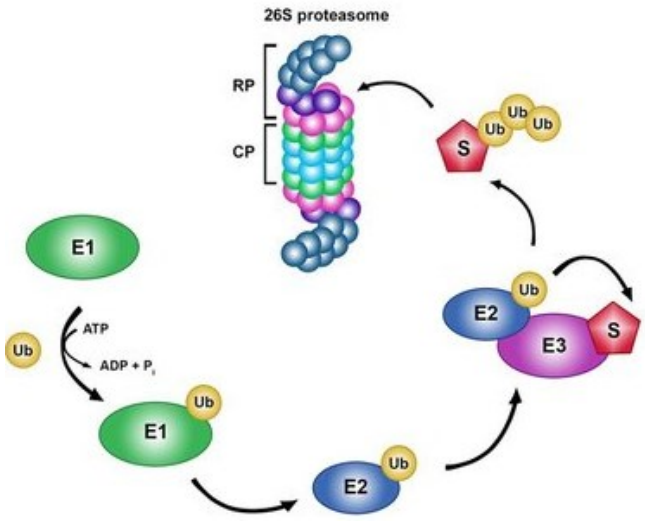

Figure 7. The ubiquitin–proteasome system (UPS). Activated ubiquitin binds to E1 and is transferred to the ubiquitin-conjugating enzyme (E2). The E2 carries the activated ubiquitin to the ubiquitin ligase E3. [62]

Dysregulation of Tau ubiquitination contributes to neuronal cell loss in the brain of AD patients, since UPS is impeded from the possibility to process filamentous forms of Tau, consequently, it is reported that Tau isolated from AD-paired helical filaments (PHF) is ubiquitinated at several lysine sites. [45,63,64]

Sixteen of 17 identified ubiquitination sites of PHF-Tau are in the microtubule-binding four-repeat domain (4RD) which forms the core of the filaments. Specifically, mono-ubiquitin was found to be linked to Lys254, Lys257, Lys311 and Lys317 [64], while single and double ubiquitination at residues Lys311 (R3) and Lys317 (R3) were identified as the most distinct PTM for differentiating between AD and control groups based on quantitative proteomic analysis of insoluble Tau in the brain. [45,54,63] The ubiquitination, in combination with other PTMs, may affect the ultrastructural organization of pathological Tau filaments. Based on the above notions, we plan to investigate the aggregation propensity of site-specifically ubiquitinated Tau proteoforms, prepared in vitro. [65]

1.4 Aggregation pathway

Amyloid proteins, under abnormal conditions, can convert into toxic aggregates, as largely discussed in paragraphs 1.2.1 and 1.2.2.

This process is common to a number of proteins including Tau, amyloid-β, polyglutamine, α-synuclein, and prions, responsible of diseases such as Alzheimer's [66], Huntington's [67], Parkinson's [68], and prion. [69] Because of its importance, kinetics mechanism of protein aggregation has gained a huge interest in the last years.

The review of Morris et all [70] elegantly collected all the theoretical and practical techniques to study aggregation kinetic. The fibrillation reaction rate depends on the protein concentration and can be accelerated by the presence of pre-aggregates components, like seeds.[71–73]

The aggregation of an intrinsically disordered protein occurs through a nucleation-dependent polymerization reaction and its typical kinetics is well-represented by a sigmoidal curve composed of three phases. The initial thermodynamically disfavoured lag phase, in which the protein is preferentially in monomeric state, the growing phase or elongation phase in which protofilaments start to aggregate, and the stationary phase in which the fibrillation process reaches the maximum rate, described by the equilibrium constant k_a (s^{-1}).

Amyloid fibrils have common optical properties such as birefringence upon binding with specific dyes like Congo red and thioflavin-T. [71,74] This characteristic allows to follow protein fibrillation through spectroscopy, monitoring the fluorescence emission.

The schematic representation of this process is presented in Figure 8.

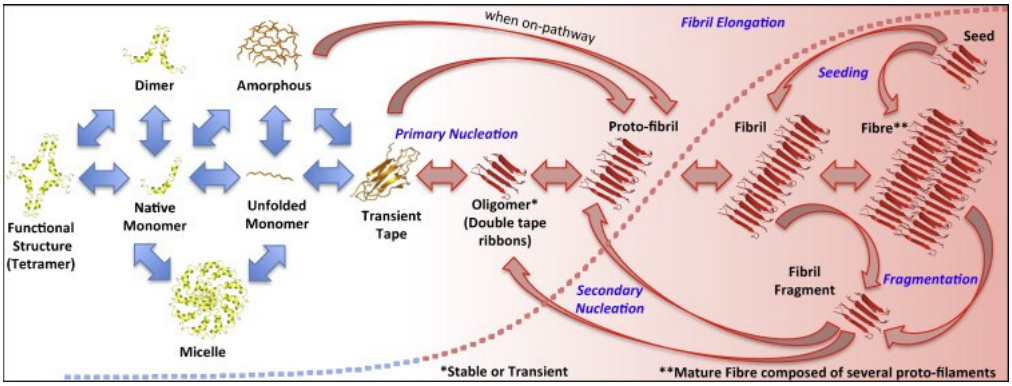

Figure 8. Schematic representation of amyloid protein fibrillation process [75]

1.5 Tau aggregation modulators

Tau aggregation is the key point for modulating the occurrence of Alzheimer disease. Different therapeutic possibilities are currently being explored that target proteins implicated in neurodegenerative disease. However, there are major challenges that hamper the development of novel therapies, including incomplete knowledge of druggable disease targets and their mechanism of action as well as a lack of biomarkers to monitor disease progression and therapeutic response. [2,76]

To achieve this goal, it is important to understand the pathogenesis of neurodegenerative conditions, i.e., a broader understanding of biochemical modifications is crucial.

In this Ph. D thesis, I explored the aggregation propensity of Tau protein when influenced by nanomaterials, by selected molecules derived from coffee beverage and upon ubiquitination modification.

1.5.1 Ubiquitin coupling reaction

Post-translational modifications are essential for good regulation of protein functions. Tau protein as an IDP, undergoes several PTMs including phosphorylation, ubiquitination, methylation and etc. Besides being important for physiological conditions, mounting evidence suggests that Tau hyperphosphorylation enhance its ability to self-assemble into paired helical filaments (PHFs) that accumulate into fibrillary tangles. This, results in the loss of axonal or dendritic transport as well as disassembly of the microtubules. Together with phosphorylation, ubiquitination, in combination with other PTMs, may play a role in modulating Tau aggregation. [35,39]

The possibility of quantifying the impact in which PTMs remodel the protein conformational landscape will pave the way for mitigating aberrant structural transformations, offering opportunities in chemical biology and molecular therapeutics.

In this work, a specific site of Tau was ubiquitinated, by chemoselective disulfide chemistry and sulfide reaction through dehydroalanine chemistry, in order to strive key information about the role of ubiquitin for Tau aggregation. The scheme of the two reactions is reported in Figure 9.

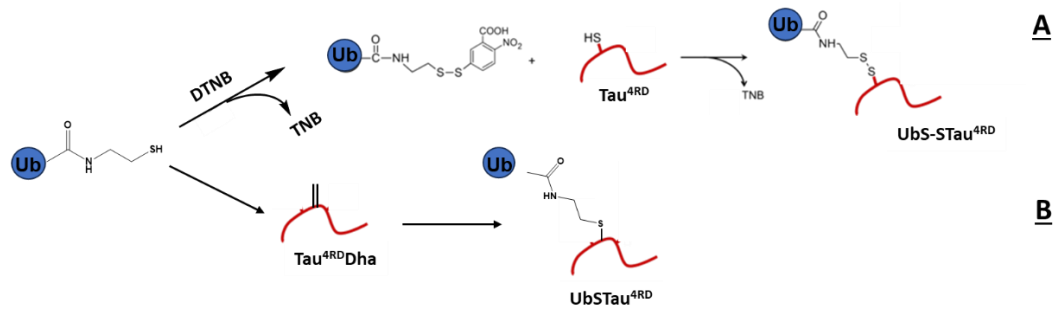

Figure 9. Ubiquitinated Tau^{4RD} species. A: Chemoselective disulfide-couplings using Ellman's reagent (DTNB; 5,5-dithio-bis-(2-nitrobenzoic acid)). B: Sulfide coupling using dehydroalanine chemistry.

1.5.2 Nanoparticles

The use of nanoparticles has a wide spread of applications and nowadays they are largely used and implemented in electronic, medical industries and food; [77,78]for instance, nanoparticles conjugated with antibodies, such as quantum dots, are used in diagnostic to determine the exact amount of the target in tissue.[79]

There are various methods for drug delivery crossing blood-brain barrier (BBB) based on nanomaterials, like poly (lactic-co-glycolic acid) (PLGA) coated nanoparticles fabricated by a nanofoil meld that produces uniform biocompatible NPs, but several methods are invasive, such as BBB osmotic modification. [80]

In the field of neurodegeneration, remarkable steps have been done including nanomaterial technology, as revealed by experiments in stem-cell showing that nanofibers can be used as nanocarrier to prevent the inflammatory response in microglia, an effect linked to neuroinflammation and degeneration. [81]

Gold nanoparticles are nanomaterials in the size range of 1 to 1000 nm, and among them, ultrasmall NPs (core size< 3nm) are promising candidates for biomedical application due to their biocompatibility, [82,83] in addition, the increased surface area-to-volume ratio of NPs increases the rate of drug loading, thereby improving drug efficacy and safety.

Here, I concentrated my attention on, dihydrolipoic acid (DHLA)-usGNPs as promising modulators for Tau aggregation. The structure of the nanoparticle used in this study is illustrated in Figure 10.

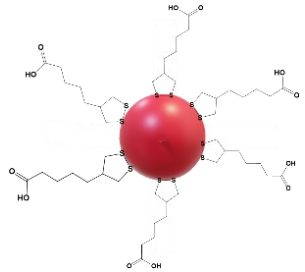

Figure 10. DHLA-usGNPs structure representation.

1.5.3 Coffee compounds

Natural compounds have been studied for a long time for their potential health benefits. Among molecules that nature provides, polyphenols are a class of compounds largely studied for their wide range of applications such as anti-inflammatory, anti-oxidant, neuroprotective and anti-aggregation activities. [84,85]

Polyphenols are prominent candidates for neurogenerative disease because their hydrophobicity property permits to cross the BBB.

Coffee is one of the most consumed beverage in the world, and helpful effects of brewed coffee are already known, such as the daily uptake of methylxanthines is correlated with a decrease in risk of stroke, suicide and depression. [86]

Despite of its positive effects on brain welfare, caffeine has not great effect on Aβ peptide and Tau fibrillization, as shown by the comparison between coffee and decaffeinated coffee. On the other hand, it has been found that the concentration of coffee molecules like theobromine and chlorogenic acids (CGAs) is inversely proportional to the formation of Aβ42 fibrils. [87,88]

Another class of newly investigated coffee derived components are phenylindanes, they are able to completely inhibit Aβ oligomerization and fibrillization in vitro and to partially decelerate Tau fibrillization. [89]

Relying on these promising perspectives, here the effects of an Italian espresso coffee mixture and of selected coffee-derived bioactive molecules towards mitigation of Tau aggregation are investigated. The structures of the molecules used in this study are illustrated in Figure 11.

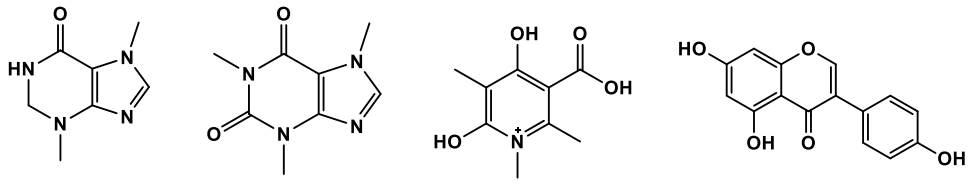

Figure 11. Structures of the molecules selected for the study: theobromine, caffeine, trigonelline and genistein (from left to right).

1.6 Liquid-Liquid Phase Separation of Tau (LLPS)

Liquid-liquid phase separation (LLPS) of biopolymers is a phenomenon leading to the formation of membraneless organelles (MLOs) in eukaryotic cells (also known as biomolecular condensates or droplets). Condensation occurs upon weak multivalent interactions, such as heterotypic electrostatic interactions between oppositely charged polyelectrolytes, or homotypic interactions involving repetitive low-complexity sequences and multiple interacting sites. LLPS is used by the eukaryotic cells for many activities like storage, processing of RNA and to facilitate intracellular reactions. [90–92] LLPS indeed, is reached when a molecule originally present in one-phase regime in solution, separates into two phases regime characterized by a highly concentrated phase (condense or dense phase) and a dilute phase, giving rise to liquid droplets. A schematic representation is reported in Figure 12.

Similar to other IDPs, Tau protein undergoes LLPS and this phenomenon has been suggested to initiate the aggregation of Tau. [47] Therefore, discovering agents that can target or alter Tau condensation can shed light into this cellular mechanism both for in vitro and in vivo studies.

In my work I studied if nanoparticles could act as condensate-targeting agents, due to their unique material properties and modes of interaction with biomolecules.

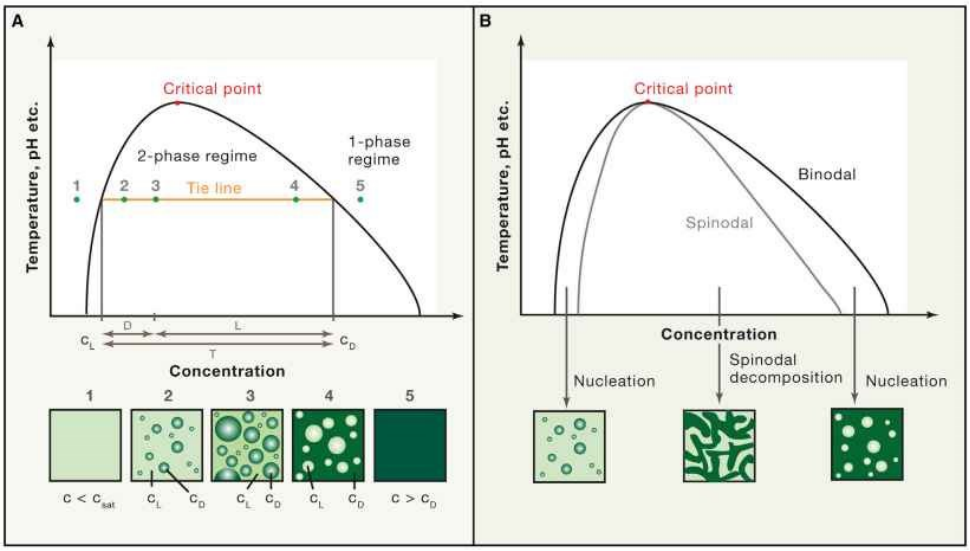

Figure 12. Schematic diagram of LLPS. On the left, the black line separates the one-phase and two-phase regime. The phase separation depends on environmental conditions, like pH and temperature. C_L refers to the concentration of the light dense component, while C_D to the dense phase. The examples 1-5 along the orange tie line represents the rearrangement of system when changing the ratio between C_L/C_D. On the right, the gray curve outlines the instability region in which the system undergoes the spinodal demixing decomposition. [93]

2 Aim of the thesis

The aim of this doctoral project is to provide new atomic-level information on the conformational changes and the aggregation kinetics of Tau protein modulated by different cofactors. For this purpose, I employed a multidisciplinary approach including organic chemistry, and a variety of spectroscopy and microscopy techniques such as CD, NMR, fluorescence, and TEM. In particular, I focused my attention on a PTM of Tau, ubiquitination, and I investigated the impact of site-specific ubiquitination on Tau aggregation. To this aim I designed a novel semi-synthetic approach via dehydroalanine to modify Tau with a ubiquitin moiety at a selected residue. I then exploited the impact of coffee extract and coffee-derived compounds and of selected nanoparticles on Tau aggregation propensity. Moreover, I elucidated the interaction and the influence of nanoparticles in the early aggregation events of Tau, described by liquid-liquid phase separation.

A deep understanding of the mechanisms of aberrant modification of amyloidogenic proteins and the investigation of molecular strategies to interfere with protein aggregation is crucial for finding new treatments for neurodegenerative diseases, which are an ever-increasing health and social problems all over the world.

3 Results and discussion

3.1 Ubiquitination

3.1.1 Introduction

A hallmark of many neurodegenerative diseases is the slow accumulation of misfolded protein deposits in the neurons of the brain. [94]

The microtubule-associated protein Tau forms pathological aggregates with the properties of amyloid fibrils in a number of neurodegenerative disorders termed Tauopathies, including Alzheimer's disease (AD) and frontotemporal dementia. [95] Tau is an intrinsically disordered protein (IDP) with little propensity for self-aggregation in solution, however in pathological conditions it readily assembles into ordered b-sheet-containing supramolecular filaments. [43] Recently, was discovered that PHFs isolated from AD-brain revealed residues 306-378, belonging to the repeat region R3 and R4, as the ordered fibril core, with the N- and C termini forming the fuzzy coat. Another fragment that has been used for in vitro assembly studies is dGAE, which comprises residues 297–391 of Tau, and was identified as the proteolytically stable core of PHFs from tangle fragments of AD.

Above this, the determinants of abnormal protein aggregation are still poorly understood but the process appears to be strongly influenced by post-translational modifications (PTMs). [33] Although the greatest research focus has been on the role of hyperphosphorylation of Tau, other PTMs, such as acetylation and ubiquitination, have also been implicated in events that lead to neurodegeneration. [45,96]

Ubiquitination (or ubiquitylation) involves the formation of an isopeptide bond between the C-terminal carboxyl group of the small regulatory protein ubiquitin (Ub) and the ε-amino group of lysine sidechains of the protein substrate. The conjugated Ub molecule can be further modified by additional Ub molecules to form elongated chains with diverse linkage topology that elicit different signals. [97] The role of ubiquitination in Tau biology and pathology is poorly understood but it has been associated with enhanced formation and impaired clearance of pathological inclusions. [64,98] Alterations to the levels of ubiquitination of Tau at various stages of disease have been observed in AD and other Tauopathies. [63] The full-length Tau isoform

(441 amino acids) has 44 lysine residues, of which 17 were reported as ubiquitination sites specific to pathological Tau. [63,99] Sixteen of these sites are in the microtubule binding domain (MTBD), which forms the core of the filaments. [43,63] Recent research suggests that ubiquitination, together with other PTMs, may play a role in the structural diversity of various Tau strains. [45]

Understanding the influence of ubiquitination on the conformational transitions of Tau requires the detailed investigation of ubiquitinated proteoforms obtained from controlled reactions. We have previously demonstrated that Tau can be ubiquitinated in vitro by an enzymatic method, using CHIP (carboxyl terminus of Hsp70 interacting protein) as the ubiquitin ligase (E3) in a chaperone-independent manner. [100–102] This approach affords facile and quantitative mono-ubiquitination of the substrate; however, the product is a mixture of regioisomers and is therefore unsuitable for establishing precise structure-function relationships. To overcome this disadvantage, we developed an alternative approach based on disulfide coupling chemistry. [100,101] This semisynthetic method generates a mimic of the native isopeptide bond, i.e. a disulfide bond between a Cys residue inserted in a specific position of the target protein and the C-terminal aminoethanethiol of a Ub derivative obtained from intein processing. [103,104] Disulfide-based coupling is advantageous as it is regio- and chemoselective, however the resulting product may prove unstable in a weakly reducing environment such as can be found in a living cell. Hence, in the present work, we explored a further strategy for the site-selective ubiquitination of Tau through stable covalent conjugation.

Dehydroalanine (Dha) chemistry has been widely exploited for the precise positioning of labels and post-translational modifications on protein substrates. [105] The noncanonical amino acid Dha can be installed at a desired position by diverse methods, [106] and sulfur-containing nucleophiles can readily attack the β-carbon atom of Dha to afford a highly selective thia-Michael adduct. The reaction can proceed in mild conditions to form a stable thioether linkage. Recent investigations demonstrated the successful application of Dha chemistry for the site-specific phosphorylation and methylation of Tau, and for the ubiquitination of a folded protein substrate. [107]

Herein, we describe an optimized chemical reaction for the preparation of Ub conjugates of Tau4RD and ADTau core (297-391) via Dha precursors.
The reaction scheme used in the present work is reported in Figure 13.

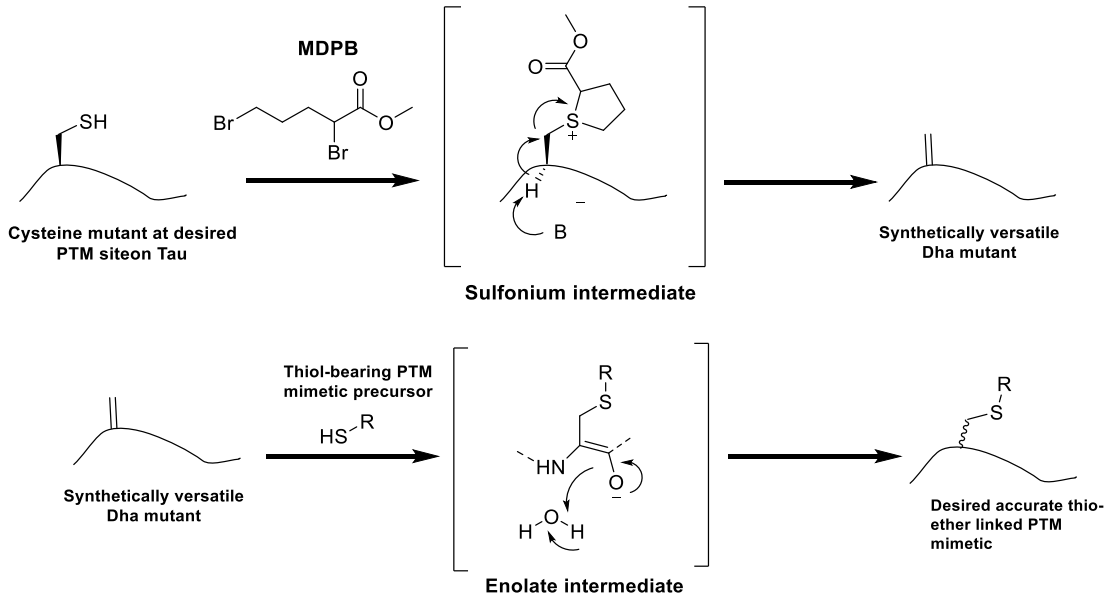

Figure 13. Ubiquitination reaction scheme. Dha protein formation (top) and ubiquitination reaction (bottom).

3.1.2 Results and discussion

Ubiquitin conjugation via dehydroalanine chemistry

Following the intein-mediated ligation approach, [108] we prepared a thiol-terminated Ub derivative (I) by expression of a Ub-intein fusion protein, followed by cysteamine-mediated cleavage of Ub from intein. The aminoethanethiol moiety becomes linked to the C-terminus of Ub via trans-thioesterification and S, N acyl shift reaction, as illustrated in Figure 14.

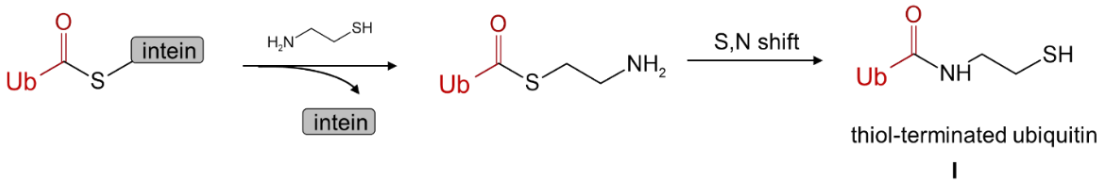

Figure 14. Intein-mediated ligation scheme

Next, we mutated the two native cysteine residues Cys297, Cys322 of Tau4RD into Ala, to obtain cysteine-free Tau4RDΔC, and introduced a non-native cysteine in the desired position Tau4RDΔC(K353C) (hereafter Tau353), using site-directed mutagenesis. The non-native Cys353 was then transformed into Dha as Tau353Dha (III), via bis-alkylation elimination using methyl 2,5-dibromopentanoate (MDBP). [107]

Dha was homogeneously introduced after incubation of the reactants for 6 h at 37 °C under shaking at 450 rpm (Figure 15).

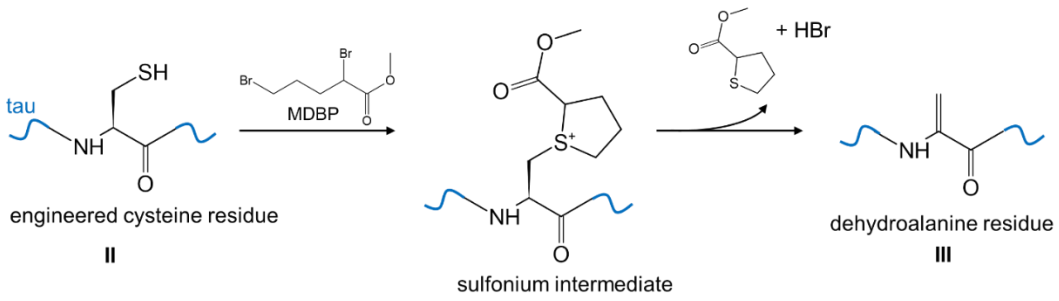

Figure 15. Dha formation via bis-alkylation elimination

The progress of the reaction was followed by SDS-PAGE analysis, by loading the samples w/o DTT as depicted in Figure 16. It is perfectly visible that Tau353 loaded w/o DTT runs like a dimer, due to disulfide bonds formation between the thiol group of the cysteines of two monomers, while, for Tau353Dha, a single band corresponding to a monomer of 14 KDa is visible thus meaning that the cysteine reacted to form dehydroalanine.

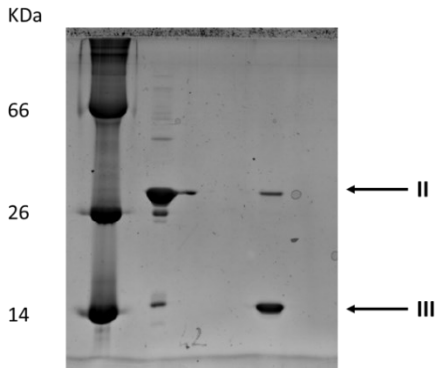

Figure 16. 15% SDS-PAGE showing Tau353Dha formation. The well for compound II is dimeric for compound III is monomeric. Samples were loaded w/o DTT.

Finally, Ub-SH was conjugated to precursor III via 1,4 thia-Michael addition, [107] producing homogeneous Tau353Ub (IV) with a thioether linkage. Figure 17

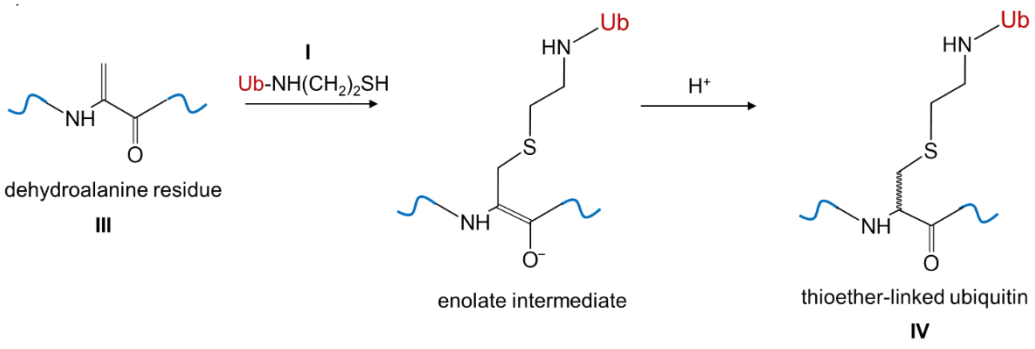

Figure 17. Thia-Michael addition for ubiquitination reaction

Proteoform IV contains a close mimic of the native conjugate, where the γ-carbon of the lysine sidechain is replaced by sulfur.

The ubiquitinated Tau formation was followed along the time by SDS-PAGE as shown in Figure 18.

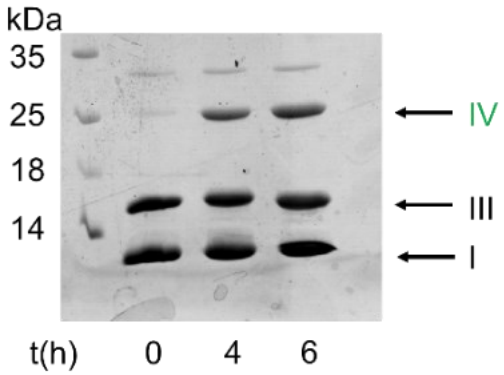

Figure 18. 15% SDS-PAGE showing the time course of the reaction to obtain the ligated product. Aliquots were taken immediately after preparation and after 4 h and 6 h of incubation. The bands correspond to reactants (compounds I, III) and product (compound IV).

Product purification and characterization

The ubiquitinated Tau product was then purified by preparative HPLC. The separation of the species was carried out using a C4 column with a gradient of acetonitrile. Figure 19

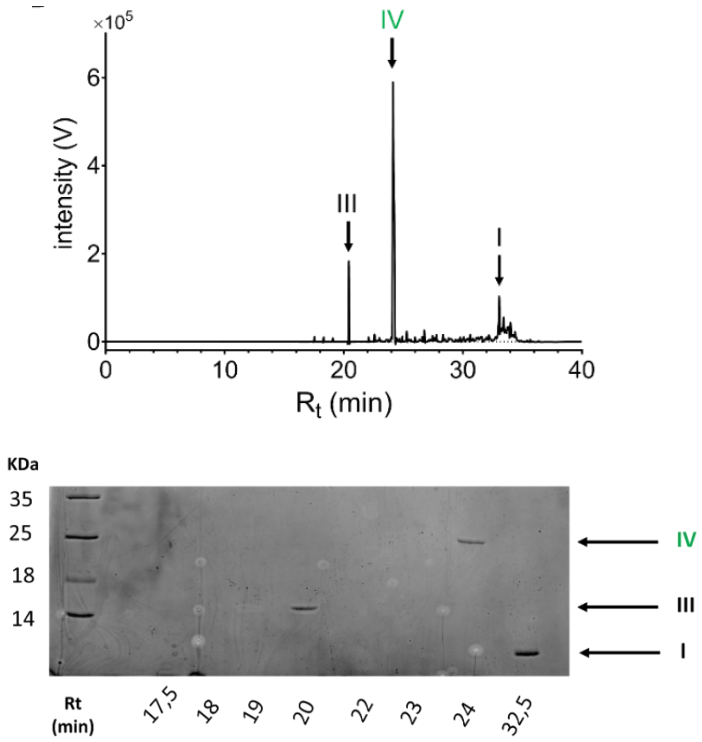

Figure 19. Top: HPLC elution profile of the reaction mixture examined after 6 h of incubation. Bottom: SDS-PAGE of HPLC fractions displaying the bands corresponding to pure reactants and product.

All the intermediate compounds and the product were characterized by MALDI-TOF mass spectrometry, using an HCCA matrix Figure 20. All the data show that we have successfully achieved the synthesis of the conjugated species Tau353Ub.

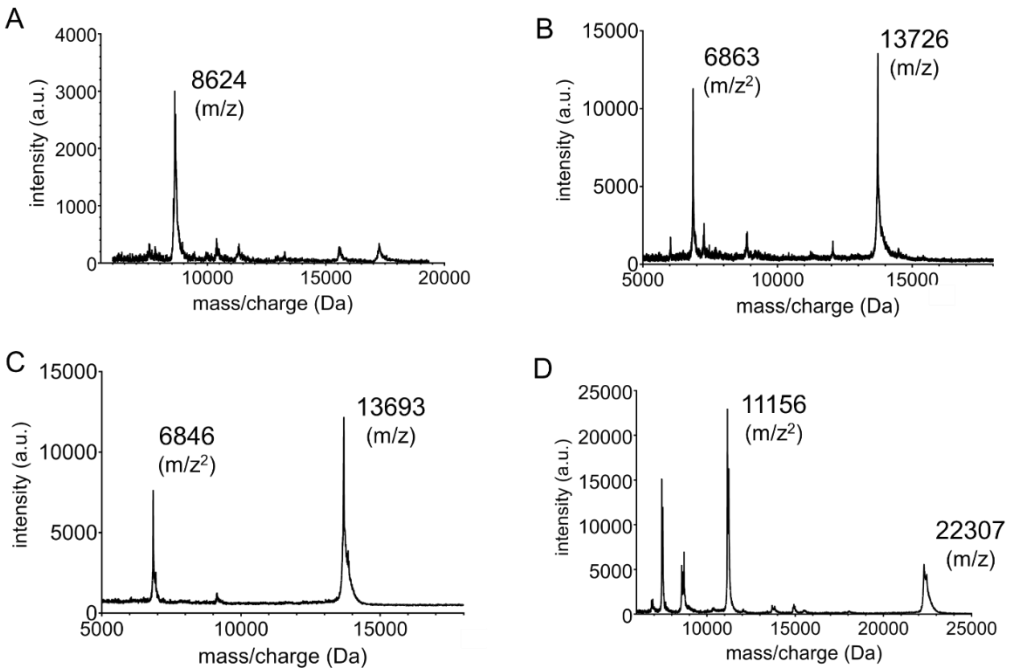

Figure 20. Mass spectrometry analysis. MALDI-TOF MS spectra of compounds I (A), II (B), III (C), and IV (D) are shown. Experimental mass values (Da) are displayed, expected values are 8624 Da (I), 13725 Da (II), 13691 Da (III), 22314 Da (IV).

Circular dichroism (CD)

The intrinsically disordered state of Tau is best described as an ensemble of rapidly interconverting conformers with no permanent global or local structural ordering. [109] Short elements of secondary structure may form transiently and potentially influence the self-interaction propensity of the polypeptide. [110] To gain insight into the conformational perturbations induced by the Ub moiety on the substrate Tau, the secondary structure of Tau353Ub was examined by far-UV circular dichroism (CD). The spectrum of TauΔC displays a deep negative ellipticity minimum at ~198 nm and no major bands at wavelengths longer than 205 nm (Figure 21, black line), in agreement with its disordered state. The spectrum of Ub reflects the presence of both b-sheet and α-helical elements of secondary structure (Figure 21, red). The spectral profile for the ubiquitinated proteoform (Figure 21, green) displays a

negative dichroic signal at 202 nm and overall stronger negative ellipticity than unmodified Tau. Since the spectrum of Tau353Ub coincides with the sum of the spectra of unconjugated protein moieties, within experimental error, it can be concluded that the disordered character of the protein is retained, and no major secondary structure motifs are induced by the modification.

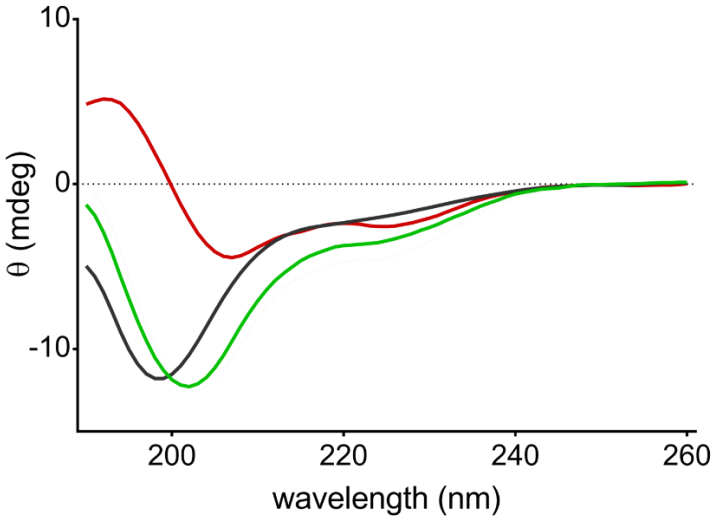

Figure 21. Far-UV CD spectra acquired on precursor III (black), precursor I (red), and on product IV (green). Protein species were 6 μM.

Thioflavin-T assay

Most Tau proteoforms and constructs, including Tau4RD, are stable in solution as monomers, therefore aggregation inducers like heparin or fatty acids are generally used to probe the aggregation mechanism. [101,111] The aggregation kinetics of the two proteoforms, in the presence of heparin, was determined by monitoring the time-dependent fluorescence signal of Thioflavin-T (ThT), a benzothiazole dye responsive to the cross-b structures characteristic of amyloid-like fibrils. [112] Here, we aimed to compare the aggregation kinetics of Tau353Ub with that of the unconjugated protein. The kinetic profile was sigmoidal-shaped and consistent with a macroscopic nucleation-growth mechanism (

Figure 22). In the used conditions, both the nucleation and growth processes were rapid for unmodified TauΔC (midpoint transition time constant, $t_{0.5}$ = 8.58 ± 0.02 h; elongation time constant, t = 0.69 ± 0.02 h). By contrast, a significantly decreased aggregation rate was observed for Tau353Ub (midpoint transition time

constant, $t_{0.5}$ = 27.47 ± 0.09 h; elongation time constant, t = 3.46 ± 0.08 h), indicating that ubiquitination in position 353 disfavours protein self-assembly. This result is in complete agreement with our previous finding obtained for a ubiquitinated TauΔC produced exploiting disulfide-coupling chemistry Tau353-SS-Ub. [100]

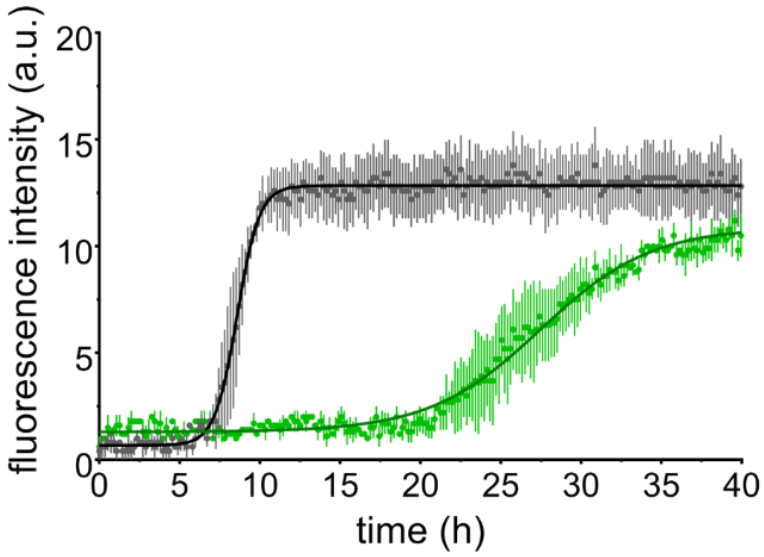

Figure 22. Aggregation assay. ThT fluorescence assay on Tau species incubated with heparin. Measurements were performed on 10 μM TauΔC (grey) and Tau353Ub (green). Data represent the mean ± SD from three replicate measurements. Solid lines correspond to the best fit curves determined using an empirical sigmoid function.

TEM analysis

The morphology of an amyloid protein aggregate can be revealed by Transmission Electron Microscopy (TEM). For our purpose, we investigate the morphological structure of fibrils of TauΔC protein and of the conjugated Tau353Ub construct, by TEM images, in order to confirm the results obtained by ThT assay.

Upon incubation with heparin for 48 h, both on unmodified and modified Tau protein images were acquired. As revealed from the pictures in Figure 23 and from the statistical analysis, the two samples display different structure parameters. TauΔC was characterized by a large width of 9±2 nm, a narrow width of 5±2 nm and a twist crossover repeat of 58±2 nm, on the contrary, Tau353Ub was characterized by a large width of 5±2 nm a narrow width of 4±2 nm and a twist crossover repeat of 20±2 nm. This results are in perfect agreement with the ThT assay, and confirmed that the presence of the ubiquitin in position 353 largely perturbs the

formation of Tau mature fibrils, but did not arrest the aggregation event, as previously demonstrated in the paper of Munari et all. [101]

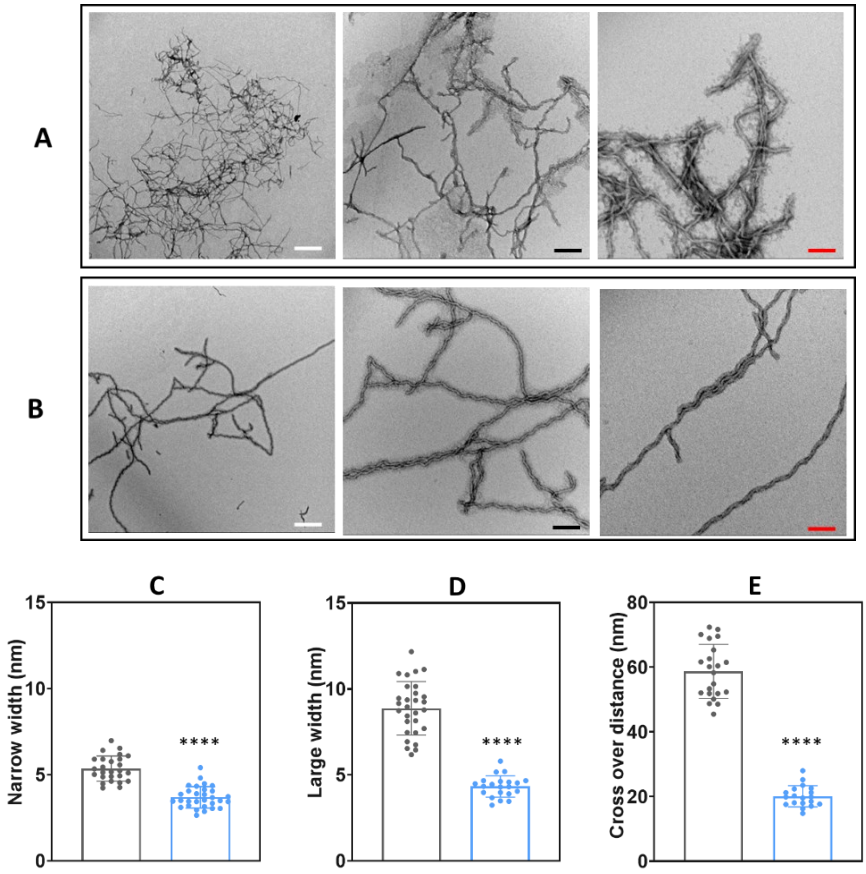

Figure 23. TEM representative images of (A) TauΔC and (B) UbTau353, after 48h of incubation at 37°C under static condition. Scale bars are reported in each image and correspond to 500 nm (white) 200 nm (black) 100 nm (red). Distribution of (C) narrow width, (D) large width and (E) crossover distances measured from TEM images of TauΔC (black) an UbTau353 (blue). Welch's statistical analysis was performed comparing the values obtained for the two samples, p = * 0.01-0.05, ** 0.001-0.01, *** 0.0001-0.001, ****<0.0001

Chemical modification of ADTau core:

The production of ubiquitinated ADTau core follows the same steps of Tau353. The purification of UbSH is the same as reported in Materials and methods.

First, we mutated the native cysteine residue, Cys322 of ADTau core into Ala, to obtain cysteine-free ADTau coreΔC, and then we introduced a non-native cysteine in the desired position obtaining ADTau coreΔC(K353C) (hereafter ADcore353 (V)), using site-directed mutagenesis. The non-native Cys353 was then transformed into Dha, as previously reported for Tau353Dha, via bis-alkylation elimination using MDBP.

Dha was homogeneously introduced after incubation of the reactants for 6 h at 37 °C under shaking at 450 rpm.

To carry out the ubiquitination reaction, we used the same molar ratio between UbSH and Dha construct as for Tau353, i.e., 300 µM of UbSH (I) and 300 µM DTT was added to 100 µM ADcore353 Dha (VI). The reaction was performed @ 37°C with a shaking of 700 rpm (**Test A,** Figure 24).

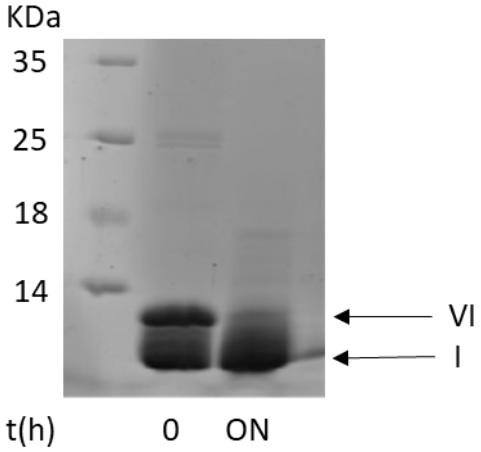

Figure 24. **Test A** 17% SDS-PAGE of the course of the ubiquitination reaction. Aliquots were taken immediately after preparation and after overnight incubation. The bands correspond to reactants I and VI.

The reaction did not produce the attended result, probably given to the aggregation of ADTau core,[113] we therefore tried other ubiquitination condition.

First of all, we reduced the shaking at 500rpm, and we kept the temperature constant at 37°C (**Test B,** Figure 25). We repeated the test by using the same amount of proteins with the same molar ratio reported above.

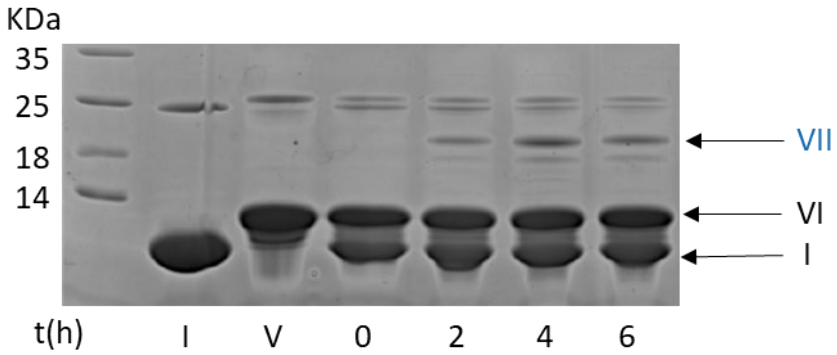

Figure 25. **Test B**. 17% SDS-PAGE of the course of the ubiquitination reaction. Aliquots were taken immediately after preparation and after 2 h, 4h and 6 h of incubation. The first line from the left correspond to compound I alone and the second line to compound V alone. The bands correspond to reactants (compounds I, VI) and product (compound VII).

Even in this case the yield was very low, so we decided to decrease the temperature to 30°C and we kept fixed the shaking at700 rpm (**Test C,** Figure 26).

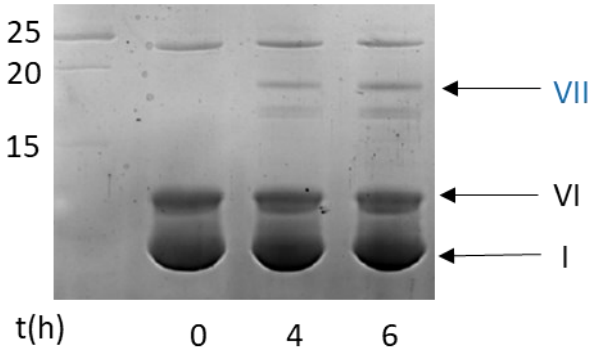

Figure 26. **Test C**. 17% SDS-PAGE of the course of the ubiquitination reaction. Aliquots were taken immediately after preparation and after 4h and 6 h of incubation. The bands correspond to reactants (compounds I, VI) and product (compound VII).

Even in this case we did not get a good yield of the product.

Product purification and characterization

ADcore353 and ADcore353Dha were characterized by MALDI-TOF mass spectrometry, using an HCCA matrix. The related calculated and experimental mass values are displayed in Figure 27.

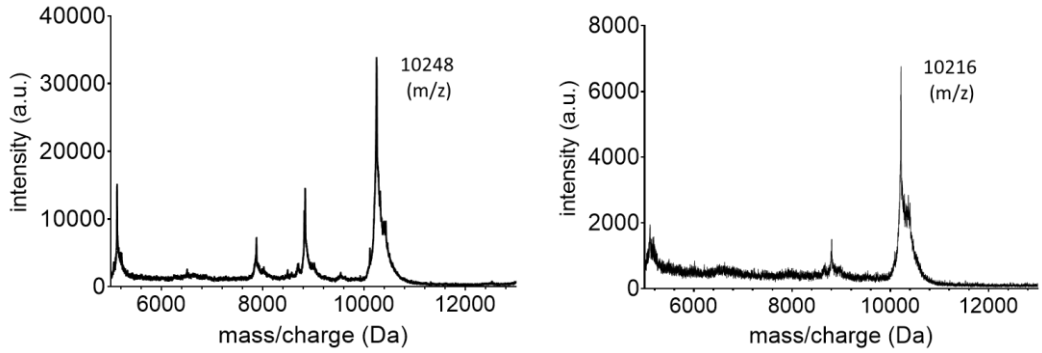

Figure 27. Mass spectrometry analysis. MALDI-TOF MS spectra of compounds V (left) and VI (right). Experimental mass values (Da) are displayed, expected values are 10296 Da (V), 10264 Da (VI).

Even though the absolute mass values are not closed to the experimental ones, the difference between the two protein is exactly 32 Da, which correspond to the loss of a thiol group.

Afterwords, we tried to purify the products of Test B and C with size exclusion chromatography (SEC) and HPLC (same method of Tau353Ub), but we did not succeed in the purification probably due to the low amount of product. (purification chromatogram and gels are not reported)

3.1.3 Conclusion

The design of novel reactions to obtain ubiquitinated conjugates is crucial to study the effect of site-specific modifications on aggregation propensity of Tau protein. Nowadays several methods are available to perform ubiquitination reactions, but none of them are regioselective or can produce stable or non-oxidating product.[61,100,102]

Here, I exploited the dehydroalanine chemistry to achieve a chemo-selective product for both Tau353 and ADcore353. For the first, pure product in a good yield was obtained. The progress of the reaction was followed by SDS-PAGE and all the intermediates' products were characterized by MALDI-ToF spectrometry. We demonstrated that the conjugation of Tau protein to the ubiquitin, in position 353, can perturb the fibrillation process and we were able to analyse the structural differences between Tau and Tau353Ub from the TEM images.

Concerning ADcore353, the dehydroalanine product was proved by MALDI-ToF spectrometry and SDS-PAGE, but the reaction, to obtain the ubiquitinated construct, needs further optimization.

3.1.4 Materials and methods

Reagents

Methyl 2,5-dibromopentanoate (MDBP), were purchased from BLDpharm (Germany). Heparin, Thioflavin-T (ThT), acetonitrile, dithiothreitol (DTT) and Trifluoroacetic acid (TFA) were obtained from Sigma-Aldrich (St Louis, MO, USA). In all preparations, high-purity deionized water from a Millipore system was used.

Recombinant protein expression and purification

For proteins expression, 20 mL of a starter culture were added to 1 L of growth medium. The culture was then incubated at specific condition according to the protein (see Table 1) and expression was induced with 0.5 mM of IPTG.

Protein	Medium	Antibiotic	O.D. $_{600}$	Time	Temp
Tau4RD	LB	Amp	0,7-1	5h	37°C
ADTau core	LB	Amp/Chl	0,8-1	5h	37°C
Ub-IntHis	Autoinducing	Amp		ON	37°C

Table 1. Cell cultures parameters for different protein. In order are reported: the growth medium, the antibiotics, optical density at 600 nm, the incubation time and the temperature.

Cells were then collected and centrifuged at 10000g for 15 min at 4°C. The resulting pellet was resuspended in 25 mL of lysis buffer (80 ml for Ub-IntHis) (see Table 2). After several sonication steps at maximum power alternating by rest periods in ice, the lysate was centrifuged for 20 min at 10000g at 4 °C and the supernatant was kept for further purification processes, briefly described in each protein section.

Tau4RD	ADTau core	Ub-IntHis
20 mM Tris-HCl pH 7.6	20 mM MES pH 6.8,	20 mM Tris-HCl pH 7.6,
50 mM NaCl	50 mM NaCl	0.5 M NaCl
Protease inhibitors 1X	Protease inhibitors 1X	20mM imidazole
PMSF 1mM	PMSF 1mM	Protease inhibitors 1X
DNase 1X	DNase 1X	PMSF 100 mM
1mM $MgCl_2$	5 mM $MgCl_2$	DNase 1X
1 mM EDTA	1 mM EGTA	3 mg of lysozyme

Table 2. Lysis buffer solution composition.

Heat shock transformation

Competent cells were transformed following the heat shock protocol:

- 50/100 µL of competent cells were thawed in ice.
- 30-50 ng of DNA were added, and the cells were incubated in ice for 20 min.
- the heat shock was performed at 42 °C for 45 sec in a water bath and then cells were placed in ice for 2 min.
- 500 µL of LB medium was added and the culture was incubated at 37 °C for 1 hour with orbital shaking.
- cells were plated on LB agar with specific antibiotic(s) and incubated O.N. at 37 °C.

Tau4RD

Tau4RD, and its mutant C291A/C322A/K353C, gene (spanning residues Q244-E372 plus initial Met, corresponding to R1-R4 repeats of Tau) (Figure 28) was cloned into a pET22b(+) vector via NdeI-BamHI sites with a stop codon to avoid insertion of a C-terminal histidine-tag (Figure 29). The plasmid pET22b (+) (purchased by Novagen) is a 5493bp expression vector with T7 promoter. It is characterized by a pelB leader sequence for subcellular targeting and tag csd, ampicillin resistance and many restrictions enzyme sites. Tau4RD, and its mutant, were expressed in BL21 (DE3) E. coli cell line, introducing the Tau4RD sequence via plasmid transformation.

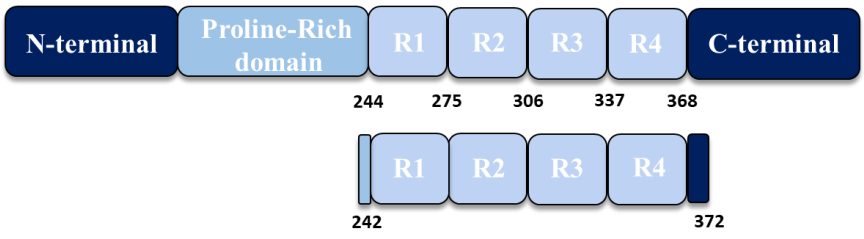

252 262 272 282 292 302
MQTAPVPMPD LKNVKSKIGS TENLKHQPGG GKVQIINKKL DLSNVQSKCG SKDNIKHVPG

312 322 332 342 352 362
GGSVQIVYKP VDLSKVTSKC GSLGNIHHKP GGGQVEVKSE KLDFKDRVQS KIGSLDNITH

372
VPGGGNKKIE

Figure 28. Schematic Tau4RD representation (top) and Tau4RD sequence (bottom).

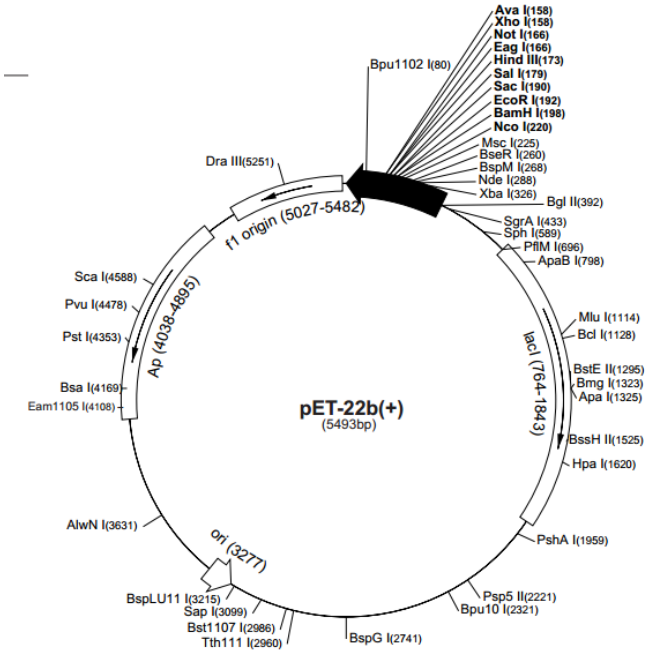

Figure 29. Schematic representation of vector pET-22b (+).

Tau4RD and its mutant were purified as described below. Briefly, the lysate was boiled for 20 min and, once it was cooled, centrifuged at 10000g for 20 min.

The soluble part was filtered and loaded onto an SP ion exchange column, pre-equilibrated with 20 mM Tris-HCl pH 7.6, 25 mM NaCl. The protein elution was performed with linear gradient from 25 mM to 500 mM NaCl.

Purified Tau4RD products were dialyzed in water.

ADTau core (a.a 297-391)

With a length of 5493 bp, the pET22b (+) plasmid features both a T7 promoter and terminator, including an AmpR gene and chloramphenicol for ampicillin and chloramphenicol resistance and a pelB leader sequence. As well as Tau4RD, also ADTau core was expressed in BL21 (DE3) E. coli cell line, introducing the ADTau core sequence via plasmid transformation. The T7 RNA polymerase-IPTG induction system suited this cell line perfectly, ensuring efficient transformation and high-level protein expression.

The plasmid used is the same for Tau4RD, reported in Figure 29, while ADTau core sequence is reported in Figure 30.

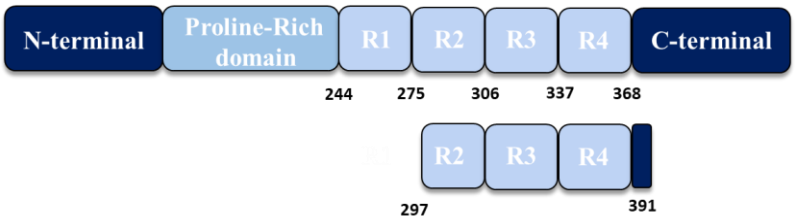


```
300        310        320        330        340        350
MIKHV PGGGSVQIVY KPVDLSKVTS KCGSLGNIHH KPGGGQVEVK SEKLDFKDRV
          360        370        380        390
QSKIGSLDNI THVPGGGNKK IETHKLTFRE NAKAKTDHGAE
```

Figure 30. Schematic ADTau core representation (top) and ADTau core sequence (bottom)

The lysate was boiled for 20 min and, once it was cooled, 1mM TCEP and DNase was added and then centrifuged at 10000g for 20 min. The supernatant was loaded in a SP-FF ion exchange column, pre-equilibrated with 20mM MES pH 6.8, 50mM NaCl, 1mM EGTA, 1mM $MgCl_2$, 0.1 mM PMSF. The elution was performed with a linear gradient from 50-250 mM NaCl. The protein was dialyzed in water.

Ubiquitin-GyrA intein-His

The ubiquitin bearing an amino ethanethiol C-terminal group (Ub-SH) required for the sulfide-coupling reaction, were produced by a chimeric protein where ubiquitin was cloned to the N-terminal of the GyrA intein in a pET22 vector. In this way, the chimeric protein has a C-terminal His-tag. The Ubiquitin-Intein-His sequence is reported in Figure 31.

```
        10         20         30         40         50         60
MQIFVKTLTG KTITLEVEPS DTIENVKAKI QDKEGIPPDQ QRLIFAGKQL EDGRTLSDYN

        70         80         90        100        110        120
IQKESTLHLV LRLRGGCITG DALVALPEGE SVRIADIVPG ARPNSDNAID LKVLDRHGNP

       130        140        150        160        170        180
VLADRLFHSG EHPVYTVRTV EGLRVTGTAN HPLLCLVDVA GVPTLLWKLI DEIKPGDYAV

       190        200        210        220        230        240
IQRSAFSVDC AGFARGKPEF APTTYTVGVP GLVRFLEAHH RDPDAQAIAD ELIDGRFYYA

       250        260        270        280
KVASVTDAGV QPVYSLRVDT ADHAFITNGF VSHATGLEHH HHHH
```

Figure 31. Ubiquitin-GyrA intein-His amino acid sequence

The lysate was filtered and then loaded onto a Ni_{2+} charged-chelating Sepharose (GE Healthcare) pre-equilibrated with 20 mM Tris pH 7.6, 500 mM NaCl, 20 mM imidazole, and eluted with a linear gradient from 20 mM to 500 mM imidazole. The protein was dialyzed in 20mM Tris-HCl pH 7.6.

Ub-SH production

Cleavage of Ub-SH was obtained by incubating the clean fusion protein in a buffer at pH 7.5 containing: Tris-HCl 20 mM, EDTA 1 mM, cysteamine 40 mM, and Tris(2-carboxyethyl) phosphine (TCEP) 3 mM for 48 h at RT. Ub-SH was purified by superdex-75 gel filtration column with 20 mM Tris and 150 mM NaCl buffer. Ub-SH amino acid sequence is illustrated in Figure 32.

1 0 2 0 3 0 4 0 5 0
MQIFVKTLTGK TITLEVEPSD TIENVKAKIQ DKEGIPPDQQ RLIFAGKQLE
6 0 7 0
DGRTLSDYNI QKESTLHLVL RLRGG(NH(CH$_2$)$_2$SH)

Figure 32. Ub-SH aminoacid sequence.

Ubiquitination reaction

Dha Formation

Tau353Dha was obtained as described above.[107] Briefly, 500µl of Tau353 (or AD-core353) was mixed with 20 mM DTT, and then heated at 37 °C for 4 minutes to remove all dimers by reducing intermolecular disulfide bonds. The sample was then loaded in a G-25M Sephadex PD-10 desalting column (GE Healthcare) and eluted with 900 µL of 20 mM NaPi pH8. Following that, was performed the reaction between Tau353 (or ADcore353) and 2, 5-dibromopentanoate (MDBP) with a molar ratio of 1:50 in 20 mM NaPi pH8. The solution was then incubated for 6h at 37°C and 450 rpm. Excess MDBP was removed by passing the reactions through G-25M Sephadex PD-10 desalting column and then conversion to Dha was verified via MALDI-TOF mass spectra.

Ubiquitination chemical reaction

To design the ubiquitinated product, Dha precursor, Ub-SH and DTT were left to react in a molar ratio 1:3:3 respectively, in water solution. The mixture was performed at 37 °C for 6h under shaking at 700 rpm (Tau353) and different combination for ADcore353. Excess DTT was removed via G-25M Sephadex PD-10 desalting column. The reaction was then purified via HPLC preparative.

Far-UV Circular Dichroism (CD) spectroscopy

CD measurements were carried out on a Jasco J-1500 spectropolarimeter equipped with a Peltier type temperature-controlled cell holder (Jasco, Easton, MD, USA). Far-UV spectra (190–260 nm) were recorded in 0.1 cm cuvettes, at 25 °C, with a scan rate of 50 nm/min, a bandwidth of 1 nm, and an integration time of 2 s. Five spectra accumulations were averaged for each sample and the spectrum of the buffer was considered as a blank and subtracted. Protein concentration was 6 μM. Data plots were generated with GraphPad Prism 9 (GraphPad Software Inc., La Jolla, CA, USA).

Thioflavin-T (ThT) aggregation assay

Solution of TauΔC was preliminarily filtered through a 100 KDa cut-off filter. The aggregation was performed in 20 mM sodium phosphate buffer at pH 7.4 and 50 mM NaCl (with 0.02% NaN3 and protease inhibitors w/o EDTA), incubating 10 μM protein with heparin in a molar ratio 1:1.

The kinetics of aggregation was monitored by measuring the fluorescence of thioflavin-T (10 μM) added to each sample in a 96-well dark plate (100 μL final volume for each well). Fluorescence measurements were performed using a TECAN Infinite M200 Pro microplate reader (Tecan Group AG, Männedorf, Switzerland) at 30 °C for ca.48 h with cycles of 30 s of shaking (250 rpm, orbital) and 10 min of rest throughout the incubation. The fluorescence intensity was measured every 11 min (excitation, 450 nm; emission, 480 nm; bottom read). Error bars of fluorescence data correspond to standard deviations of at least four independent experiments.

Transmission Electron Microscopy (TEM)

For TEM measurements, samples were prepared as described for the ThT assay in a final volume of 100 μL and incubated at 37 °C for 48 h in static condition. Subsequently, 30 μL of aggregates samples (5 μM) in mQ H2O were adsorbed onto 400 mesh holey film grids; after staining with 2% uranyl acetate (for 2 min), the sample was observed with a Tecnai G2 (FEI) transmission electron microscope operating at 100 kV. Images were captured with a Veleta (Olympus Soft Imaging System, Münster, Germany) digital camera using FEI TIA acquisition software (Version 4.0).

Mass Spectroscopy

Mass spectra were acquired on a Bruker Ultraflextreme MALDI-TOF/TOF instrument (Bruker Daltonics, Billerica, MA, USA) at the Centro Piattaforme Tecnologiche (CPT) of the University of Verona. Samples were acidified with TA30 solution (30% Acetonitrile (ACN), 0.1% trifluoroacetic acid (TFA) in water). The resulting solutions were mixed 1:1 (v/v) with the matrix HCCA (α-cyano-4-hydroxycinnamic acid) and 1 μL of the sample/matrix solution was spotted in triplicate onto a Ground steel MALDI target plate (Bruker Daltonics) and dried at room temperature.

3.2 Published article: Tau Nanoparticle

Ultrasmall gold nanoparticles form multi-molecular assemblies with the unstructured protein Tau and inhibit disease-related conformational transitions.

Giovanna Viola,[a,*] Carlo Giorgio Barracchia,[a,*] Roberto Tira,[a] Francesca Parolini,[a] Giulia Leo,[a] Massimo Bellanda,[b] Francesca Munari,[a] Stefano Capaldi,[a] Mariapina D'Onofrio [a] and Michael Assfalg[a,**]

a Department of Biotechnology, University of Verona, 37134 Verona, Italy
b Department of Chemistry, University of Padova, 35131 Padova, Italy

* Contributed equally to this work
** Corresponding author: Michael Assfalg

Department of Biotechnology
University of Verona
Strada Le Grazie 15
37134 Verona, Italy
Email: michael.assfalg@univr.it

Keywords: intrinsically disordered proteins; NMR spectroscopy; protein aggregation ; protein-nanoparticle interaction ; ultrasmall nanoparticles

ABSTRACT

Understanding the interactions between nanoparticles (NPs) and proteins is crucial for the successful application of NPs in biological contexts. Protein adsorption is dependent on particle size, and protein binding to ultrasmall (1−3 nm) NPs is considered to be generally weak. However, most studies have involved structured biomacromolecules, while the interactions of ultrasmall NPs with intrinsically disordered proteins (IDPs) have remained elusive. IDPs are abundant in eukaryotes and found to associate with NPs intracellularly. As a model system, we focused on ultrasmall gold nanoparticles (usGNPs) and Tau, a cytosolic IDP associated with Alzheimer's disease. Using site-resolved NMR, steady-state fluorescence, calorimetry, and circular dichroism, we reveal that Tau and usGNPs form stable multimolecular assemblies, representing a new type of nano−bio interaction. Specifically, the observed interaction hot spots explain the influence of usGNPs on Tau conformational transitions, with implications for the intracellular targeting of aberrant IDP aggregation.

Graphical abstract

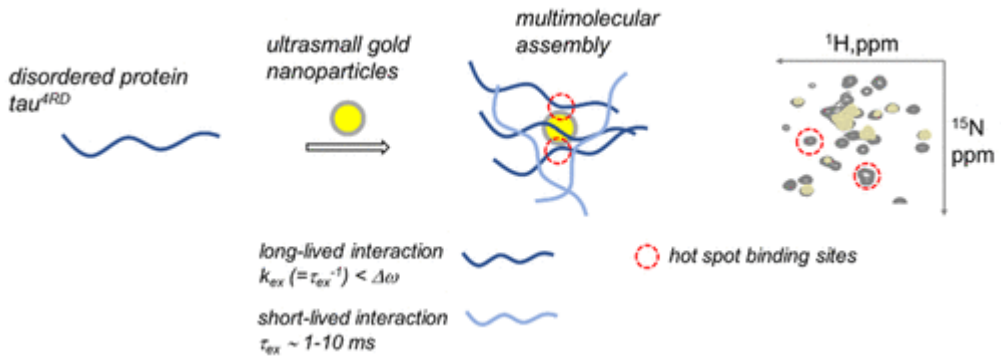

The successful development of nanoparticle (NP)-based tools for use in biological contexts requires a thorough understanding of the nano−bio interactions.[1] Despite the inherent complexity of interfaces, significant progress has been made in the description of the physicochemical interactions between nanomaterials and biological components.[2] A major result is the observation that most NPs readily interact with biomolecules that adsorb on their surface, forming a biomolecular corona which influences their biodistribution and bio-activity.[3,4]

Among NPs, ultrasmall NPs (usNPs), usually defined as particles with core size in the range 1−3 nm, present attractive features for biomedical purposes, including efficient renal clearance, limited accumulation in the liver, in vivo tumour accumulation, enhanced cell and nuclear penetration, and capability to cross the blood−brain barrier.[5−8] Ultrasmall gold NPs (usGNPs) have the advantage of controllable synthesis, ease of surface modification, emergent optical properties, and low toxicity.[9,10] Therefore, usGNPs show great promise for applications in biosensing, cellular imaging, drug delivery, and disease therapy.[11,12]

A systematic investigation of protein adsorption to citrate- stabilized GNPs upon exposure to biological media provided clear evidence that the characteristics of the protein corona are particle-size-dependent.[13] Thus, large NPs become coated by a thick, multilayered corona, while medium-sized NPs display a near-single dense protein corona layer, and small NPs exhibit an incomplete corona. In the ultrasmall scale, the nature of protein−NP interactions differs from the case of larger NPs, being characterized by transient particle−biomolecule associations and by the absence of hard coatings.[14,15] Indeed, usNPs are of comparable size or smaller than common proteins and may display macromolecule-like or even drug-like features. The formed supramolecular species can be defined as usNP/protein complexes.[16]

A significant fraction of proteins interacting with NPs in a living system is constituted by macromolecules of defined tertiary structure, including albumin, immunoglobulins, and others that are abundant in peripheral biofluids.[17,18] However, a recent study revealed that NP-associated intracellular proteomes are enriched in intrinsically disordered, RNA- processing proteins, suggesting that conformational disorder facilitates the binding of proteins to NPs.[19] In addition to RNA-binding proteins, biologically active intrinsically disordered proteins (IDPs) and proteins

containing disordered regions (IDRs) are abundant in eukaryotic proteomes.[20] Besides being involved in key biological functions, an increasing number of IDPs are found to undergo aberrant aggregation, under defined conditions, and are associated with irreversible neurodegenerative diseases.[21] In this context, the binding to NPs could provide the means to redirect aggregation pathways and mitigate the formation of neurotoxic assemblies, opening the way to new therapeutic strategies.[22,23] Classical NPs offer large surface areas for accommodating disordered polypeptides, whose conformational adaptability allows establishing a large number of noncovalent interactions. The adsorption of amyloidogenic proteins and peptides onto NPs and the consequences on protein fibrillation have been extensively explored.[22,24] At the macroscopic level, NPs were found to either accelerate or retard protein fibril formation, depending on surface properties.[23,25] In the ultrasmall regime, the interactions of IDPs with NPs remain poorly characterized.[26−28]

Herein, we focus on the interaction of usGNPs with a prototypical IDP: the aggregation-prone, four-repeat domain of Tau (Tau^{4RD}, Supporting Information Figure S1A). Tau is a cytosolic IDP that supports neuronal cell function and that, in pathological conditions, transitions from a soluble monomeric state to oligomers and fibrils (hallmark aggregates in Alzheimer's disease, AD).[29,30] A high number of basic amino acid residues mediate the interaction of Tau^{4RD} with biological and exogeneous anionic surfaces (microtubules, lipid mem- branes, NPs). To characterize the mode of interaction between usGNPs and Tau^{4RD}, we applied gel electrophoresis, steady- state fluorescence spectroscopy, isothermal titration calorimetry, circular dichroism spectroscopy, and site-resolved solution NMR. We further explored the influence of usGNPs on disease-related protein conformational transitions.

We prepared dihydrolipoic acid (DHLA)-capped usGNPs (ligand structure is displayed in Figure S1B) with a previously described one-pot synthetic approach.[31] DHLA-capped usGNPs (hereafter referred to as usGNPs for simplicity) exhibit limited ligand desorption due to the strong Au−S bonds and form stable colloids in aqueous solution due to electrostatic repulsion between carboxylates.[31,32] The colloidal solution of usGNPs appeared pale brown and displayed bright red luminescence on exposure to UV light (Figure S2A). The particles were characterized by UV−visible absorption spectroscopy, transmission electron microscopy (TEM),

dynamic light scattering (DLS), and ^{1}H NMR spectroscopy (Figure S2 B−H). The mean core size was ca. 1.9 nm, and the ζ- potential value in neutral solution was $\zeta = -36 \pm 6$ mV.

To investigate protein binding to usGNPs, we first applied agarose gel electrophoresis. UsGNPs are expected to migrate toward the positive electrode. Conversely, Tau^{4RD} is a lysine- rich, highly basic polypeptide that displays positive ζ potential ($\zeta = 22 \pm 1$ mV, pI = 9.7) and is predicted to migrate toward the cathode. In this work, we used a cysteine-free protein variant (hereafter, Tau^{4RD}) to avoid uncontrolled formation of Au−S and S−S bonds. The observed progressive decrease of usGNP electrophoretic mobility toward the anode on increasing protein concentration (Figure 1A) likely originated from both an increased size and a surface charge variation determined by the association of usGNPs with Tau^{4RD}.

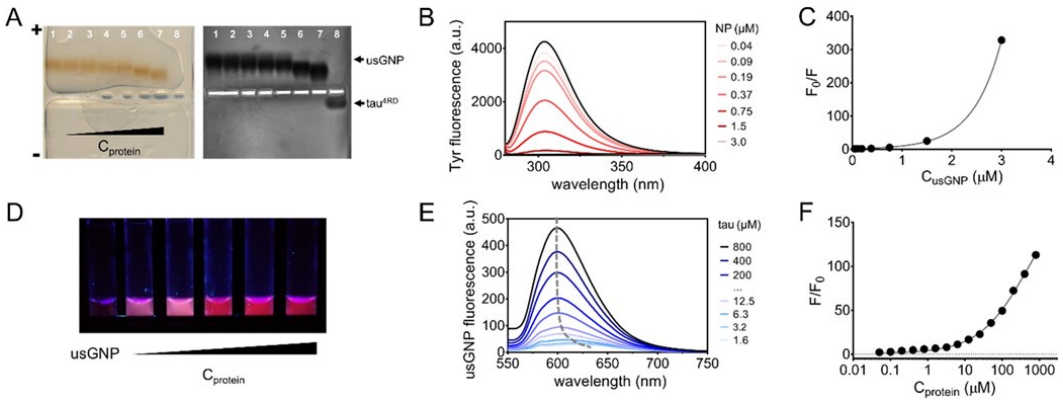

Figure 1. Gel electrophoresis and photophysical measurements. (A) Agarose native gel electrophoresis: left, unstained; right, Coomassie staining. Lanes 1−7 were loaded with 6.5 μM usGNPs; lanes 2−8 contained Tau^{4RD} at concentrations 3.25, 6.5, 13, 19.5, 43.5, and 65 μM; all components were dissolved in 0.5% TBE, pH 9 (1% agarose, 50 V, 40 min). (B) Tyrosine fluorescence emission spectra (λ_{ex} = 270 nm) measured on 6 μM Tau^{4RD} in the presence of usGNPs at varying concentration. The spectrum of the free protein is shown in black (λ_{max} = 304 nm). (C) Relative Tyr fluorescence intensity as a function of usGNP concentration (Stern−Volmer plot). The solid line corresponds to an exponential function fit. (D) Colloidal solutions of 0.5 μM usGNPs in the presence of varying concentration of protein, visualized under UV lamp. (E) Fluorescence emission spectra (λ_{ex} = 530 nm) of 0.25 μM usGNP in the presence of Tau^{4RD} at varying concentration. The dashed line indicates the shift of the peak maximum. (F) Relative usGNP fluorescence intensity as a function of protein concentration (logarithmic scale). The solid line corresponds to the best-fit curve (Hill function)

We further examined the effect of the interaction on the photophysical properties of protein and usGNPs. The intrinsic fluorescence of the protein, due to the single fluorescent residue Tyr310, was effectively quenched on addition of usGNPs (Figure 1B), suggesting that the repeat region R3 closely approached the particle

surface. The nonlinear dependence of the relative fluorescence intensity, F_0/F, on usGNPs concentration (Figure 1C) indicates that the quenching mechanism was not of a single type (dynamic or static). Previous work established that fluorescence quenching of organic dyes by usGNPs lacking a surface plasmon band was dominated by nanometal surface energy transfer.[33]

As noted earlier, the photoluminescence of usGNPs is generally affected by protein binding.[34] Here, we observed a progressive enhancement of intrinsic luminescence on increasing the concentration of Tau^{4RD} (Figure 1D), with up to 20-fold higher intensity for the highest concentration of Tau^{4RD} considered, and a blue shift of the emission band maximum (up to 40 nm) (Figure 1E). The latter observation indicates that adsorbed protein molecules reduced the polarity of the local dielectric environment at the particle surface and suggests that Tau^{4RD} has a greater capability to shield the usGNP surface from the solvent, compared to compact globular proteins.[34] The fluorescence intensity did not show saturation behaviour in the investigated concentration range (Figure 1F); therefore, an accurate quantitative analysis of the experimental curve was not possible. Nonetheless, a tentative fit of the data with a Hill model yielded a Hill coefficient $n = 0.66$, suggestive of anti-cooperative binding.

To gain insight into the mechanism of association, we performed isothermal titration calorimetry (ITC) experiments. The calorimetric response obtained by titrating Tau^{4RD} into a solution of usGNPs appeared nonmonotonic, with a net heat release in the first half and endothermic behaviour in the second half of the titration (Figures 2A,S3). Interestingly, the titration of another IDP, α-synuclein, into usGNPs generated a different calorimetric profile, lacking net endothermic signals (Figure S4) but also reflecting the occurrence of multiple processes during titration. The calorimetric curves for both protein systems were ionic-strength-dependent, displaying reduced heat exchange at high salt concentration (Figures 2B,S3, and S4), thus pointing to a contribution of electrostatic interactions to the underlying phenomena. The effect was particularly evident in the second part of the process: at high salt concentration, the positive hump in the calorimetric profile of Tau^{4RD} and the negative shoulder in that of α-synuclein were attenuated. In the case of Tau^{4RD} in salt-containing solutions, the early titration heat signals departed from the general

trend of the following titration points (note that solution buffers for injectant and analyte were identical) (Figures 2B, S3). This behavior was not observed for α-synuclein (Figure S4), indicating that the effect was protein-specific. Calorimetric data for Tau^{4RD} were analyzed with a two-sets-of-sites binding model to estimate thermodynamic quantities (Tables 1, S1). In the absence of NaCl, binding was strong for both sets, driven by enthalpy in the first and by entropy in the second event. The number of involved binding sites was larger for the second set than for the first set. The energetic terms and affinity constants were reduced in the presence of 100 mM NaCl. The favourable enthalpic term likely resulted from strong electrostatic attraction between the negatively charged usGNPs and the polycationic protein, while the favorable entropic component of the second event may reflect, among various possible contributing factors, the conformational disorder of bound protein molecules. Thus, the proposed model identified two main modes of association of Tau^{4RD} with usNPs: the one characterized by greater affinity may correspond to unhindered docking of protein molecules to free surface areas on usNPs, while the lower affinity mode may correspond to the binding to already coated usNPs. The occurrence of two distinct types of interaction recalls the concept of hard and soft corona described for larger NPs. However, differently from a typical hard corona where folded proteins form a densely packed and sterically defined adlayer, Tau molecules bound to usGNPs are probably best described as a "fuzzy" assembly, where fuzziness refers to the conformational heterogeneity of bound-state ensembles of IDPs observed in many protein−protein complexes.[35] On binding to usNPs, IDPs will engage small contact regions, by contrast larger NPs may accommodate long polypeptide stretches and multiple regions. Thus, IDPs interacting with larger NPs can form fuzzy complexes[36] as well as more static and compact protein coronas.[37]

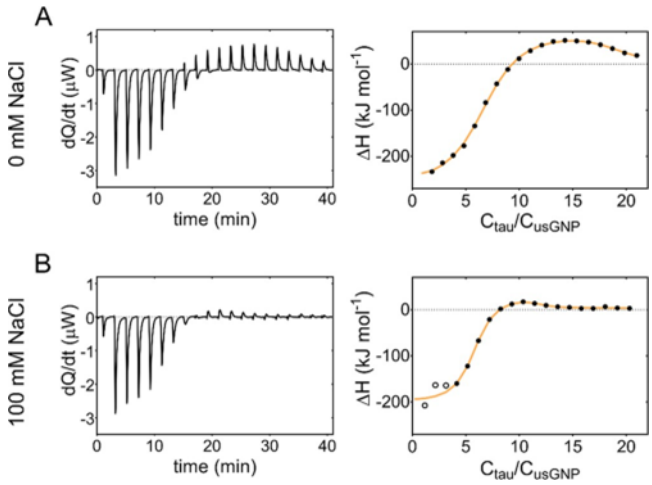

Figure 2. Energetics of the interaction between Tau4RD and usGNPs. Isothermal titration calorimetry data obtained on titrating Tau4RD into usGNPs, in the presence of 0 mM (A) and 100 mM (B) NaCl (see Figure S3 for additional NaCl concentration points). Left panels display corrected heat transfer rates; right panels display integrated heat plots. Orange lines are best-fit curves based on a two-sets-of-sites binding model; data displayed as empty circles were excluded from fitting.

Table 1. Thermodynamic Parameters for the Binding of Tau^{4RD} to usGNPs[a]

NaCl	*b*	K_a (M^{-1})	ΔG (kJ mol^{-1})	ΔH (kJ mol^{-1})	$-T\Delta S$ (kJ mol^{-1})	*n*
0 mM	I	(6.1 ± 0.9) × 10^7	−44.5 ± 0.4	−268 ± 5	224 ± 5	5.8 ± 0.1
	I	(2.7 ± 0.3) × 10^6	−36.8 ± 0.3	74 ± 5	−110 ± 5	12.5 ± 0.1
100 mM	I	(8.1 ± 1.2) × 10^6	−39.5 ± 0.4	−216 ± 20	177 ± 20	5.5 ± 0.8
	I	(3.1 ± 0.5) × 10^5	−31.4 ± 0.4	65 ± 10	−96 ± 10	6 ± 3

Given errors are from data fitting. [b]I, first binding event; II, second binding event.

The disordered character of Tau^{4RD} entails strong conformational plasticity and adaptability to binding surfaces.[23] To obtain insight into protein structural changes resulting from adsorption to usGNPs, we performed circular dichroism (CD) measurements. The far-UV CD spectrum of Tau^{4RD} free in solution featured a deep ellipticity minimum centered at 198 nm (Figure S5A), consistent with a prevalently unstructured state. The addition of usGNPs elicited the progressive reduction of signal ellipticity and a shift of the peak minimum toward longer wavelengths. We interpret these spectral changes as being due to a binding-induced redistribution of conformational states and formation of a heterogeneous ensemble of bound molecules with mixed-type local secondary structure elements.[38,39] The peak wavelength change as a function of usGNP concentration was found to follow an apparent Langmuir-type dependence (Figure S5B), indicating saturable binding.

To identify the NP-binding site(s) on Tau^{4RD}, we performed site-resolved NMR spectroscopy experiments. Previous works demonstrated the power of NMR to elucidate the binding modes and dynamics of proteins, both folded and unstructured, on NP surfaces with single residue resolution.[36,40–47] The $^{1}H–^{15}N$ HSQC spectrum of [^{15}N]Tau^{4RD} displays HN correlation signals for virtually all non-proline amino acid residues (Figures 3A,S6). After addition of small amounts of usGNPs, the position of individual peaks was minimally perturbed (for P:usGNP = 0.02, $\Delta\delta_{HN}$ were <0.015 ppm); by contrast signal intensities were significantly reduced (Figures 3A,B, S6). In the initial titration steps, no new signals appeared; however, at higher usGNP concentration, a number of broad, low-intensity peaks became visible at different positions from those of the unbound protein (Figure 3A). This behavior, also in consideration of the binding strength determined by ITC, is consistent with the partitioning of protein molecules to a particle-bound state in a slow− intermediate exchange regime. The absence of sharp bound- state resonances can be attributed to multiple molecules interacting with each particle, forming assemblies with reduced rotational diffusion, and to structural disorder and dynamics of the bound-state conformational ensemble contributing to peak broadening. The residue-by-residue signal intensity attenuation was not uniform along the peptide sequence, with a similar profile at low (Figure 3B) and high ionic strength (Figure S7), indicating preferential involvement of discrete regions in binding to usGNPs. For example, the strong attenuations in segment 276−283, encompassing part of one hexapeptide motif (PHF6*, 275−280), suggest that this region represents a preferential anchoring site for usGNPs. Indeed, two adjacent lysine residues (Lys280, Lys281), a unique occurrence in the entire polypeptide, may promote the association via strong electrostatic attraction. Interestingly, intensity perturbations were also strong (>80%, Figure 3B) in the stretch 309−311, which belongs to the second hexapeptide motif (PHF6, 306- 311) and terminates with Lys311, hinting at a central role of these motifs in the protein's slow exchange dynamics.

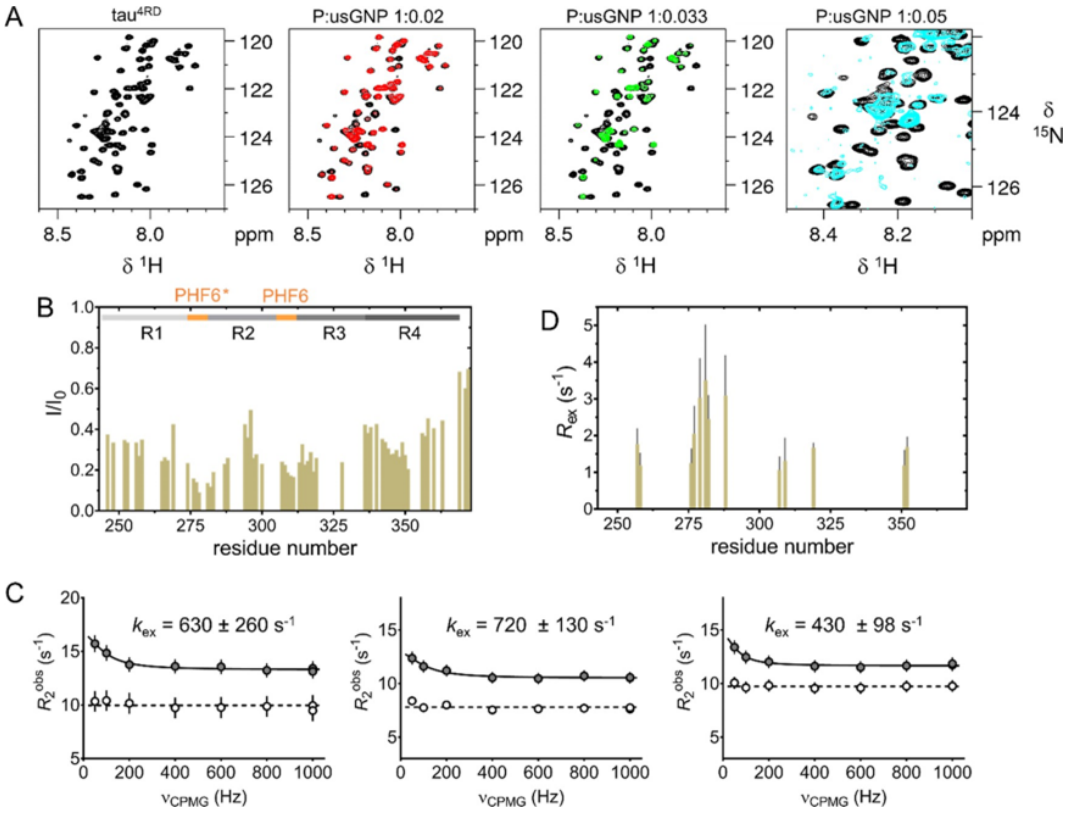

Figure 3. Mapping of contact sites and conformational dynamics. (A) Selected portions of HN-HSQC spectra (600 MHz) of 50 μM [^{15}N] Tau^{4RD} (black) in the absence (top left) or presence of usGNPs (colored maps overlaid on black) at the reported molar ratios. Red and green maps areshown in scale with black spectrum, the cyan map is displayed with increased intensity for better visualization of the peak position changes; the rightmost panel displays an enlarged view for better appreciation of peak details; and protein (P):usGNP molar ratios are indicated on top. (B)Residue-specific HSQC-peak intensity versus residue number. Peak intensities were measured on Tau^{4RD} in the absence (I_0) or presence (I) of usGNPs at a molar ratio P:usGNPs = 0.02; only isolated peaks were included in the analysis; the protein domain organization is schematized with bars of different gray shading for the four repeat motifs (R1−R4); and the hexapeptide motifs are indicated in orange. (C) Representative ^{15}N- CPMG relaxation dispersion curves at 700 MHz spectrometer frequency observed for 200 μM [^{15}N]Tau^{4RD} in the absence (empty circles) or presence (filled circles) of 2 μM usGNPs (from left to right: Lys281, Leu282, Gln288) and 10 mM NaCl. Uncertainties were estimated fromduplicate measurements; solid lines are the best-fit curves obtained by fitting the relaxation data to a two-state exchange model, the fitted exchangerate constants are reported; and dashed lines indicate the average R_2^{obs} for no exchange. (D) Exchange contributions to relaxation rates obtained from relaxation dispersion experiments on samples containing Tau^{4RD} and usGNPs. Gray bars are errors propagated from the uncertainties of fitted parameters.

To gain additional insight into the dynamics of Tau4RD in the presence of usGNPs, we carried out ^{15}N-spin Carr−Purcell−Meiboom−Gill relaxation dispersion (CPMG-RD) experiments, which are sensitive to exchange processes in the 0.3− 10 ms time window.[48] Chemical exchange signal broadening, resulting from an enhanced relaxation rate (line width $\lambda = 2R_2^{obs}$, where $R_2^{obs} = R_2^0 + R_{ex}$), is modulated by the frequency of the CPMG pulse train (ν_{CPMG}) applied during the T_{CPMG} relaxation delay of the NMR experiment. The analysis of R_2^{obs} versus ν_{CPMG} dispersion

curves provides information on the underlying dynamic process. The protein alone displayed virtually no relaxation dispersion, by contrast small but clear-cut RD effects for some residues were apparent in the presence of usGNPs (Figure 3C, D). Dispersion curves were analyzed with two-state exchange models, and all data were found to best fit to an exchange process in the fast-limit regime. This process likely corresponds to the weak binding of protein molecules to already coated NPs since the experiment was performed with protein in large excess. Observing the effects of the intermediate dynamics that characterizes the protein−NP interactions would require comparable concentrations of protein and NPs corresponding to conditions unsuitable for relaxation dispersion measurements. Relaxation dispersion originates from changes in the chemical environment at the observed site, and, interestingly, the largest chemical exchange contribution to transverse relaxation, R_{ex}, was observed in the region 277−282 and for residue 288 (Figure 3D). We further note that the effective relaxation rate values at high CPMG field strength ($\nu_{CPMG} \rightarrow \infty$), R_2^0 , corresponding to relaxation in the absence of exchange, were invariably larger for Tau4RD in the presence of usGNPs than for the protein alone. The residue-by-residue variation of ΔR_2 (with/without usGNP, Figure S8), measured at a CPMG field of 595 Hz to suppress exchange-induced line broadening, reports on contributions to $R2$ from the NP-bound state.49,50 The patterned profile again indicates the prevalent involvement of the PHF6 regions in the assembly with usGNPs.

Following the observation that aggregation-prone hexapeptide motif regions were key mediators of binding to usGNPs in both slower and faster exchange regimes, we set to explore the influence of usGNPs on protein aggregation. The aggregation kinetics of Tau4RD was followed by monitoring the time dependent fluorescence signal of thioflavin-T (ThT). The kinetic profile was sigmoidal-shaped and consistent with a macroscopic nucleation−growth mechanism (Figure 4A). The presence of low amounts of usGNPs (P:NP < 0.005) showed modest influence on the kinetics of the process, as evident from the little changes in transition midpoints compared to the particle-free sample. However, the addition of usGNPs at a P:NP ratio of 1:0.03 resulted in a significantly delayed aggregation (midpoint transition time constant, $t0.5$ = 30.1 ± 0.4 h versus 20.7 ± 0.1 h in the absence of NPs) and almost unchanged fibril elongation rate (elongation time constant, τ =1.6 ± 0.3 h

versus 1.4 ± 0.1 h). The fluorescence intensity at plateau decreased progressively on increasing the concentration of usGNPs until complete quenching in the case of a P:NP molar ratio of 1:0.1 (Figure 4A), possibly indicating the formation of smaller amounts of fibrils.

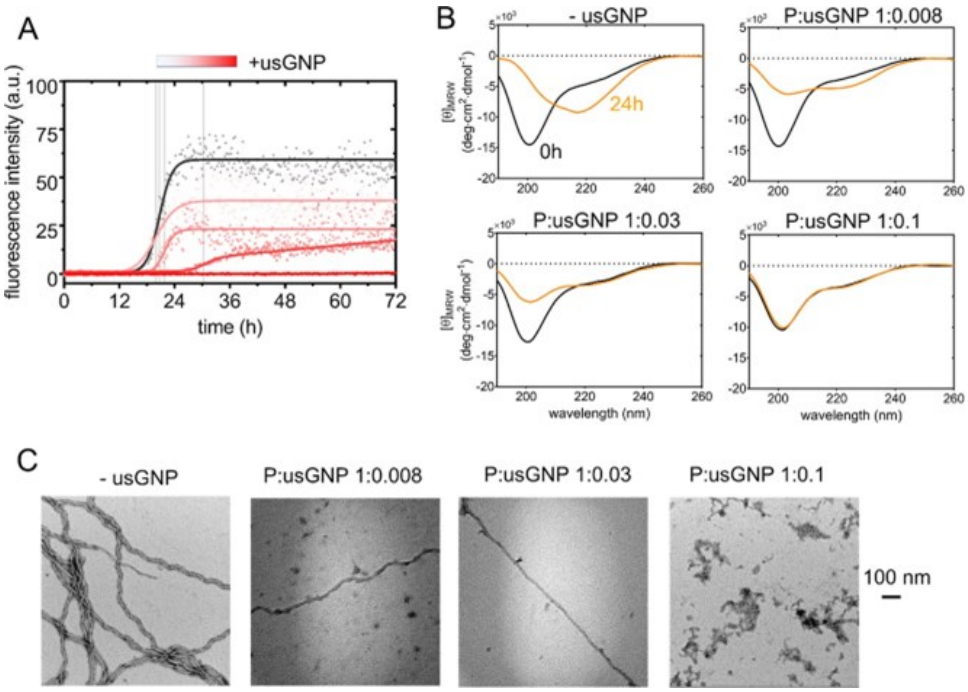

Figure 4. Protein conformational transitions and aggregation. (A) Aggregation kinetics monitored by ThT fluorescence. Measurements were performed on Tau^{4RD} in the absence (gray dots) or presence (light-to-dark red dots) of usGNPs (P:usGNP molar ratios 1:0, 1:0.002, 1:0.004, 1:0.03, 1:0.1); solid lines correspond to the best-fit curves determined using an empirical sigmoid function; data represent the mean of five replicatemeasurements; and vertical gray lines indicate transition midpoints. (B) Far-UV CD spectra acquired on 6 μM Tau^{4RD} after 0 h (black) and 24 h(brown) incubation, in the absence or presence of usGNPs at the indicated molar ratios. (C) Representative TEM images of Tau^{4RD} samples after48 h incubation in aggregating conditions, in the absence (left panel) or presence (remaining panels) of usGNPs (see Figure S9 for additional images). Scale bar is 100 nm.

The protein conformational transitions taking place during aggregation were further monitored by far-UV CD (Figure 4B). The spectrum of Tau4RD in the absence of usGNPs revealed a major change in secondary structure content after 24 h of incubation: the ellipticity minimum shifted to larger wavelengths (217 nm), consistent with the formation of β- structure, and a shoulder appeared around 207 nm, possibly corresponding to mixed-type secondary structures.39 In the presence of usGNPs at a P:NP ratio of 1:0.1, no conformational conversion was observed after the incubation period, while experiments conducted with lower amounts of particles revealed an intermediate situation with a smaller signal of the disordered protein and slightly

increased ellipticity around ~220 nm (Figure 4B). Thus, the CD data were consistent with the concentration-dependent trend observed in the ThT fluorescence assay. TEM analysis of samples incubated for 48 h showed that filamentous aggregates could form in the presence of low−intermediate concentrations of usGNPs but not when particles were added at a P:NP ratio of 1:0.1 (Figures 4C, S9). By coarse visual inspection of the micrographs, we found that the amount of fibrillar aggregates decreased with increasing usGNP concentration, confirming the inhibitory effect of usGNPs. The inhibitory action of usGNPs was retained at higher (near-physiological) ionic strength (Figure S7).

The possibility to use usNPs for modulating the conformational states of IDPs intracellularly stimulated us to verify two fundamental requirements for usGNPs: (i) their biocompatibility and (ii) their ability to get internalized into live neuronal cell models. To assess the biocompatibility, we evaluated the viability of two different human cell lines, the neuroglioma derived H4swe and the nontumoral human embryonic kidney (HEK-293), after 72 h treatment with various concentrations of usGNPs. We observed no significant decrease in cell viability for both lines (Figure S10A), demonstrating that usGNP does not display acute cytotoxicity. Next, we monitored the cellular uptake and the internalization efficiency of usGNPs in H4swe cells by confocal microscopy. Since autofluorescence of usGNPs was insufficient to provide a clear signal at the used concentrations, we resorted to labelling the particles with cysteamine-FITC. Small granular aggregates were clearly visible in the cytoplasm of cells treated for 48 h with labelled nanoparticles (Figure S10B). Overall, these results indicate that usGNPs are internalized by the cells with little or no toxicity in the short term, making them suitable for in-cell applications.

The observation that usGNPs concentrated intracellularly in discrete sites stimulated us to verify whether they localized in stress granules (SGs). These cytoplasmic membraneless organelles contain several RNA-binding proteins which are enriched for intrinsically disordered regions (IDRs) and thus could represent targets for usGNPs. Colocalization experiments showed that upon simple incubation, usGNPs did not apparently partition into SGs induced by arsenite treatment nor did they trigger SG formation (Figure S11). However, if cell membrane permeabilization was applied to facilitate particle uptake after SG induction, usGNPs distributed

throughout the cell interior and partitioned into SGs (Figure S12), suggesting that usGNPs may interact with IDRs/IDPs in these organelles.

In conclusion, usNPs are attracting considerable interest for potential applications in the life sciences. The possibility to design usNPs that target biologically active macromolecules and modulate their function requires in-depth characterization of their interactions with biomolecules. It has been observed that particle size strongly influences NP−protein interactions and that protein binding to usNPs is generally weak, at least in the case of globular folded proteins. However, the nature of the interactions of usNPs with disordered proteins (IDPs) has been poorly investigated. In our study, we aimed at a detailed, sub molecular level characterization of a prototypical system consisting of usGNPs and the disordered Tau protein. We found that usGNPs engage the protein Tau4RD in the formation of stable (Ka = ∼ 10^7 M^{-1}) multimolecular assemblies (Figure 5), in contrast to the notion of weak protein association to usNPs. Additional short-lived (τ_{ex} = 1−10 ms) interactions were also detected, likely corresponding to binding events on the exterior of usGNP/Tau complexes. The formed assemblies are best described as “fuzzy” complexes, with reference to bound-state conformational heterogeneity. Different from assemblies with larger NPs, the interaction of IDPs with usNPs cannot involve long polypeptide stretches and may not result in the formation of a sterically defined and compact protein corona. This type of assembly can affect biological behaviour: specifically, by targeting disease-related protein aggregation sites of Tau, usGNPs were found to act as aggregation inhibitors. Given the observation that usGNPs are not cytotoxic and are taken up by neuronal cells, they could find application for aggregation studies in both in vitro and cellular models of neurodegeneration.

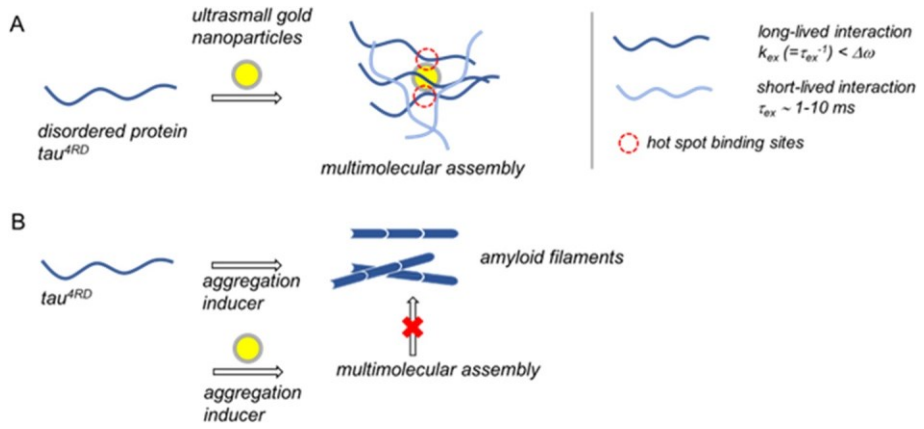

Figure 5. (A) Schematic representation of the multimolecular assembly formed by ultrasmall gold NPs and a prototypical intrinsically disordered protein, characterized by two distinct exchange regimes. (B) Schematic representation of the influence of usGNPs on disease-related amyloid deposition of Tau^{4RD}

Author Contributions

G.V. and C.G.B contributed equally to this work.

Conflict of interest

The authors declare no competing financial interest.

■ ACKNOWLEDGMENTS

We thank Vincenzo Amendola for critical reading of an early version of the manuscript. The Italian Ministry of University and Research (MIUR) is acknowledged for support via the grant "Fondo per il finanziamento delle attività base di ricerca (FFABR)-MIUR 2018" (to M.A.) and through the program "Dipartimenti di Eccellenza 2018−2022". This work benefited from access to CERM/CIRMMP, an Instruct-ERIC center. Financial support was provided by Instruct-ERIC (PID 12742). We thank Dr. Fabio Calogiuri for expert technical assistance with NMR measurements. Centro Piattaforme Tecnologiche of the University of Verona is acknowledged for providing access to the Microscopy Facility and ITC Instruments. The University of Padova is acknowledged for providing access to the electron microscope (DiBio Imaging Facility) and to the NMR spectrometer (Department of Chemistry). C.G.B. received a fellowship grant (Assegno di Ricerca) from the Department of Biotechnology

REFERENCES

(1) Mahmoudi, M.; Lynch, I.; Ejtehadi, M. R.; Monopoli, M. P.;Bombelli, F. B.; Laurent, S. Protein−Nanoparticle Interactions:Opportunities and Challenges. *Chem. Rev.* 2011, *111*, 5610−5637.

(2) Nel, A. E.; Madler, L.; Velegol, D.; Xia, T.; Hoek, E. M. V.;Somasundaran, P.; Klaessig, F.; Castranova, V.; Thompson, M.Understanding Biophysicochemical Interactions at the Nano−Bio Interface. *Nat. Mater.* 2009, *8*, 543−557.

(3) Cedervall, T.; Lynch, I.; Lindman, S.; Berggard, T.; Thulin, E.;Nilsson, H.; Dawson, K. A.; Linse, S. Understanding the Nanoparticle-Protein Corona Using Methods to Quantify Exchange Rates and Affinities of Proteins for Nanoparticles. *Proc. Natl. Acad. Sci. U. S.A.* 2007, *104*, 2050−2055.

(4) Monopoli, M. P.; Aberg, C.; Salvati, A.; Dawson, K. A.Biomolecular Coronas Provide the Biological Identity of Nanosized Materials. *Nat. Nanotechnol.* 2012, *7*, 779−786.

(5) Liu, J.; Yu, M.; Zhou, C.; Yang, S.; Ning, X.; Zheng, J. Passive Tumor Targeting of Renal-Clearable Luminescent Gold Nanoparticles:Long Tumor Retention and Fast Normal Tissue Clearance. *J. Am. Chem. Soc.* 2013, *135*, 4978−4981.

(6) Loynachan, C. N.; Soleimany, A. P.; Dudani, J. S.; Lin, Y.; Najer,A.; Bekdemir, A.; Chen, Q.; Bhatia, S. N.; Stevens, M. M. Renal Clearable Catalytic Gold Nanoclusters for in Vivo Disease Monitoring. *Nat. Nanotechnol.* 2019, *14*, 883−890.

(7) Sokolova, V.; Nzou, G.; van der Meer, S. B.; Ruks, T.; Heggen, M.; Loza, K.; Hagemann, N.; Murke, F.; Giebel, B.; Hermann, D. M.; et al. Ultrasmall Gold Nanoparticles (2 Nm) Can Penetrate and Enter Cell Nuclei in an in Vitro 3D Brain Spheroid Model. *Acta Biomaterialia* 2020, *111*, 349−362.

(8) Sokolova, V.; Mekky, G.; van der Meer, S. B.; Seeds, M. C.;Atala, A. J.; Epple, M. Transport of Ultrasmall Gold Nanoparticles (2Nm) across the Blood−Brain Barrier in a Six-Cell Brain Spheroid Model. *Sci. Rep* 2020, *10*, 18033.

(9) Kim, B. H.; Hackett, M. J.; Park, J.; Hyeon, T. Synthesis,Characterization, and Application of Ultrasmall Nanoparticles. *Chem.Mater.* 2014, *26*, 59−71.

(10) Nienhaus, K.; Wang, H.; Nienhaus, G. U. Nanoparticles for Biomedical Applications: Exploring and Exploiting Molecular Interactions at the Nano-Bio Interface. *Materials Today Advances* 2020, *5*, 100036.

(11) Zarschler, K.; Rocks, L.; Licciardello, N.; Boselli, L.; Polo, E.; Garcia, K. P.; De Cola, L.; Stephan, H.; Dawson, K. A. Ultrasmall Inorganic Nanoparticles: State-of-the-Art and

Perspectives for Biomedical Applications. *Nanomedicine: Nanotechnology, Biology and Medicine* 2016, *12*, 1663−1701.
(12) Shang, L.; Dong, S.; Nienhaus, G. U. Ultra-Small Fluorescent Metal Nanoclusters: Synthesis and Biological Applications. *Nano Today* 2011, *6*, 401−418.
(13) Piella, J.; Bastús, N. G.; Puntes, V. Size-Dependent Protein−Nanoparticle Interactions in Citrate-Stabilized Gold Nanoparticles: The Emergence of the Protein Corona. *Bioconjugate Chem.* 2017, *28*, 88−97.
(14) Boselli, L.; Polo, E.; Castagnola, V.; Dawson, K. A. Regimes of Biomolecular Ultrasmall Nanoparticle Interactions. *Angew. Chem., Int.Ed.* 2017, *56*, 4215−4218.
(15) Lira, A. L.; Ferreira, R. S.; Torquato, R. J. S.; Zhao, H.; Oliva, M. L. V.; Hassan, S. A.; Schuck, P.; Sousa, A. A. Binding Kinetics of Ultrasmall Gold Nanoparticles with Proteins. *Nanoscale* 2018, *10*, 3235−3244.
(16) Sousa, A. A.; Schuck, P.; Hassan, S. A. Biomolecular Interactions of Ultrasmall Metallic Nanoparticles and Nanoclusters. *Nanoscale Adv.* 2021, *3*, 2995−3027.
(17) Cedervall, T.; Lynch, I.; Foy, M.; Berggard, T.; Donnelly, S. C.; Cagney, G.; Linse, S.; Dawson, K. A. Detailed Identification of Plasma Proteins Adsorbed on Copolymer Nanoparticles. *Angew. Chem., Int. Ed.* 2007, *46*, 5754−5756.
(18) Tenzer, S.; Docter, D.; Rosfa, S.; Wlodarski, A.; Kuharev, J.; Rekik, A.; Knauer, S. K.; Bantz, C.; Nawroth, T.; Bier, C.; et al. Nanoparticle Size Is a Critical Physicochemical Determinant of the Human Blood Plasma Corona: A Comprehensive Quantitative Proteomic Analysis. *ACS Nano* 2011, *5*, 7155−7167.
(19) Romashchenko, A. V.; Kan, T.-W.; Petrovski, D. V.; Gerlinskaya, L. A.; Moshkin, M. P.; Moshkin, Y. M. Nanoparticles Associate with Intrinsically Disordered RNA-Binding Proteins. *ACS Nano* 2017, *11*, 1328−1339.
(20) Uversky, V. N. Unusual Biophysics of Intrinsically Disordered Proteins. *Biochimica et Biophysica Acta (BBA) - Proteins and Proteomics* 2013, *1834*, 932−951.
(21) Chiti, F.; Dobson, C. M. Protein Misfolding, Amyloid Formation, and Human Disease: A Summary of Progress Over the Last Decade. *Annu. Rev. Biochem.* 2017, *86*, 27−68.
(22) Mahmoudi, M.; Kalhor, H. R.; Laurent, S.; Lynch, I. Protein Fibrillation and Nanoparticle Interactions: Opportunities and Challenges. *Nanoscale* 2013, *5*, 2570.
(23) D'Onofrio, M.; Munari, F.; Assfalg, M. Alpha-Synuclein_Nanoparticle Interactions: Understanding, Controlling and Exploiting Conformational Plasticity. *Molecules* 2020, *25*, 5625.

(24) Barracchia, C. G.; Parolini, F.; Volpe, A.; Gori, D.; Munari, F.; Capaldi, S.; D'Onofrio, M.; Assfalg, M. Camouflaged Fluorescent Silica Nanoparticles Target Aggregates and Condensates of the Amyloidogenic Protein Tau. *Bioconjugate Chem.* 2022, *33*, 1261.
(25) Vacha, R.; Linse, S.; Lund, M. Surface Effects on Aggregation Kinetics of Amyloidogenic Peptides. *J. Am. Chem. Soc.* 2014, *136*, 11776−11782.
(26) Gao, G.; Zhang, M.; Gong, D.; Chen, R.; Hu, X.; Sun, T. The Size-Effect of Gold Nanoparticles and Nanoclusters in the Inhibition of Amyloid-*β* Fibrillation. *Nanoscale* 2017, *9*, 4107−4113.
(27) Chan, H.-M.; Xiao, L.; Yeung, K.-M.; Ho, S.-L.; Zhao, D.; Chan, W.-H.; Li, H.-W. Effect of Surface-Functionalized Nanoparticles on the Elongation Phase of Beta-Amyloid (1−40) Fibrillogenesis.
Biomaterials 2012, *33*, 4443−4450.
(28) Mahapatra, A.; Sarkar, S.; Biswas, S. C.; Chattopadhyay, K. Modulation of *α*-Synuclein Fibrillation by Ultrasmall and Biocompatible Gold Nanoclusters. *ACS Chem. Neurosci.* 2020, *11*, 3442−3454.
(29) Grundke-Iqbal, I.; Iqbal, K.; Quinlan, M.; Tung, Y. C.; Zaidi, M. S.; Wisniewski, H. M. Microtubule-Associated Protein Tau. A Component of Alzheimer Paired Helical Filaments. *J. Biol. Chem.* 1986, *261*, 6084−6089.
(30) Kosik, K. S.; Joachim, C. L.; Selkoe, D. J. Microtubule-Associated Protein Tau (Tau) Is a Major Antigenic Component of Paired Helical Filaments in Alzheimer Disease. *Proc. Natl. Acad. Sci.U.S.A.* 1986, *83*, 4044−4048.
(31) Shang, L.; Azadfar, N.; Stockmar, F.; Send, W.; Trouillet, V.; Bruns, M.; Gerthsen, D.; Nienhaus, G. U. One-Pot Synthesis of Near- Infrared Fluorescent Gold Clusters for Cellular Fluorescence Lifetime Imaging. *Small* 2011, *7*, 2614−2620.
(32) Roux, S.; Garcia, B.; Bridot, J.-L.; Salome, M.; Marquette, C.; Lemelle, L.; Gillet, P.; Blum, L.; Perriat, P.; Tillement, O. Synthesis, Characterization of Dihydrolipoic Acid Capped Gold Nanoparticles, and Functionalization by the Electroluminescent Luminol. *Langmuir* 2005, *21*, 2526−2536.
(33) Jennings, T. L.; Singh, M. P.; Strouse, G. F. Fluorescent Lifetime Quenching near d = 1.5 Nm Gold Nanoparticles: Probing NSET Validity. *J. Am. Chem. Soc.* 2006, *128*, 5462−5467.
(34) Shang, L.; Brandholt, S.; Stockmar, F.; Trouillet, V.; Bruns, M.; Nienhaus, G. U. Effect of Protein Adsorption on the Fluorescence of Ultrasmall Gold Nanoclusters. *Small* 2012, *8*, 661−665.

(35) Tompa, P.; Fuxreiter, M. Fuzzy Complexes: Polymorphism and Structural Disorder in Protein−Protein Interactions. *Trends Biochem. Sci.* 2008, *33*, 2−8.
(36) Li, D.-W.; Xie, M.; Brüschweiler, R. Quantitative Cooperative Binding Model for Intrinsically Disordered Proteins Interacting with Nanomaterials. *J. Am. Chem. Soc.* 2020, *142*, 10730−10738.
(37) Vitali, M.; Rigamonti, V.; Natalello, A.; Colzani, B.; Avvakumova, S.; Brocca, S.; Santambrogio, C.; Narkiewicz, J.; Legname, G.; Colombo, M.; et al. Conformational Properties of Intrinsically Disordered Proteins Bound to the Surface of Silica Nanoparticles. *Biochimica et Biophysica Acta (BBA) - General Subjects*
2018, *1862*, 1556−1564.
(38) Barracchia, C. G.; Tira, R.; Parolini, F.; Munari, F.; Bubacco, L.; Spyroulias, G. A.; D'Onofrio, M.; Assfalg, M. Unsaturated Fatty Acid-Induced Conformational Transitions and Aggregation of the Repeat
Domain of Tau. *Molecules* 2020, *25*, 2716.
(39) Tira, R.; De Cecco, E.; Rigamonti, V.; Santambrogio, C.; Barracchia, C. G.; Munari, F.; Romeo, A.; Legname, G.; Prosperi, D.; Grandori, R.; et al. Dynamic Molecular Exchange and Conformational Transitions of Alpha-Synuclein at the Nano-Bio Interface. *Int. J. Biol. Macromol.* 2020, *154*, 206−216.
(40) Ceccon, A.; Lelli, M.; D'Onofrio, M.; Molinari, H.; Assfalg, M. Dynamics of a Globular Protein Adsorbed to Liposomal Nanoparticles. *J. Am. Chem. Soc.* 2014, *136*, 13158−13161.
(41) Zanzoni, S.; Pedroni, M.; D'Onofrio, M.; Speghini, A.; Assfalg, M. Paramagnetic Nanoparticles Leave Their Mark on Nuclear Spins of Transiently Adsorbed Proteins. *J. Am. Chem. Soc.* 2016, *138*, 72−75.
(42) Ceccon, A.; Tugarinov, V.; Bax, A.; Clore, G. M. Global Dynamics and Exchange Kinetics of a Protein on the Surface of Nanoparticles Revealed by Relaxation-Based Solution NMR Spectroscopy. *J. Am. Chem. Soc.* 2016, *138*, 5789−5792.
(43) Randika Perera, Y.; Hill, R. A.; Fitzkee, N. C. Protein Interactions with Nanoparticle Surfaces: Highlighting Solution NMR Techniques. *Isr. J. Chem.* 2019, *59*, 962−979.
(44) Brancolini, G.; Corazza, A.; Vuano, M.; Fogolari, F.; Mimmi, M. C.; Bellotti, V.; Stoppini, M.; Corni, S.; Esposito, G. Probing the Influence of Citrate-Capped Gold Nanoparticles on an Amyloidogenic Protein. *ACS Nano* 2015, *9*, 2600−2613.
(45) Lin, W.; Insley, T.; Tuttle, M. D.; Zhu, L.; Berthold, D. A.; Kral, P.; Rienstra, C. M.; Murphy, C. J. Control of Protein Orientation on Gold Nanoparticles. *J. Phys. Chem. C* 2015, *119*, 21035−21043.

(46) Shrivastava, S.; McCallum, S. A.; Nuffer, J. H.; Qian, X.; Siegel, R. W.; Dordick, J. S. Identifying Specific Protein Residues That Guide Surface Interactions and Orientation on Silica Nanoparticles. *Langmuir* 2013, *29*, 10841−10849.
(47) Calzolai, L.; Franchini, F.; Gilliland, D.; Rossi, F. Protein−Nanoparticle Interaction: Identification of the Ubiquitin−Gold Nanoparticle Interaction Site. *Nano Lett.* 2010, *10*, 3101−3105.
(48) Kleckner, I. R.; Foster, M. P. An Introduction to NMR-Based Approaches for Measuring Protein Dynamics. *Biochim. Biophys. Acta* 2011, *1814*, 942−968.
(49) Libich, D. S.; Fawzi, N. L.; Ying, J.; Clore, G. M. Probing the Transient Dark State of Substrate Binding to GroEL by Relaxation-Based Solution NMR. *Proc. Natl. Acad. Sci. U. S. A.* 2013, *110*, 11361−11366.
(50) Munari, F.; D'Onofrio, M.; Assfalg, M. Solution NMR Insights into Dynamic Supramolecular Assemblies of Disordered Amyloidogenic Proteins. *Arch. Biochem. Biophys.* 2020, *683*, 108304.

SUPPORTING INFORMAITON

CONTENT:

- Experimental methods

- Tables S1, S2

- Figures S1-S12

METHODS

Reagents

Tetrachloroauric acid trihydrate ($HAuCl_4$), lipoic acid (LA), and sodium borohydride ($NaBH_4$) were purchased from Alfa Aesar (MA, USA). Heparin and all chemical reagents were obtained from Sigma-Aldrich (St Louis, MO, USA). In all preparations, high-purity deionized water from a Millipore system was used.

Recombinant protein expression and purification

Recombinant Tau^{4RD} (region Q244-E372 of human full-length Tau, plus initial Met) was expressed and purified as described previously,[1] with the mutations C291A and C322A to avoid unintended disulfide bond formation (hereafter referred to as Tau^{4RD} for simplicity). Briefly, the protein was expressed in BL21 (DE3) cells grown in LB medium at 37 °C for 5 h, with 0.5 mM IPTG. Protein purification was achieved by thermal treatment of the soluble bacterial extract (80–100 °C) and SP-ion exchange chromatography. To label Tau^{4RD} with ^{15}N, the *E. coli* culture was grown in M9 minimal medium supplemented with $^{15}NH_4Cl$ (1 g/L). Purified Tau^{4RD} products were dialyzed in the final buffer (10 mM phosphate buffer pH 7.4, hereafter called working buffer). Recombinant human α-synuclein was produced in *E. coli* BL21 (DE3) cells and purified as reported previously. [2]

Synthesis of lipoic acid-stabilized ultrasmall gold nanoparticles

For synthetic procedures, all glassware was cleaned with 70% HNO_3 and rinsed thoroughly in Millipore water prior to use. Dihydrolipoic acid (DHLA)-capped ultrasmall gold nanoparticles (usGNPs) were synthesized following a previously reported protocol [3,4]. Briefly, 70 mg of lipoic acid were dissolved in 188.6 ml aqueous solution containing 484 µL NaOH (2 M), followed by addition of $HAuCl_4$ solution (1.96 mL, 2% by mass). After stirring for 5 min, an aqueous solution of $NaBH_4$ (4.06 mL, 50 mM) was slowly added drop by drop, under rapid stirring. The reaction was stopped after stirring overnight. The brownish solution was dialysed against ultrapure water, and then overnight against working

buffer, using a 3.5 kDa molecular weight cut-off membrane. The solution was purified by centrifugal filtration, using Amicon Ultra (Merck, Millipore) centrifugal filters with a 10 kDa cut-off. The pale brown solution containing the usGNPs was stored at 4 °C for later use.

The nanoparticle concentration was estimated from the absorbance at 450 nm using the extinction coefficient ($4.25\ 10^5$) $M^{-1}\ cm^{-1}$, as reported by Haiss.[5] UV-vis absorption spectra were recorded with a NanoDrop™ 2000 Spectrophotometer (Thermofisher), using 1 cm path-length quartz cuvettes.

Cysteamine-FITC/DHLA-capped usGNPs were synthesized following the same protocol described above. [3,4] Cysteamine (0.05 M) was mixed with FITC 8 mg/ml in sodium carbonate buffer, pH 9.0, for 24 h at room temperature in the dark. The product was then mixed with lipoic acid in a molar ratio of 16:1.

Dynamic Light Scattering (DLS)

Hydrodynamic diameter and ζ-potential measurements were performed using a Zetasizer Nano ZS (Malvern Instruments, Malvern, UK) at room temperature, operating at λ = 633 nm and equipped with a back scattering detector of 173°. For determining size distribution by DLS, a solution of 13 μM usGNPs in working buffer was recorded in triplicate and the average of three measurements was plotted. For ζ-potential measurements, samples were loaded into a folded capillary cell and the voltage was automatically set to 148 V. The ζ- potential values were derived from the electrophoretic mobility by means of the Henry equation over five replicates.

Fluorescence Spectroscopy

Fluorescence measurements were performed on a Jasco FP-8500 spectrofluorometer (Jasco, Easton, MD, USA) using 1 cm path-length quartz cuvettes. The used concentrations of usGNPs and Tau^{4RD} were such that the absorbance at the excitation wavelength was less than 0.05, to avoid self-absorption and inner filter effects.

Fluorescence emission spectra of usGNPs were recorded in the range of 550-750 nm using an excitation wavelength of 530 nm (slit width 5 nm). A fixed

concentration of usGNPs (0.25 μM) was titrated with Tau^{4RD} (800-0.05 μM). Samples were prepared in working buffer.

Tyrosine fluorescence measurements were performed on a Jasco FP-8500 spectrophotometer (Jasco, Easton, MD, USA). The excitation wavelength was 270 nm (slid width 10 nm) and emission spectra were collected in the range of 275-400 nm. A fixed concentration of Tau^{4RD} (60 μM) was titrated with usGNPs (3-0.1 μM).

All experiments were performed at room temperature. Three spectra accumulations were averaged for each sample and the spectrum of the buffer was considered as a blank and subtracted.

Isothermal Titration Calorimetry (ITC)

ITC measurements were performed with a MicroCal PEAQ-ITC instrument (Malvern Panalytical, UK) at 25 °C.

1.5 μM of usGNPs were titrated with Tau^{4RD} or α-synuclein (150 μM and 250 μM, respectively). Nineteen injections of 2 μL were performed, setting the stirring speed to 500 rpm, with 150 s interval between subsequent injections. For all titrations, samples were dialysed against the same working buffer. Number of sites (N), dissociation constant (K_D) and enthalpy change (ΔH) were the experimental parameters obtained by the best performing fitting model (two sets of sites). Data were analyzed by using the MicroCal PEAQ-ITC Analysis Software (Malvern). The titrations were repeated in the presence of different concentrations of NaCl (10, 50, 100 and 200 mM NaCl for Tau^{4RD}, 10 and 200 mM NaCl for α-synuclein).

Nuclear Magnetic Resonance (NMR) spectroscopy

NMR spectra were recorded on a Bruker Avance IV 700 MHz spectrometer, equipped with a TCI cryoprobe, or on a Bruker Avance NEO 600 MHz spectrometer equipped with a Prodigy TCI cryoprobe. All the spectra were recorded at 10 °C.

One-dimensional ^1H spectra were acquired on DHLA-stabilized usGNPs (5 μM) and DHLA solutions, in working buffer and 10% D_2O, for general

characterization. Experiments were performed using a standard pulse sequence incorporating the excitation sculpting water suppression scheme. A total of 8 transients were acquired over a spectral width of 9615 Hz and 32768 complex points with recycle delay of 1.7 s.

NMR titration experiments were run on samples with a protein concentration of 50 μM and usGNPs concentration in the range 0-5 μM, corresponding to protein/usGNPs molar ratios of: 10:1, 20:1, 25:1, 30:1, 40:1, 50:1, 60:1, and 80:1. The solutions were prepared in working buffer and 10% D_2O. One-dimensional ^{1}H-NMR experiments were acquired with 16 transients over a spectral width of 11363 Hz and 32768 complex points, with a recycle delay of 1.2 s. Typical two-dimensional ^{1}H-^{15}N HSQC spectra were acquired with a data matrix consisting of 2048 (F2, ^{1}H) x 256 (F1, ^{15}N) complex points, 12 scans, 1.2 s recycle delay, and spectral widths of 9615 (F2) x 1776 (F1) Hz.

Nuclear spin relaxation rate measurements were performed at 16.4 T magnetic field strength. Protein backbone ^{15}N-spin T_2 (=R_2^{-1}) spectra were recorded on 200 μM [^{15}N]Tau^{4RD} in the absence or presence of usGNPs. Experiments were performed in gradient-selected sensitivity-enhanced mode and in interleaved fashion; matrix: 2048(^{1}H) × 128(^{15}N) complex data points for each relaxation delay; spectral widths: 13 (^{1}H) and 33 ppm (^{15}N). Water signal suppression was obtained with a flip-back pulse. The recycle delay was set to 3 s. T_2 relaxation delays were 0.016 (duplicate), 0.032, 0.064, 0.128, 0.192, 0.224, 0.272 (duplicate) s. The echo delay was 0.42 ms. Relaxation times T_2 were determined by fitting peak intensities to a single exponential decay.

Carr–Purcell Meiboom–Gill relaxation dispersion (CPMG-RD) experiments were performed using a constant- time relaxation-compensated pulse program (constant-time period, T_{CPMG}= 100 ms; CPMG frequencies, (ν_{CPMG} = 50, 100, 200, 400, 600, 800, 1000(duplicate) Hz). Two-dimensional data sets were acquired in an interleaved manner (inter-scan delay = 3 s; 256 increments in the nitrogen dimension). The transverse relaxation rate, R_2^{obs}, for each frequency point was obtained from the signal intensity measured at the end of the T_{CPMG} period according to:

$$R_2^{obs} = -\frac{ln\,(I_{\nu CPMG}/I_0)}{T_{CPMG}} \qquad \text{Eq 1}$$

where I_0 is the signal intensity measured in a reference spectrum lacking the CPMG period, and I_{vCPMG} is the residual intensity at the end of the CPMG pulse sequence for a particular spin-lock frequency. R_2^{obs} uncertainties were estimated from duplicate measurements of one data point and were in most cases below 5%. The minimum error was set to 5% for all points.

Relaxation dispersion curves were modelled with a simple two-state exchange process in RING-NMR.[6] Fast- limit ($k_{ex} \gg \delta\omega$) and slow-limit ($k_{ex} \ll \delta\omega$) exchange models between the sites were considered, model selection was based on the Akaike information criterion. Dispersion curves were then fitted individually with the resulting fast-exchange model using GraphPad Prism 9 (GraphPad Software Inc., La Jolla, CA, USA). The fitting parameters were k_{ex}, $R_2{}^0$, and $\delta_{ppm}{}^{min}$; the latter is a field-independent variable representing the chemical shift change expected for equal populations of the exchanging states. The exchange contributions to relaxation rates were calculated from the expression:

$$R_{ex} = \frac{\left(2\pi B_0 \delta_{ppm}^{min}\right)^2}{4K_{ex}} \qquad \text{Eq. 2}$$

Far-UV Circular Dichroism (CD) spectroscopy

CD measurements were carried out on a Jasco J-1500 spectropolarimeter equipped with a Peltier type temperature-controlled cell holder (Jasco, Easton, MD, USA). Far-UV spectra (190–260 nm) were recorded in cm cuvettes, at 25 °C, with a scan rate of 50 nm min^{-1}, a bandwidth of 1 nm, and an integration time of 2s. Spectra were recorded on samples of Tau^{4RD} in the absence or presence of usGNPs at various molar ratios. Five spectra accumulations were averaged for each sample and the spectrum of the buffer was considered as a blank and subtracted. The protein concentration was 6 µM.

Prior to running aggregation assays, solutions of Tau^{4RD} were filtered through a 100 kDa cut-off filter (Sartorius Stedim Biotech GmbH, Göttingen, Germany) to remove pre-existing large oligomers and fibrils. To monitor time-dependent spectral changes, samples were incubated for 48 h at 30 °C. Aggregation reactions were

prepared in 300 µL aqueous buffer (10 mM KPi, pH 7.4, protease inhibitors, in the absence or presence of 100 mM NaF) by mixing 50 µM Tau^{4RD}, (0.4, 1.5, 5) µM usGNPs, and 50 µM heparin.
Data plots were generated with GraphPad Prism 9 (GraphPad Software Inc., La Jolla, CA, USA).

Thioflavin-T (ThT) aggregation assay

Solutions of Tau^{4RD} were preliminarily filtered through a 100 kDa cut-off filter. The aggregation was induced by incubating the soluble protein in the presence of heparin at various concentrations of usGNPs; protein:NP was (10:0, 10:0.02, 10:0.04, 10:0.3, 10:1) µM in working buffer (in the absence or presence of 100 mM NaCl). Control reactions were carried out in the absence of usGNPs (protein:HEP was 10:10 µM).
The kinetics of aggregation was monitored by measuring the fluorescence of thioflavin-T (10 µM) added to each sample in a 96-well dark plate (100 µL final volume for each well). Fluorescence measurements were performed using a TECAN Infinite M200 Pro microplate reader (Tecan Group AG, Männedorf, Switzerland) at 30 °C for ca.72 h with cycles of 30 s of shaking (250 rpm, orbital) and 10 min of rest throughout the incubation. The fluorescence intensity was measured every 11 min (excitation, 450 nm; emission, 480 nm; bottom read). Error bars of fluorescence data correspond to standard deviations of at least four independent experiments.

Transmission Electron Microscopy (TEM)

For TEM measurements, samples were prepared as described for the ThT assay at the final volume of 100 µL and incubated at 30 °C for 48 h in static condition. Subsequently, 30 µL of aggregates samples (5 µM) in mQ H2O were adsorbed onto 400 mesh holey film grids; after staining with 2% uranyl acetate (for 2 min), the sample was observed with a Tecnai G^2 (FEI) transmission electron microscope operating at 100 kV. Images were captured with a Veleta (Olympus Soft Imaging System, Münster, Germany) digital camera using FEI TIA acquisition software (Version 4.0).

Cellular viability and nanoparticle uptake assays

APP-swe expressing cells (H4-swe cells) and Hek-293 cells were cultured in a humidified atmosphere of 5% CO2, and passaged in complete growth medium: Dulbecco's modified Eagle's medium (DMEM) High Glucose (Aurogene) containing 10% fetal bovine serum (FBS) (Aurogene) supplemented with 2 mM glutamine (Aurogene), 100 U/ml penicillin and 100 U/ml streptomycin (Aurogene). Once 70–80% confluence was reached, cells were collected using trypsin, washed, and counted.

usGNPs were dialyzed against phosphate-buffered saline (PBS) prior to administration to cells. For the treatment, FBS was replaced with 2% B27 Supplement. Cell viability after usGNPs treatment was evaluated by the reduction of the tetrazolium salt MTT 1-(4,5-Dimethylthiazol-2-yl)-3,5-diphenylformazan, Thiazolyl blue formazan Sigma Aldrich), following the manufacturer's protocol. Briefly, 10000 H4-swe cells/well were seeded in their exponential growth phase in a flat-bottomed 96-well plate and were incubated at 37 °C in a 5% CO2 incubator. After 24 h, cells were treated with different concentrations of usGNPs (0.5, 0.1, 0.05, and 0.01 μM). After 72 h of treatment, cells were incubated with 0.5 mg/ml MTT for 3 h at 37 °C and insoluble formazan crystals were dissolved in 200 μL DMSO. Reduced MTT was evaluated by measuring the absorbance at 560 nm. Experiments were performed in triplicate on an Infinite M200 PRO fluorescence microplate reader (Tecan).

For usGNPs uptake experiments, human H4-swe cells were seeded on coverslip glasses in a 24-multiwell microplate. Cells were treated for 48 h with 0.5 μM FITC-usGNPs in complete medium (replacing 10% FBS with 2% B27 Supplement). After treatment, cells were washed with PBS and fixed with ice-cold 4% PFA in PBS for 15 min at room temperature. After blocking with 2% bovine serum albumin and 2% Fetal Goat Serum in PBS for 1 h at room temperature, cells were incubated with 2 μg/ml of anti β-tubulin III primary antibody (Merck) diluted in the blocking buffer for 2 h at room temperature. After 3 PBS washes, cells were incubated with 0.5 μg/ml anti-rabbit-Alexa Fluor 594 secondary antibody (Thermo Scientific) diluted

in the blocking buffer for 1 h at room temperature. After PBS washes, nuclei were stained with 1 μg/ml Hoechst diluted in PBS.

For stress granules (SG) colocalization experiments, H4-swe cells (104 cells/well) were seeded on coverslip glasses in a 24-multiwell microplate. Cells were treated overnight with 0.5 μM FITC-usGNP as described above. The next day, coverslips were washed twice with complete DMEM medium and incubated 1 h at 37 °C in presence or absence of 0.5 mM sodium arsenite (AS). Cells were washed three times with PBS, fixed with ice-cold 4% PFA for 20 min and permeabilized with 0.2% Triton X-100 in PBS. After blocking with 1% bovine serum albumin in PBS, cells were incubated for 2 h with CoraLite®594-conjugated G3BP1 monoclonal antibody (Proteintech) diluted in blocking solution. After 3□ PBS washes, nuclei were stained with 1 μg/ml Hoechst diluted in PBS and coverslips were sealed with nail polish. Alternatively, live cells were first treated with 0.5 mM AS (1 h) and subsequently permeabilized with 0.01% Triton X-100 in HHBS [Hanks' Buffer with 20 mM Hepes] for 5 min. After 2 washes with HHBS, coverslips were incubated with 0.5 μM FITC-usGNP diluted in the same buffer at 37 °C for 30 min. After 3 washes with HHBS, cells were fixed and immunostained as described above.

Microscopy images were acquired using a Leica DM2500 fluorescence microscope or a confocal laser- scanning fluorescence microscope Leica TCS SP5 with a 63x HCX PL APO objective, and analyzed with LAS AF (Leica) and ImageJ software.

Table S1. Thermodynamic parameters for the binding of Tau^{4RD} to usGNPs. Given uncertainties are from data fitting.

NaCl	*	K_a (M^{-1})	ΔG ($kJmol^{-1}$)	ΔH ($kJmol^{-1}$)	$-T\Delta S$ ($kJmol^{-1}$)	n
0 mM	I)	$(6.1 \pm 0.9) \times 10^7$	-44.5 ± 0.4	-268 ± 5	224 ± 5	5.8 ± 0.1
	II)	$(2.7 \pm 0.3) \times 10^6$	-36.8 ± 0.3	74 ± 5	-110 ± 5	12.5 ± 0.1
10 mM	I)	$(1.3 \pm 0.1) \times 10^8$	-46.4 ± 0.2	-290 ± 6	244 ± 6	5.7 ± 0.1
	II)	$(3.6 \pm 0.1) \times 10^6$	-37.5 ± 0.1	70 ± 3	-107 ± 3	8.5 ± 0.2
50 mM	I)	$(2.4 \pm 0.5) \times 10^7$	-42.3 ± 0.5	-231 ± 50	189 ± 50	5.5 ± 0.5
	II)	$(1.2 \pm 0.2) \times 10^6$	-34.7 ± 0.4	69 ± 30	-104 ± 30	7.3 ± 0.2
100 mM	I)	$(8.1 \pm 1.2) \times 10^6$	-39.5 ± 0.4	-216 ± 20	177 ± 20	5.5 ± 0.8
	II)	$(3.1 \pm 0.5) \times 10^5$	-31.4 ± 0.4	65 ± 10	-96 ± 10	6 ± 3

* I) first binding event, II) second binding event

Table S2. Thermodynamic parameters for the binding of α-syn to usGNPs. Given uncertainties are from datafitting.

NaCl	*	K_a (M^{-1})	ΔG ($kJmol^{-1}$)	ΔH ($kJmol^{-1}$)	$-T\Delta S$ ($kJmol^{-1}$)	n
0 mM	I)	$(1.5 \pm 0.2) \times 10^7$	-41.0 ± 0.3	-195 ± 10	154 ± 10	2.4 ± 0.1
	II)	$(8.3 \pm 0.4) \times 10^5$	-34 ± 2	-48 ± 2	14 ± 4	12.7 ± 0.3
10 mM	I)	$(1.7 \pm 0.4) \times 10^7$	-41 ± 2	-173 ± 9	132 ± 11	2.4 ± 0.1
	II)	$(7.0 \pm 0.5) \times 10^5$	-33 ± 2	-42 ± 2	9 ± 4	12.2 ± 0.4
200 mM	**	$(6.6 \pm 0.8) \times 10^5$	-33.2 ± 0.3	-182 ± 20	149 ± 20	2.2 ± 0.2

* I) first binding event, II) second binding event
** one-site binding model

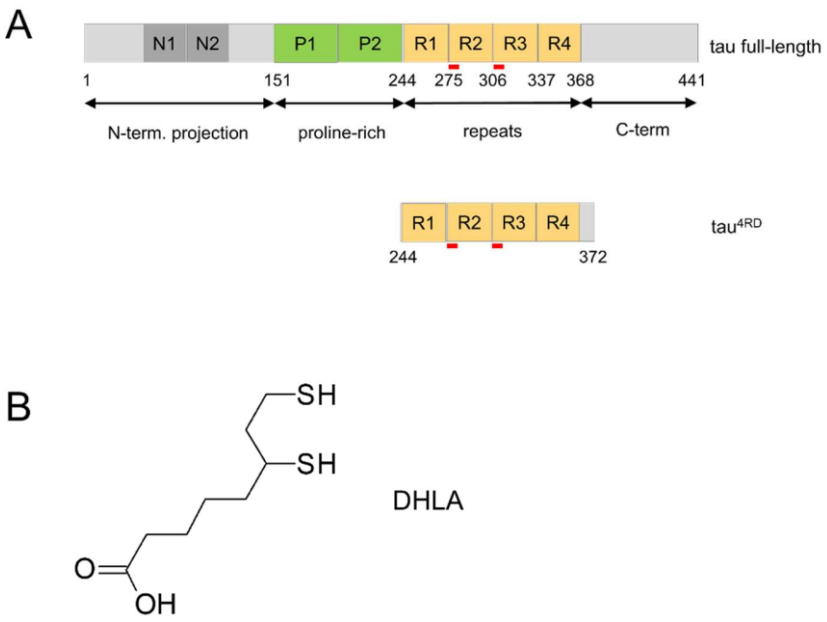

Figure S1. *Molecules used in the study*. A) Domain organization of Tau full-length and Tau^{4RD}; the position of the hexapeptide motifs is indicated by red bars. B) Structure of dihydrolipoic acid (DHLA).

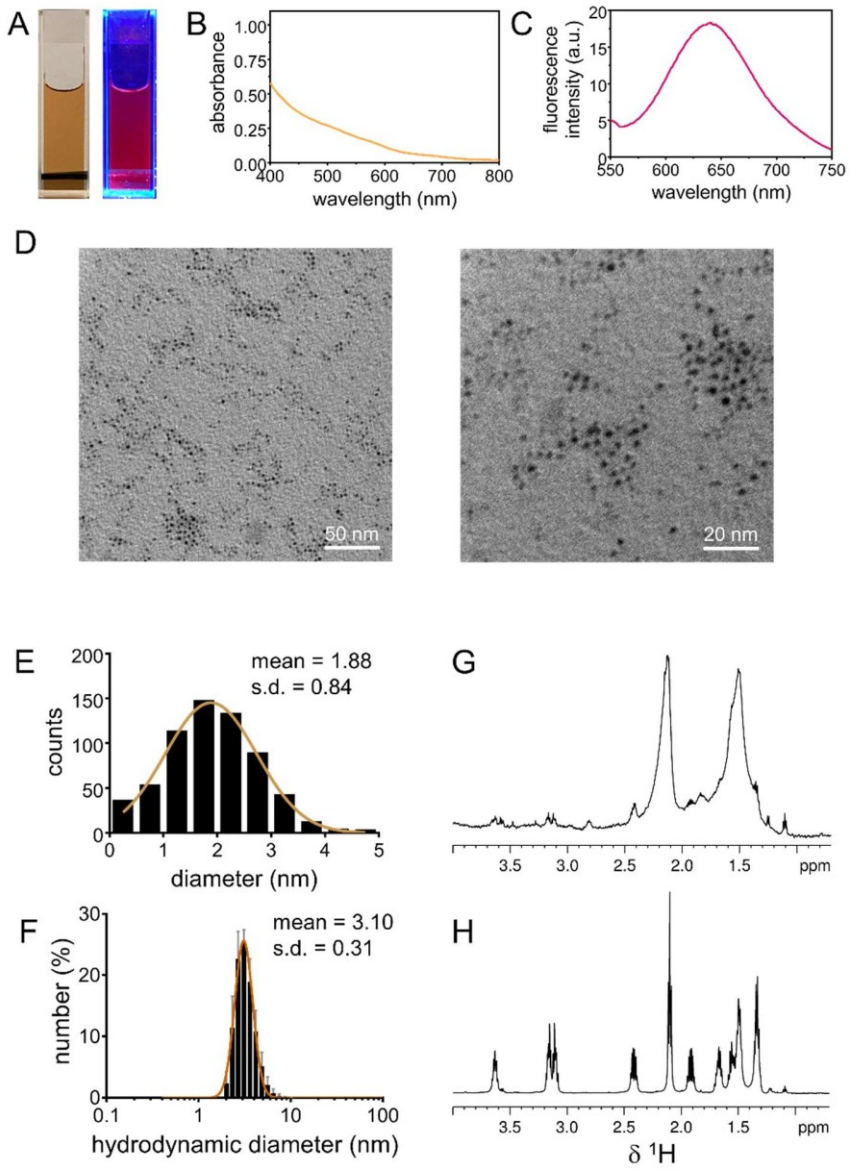

Figure S2. Characterization of synthesized ultrasmall gold nanoparticles. A) Colloidal solution of usGNPs visualized under daylight (left) and UV lamp (right). B) The absence of a surface plasmon resonance band in the visible light absorption spectrum is consistent with the ultrasmall size. C) Fluorescence emission spectrum (ex = 530 nm, max = 640 nm). D) Representative TEM images. E) Diameter distribution histogram derived from TEM micrographs; continuous line is the best-fit Gaussian curve. F) Hydrodynamic diameter distribution as determined from dynamic light scattering; continuous line is the best-fit Log-Gaussian curve. G) The 1H- NMR spectrum of DHLA-capped usGNPs displays broad, poorly resolved signals representing surface-bound DHLA; line broadening results from restricted mobility of the ligand compared to its free state (panel H) and frequency shifts originate from magnetic interactions near the metal surface.[7] H) 1H-NMR spectrum of the unbound capping ligand.

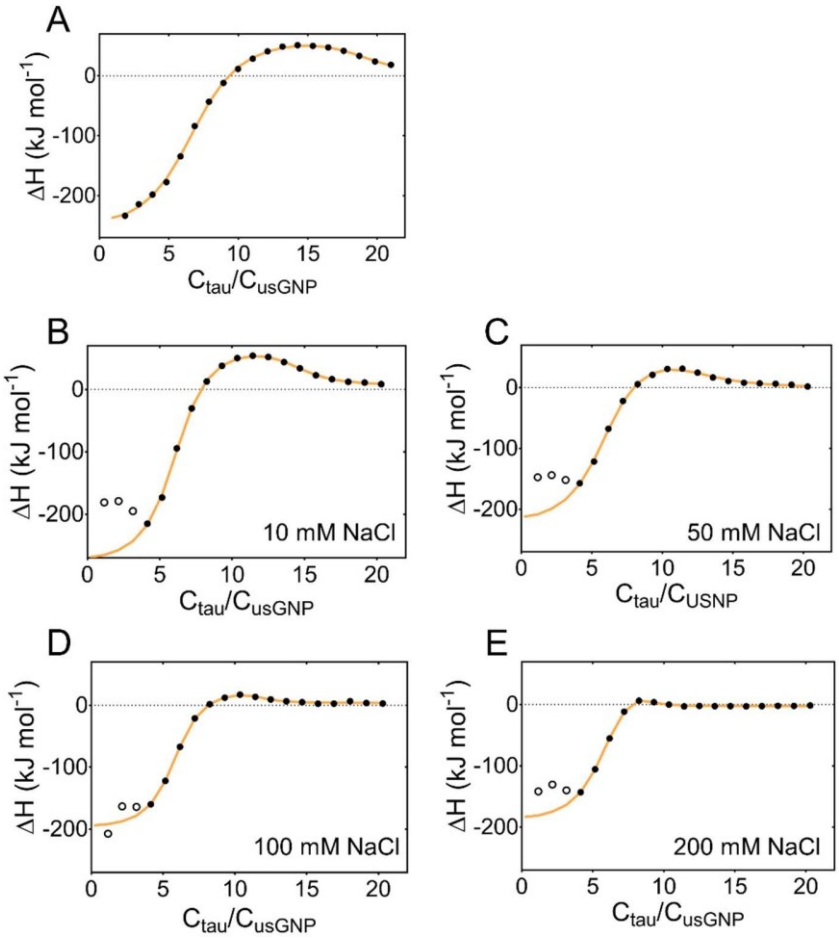

Figure S3. *Ionic strength-dependent thermal response for the interaction between Tau^{4RD} and usGNPs*. Isothermal titration calorimetry data obtained on titrating Tau^{4RD} into usGNPs, in the presence of A) 0 mM,B) 10 mM, C) 50 mM, D) 100 mM, and E) 200 mM NaCl. All panels display integrated enthalpy plots. Orange lines are best-fit curves based on a two-sets-of-sites binding model; data displayed as empty circles were excluded from fitting. The fitted parameters for A-D are reported in Table S1. For dataset E, no binding parameters are reported as the fitting was unstable

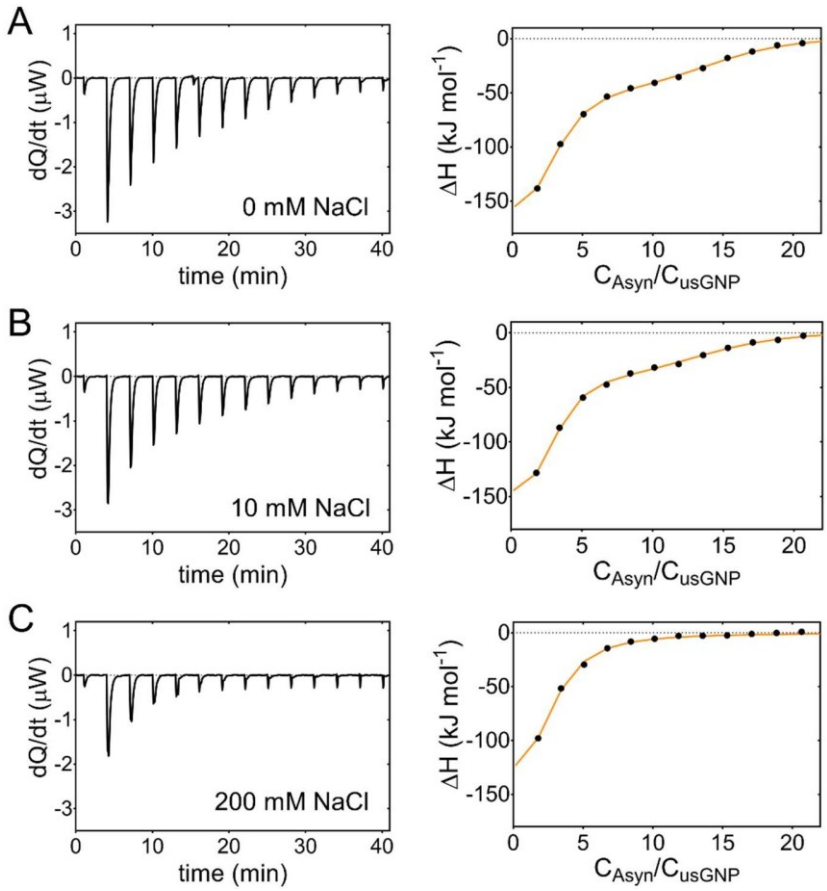

Figure S4. *Isothermal titration calorimetry on α-synuclein/usGNPs*. ITC data obtained on titrating α-synuclein (α-syn) into usGNPs, in the presence of A) 0 mM, B) 10 mM, and C) 200 mM NaCl. All panels display heat flow(left) and integrated enthalpy plots (right). Orange lines are best-fit curves based on (A,B) two-sets-of-sitesor (C) one-set-of-sites binding models. The corresponding binding parameters are reported in Table S2.

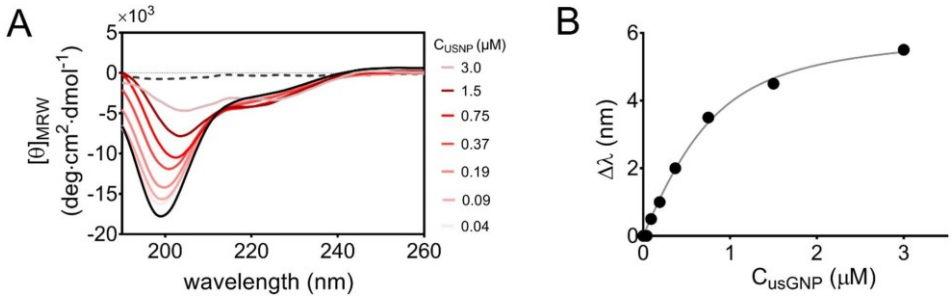

Figure S5. *Secondary structure perturbations.* A) Far-UV CD spectra measured on 6 μM Tau^{4RD} in the presence of usGNPs at the indicated concentrations; black continuous line refers to Tau^{4RD} alone, dashed line refers tousGNPs alone. B) Concentration dependence of the position of the CD peak with largest ellipticity (ca. 200nm); solid line corresponds to the best-fit hyperbolic curve

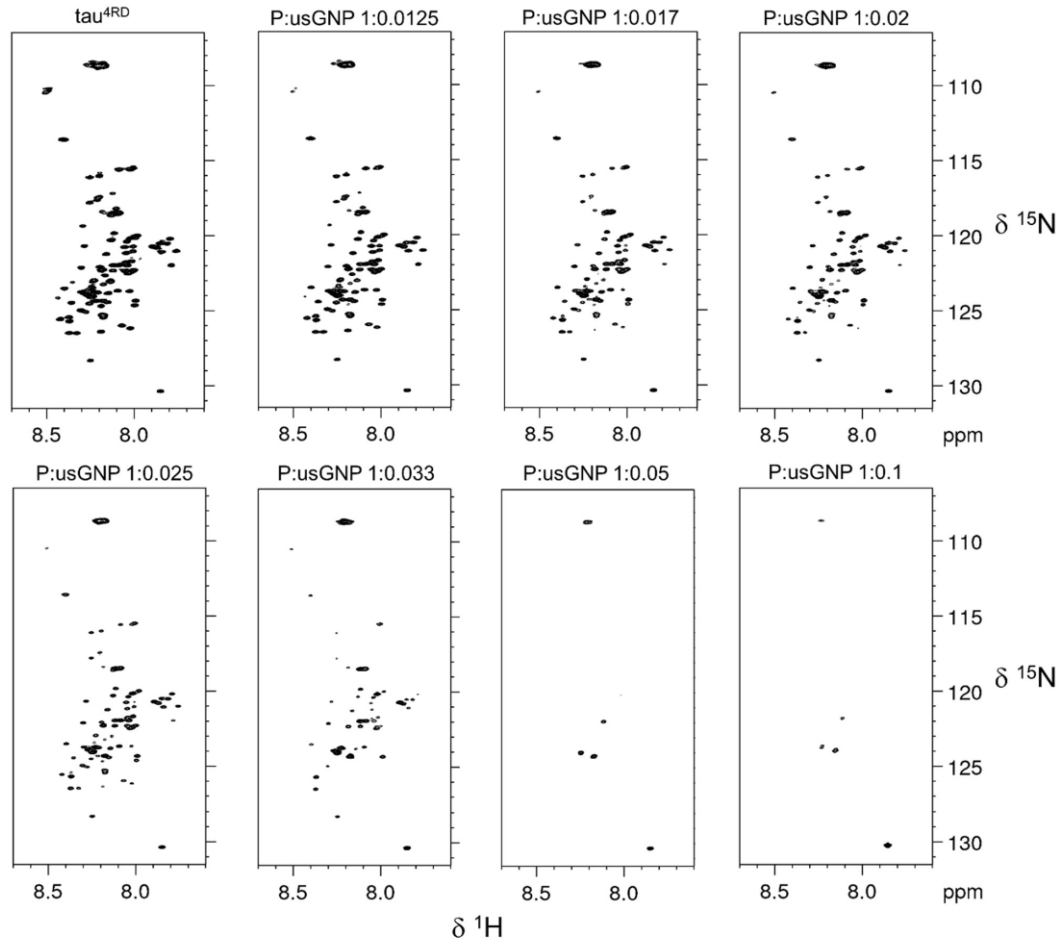

Figure S6. *Protein-observed NMR spectra.* HN-HSQC spectra of Tau^{4RD} in the absence (top left) or presence of usGNPs at increasing concentration; the spectral region of side chain amide signals is excluded for better visualization.

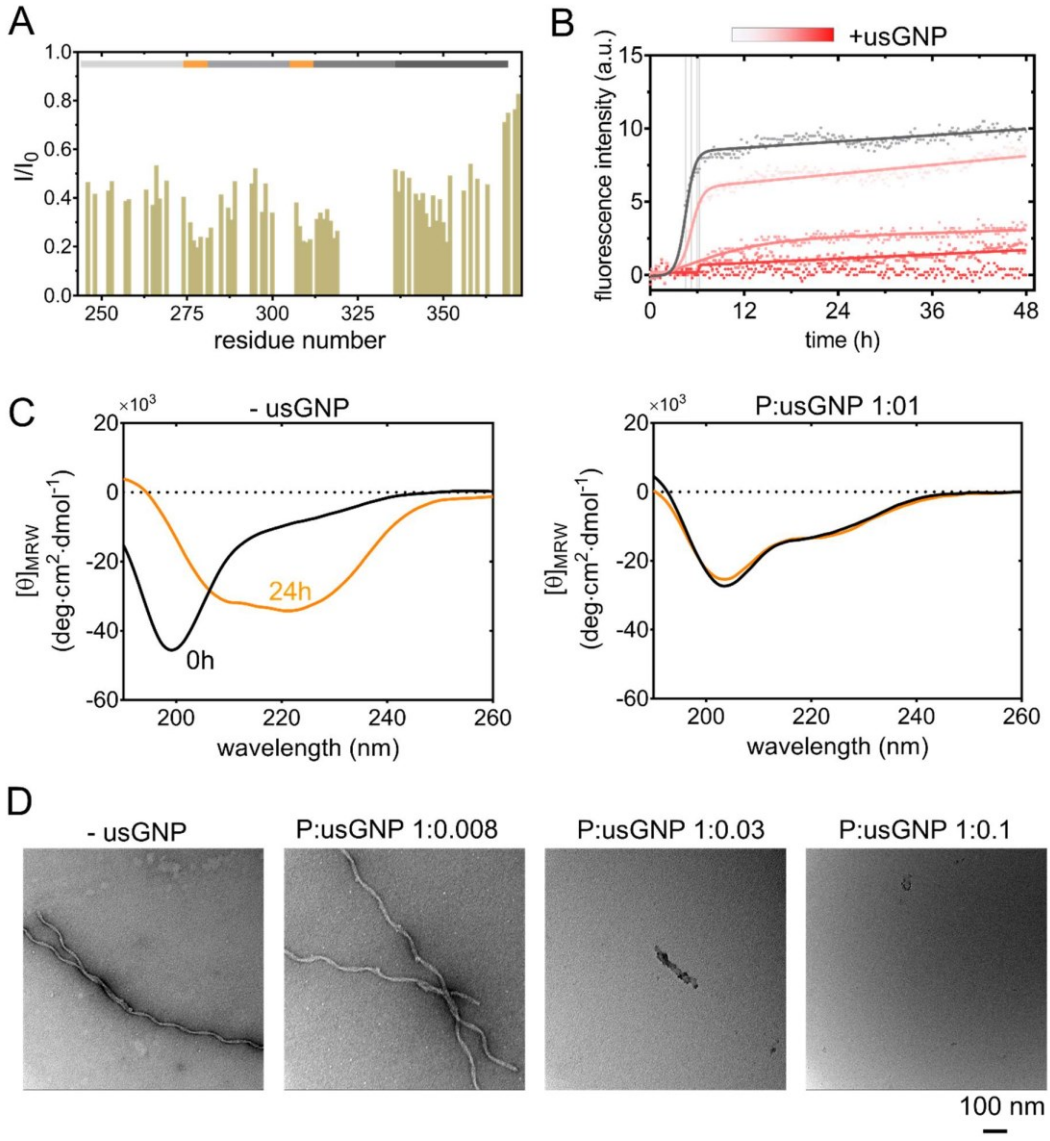

Figure S7. *Binding and aggregation experiments at high ionic strength.* A) Residue-specific HSQC-peak intensity versus residue number; peak intensities were measured on Tau^{4RD} in the absence (*I*0) or presence (*I*) of usGNPs at a molar ratio P:usGNPs = 1:0.02; only isolated peaks were included in the analysis; the protein domain organization is shown on top. B) Aggregation kinetics monitored by ThT fluorescence; measurements were performed on Tau^{4RD} in the absence (grey dots) or presence (light-to-dark red dots) of usGNPs (P:usGNP molar ratios 1:0, 1:0.002, 1:0.004, 1:0.03, 1:0.1); solid lines correspond to the best-fit curves; vertical grey lines indicate transition midpoints. C) Far-UV CD spectra acquired on Tau^{4RD} after 0 h (black) and 24 h (brown) incubation with heparin, in the absence (left) or presence (right) of usGNPs at the indicated molar ratio. Samples were prepared with 100 mM NaCl (NMR, ThT assay) or NaF (CD). D) Representative TEM images of Tau^{4RD} samples after 48 h incubation in aggregating conditions and with 100 mM NaCl, in the absence (left panel) or presence (remaining panels) of usGNPs.

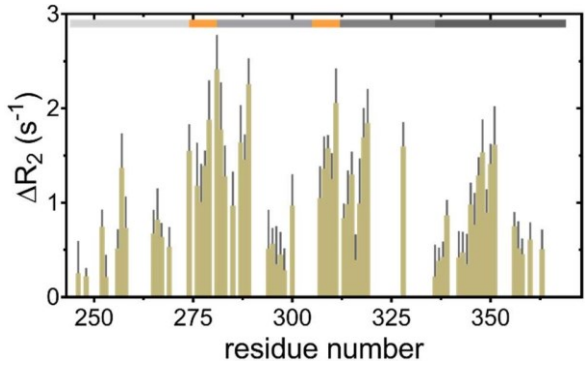

Figure S8. ^{15}N-ΔR_2 (CPMG field = 595 Hz) for 200 μM [^{15}N]Tau^{4RD} in the presence of 2 μM usGNPs, 10 mM NaCl, at a spectrometer frequency of 700 MHz Grey bars are errors derived from exponential fitting of experimental data. Protein domain organization is schematically depicted on the top.

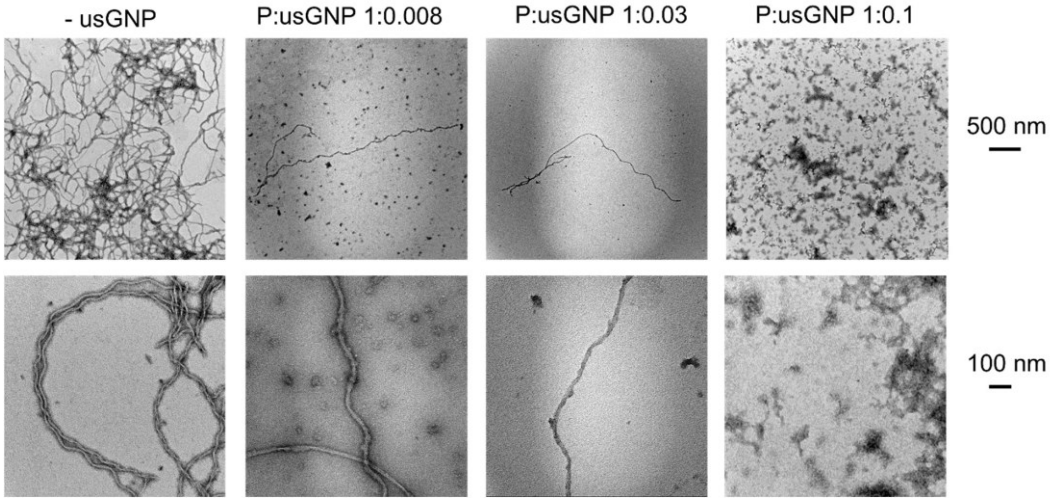

Figure S9. Representative TEM images of Tau^{4RD} samples after 48 h incubation in aggregating conditions, inthe absence (left panel) or presence (remaining panels) of usGNPs; scale bar for all images in the top (bottom) panels is 500 (100) nm.

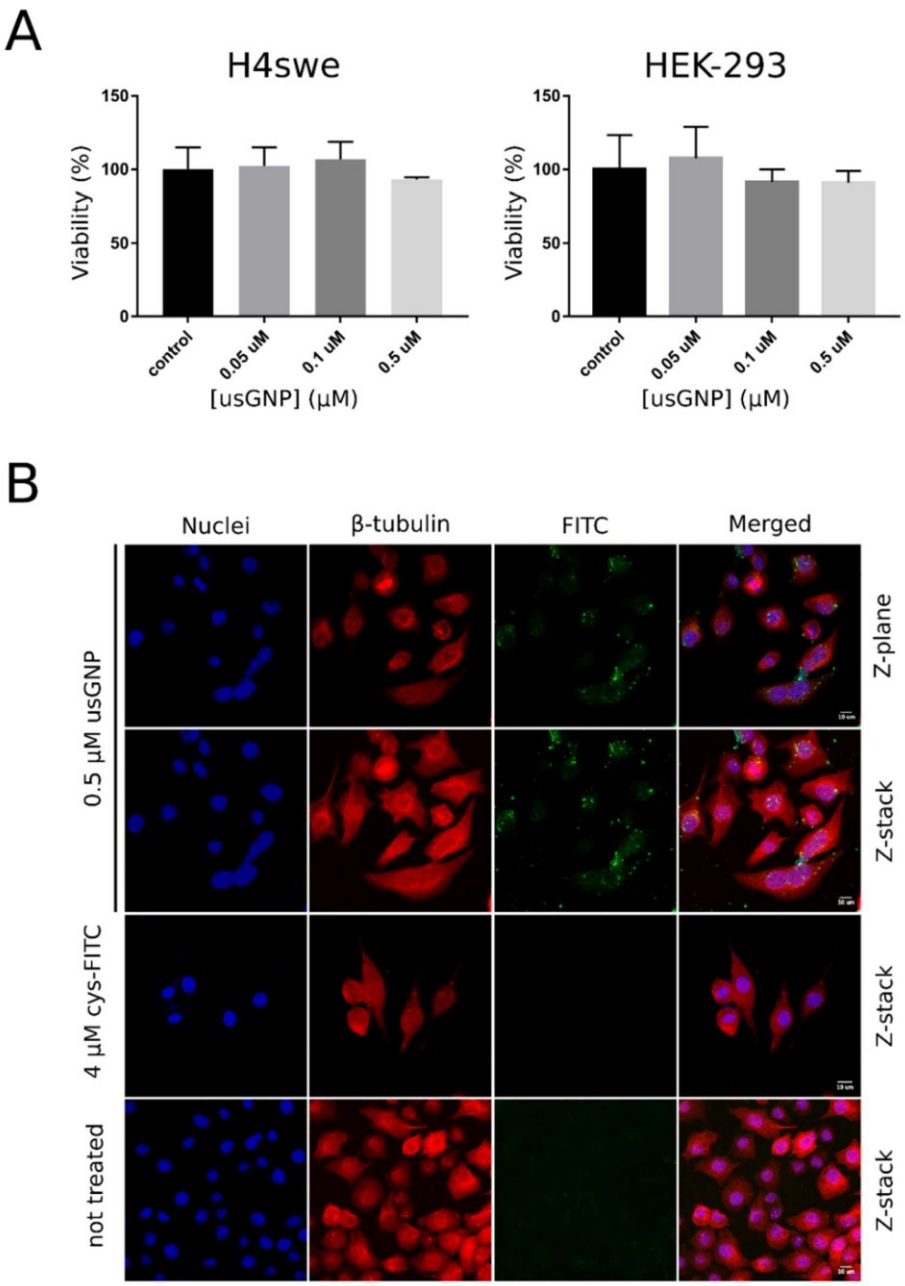

Figure S10. *Biocompatibility and internalization of usGNPs*. A) Cell viability measured by MTT proliferation assay in H4swe (left) and HEK-293 (right) adherent cells treated for 72 h with different concentrations of usGNPs. The results are shown as mean ± S.D. of three independent experiments. One-way ANOVA and Dunnett's multiple comparisons test revealed no statistically relevant differences between the treated samples and the control. B) Representative confocal microscopy images of H4swe cells after 48 h of treatment with 0.5 µM usGNPs (single Z-plane and Z-stack), 4 µM free cysteamine-FITC, and control (not treated). β-tubulin (cytoskeleton) is stained in red; cell nuclei are stained with Hoechst 33342 (blue). Scalebars are 10 µm.

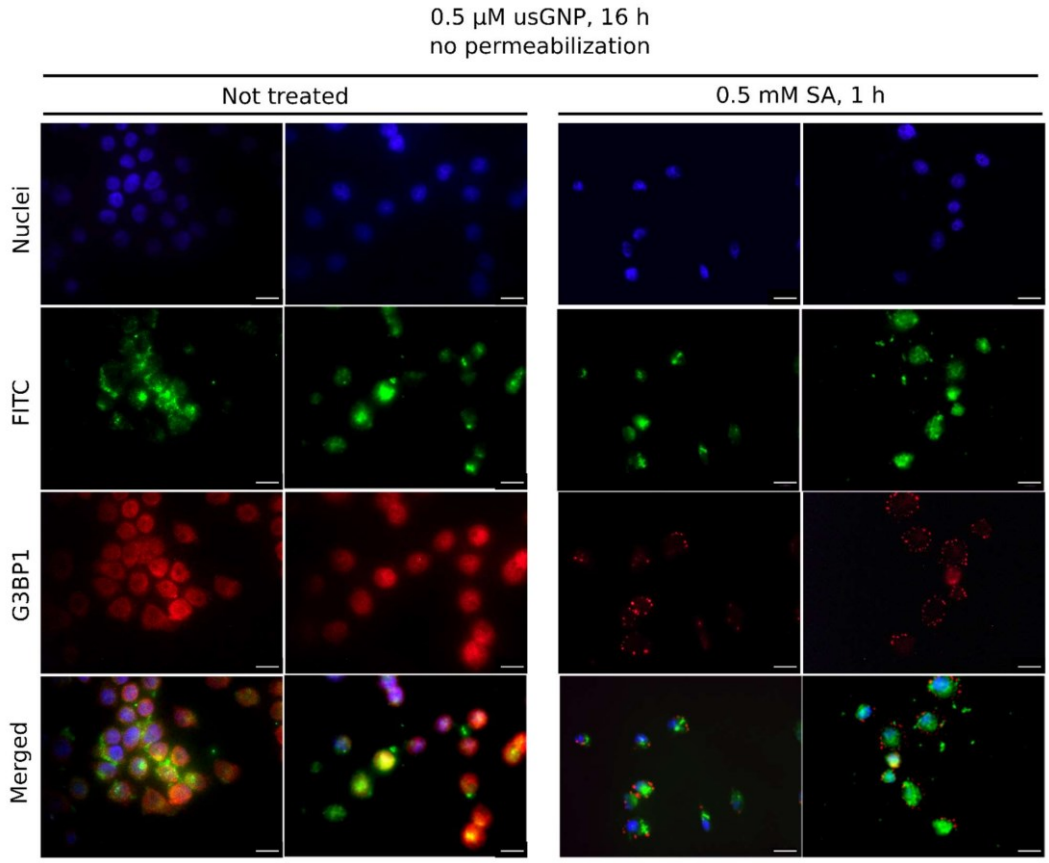

Figure S11. Representative fluorescence microscopy images of unpermeabilized H4-swe cells treated for 16h with 0.5 µM FITC-usGNPs and subsequently incubated for 1 h in the absence (left) or in the presence (right) of 0.5 mM sodium arsenite (SA). Stress granule marker G3BP1 is stained in red and nuclei in blue (DAPI). Scale bars: 20 µm.

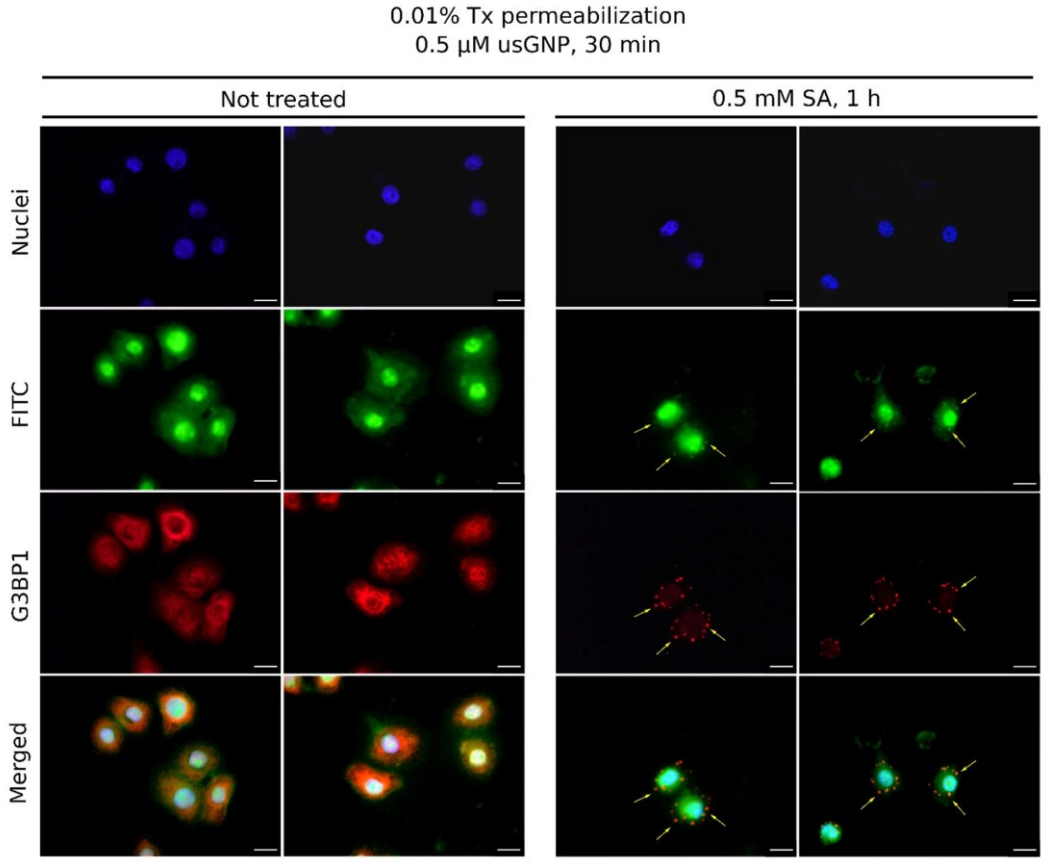

Figure S12. Representative fluorescence microscopy images of H4-swe cells, not treated (left) or treated with 0.5 mM SA (right), incubated for 30 min with 0.5 µM FITC-usGNPs after membrane permeabilization with 0.01% Triton-X100. Stress granule marker G3BP1 is stained in red and nuclei in blue (DAPI). Colocalization ofusGNPs with SGs is indicated by the yellow arrows. Scale bars: 20 µm.

REFERENCES

(1) Munari, F.; Barracchia, C.G.; Franchin, C.; Parolini, F.; Capaldi, S.; Romeo, A.; Bubacco, L.; Assfalg, M.; Arrigoni, G.; D'Onofrio, M. Semisynthetic and Enzyme-Mediated Conjugate Preparations Illuminate the Ubiquitination-Dependent Aggregation of Tau Protein. *Angew. Chem. Int. Ed Engl.* **2020**, *59*, 6607– 6611, doi:10.1002/anie.201916756.

(2) Tira, R.; De Cecco, E.; Rigamonti, V.; Santambrogio, C.; Barracchia, C.G.; Munari, F.; Romeo, A.; Legname, G.; Prosperi, D.; Grandori, R.; et al. Dynamic Molecular Exchange and Conformational Transitions of Alpha-Synuclein at the Nano-Bio Interface. *Int. J. Biol. Macromol.* **2020**, *154*, 206–216, doi:10.1016/j.ijbiomac.2020.03.118.

(3) Shang, L.; Brandholt, S.; Stockmar, F.; Trouillet, V.; Bruns, M.; Nienhaus, G.U. Effect of Protein Adsorption on the Fluorescence of Ultrasmall Gold Nanoclusters. *Small* **2012**, *8*, 661–665, doi:https://doi.org/10.1002/smll.201101353.

(4) Shang, L.; Azadfar, N.; Stockmar, F.; Send, W.; Trouillet, V.; Bruns, M.; Gerthsen, D.; Nienhaus, G.U. One-Pot Synthesis of Near-Infrared Fluorescent Gold Clusters for Cellular Fluorescence Lifetime Imaging. *Small* **2011**, *7*, 2614–2620, doi:https://doi.org/10.1002/smll.201100746.

(5) Haiss, W.; Thanh, N.T.K.; Aveyard, J.; Fernig, D.G. Determination of Size and Concentration of Gold Nanoparticles from UV−Vis Spectra. *Anal. Chem.* **2007**, *79*, 4215–4221, doi:10.1021/ac0702084.

(6) Beckwith, M.A.; Erazo-Colon, T.; Johnson, B.A. RING NMR Dynamics: Software for Analysis of Multiple NMR Relaxation Experiments. *J. Biomol. NMR* **2021**, *75*, 9–23, doi:10.1007/s10858-020-00350-w.

(7) Ruks, T.; Beuck, C.; Schaller, T.; Niemeyer, F.; Zähres, M.; Loza, K.; Heggen, M.; Hagemann, U.; Mayer, C.; Bayer, P.; et al. Solution NMR Spectroscopy with Isotope-Labeled Cysteine (^{13}C and ^{15}N) Reveals the Surface Structure of L -Cysteine-Coated Ultrasmall Gold Nanoparticles (1.8 Nm). *Langmuir* **2019**, *35*, 767–778, doi:10.1021/acs.langmuir.8b03840.

3.3 Published article: Tau-coffee.

Italian espresso coffee mitigates the aggregation and condensation of Alzheimer's associated Tau protein

Roberto Tira[1], Giovanna Viola[1], Carlo Giorgio Barracchia[1], Francesca Parolini[1], Francesca Munari[1], Stefano Capaldi[1], Michael Assfalg[1], Mariapina D'Onofrio[1*].

[1] Department of Biotechnology, University of Verona, Strada le Grazie 15, 34134 Verona, Italy

*Corresponding author at: Department of Biotechnology, University of Verona, Strada le Grazie 15, 34134 Verona, Italy

E-mail address: mariapina.donofrio@univr.it

Keywords: Tau protein, coffee extract, protein aggregation, NMR, bioactive molecules, liquid-liquid phase separation, Alzheimer's disease

ABSTRACT

Espresso coffee is among the most consumed beverages in the world. Recent studies report a protective activity of the coffee beverage against neurodegenerative disorders such as Alzheimer's disease. Alzheimer's disease belongs to a group of disorders, called Tauopathies, which are characterized by the intraneuronal accumulation of the microtubule-associated protein Tau in fibrillar aggregates. In this work, we characterized by NMR the molecular composition of the espresso coffee extract and identified its main components. We then demonstrated with in vitro and in cell experiments that the whole coffee extract, caffeine, and genistein have biological properties in preventing aggregation, condensation, and seeding activity of the repeat region of Tau. We also identified a set of coffee compounds capable of binding to preformed Tau fibrils. These results add insights into the neuroprotective potential of espresso coffee and suggest candidate molecular scaffolds for designing therapies targeting monomeric or fibrillized forms of Tau.

Graphical abstract

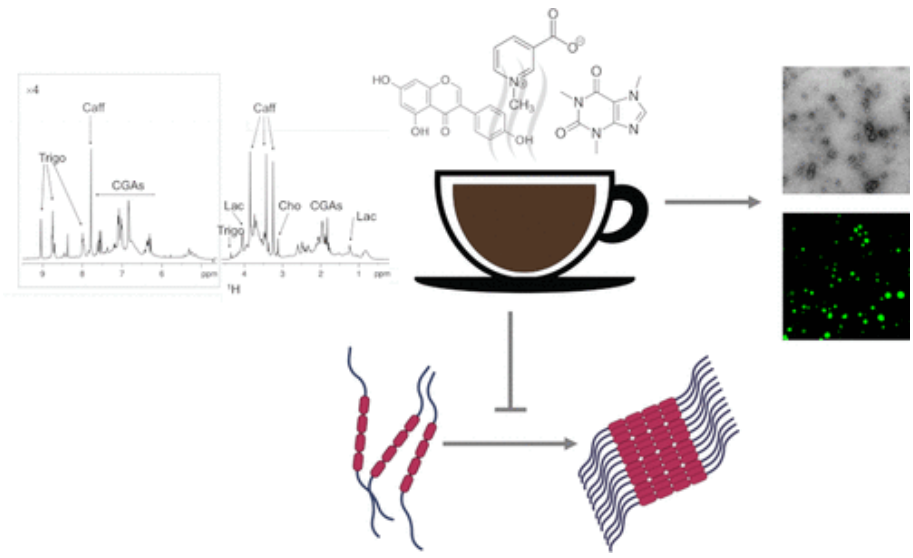

INTRODUCTION

Espresso coffee is among the best known beverages worldwide, and drinking espresso has become a habit in many countries due to its pleasant taste. For many years, coffee consumption was associated with health risks; however, recent studies showed that when consumed in moderation, this soft drink could have beneficial effects on human health thanks to its biological properties.[1,2] The analysis and review of observational studies present in the literature suggest that consuming coffee could be advantageous against a number of chronic diseases, including some cancers (liver, colorectal, endometrial, and prostate),[3] metabolic diseases (type-2 diabetes and metabolic syndrome), and neurological disorders (Parkinson′s disease, Alzheimer′s disease, and depression).[1] In particular, numerous studies report that moderate and, sometimes, even high coffee consumption exerts a neuroprotective action against two of the most common neurodegenerative diseases, i.e., Parkinson′s and Alzheimer′s.[4–6] Many coffee compounds display beneficial properties in alleviating disease symptoms, for instance by reducing cognitive and memory impairment,[2] as antioxidants,[7] or by preventing amyloid formation and neurotoxicity.[8] The coffee beverage consists of more than a thousand compounds; the beverage as a whole and its components show a bioactive role, and therefore, coffee is considered a potential functional food.

Tauopathies is the term used to define a set of neuro- degenerative disorders with symptoms of dementia and parkinsonism.[9] Among the Tauopathies identified so far, Alzheimer′s disease is the most common, with a worldwide prevalence of 50 million people, especially the elderly (age > 65 years). The primary feature of Tauopathies is the abnormal accumulation of the microtubule-associated protein Tau in the brain (neurons or glial cells or both). The mechanisms underlying the onset of these diseases are complex and currently unclear, but Tau aggregation and spreading are thought to play a crucial role. The microtubule-associated protein Tau (hereafter Tau) binds to microtubules and regulates their assembly and axon outgrowth and integrity. Tau is expressed in six isoforms in the adult human brain, the most abundant being 441 amino acids long (Figure 1);[10] it is an intrinsically disordered protein, highly soluble and with little tendency to aggregate. The repeat region is responsible for binding to microtubules and contains two hexapeptide

motives, at the beginning of the second (R2) and third (R3) repeats, which drive Tau aggregation (Figure 1). The dissociation of Tau from microtubules is considered the leading cause of its pathological accumulation; however, the molecular mechanisms involved in the early events of pathogenesis are still not completely clear.[11] Due to the increase in the elderly population, the number of patients with Tauopathies expected in the future years is very high: this will represent a high socio- economic burden worldwide unless the means to prevent or treat these diseases are found. It is worth emphasizing that these diseases are currently incurable, as there are no effective disease-modifying treatments. In this complex scenario, nutraceuticals offer an attractive means for prevention strategies or for designing food-based therapeutics to interfere with the progression of the disease and mitigate its symptoms. Green and roasted coffee extracts and their main compounds have been previously investigated for their ability to target Aβ oligomers, involved in the progression of Alzheimer's disease, hindering their fibrillization and neurotoxicity.[8]

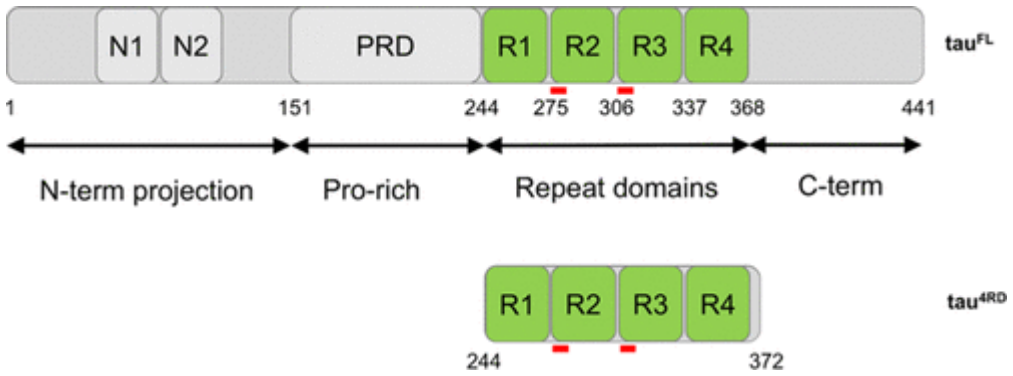

Figure 1. Domain organization of full-length Tau, Tau^{FL}, and of the shorter construct comprising the four-repeat region, Tau^{4RD}. Red bars indicate the position of hexapeptide motifs known as aggregation nuclei.

In this work, we started with the NMR characterization of the molecular composition of the coffee extract to identify its main components. Next, we interrogated the biological properties of the whole coffee extract and of selected components, i.e., caffeine and genistein, and observed their ability to prevent aggregation, condensation, and the seeding activity of the Tau protein. Moreover, we identified molecules among coffee compounds, able to bind to preformed fibrils of Tau. Taken together,

these results add insights into the neuroprotective potential of espresso coffee and suggest candidate molecular scaffolds for designing therapies targeting monomeric or fibrillized forms of the Tau protein.

MATERIALS AND METHODS

Chemicals.

Trigonelline (analytical standard) was purchased from Sigma-Aldrich (St Louis, MO); caffeine (99% purity), genistein (99% purity), and theobromine (99% purity) were purchased from Alfa Aesar by Thermo Fisher Scientific (Kandel, Germany). Stock solutions of all compounds were prepared in mQ H_2O at a concentration of 1 mg/mL and stored at −20 °C. All other reagents were purchased from Sigma-Aldrich (St Louis, MO) unless otherwise indicated.

Espresso Extraction.

The medium roast ground coffee used in this study is a blend of Arabica coffee from South America and Robusta coffee from Africa and Southwest Asia (commercial brand). The espresso coffee extract was obtained from 15 g of powder using a two-cups coffee machine (Gaggia espresso machine, Gaggia Milano, Italy) for a final volume of 80 mL of beverage. The extraction lasted for 30 s at 80 °C in mQ H_2O. The final product was distributed in 15 mL Falcon tubes, freeze-dried, and stored at +4 °C.

Recombinant Tau^{4RD} Expression and Purification.

All Tau^{4RD} variants were expressed in BL21(DE3) cells grown in LB medium, at 37 °C for 5 h with 0.5 mM IPTG. Protein purification was achieved by thermal treatment of the soluble bacterial extract (80 °C) followed by the SP-ion exchange chromatography step.[12−14]

Thioflavin-T Aggregation Assay.

Solutions of the 50 μM Tau^{4RD} protein in 20 mM sodium phosphate buffer at pH 7.4, 50 mM NaCl, 1 mM DTT, 0.02% NaN_3, and protease inhibitors with EDTA

were incubated in the absence or presence of coffee extract or different compounds in 96-well dark plates at 37 °C for 40 h. Heparin and Thioflavin-T (ThT) were added to the sample solutions in a molar ratio of 1:1 with respect to the protein. Fluorescence measurements (λ_{ex}.: 450 nm and λ_{em}: 482 nm) were performed with a Tecan Infinite M200 Pro Microplate Reader (Tecan Group AG, Männedorf, Switzerland) with cycles of 30 s of orbital shaking at 140 rpm and 10 min of rest before the fluorescence reading throughout the incubation, as described in previous work.[15] The fluorescence intensity and lag- phase duration of four replicates of each sample were analyzed with GraphPad Prism 8.2 software (GraphPad Software, San Diego, California, www.graphpad.com). Any pre-existing aggregate was removed by filtering the protein stock solutions through a 100 MWCO cut-off filter (Sartorius Stedim Biotech GmbH, Göttingen, Germany), before the aggregation reaction. Error bars of ThT curves correspond to standard deviations of four independent experiments.

Sample Preparation for CD and TEM Analysis.

Solutions of the 50 μM filtered Tau^{4RD} protein in 20 mM sodium phosphate buffer at pH 7.4, 50 mM NaCl, 1 mM DTT, 0.02% NaN_3, and protease inhibitors with EDTA were incubated in the absence or presence of coffee extract or different compounds in static conditions at 37 °C for 48/72 h using heparin at a 1:1 molar ratio as the aggregation initiator.

CD Analysis.

Circular dichroism (CD) spectra were collected using a Jasco J-1500 spectropolarimeter equipped with a Peltier-type cell holder for temperature control (Jasco, Easton, MD). Solutions containing Tau^{4RD} aggregates were diluted in 20 mM sodium phosphate buffer, pH 7.4, to a final concentration of 6 μM. Far-UV spectra (190−260 nm) were recorded at 25 °C with a scan rate of 50 nm min^{-1}, a bandwidth of 1 nm, and an integration time of 2 s, in 0.1 cm cuvettes. Three spectra accumulations were collected and averaged for each sample at different times (0 and 72 h). The spectrum of the buffer alone (with or without the compounds) was subtracted

from the spectrum of the corresponding sample. Data were analyzed with Spectra Manager and graphs were generated with GraphPad Prism 8.2 software.

TEM Analysis.

For transmission electron microscopy (TEM) measurements, 10 μL of Tau^{4RD} aggregates (obtained after 48 h incubation with or without coffee extract or different compounds) were washed and diluted in mQ H_2O to a final concentration of 5 μM (monomer concentration). 30 μL of diluted aggregates were adsorbed onto a film grid (400 mesh) and stained for 2 min with 2% uranyl acetate. A Tecnai G2 (FEI) transmission electron microscope instrument operating at 100 kV was employed to analyze the samples. Images were acquired with a Veleta digital camera (Olympus Soft Imaging System, Münster, Germany) using FEI TIA software (version 4.0). Fibril characteristics were analyzed with ImageJ software (v2.0).

NMR Spectroscopy.

NMR experiments were acquired at 600 MHz on a Bruker Avance III spectrometer equipped with a triple resonance TCI cryoprobe or on a Bruker Avance NEO spectrometer equipped with a cryoprobe Prodigy TCI. All NMR spectra were processed with Topspin 4.1.1 software (Bruker, Karlsruhe, Germany) and analyzed using NMRFAM-SPARKY. One-dimensional ^1H spectra were acquired at 25 °C on samples dissolved in deuterated buffer (20 mM sodium phosphate at pH 7.4, 50 mM NaCl). A total of 8 transients were acquired over a spectral width of 9615 Hz and 32,768 complex points with a recycle delay of 4 s. Saturation transfer difference (STD) experiments were acquired at 600 MHz, with 8 scans at 25 °C. Tau^{4RD} aggregates (obtained after 48 h incubation) were extensively washed to eliminate any other species eventually present. Selective saturation of the protein at 0.4 ppm frequency was carried out with a 2 s pulse train (40 Gaussian-shaped pulses of 50 ms separated by 1 ms intervals, field strength of 90 Hz) included in the relaxation delay, and a 25 ms spin-lock was used to reduce the broad background protein signal. The STD spectrum was obtained by subtracting the on-resonance spectrum from the off-resonance spectrum. WaterLOGSY experiments were performed with a 180° inversion pulse applied to the water signal at ~4.7 ppm using a Gaussian-shaped

selective pulse of 7.5 ms. Each WaterLOGSY spectrum was acquired with 240 scans and a mixing time of 1.5 s. In all experiments, water suppression was obtained using the excitation sculpting pulse scheme. Experiments with samples containing only the free compounds were acquired as a reference to verify the binding.

Tau^{4RD} Condensates in the Presence of Coffee, Caffeine, and Genistein.
Tau^{4RD} was mixed with a small amount (1.2% of the total protein) of Tau^{4RD} labeled with fluorescein isothiocyanate (FITC) or with Alexa Fluor 488 (Thermo Fisher Scientific) to report its liquid−liquid phase separation, as previously reported.[16] Liquid−liquid phase separation of Tau^{4RD} was induced using heparin, in the absence or presence of espresso coffee, caffeine, or genistein at different concentrations (35−280 μg/mL). Where indicated, coffee, caffeine, and genistein were added to already-formed droplets (after 5 min). In all samples, 35 μM protein in 20 mM sodium phosphate buffer, pH 6.0, 30 mM NaCl, and 5 mM DTT was mixed with 8.75 μM heparin. For phase separation imaging, 7 μL of the solution was spotted onto a microscope slide, covered with a circular coverslip, and sealed with nail polish. Condensate images were acquired on a Leica TCS SP5 AOBS microscope to visualize the formation of droplets over time. Image analysis was performed with FIJI ImageJ software (v2.0).

Sample Preparation for Cellular Viability and Seeding- Based Aggregation Assays.
Solutions containing the 100 μM Tau^{4RD} protein (in 20 mM sodium phosphate buffer at pH 7.4, 50 mM NaCl, 1 mM DTT, and protease inhibitor with EDTA) were filtered and then incubated in the absence or presence of 50 or 400 μg/mL coffee extract in static conditions at 37 °C for 24 h. The protein and heparin were in a 4:1 molar ratio. After the incubation of Tau^{4RD} in buffer or with coffee extracts, a centrifugation step was performed at 20,000*g* for 30 min to separate the fibrils as a pellet (Figure 7A). The sample obtained from Tau^{4RD} incubated in the presence of 400 μg/mL coffee extract did not contain insoluble aggregates and therefore the first centrifugation did not produce pellets. The sample was further treated as described below. The solution was separated by filtration through a 100 kDa MWCO filter to isolate the monomeric forms (Figure 7A red frame, filtrate) from the higher

molecular weight aggregates of Tau^{4RD} (Figure 7A red frame, retentate). All samples were verified by sodium dodecyl sulfate−polyacrylamide gel electrophoresis (SDS−PAGE, Figure S12A).

Seeding-Based Aggregation and Immunoblot Analysis.

Nontumoral human embryonic kidney cell lines (HEK293) stably expressing human full-length Tau P301L fused with GFP[17] were cultured in DMEM high glucose (Aurogene) supplemented with 10% FBS (fetal bovine serum, Aurogene), antibiotics (100 U of penicillin/ mL, and 100 U of streptomycin/mL), and 1% L-glutamine (Aurogene) at 37 °C, 5% CO_2 in a humidified incubator. Once 70−80% confluence was reached, the cells were collected using trypsin, counted, and seeded for the experiments. HEK293 cells were treated with 5 μM Tau^{4RD} fibrils obtained in the absence or presence of 50 μg/mL coffee extract (pellet) or with the filtrate and the retentate obtained as described from Tau^{4RD} aggregated in the presence of 400 μg/mL coffee extract. Lipofectamine LTX at 0.5% was employed as a transfection agent. For immunoblot analysis, 100,000 cells/well were seeded in a 24-well plate. After treatment, the cells were first scraped into Triton lysis buffer (1% Triton X-100 in 50 mM Tris, 150 mM NaCl, pH 7.6) containing protease and phosphatase inhibitors and incubated on ice for 15 min. Lysates were centrifuged at 20,000*g* for 30 min at 4 °C. Supernatants were kept as the "Triton 1 fraction," whereas the pellets were washed once in Triton lysis buffer, separated again with centrifugation, resuspended in SDS lysis buffer (1% SDS in 50 mM Tris, pH 7.6) at a volume that is 1/3 of the Triton lysis buffer, and heated for 15 min at 80 °C. After centrifugation at 20,000*g*, supernatants were kept as the "SDS fraction". Protein concentrations of Triton 1 fractions were determined with the BCA assay. According to protein concentration in the Triton 1 soluble fraction (considered as the protein standard), a proper amount of the SDS fraction was separated by SDS−PAGE and probed with the TAU-5 antibody, specific for the human Tau^{FL}. Immunoreactive proteins were detected using the ECL prime western blotting detection reagents (Ge Healthcare) according to the manufacturer′s instructions.

Cell Viability Assay.

H4-APPswe neuroglioma cells (stably expressing the APP Swedish mutation) were a generous gift from Prof. Mario Buffelli. The cell line was cultured in a humidified atmosphere of 5% CO_2 and passaged in a complete growth medium: Dulbecco′s modified Eagle medium (DMEM) high glucose (Aurogene) containing 10% fetal bovine serum (FBS, Aurogene) supplemented with antibiotics (1% penicillin/streptomycin) and 1% glutamine (Aurogene). Once 70−80% confluence was reached, the cells were collected using trypsin, washed, and counted. Cell viability after Tau^{4RD} sample treatment was evaluated by the reduction of the tetrazolium salt MTT (1-(4,5-dimethylthiazol-2-yl)-3,5-diphenylformazan, thiazolyl blue formazan), following the manufacturer′s protocol. Briefly, 1000 H4-APPswe cells/well were seeded in their exponential growth phase in a flat-bottom 96-well plate and were incubated at 37 °C in a 5% CO_2 incubator.

After 24 h, the cells were treated with Tau^{4RD} samples (pellet or retentate at 5 μM) obtained as previously described. After 48 h of treatment, the cells were incubated with 0.5 mg/mL MTT for 3 h at 37 °C, and insoluble formazan crystals were dissolved in 200 μL of DMSO. The absorbance measurement at 560 nm was employed to evaluate the reduced MTT. Experiments were performed in triplicate on a Tecan Infinite M200 Pro Microplate Reader.

Statistical Analysis.

Statistical analysis was applied to cell viability data and TEM morphological data on fibrils. Any statistically significant difference between samples was determined using one- way ANOVA analysis of variance followed by Dunnett′s multiple comparison test to compare the means from sample groups against a control group. The significance threshold was set at $P = 0.05$. For the cell viability assay, measurements were performed in triplicates. For TEM analysis, 10−20 measurements (from different images) for each parameter were analyzed. All sets of samples comply with normal distribution for the D′Agostino and Pearson test. Standard deviation (SD) was homogeneous according to Brown−Forsythe and Bartlett′s tests.

For both analyses, P values were indicated as follows: * = 0.01− 0.05, ** = 0.001−0.01, *** = 0.0001−0.001, and **** <0.0001.

RESULTS

NMR Characterization of the Extract from Arabica and Robusta Coffee Beans.

Coffee samples were prepared with espresso extraction and examined by NMR spectroscopy in order to identify the main compounds constituting the beverage. The one-dimensional (1D) ^{1}H NMR spectrum of espresso brew (Figure 2A) exhibits a complex profile in which the proton resonances are considerably overlapped. The identification of the main metabolites was obtained from the analysis of one- (^{1}H) and two-dimensional (^{1}H–^{1}H TOCSY, ^{1}H–^{13}C HSQC) spectra and by comparison with previously reported data.[7,18,19] The assignment of compounds such as trigonelline, caffeine, lactate, and chlorogenic acids (CGAs) was obtained from the observation of typical patterns of signals. The profiling of the coffee extract revealed the presence of compounds that are commonly found in brews from Arabica and Robusta coffee.[7]

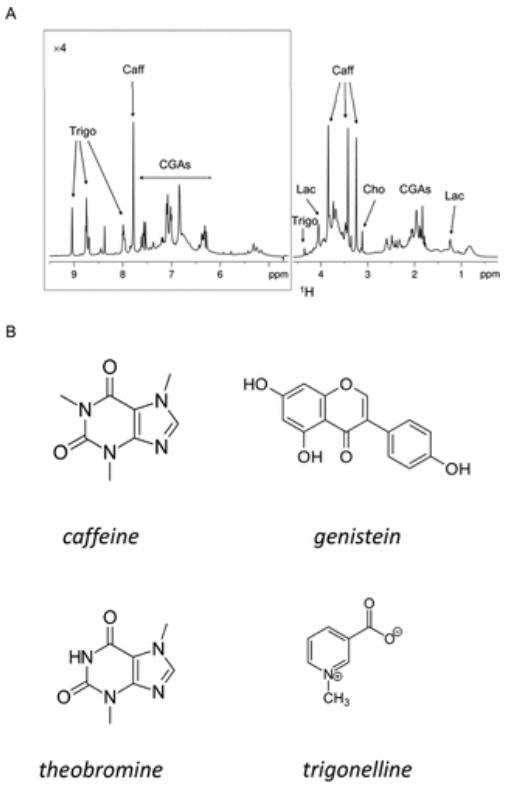

Figure 2. (A) ^{1}H NMR profile of 5 mg/mL lyophilized espresso coffee extract. The downfield spectral region (5–10 ppm) is displayed with 4-fold higher intensity than the highfield region for better visualization. The spectrum has been recorded at 600 MHz and 25 °C. Peak assignments are indicated. Caff: caffeine, Trigo: trigonelline, CGAs: chlorogenic acids, Lac: lactate, and Cho: choline. (B) Molecular structures of coffee-derived molecules analyzed in this study.

Coffee Extract and Single Compounds Influence the Aggregation Kinetics of Tau^{4RD}.

Following the identification of the main compounds contained in the coffee brew, we tested the impact of both the complex mixture and selected isolated compounds (Figure 2B) on protein Tau fibril formation. We chose to focus on some compounds found in coffee extracts: two alkaloids, caffeine and trigonelline, and an isoflavone compound, genistein.[8,20,21] Additionally, we employed the compound theobromine, a methylxanthine analogue to caffeine lacking the methyl group at position 1.

For aggregation experiments, we focused on a shorter construct of Tau, hereafter Tau^{4RD}, spanning residues Q244- E372 (Figure 1). Tau^{4RD} comprises the microtubule-binding region and most of the residues involved in the assembly of pathological filaments,[22] and it is widely used as a model system to test the aggregating properties of Tau.[23,24]

To assess the aggregation kinetics of Tau^{4RD} in the presence and absence of coffee extract, we performed a ThT fluorescence assay. The fluorescence of ThT increases upon binding to β-sheet-rich amyloid structures and its change over time allows us to monitor fibril formation. In the presence of a low amount of coffee extract (50 μg/mL), the aggregation kinetics of Tau^{4RD} followed a typical sigmoidal trend, comparable in shape to that observed for Tau^{4RD} alone; however, it represents a significantly extended lag phase and a decreased rate of fibril growth (Figure 3A and Table 1). Interestingly, in the presence of 400 μg/mL coffee extract, there was almost no increase in ThT fluorescence and the typical sigmoidal shape was not discernable. These observations suggest an inhibitory effect of the coffee extract on Tau fibril formation in a concentration-dependent manner (Figure 3A). This finding differs slightly from results described in a previous report,[25] in which an effect on Tau^{FL} fibrillization was observed only at a high concentration (200 μg/mL) of three different varieties of 100% Arabica instant coffee, while low concentrations (5 or 40 μg/mL) produced no or negligible variation of aggregation rates. We conclude that the specific coffee beans and the composition of the extracts determine a unique activity.

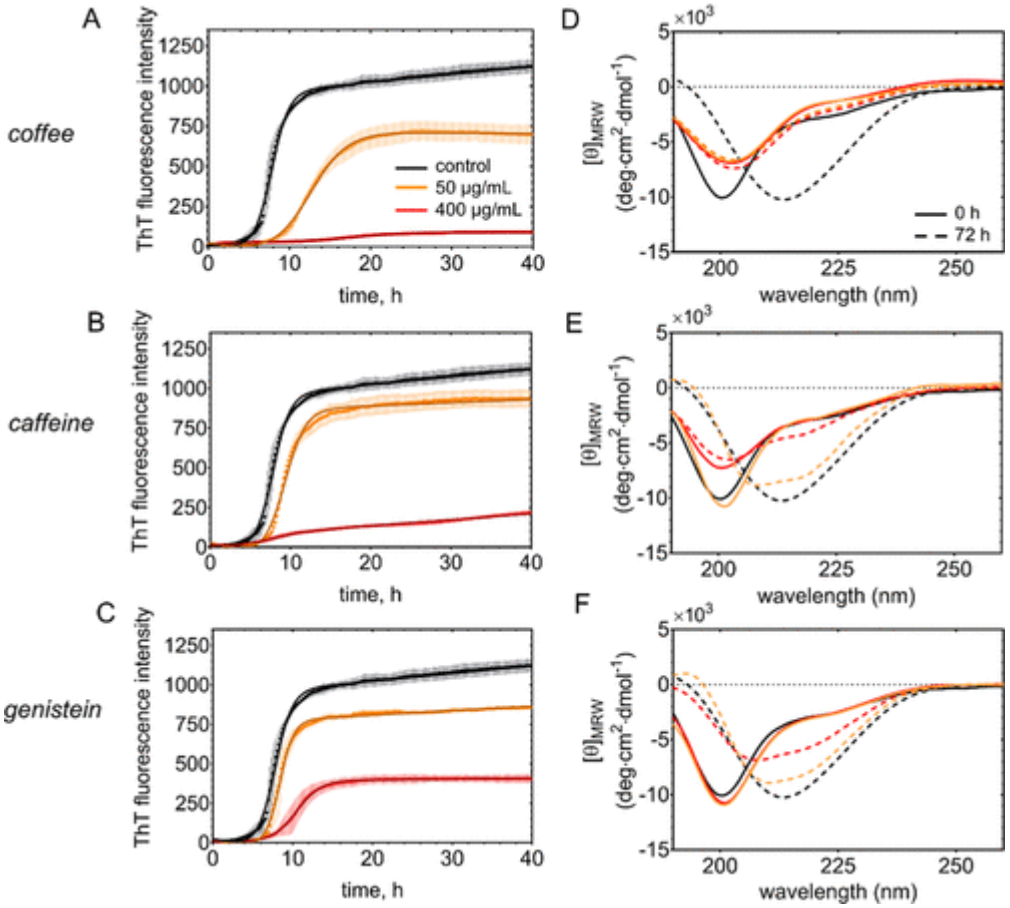

Figure 3. Time course of Tau conformational transitions. (A–C) ThT fluorescence-based aggregation kinetics curves measured on 50 µM Tau^{4RD} in the presence of coffee extract (A), caffeine (B), or genistein (C). Compound concentrations were 0 (black), 50 (orange), or 400 (red) µg/mL. Measurements were carried out on four replicates and data are reported as mean ± s.d. Solid lines correspond to the best-fit curves determined using an empirical sigmoid function. (D–F) Far-UV CD spectra recorded on 6 µM Tau^{4RD} in the absence or presence of coffee compounds. Measurements were performed immediately after sample preparation (continuous curves) and after 72 h (dotted curves) incubation of a concentrated stock (50 µM protein and 50 or 400 µg/mL compounds) in static conditions at 37 °C. Molar concentrations of compounds were 0.26 mM (50 µg/mL) and 2 mM (400 µg/mL) caffeine and 0.18 mM (50 µg/mL) and 1.5 mM (400 µg/mL) genistein.

Table 1. Kinetic Parameters for the Aggregation of Tau^{4RD}, Determined on the Basis of ThT Fluorescence Assays [a]. [a] $t_{0.5}$: midpoint of the transition; τ: elongation time constant; $t_{lag} = t_{0.5} - 2\tau$; nd: not determined.

	concentration (µg/mL)	$t_{0.5}$ (h)	τ (h)	t_{lag} (h)
control		7.85 ± 0.02	1.03 ± 0.02	5.79 ± 0.06
coffee	50	12.90 ± 0.06	2.09 ± 0.03	8.72 ± 0.12
	400	nd	nd	nd
caffeine	50	9.45 ± 0.03	1.17 ± 0.02	7.11 ± 0.07
	400	nd	nd	nd
genistein	50	8.43 ± 0.01	0.84 ± 0.01	6.75 ± 0.03
	400	10.50 ± 0.02	1.50 ± 0.01	7.50 ± 0.04
theobromine	50	9.10 ± 0.05	1.19 ± 0.04	6.72 ± 0.13
	400	8.46 ± 0.02	1.16 ± 0.02	6.14 ± 0.06
trigonelline	50	7.24 ± 0.02	1.00 ± 0.02	5.24 ± 0.06
	400	6.73 ± 0.01	0.56 ± 0.01	5.61 ± 0.03

Next, we tried to determine if any of the components of the coffee extract were responsible for the inhibitory activity toward fibril formation. To this aim, we analyzed the aggregation kinetics of Tau^{4RD} in the presence of increasing amounts of selected isolated molecules (Figures 3B,C and S1A,B). At a concentration of 50 μg/mL, the tested molecules showed moderate effects on fibril formation, with a consistently extended lag phase, except for trigonelline (Table 1). At a higher concentration (400 μg/mL), caffeine and genistein were found to strongly interfere with fibril formation. In particular, the ThT fluorescence response in the case of caffeine was very poor, similar to what was observed with the coffee extract (Figure 3A,B and Table 1). We also examined the effect of a mixture of the selected molecules at concentrations comparable to those estimated for the extract. The corresponding ThT fluorescence data indicate that the pool of compounds had some inhibitory effect on Tau^{4RD} fibril formation, albeit not as strong as that of the coffee extract (Figure S1E). In order to exclude that the observed inhibitory effects were due to an interaction of the selected compounds with ThT (the fluorescence probe) or with heparin (the aggregation inducer), we acquired ^{1}H NMR spectra of heparin or ThT in the absence and presence of different concentrations of each molecule (Figures S2−S5). The invariance of the signals of heparin or ThT, and of the compounds, indicated that no strong interactions occurred and that the effects observed during the fibrillization reactions originated from an interaction of the pure compounds with the protein substrate. The described experiments indicate that the ensemble of compounds constituting the coffee extract is more effective in inhibiting Tau^{4RD} fibril formation than any single component. Nonetheless, among the selected molecules, caffeine and genistein were capable to mitigate the process of Tau^{4RD} aggregation.

Conformational Transitions of Tau^{4RD} Analyzed by CD Spectroscopy.

The maturation of amyloid fibers is triggered by the formation of aggregates characterized by a β- sheet secondary structure. To assess the effects of the coffee extract and of bioactive compounds on the conformational transitions of Tau^{4RD} during aggregation, we acquired circular dichroism (CD) spectra and examined their overall shapes. Monomeric Tau^{4RD} displays a far-UV CD spectrum typical of

disordered polypeptides, characterized by a negative ellipticity peak centered at about 200 nm[23] and the absence of strong signals at 220 nm (Figure 3D−F, black continuous line). This feature of the spectrum was maintained in all CD traces at the starting points of aggregation, independently of sample condition (Figure 3D−F), thus showing the inability of the compounds to modify the structure of soluble Tau^{4RD}. Changes in the secondary structure of Tau^{4RD} were monitored after 72 h of incubation with heparin (Figure 3D−F, black dashed lines). The CD spectrum of the aggregated protein was characterized by a substantial change in shape and a shift of the curve minimum to longer wavelengths (~215 nm), which is indicative of a structural reorganization consistent with the formation of β-sheet structures.

The latter behavior was retained in samples of Tau^{4RD} co-incubated with theobromine and trigonelline (Figure S1C,D), indicating that these compounds were unable to prevent aggregation. By contrast, a different behavior was observed when Tau^{4RD} was incubated with genistein or caffeine, dependent on the concentration of the compounds (Figure 3E,F). At low molecule concentrations (Figure 3E,F orange lines), the conformational transformation of Tau^{4RD} was affected to a small extent. At a higher concentration of genistein, we still observed a shift of the peak minimum but with smaller negative ellipticity. The impact of caffeine appeared even more pronounced: at 400 μg/mL concentration, the CD spectrum recorded after 72 h of incubation was only slightly altered from its initial shape (Figure 3E red lines), implying the prevalence of a disordered structure as a result of the inhibitory effect of caffeine on aggregation. Finally, the effect of coffee extract was quite strong, regardless of the concentration. The CD spectra were characterized by a reduced peak minimum suggestive of scattering effects in the samples and retained the initial shape after 72 h of incubation (Figure 3D). The conformational transitions of Tau^{4RD} after 72 h of incubation with 50 μg/mL coffee extract (Figure 3D) were not detected by CD, possibly due to the complex composition of the sample and the heterogeneous nature of polymorphic nonfibrillar and fibrillar aggregates, which would not correspond to a unique secondary structure signature.

Overall, the results of CD experiments confirm that the compound mixture of coffee brew prevents the formation of ordered fibrillar structures. The conformational analysis agrees with the ThT analysis and indicates a variable impact on the

aggregation properties of Tau^{4RD} exerted by the coffee extract and by the single bioactive compounds.

Morphological Analysis of Tau^{4RD} Aggregates.

As a next step, we performed a TEM analysis of Tau^{4RD} aggregates obtained in the absence or presence of coffee extract or single compounds (Figures 4 and S6). The collected images clearly show that Tau^{4RD} was able to form abundant mature fibrils after 48 h of incubation in the presence of heparin. Furthermore, TEM analysis confirmed the different abilities of the tested compounds to interfere with Tau^{4RD} fibril formation. The presence of trigonelline and theobromine had a modest impact on Tau^{4RD} fibril assembly, and long straight and twisted fibrils were observed at all tested concentrations (Figure S6); these data agree with aggregation kinetics results obtained by ThT fluorescence and with CD analysis. A different behavior was observed when caffeine and genistein were present during the fibrillization process (Figure 4D−G). Both molecules displayed significant inhibitory activity toward Tau^{4RD} fibrillization, with a stronger effect at a higher compound concentration. In the presence of 50 μg/mL compounds, long fibrils could still form but short filaments were also visible. Upon increasing the amount of the compounds to 400 μg/mL, almost all structures visible in TEM images were short filaments with a morphology comparable to that of Tau^{4RD} alone (Figure S7).

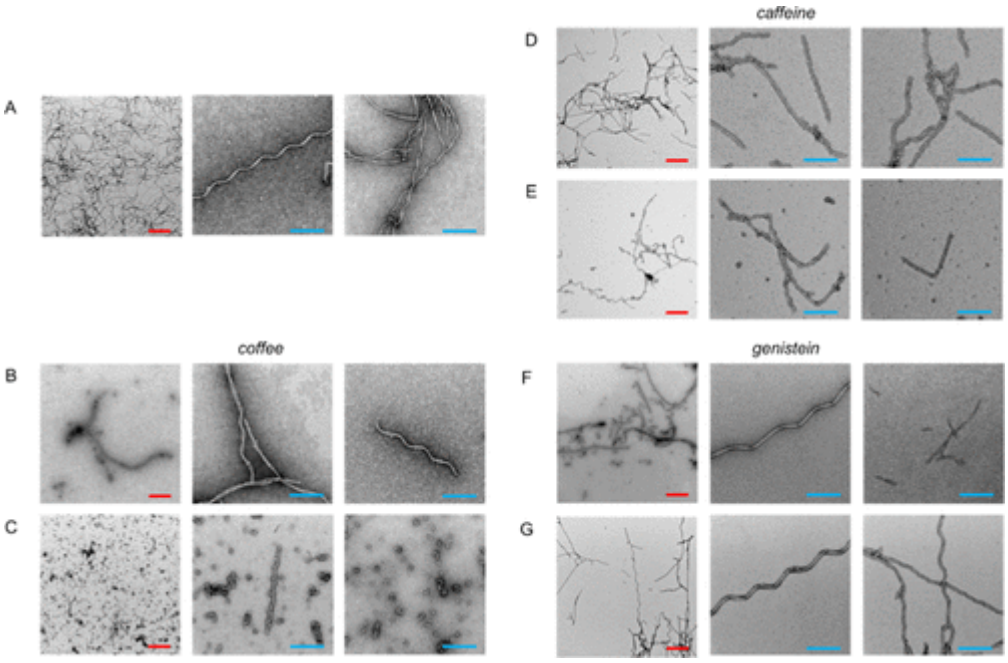

Figure 4. Transmission electron microscopy of Tau^{4RD} aggregates. Representative TEM images of Tau^{4RD} aggregates in the presence of different concentrations of coffee extract or single compounds. Samples contained Tau^{4RD} in buffer (A) with 50 μg/mL (B) or 400 μg/mL (C) coffee extract, 50 μg/mL (D) or 400 μg/mL (E) caffeine, 50 μg/mL (F) or 400 μg/mL (G) genistein. The protein was 50 μM. Samples were incubated for 48 h at 37 °C in static conditions. Scale bars are 500 nm (red) and 200 nm (light blue).

The effect of coffee extract was remarkable: even in the presence of low quantities of the mixture, the formation of long fibrils was compromised and only few short fibrils were visible (Figure 4B,C). The coffee extract at high concentrations strongly interfered with fibril formation: the few observable fibrils showed a modified morphology, and a large amount of spheroidal oligomeric species, with a diameter of about 20 nm, were observed in the images (Figures 4B,C and S7). The morphological analysis of all of the samples showed that the overall shape of fibrils of Tau^{4RD} alone (Figure S7) was maintained also when the fibrils were formed in the presence of the selected molecules; the differences observed in some structural parameters are attributable to the different quality of images rather than to a real morphological difference. The results obtained using a coffee extract generally agree with previously reported data obtained on Tau^{FL} in the presence of instant coffee brews;[2525] however, no influence of caffeine on fibril growth was found in the previous study. The discrepancy could be due to the different Tau constructs used in the two studies. It is worth noticing that another work[26] provided evidence that full-length Tau can interact with caffeine. The docking study indicated that the

R2 and R4 repeats of the MBD of Tau (Figure 1) are the most likely binding sites for caffeine, and localized surface plasmon resonance spectroscopy data revealed that the binding of caffeine molecules to Tau significantly reduced the formation of Tau−Tau complexes. These results could explain our finding that caffeine inhibits fibril formation, as the assembly of a Tau−Tau complex is a prerequisite for protein aggregation. Moreover, the presence of spheroidal aggregates in TEM images of Tau^{4RD} obtained in the presence of 400 μg/mL coffee extract or caffeine is in agreement with the decreased rate constants determined from ThT experiments. Altogether, the collected pieces of evidence suggest that fibril elongation and possibly secondary nucleation processes are inhibited in particular by caffeine and bioactive compounds of coffee extracts.

Condensation-Linked Aggregation of Tau^{4RD}.

Accumulating evidence indicates that Tau is able to form and participate in biomolecular condensates.[24,27,28] Cellular bio- molecular condensates often contain proteins and RNA, they are thought to form through liquid−liquid phase separation (LLPS) and exhibit liquid-like properties.[29] LLPS has been recognized as one of the key organizing principles by which eukaryotic cells control molecular localization and biochemical reactions.[30] However, condensates are metastable and may transition from liquid-like to gel or solid-like states.[30] In particular, age-related changes and pathological insults may promote abnormal phase transitions.[31] The observation that Tau undergoes LLPS has stimulated efforts to understand whether condensation may be linked to pathological aggregation.[24,27,28]

Polyanionic cofactors, including RNA and heparin, stimulate condensation of Tau in vitro.[32] Heparin is commonly used as an aggregation inducer, and it is increasingly employed in model systems to investigate condensation-linked aggregation.[16,33,34] Indeed, heparin-induced liquid condensates of Tau^{4RD} proved unstable and were found to rapidly evolve into irregularly shaped assemblies.[16,35] Here, we prepared the condensates in the absence or presence of coffee extracts or single bioactive compounds and observed the liquid droplets by fluorescence microscopy using Alexa488-Tau^{4RD} as a reporter molecule (Figures 5 and S8−S10). Small spherical droplets formed immediately after mixing Tau^{4RD} and heparin, then grew

over the following 5 min, and partly dissolved or lost their regular shape after 30 min (Figure 5A).

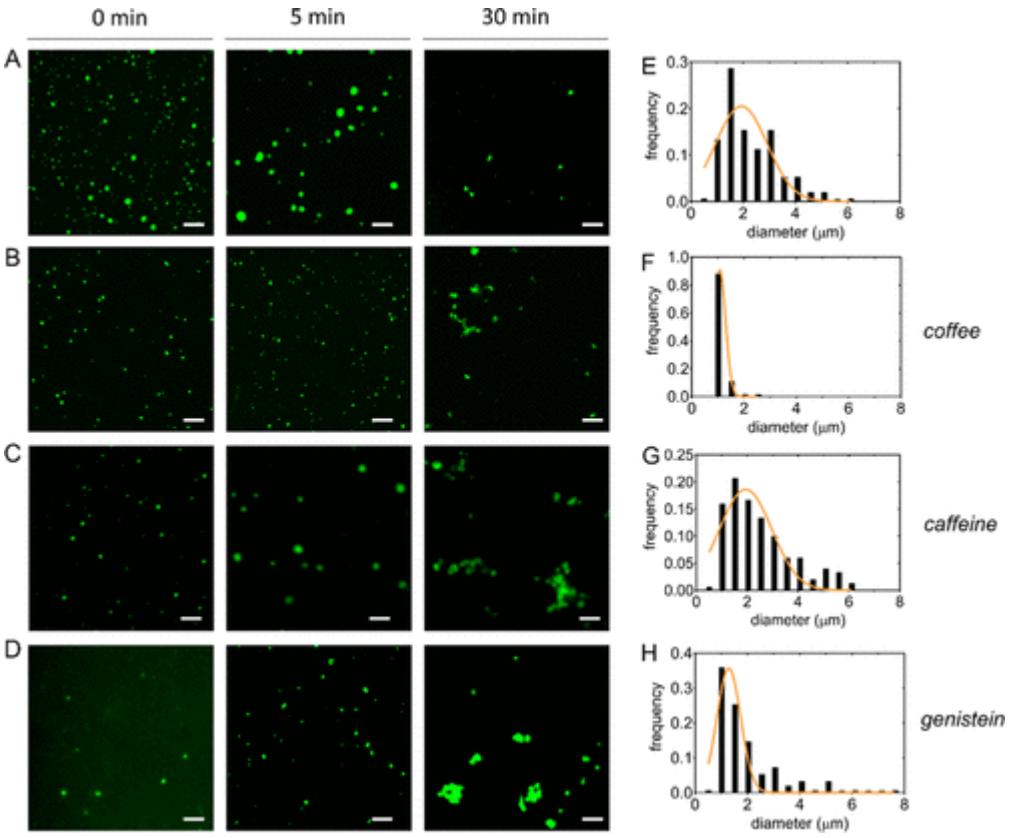

Figure 5. Influence of coffee compounds on Tau condensation. Representative fluorescence microscopy images displaying condensates of Tau^{4RD}/heparin in simple buffer (A) or in the presence of 280 μg/mL coffee extract (B), caffeine (1.4 mM) (C), and genistein (1 mM) (D). Images were acquired at 0, 5, and 30 min after mixing components. Protein was 35 μM and heparin was 8.75 μM. The scale bar is 10 μm. (E–H) Distribution plots of droplet diameters corresponding to conditions of panels (A–D) at 5 min; orange lines are best-fit log-normal curves.

A similar evolution was observed in the presence of bioactive compounds; however, few differences emerged (Figure 5B− D): the size distribution of droplets in the presence of caffeine was similar to the control; by contrast, narrower distributions and smaller mean sizes were observed in the case of coffee extract and genistein. The endpoint (30 min) images displayed irregular assemblies for coffee and caffeine, while clustered spherical droplets appeared in the case of genistein. We further investigated if the bioactive compounds were able to perturb preformed condensates (Figures S8D,E, S9D,E, and S10D,E). We observed that condensates were minimally perturbed by the subsequent addition of compounds, with the

exception of the case of 280 μg/mL genistein, which appeared to promote the coalescence of initially formed droplets into larger condensates.

In summary, the tested compounds did not dramatically impact the formation and evolution of Tau^{4RD}/heparin condensates with two main exceptions: coffee extracts prevented the formation of larger droplets, and concentrated genistein disfavored the aggregation-linked dispersion and transformation of droplets. This finding suggests that the coffee extract can influence the physicochemical properties of a condensate, modulating its stability and maturation, with important implications for disease-related condensation, an aspect that warrants further scrutiny.

NMR-Based Assessment of the Binding of Coffee Extract and Caffeine to Tau^{4RD} Fibrils.

The identification of soluble molecules able to interact with preformed fibrils is attracting increasing attention, as it opens new options for the design of novel therapeutics or specific probes for the diagnosis of a variety of neurodegenerative disorders.[36] We therefore investigated the ability of coffee extract and caffeine to recognize and bind preformed Tau fibrils by employing NMR spectroscopy, specifically a combination of STD[37] and WaterLOGSY experiments.[38] These experiments are quite powerful for assessing the interaction between a small molecule and a high-molecular-weight species. The latter are, in this case, the preformed Tau fibrils dissolved in deuterated phosphate buffer. Both STD and WaterLOGSY are based on intermolecular nuclear Overhauser effects (NOEs) to the ^{1}H nuclei of a ligand transiently bound to a large biomolecule.[39] The STD spectra of the coffee extract were acquired in the presence and absence (control experiment) of the protein fibrils, setting the on-resonance frequency at 0.4 ppm, to achieve saturation of protein aliphatic resonances. The signals in the STD spectrum (obtained by subtracting the on- resonance from the off-resonance spectrum) of the coffee extract contained several NMR signals (Figures 6A,E and S11A); however, the comparison with the control experiment acquired in the absence of fibrils revealed that only a subset of peaks experienced a signal build-up. Thus, a group of atoms of the molecules present in the coffee extract received saturation transfer from the protein via NOE, proving their interaction with the aggregates.[37] We considered the results

obtained with STD experiments definitive only if confirmed by WaterLOGSY experiments acquired in the same conditions (Figure 6C,E).[39,40] In the case of WaterLOGSY, the ^{1}H nuclei of bulk water are excited, and the magnetization is transferred from transiently bound water ^{1}H to protons of a small molecule bound to the protein.[38] Also, in the WaterLOGSY spectrum, a group of peaks experienced a signal build-up with respect to the control experiment. The comparison of the signals in STD and WaterLOGSY experiments with the ^{1}H NMR spectrum of the coffee extract (Figure 6E) clearly indicates that caffeine and chlorogenic acids were able to interact with fibrils. To further prove the ability of caffeine to interact with Tau^{4RD} fibrils, the STD and WaterLOGSY experiments were repeated on the pure compound in the same conditions (Figures 6B,D,F and S11B). All of the NMR peaks of caffeine experienced a signal build-up in the two experiments, thus confirming the ability of this bioactive molecule to bind to preformed Tau^{4RD} fibrils.

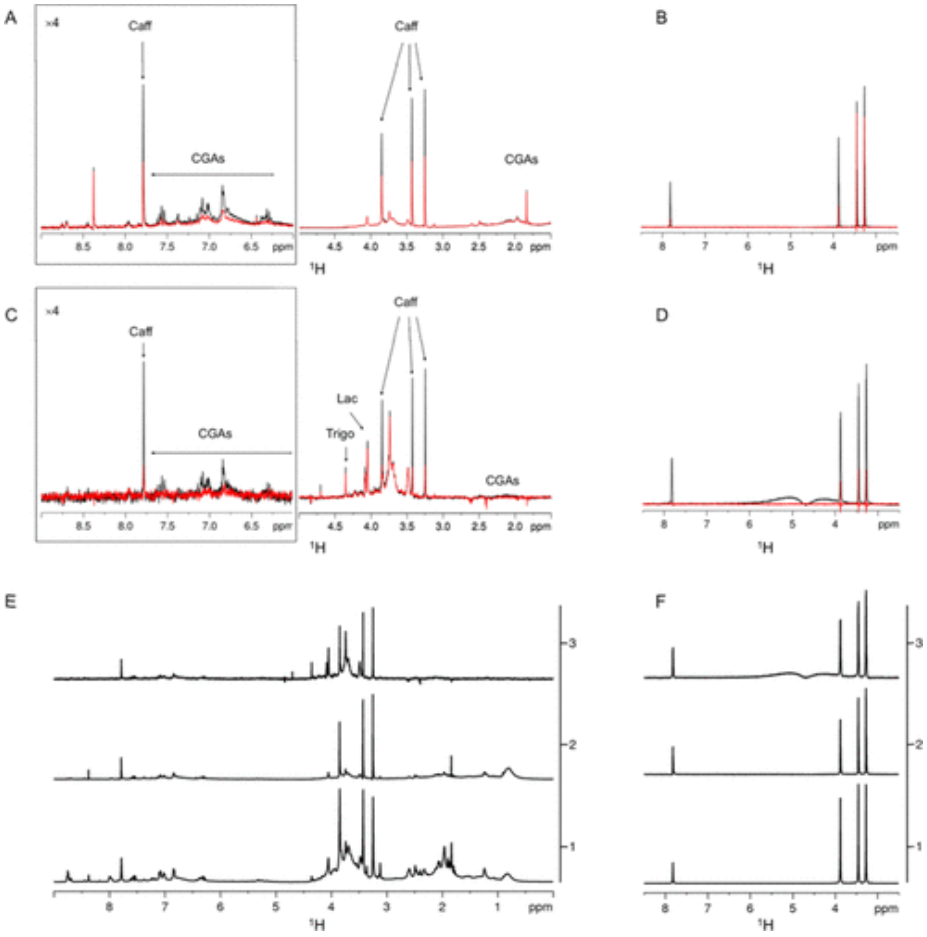

Figure 6. Interaction of coffee compounds with Tau aggregates. Saturation transfer difference (A, B) and WaterLOGSY (C, D) NMR spectra acquired on a 5 mg/mL espresso coffee mixture (A, C) or 0.8 mg/mL (4 mM) caffeine (B, D) in the absence (red) and presence (black) of Tau^{4RD} filaments (80 µM monomer) in 20 mM deuterated phosphate buffer, pH 7.4 at 25 °C. The downfield regions in (A, C) are displayed with four-fold higher intensity compared to the highfield regions on the right. (E, F) ^{1}H NMR spectrum of 5 mg/mL coffee (E) or 0.8 mg/mL caffeine (F) in 20 mM deuterated phosphate buffer, pH 7.4 (1), STD (2), and WaterLOGSY (3) spectra acquired on 5 mg/mL coffee (E) or 0.8 mg/mL caffeine (F) in the presence of Tau^{4RD} filaments.

Taken together, the NMR data provide clear evidence that specific bioactive molecules present in the coffee extract, i.e., caffeine and chlorogenic acids, can interact with preformed fibrils of Tau^{4RD}.

Coffee Extract Modulates Tau-Mediated Cytotoxicity and Intracellular Tau Accumulation.

The above reported data point to the ability of the coffee extract to interfere with Tau filament formation in vitro, redirecting the assembly of Tau into off-pathway amorphous oligomeric species. We therefore decided to test the toxicity of Tau^{4RD} aggregates formed in the absence and presence of different amounts of coffee

extract. To this aim, neuroglioma-derived H4swe cells were treated for 48 h with three different samples obtained as depicted in Figure 7A. Fibrils were obtained by preincubating Tau^{4RD} with heparin (4:1 ratio) and 50 μg/mL coffee extract and then sedimented by centrifugation (Figure 7A, orange frame, and S12A), showed decreased toxicity compared to fibrils obtained in simple buffer (Figure 7A, gray frame, and S12A), with cell viability increasing from 53 to 72% (100% refers to nontreated cells, Figure 7B).

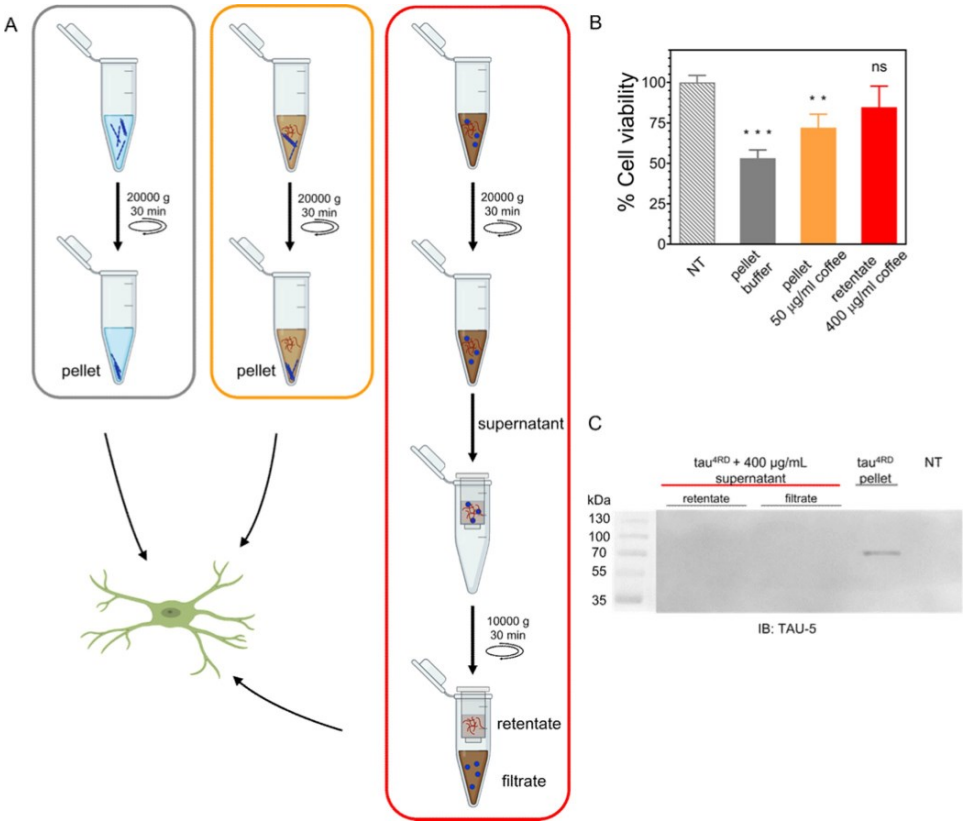

Figure 7. (A) Schematic depiction of sample preparation for cell viability and seeding-based aggregation assays in cellular models. A first centrifugation step was performed for the isolation of the fibrils (pellets in blue) from soluble Tau (aggregates in dark red and monomers as blue spheres) obtained after the fibrillization reaction of Tau^{4RD} in buffer (gray frame), in the presence of 50 µg/mL coffee extract (orange frame) and in the presence of 400 µg/mL coffee extract (red frame). The latter sample did not contain any aggregate and therefore the first centrifugation did not produce pellets. The solution obtained after centrifugation of Tau^{4RD} aggregated in the presence of 400 µg/mL coffee extract was further treated: a filtration step (through 100 kDa MWCO) was performed to separate monomers (filtrate) from soluble aggregates (retentate) used for seeding-based aggregation assays. The figure was created with BioRender.com. (B) Cell viability assay performed on H4-APPswe neuroglioma cells nontreated (NT) or treated for 48 h with pellets or retentate obtained as depicted in A (the color code is maintained). One-way statistical analysis ANOVA followed by Dunnett′s multiple comparison test was performed, ns = nonsignificant, p = *0.01–0.05, **0.001–0.01, ***0.0001–0.001. (C) Immunoblot analysis of the cellular insoluble fraction after treatment with samples of Tau^{4RD} aggregated in buffer and in the presence of 400 µg/mL coffee extract (prepared as depicted in A, red frame). HEK293 cells overexpressing Tau^{FL}/P310L-GFP were treated with the samples for 48 h and the Triton-insoluble fractions were blotted with the TAU-5 antibody. The last lane represents cells without the treatment (NT).

We have shown that Tau^{4RD} incubated in buffer containing 400 μg/mL coffee extract was unable to form fibrils but rather underwent structural transitions, giving rise to nonfibrillar aggregates/oligomeric species. Previous studies reported the ability of Tau oligomers to act as primary culprits of toxicity;[41−43] therefore, we sought to investigate if the amorphous, aggregated species formed in the presence of large quantities of coffee extract could interfere with cell survival. A sample containing Tau^{4RD} aggregated species formed in the presence of 400 μg/mL coffee extract was first sedimented using centrifugation and checked on SDS−PAGE (Figure S12A). The soluble supernatant was then separated into monomers and mixtures of oligomers by filtration through a 100 kDa MWCO filter (Figures 7A red frame, and S12A). Interestingly, the viability of the cells treated with the retentate that contained amorphous/oligomeric species showed a nonsignificant difference with respect to the viability of nontreated cells (Figure 7B), thus indicating that the presence of coffee extract not only interferes with Tau^{4RD} fibril formation but also promotes the formation of aggregated species with reduced or no toxicity.

Previous studies demonstrated the ability of synthetic preformed Tau fibrils to act as a template in soluble Tau fibrillization, both in vitro and in cell culture models.[17] To test whether Tau^{4RD} aggregates formed in the presence of coffee extract retained the seeding capacity, we employed HEK293 cells stably expressing Tau^{FL}/P301L-GFP and used lipofect- amine to promote the cellular uptake of the selected samples. First, we treated the HEK293 Tau^{FL}/P301L-GFP cells with pellets isolated by centrifugation deriving from Tau^{4RD} aggregated in the absence and presence of different amounts of coffee extract (sample preparation is depicted in Figure 7A). The immunoblot analysis of the Triton-insoluble fraction of cells after treatment with the tested samples showed that the seeded fibrillization propensity of Tau^{4RD} was perturbed when the aggregates were obtained in the presence of coffee extract (Figure S12B). However, since the pellet of the sample obtained in the presence of 400 μg/mL coffee extract did not contain a detectable protein fraction (Figure S12A), we decided to treat the cells with the two components isolated by filtration of the soluble supernatant: the retentate and the filtrate (Figure 7A red frame). The immunoblot analysis confirmed the inability of the aggregates obtained in the presence of a high amount of coffee to induce intracellular Tau fibrillization (Figure

7C). These data suggest that the molecules constituting the espresso coffee extract could have a bioactive role in the modulation of Tau-mediated cell toxicity and reduce the Tau-seeding activity in cultured cells.

DISCUSSION

Neurodegenerative diseases are often associated with the aggregation and deposition of incorrectly folded proteins. The predominant pathological feature of Tauopathies, including Alzheimer′s disease, is the intraneuronal deposition of the Tau protein, hence the development of novel forms of treatments and prevention targeting Tau protein is considered a promising strategy.[44] Toward this direction, a possible approach is to test small compounds for their inhibitory activity against the aggregation of Tau.

In recent years, the potential health benefits of the consumption of functional foods have been extensively investigated,[45−48] and a large number of food components showed biological activity.[49,50] In this work, we investigated the antiaggregation property of espresso coffee extract and some of its components toward the Tau protein. Taken together, ThT fluorescence, TEM analysis, and CD spectra indicate that the espresso extract has a strong antiaggregation effect in a dose-dependent manner. The length of Tau^{4RD} fibrils decreased upon increasing coffee extract concentration and only small spheroidal oligomeric species were observed at a high coffee concentration.

We also found that the coffee extract can modulate the stability and maturation of Tau condensates. Condensate formation has been suggested as a possible mechanism initiating the aggregation of Tau;[27] therefore, our results show a further interesting property of the coffee extract in interfering with the early events, leading to the pathological accumulation of Tau.

Coffee extracts contain a large variety of bioactive compounds exhibiting health-beneficial effects.[2] Using NMR- based analysis, we were able to identify the most abundant constituents of espresso coffee. Among these, we focused on caffeine and trigonelline, as well as on less abundant molecules, i.e., genistein and theobromine, to test their effects on Tau^{4RD} aggregation. Among the tested compounds, only caffeine and genistein showed significant modulation of Tau^{4RD} aggregation kinetics

in a dose-dependent manner, and only short protofilaments were observed after incubation. Moreover, concentrated genistein modulates the transformation of droplets, suggesting a possible concerted bioactive function toward Tau condensation and aggregation. It is interesting to point out that previous data showed an inhibitory activity of genistein against Aβ aggregation and toxicity.[50] This dual inhibition function against Tau and Aβ aggregation makes genistein an attractive biomolecule for designing genistein- based therapies.

It has been previously shown that caffeine, the well-known psychoactive alkaloid abundantly found in coffee extracts,[2] does not prevent Aβ aggregation and neurotoxicity, therefore making this molecule less interesting as a bioactive compound.[8] By contrast, our large panel of experiments clearly shows that caffeine exhibits a significant inhibitory activity toward Tau^{4RD} aggregation. Furthermore, ligand-based NMR experiments showed that among all of the coffee components, caffeine has the additional property of binding preformed Tau^{4RD} fibrils. All these findings are particularly interesting because caffeine could provide a structural template to treat Tauopathies targeting Tau fibrils or to design molecular probes with improved specificity and binding properties for the detection of pathological aggregates useful for the clinical diagnosis of Tau-based diseases.

The formation of amorphous spheroidal aggregates in the presence of coffee extract prompted us to study their toxicity on H4-APPswe cells, as Tau oligomers are considered to be the most toxic Tau species. Tau^{4RD} aggregated in the presence of coffee extract showed a significantly decreased cytotoxicity compared with untreated Tau^{4RD} fibrils, in line with previously reported data on natural compounds such as limonoids and xanthohumol.[51,52] Additional experiments also showed the reduced ability of the amorphous aggregates to induce intracellular Tau fibrillization, thus suggesting a neuroprotective effect of coffee extracts against Tau-induced toxicity in cultured cells. These results are in line with previous studies showing a reduced seeding propensity of Tau oligomers pretreated with a curcumin derivative.[53]

The association of coffee intake with a decreased risk of neurodegenerative disorders has been largely investigated.[2,54] A moderate espresso coffee consumption of 2/3 cups per day (40 mL/cup) provides about 250 mg of caffeine and 25 μg of genistein, in addition to numerous other bioactive com- pounds.[7,20] Many of these

compounds, including caffeine and genistein, can cross the blood−brain barrier via different mechanisms[55,56] and exert neuroprotective effects.[6]

Here, we show that aggregation of the Tau protein is modulated by espresso coffee extract and some of its components, at both concentrations used in the experiments (i.e., 50 and 400 μg/mL). Intraneuronal Tau concentration has been estimated to be about 2 μM,[57] 25 times less than what we have used in our experiments. Based on the bioavailability of coffee components in the brain, and on the results of our study, we expect that moderate coffee consumption may provide a sufficient amount of bioactive molecules to act separately or synergistically as modulators of Tau protein aggregation and toxicity.

In conclusion, we have presented a large body of evidence that espresso coffee, a widely consumed beverage, is a source of natural compounds showing beneficial properties in ameliorating Tau-related pathologies. Our findings could pave the way for further investigation into the design of bioactive compounds in the prevention and treatment of Tauopathies.

Conflict of interest

The authors declare no competing financial interest.

ACKNOWLEDGMENTS

Centro Piattaforme Tecnologiche of the University of Verona is acknowledged for providing access to the Microscopy Facility and to the NMR and CD instruments. The University of Padova is acknowledged for providing access to the electron microscope (DiBio Imaging Facility) and the NMR spectrometer (Department of Chemistry). C.G.B. received a fellowship grant (Assegno di Ricerca) from the Department of Biotechnology. The authors thank Fulvio Floriani for help with the experiments on liquid condensates.

ABBREVIATIONS

CD circula dichroism

CGAs chlorogenic acids

GFP green fluorescent protein

HEK293 nontumoral human embryonic kidney cells

LLPS liquid-liquid phase separation

MBD microtubule-binding domain

MWCO molecular weight cutoff

NMR nuclear magnetic resonance

STD saturation transfer difference

TEM transmission electron microscopy

ThT Thioflavin-T

REFERENCES

(1) Grosso, G.; Godos, J.; Galvano, F.; Giovannucci, E. L. Coffee, Caffeine, and Health Outcomes: An Umbrella Review. Annu. Rev. Nutr. 2017, 37, 131−156.
(2) Carneiro, S. M.; Oliveira, M. B. P. P.; Alves, R. C. Neuroprotective properties of coffee: An update. Trends Food Sci. Technol. 2021, 113, 167−179.
(3) Fan, F. S. Coffee reduces the risk of hepatocellular carcinoma probably through inhibition of NLRP3 inflammasome activation by caffeine. Front. Oncol. 2022, 12, No. 1029491.
(4) Carman, A. J.; Dacks, P. A.; Lane, R. F.; Shineman, D. W.; Fillit, H. M. Current evidence for the use of coffee and caffeine to prevent age-related cognitive decline and Alzheimer′s disease. J. Nutr., Health Aging 2014, 18, 383−392.
(5) Santos, C.; Costa, J.; Santos, J.; Vaz-Carneiro, A.; Lunet, N. Caffeine intake and dementia: systematic review and meta-analysis. J. Alzheimer's Dis. 2010, 20, S187−204.
(6) Socała, K.; Szopa, A.; Serefko, A.; Poleszak, E.; Wlaz, P. Neuroprotective Effects of Coffee Bioactive Compounds: A Review. Int. J. Mol. Sci. 2021, 22, No. 107.
(7) Ciaramelli, C.; Palmioli, A.; Airoldi, C. Coffee variety, origin and extraction procedure: Implications for coffee beneficial effects on human health. Food Chem. 2019, 278, 47−55.
(8) Ciaramelli, C.; Palmioli, A.; De Luigi, A.; Colombo, L.; Sala, G.; Riva, C.; Zoia, C. P.; Salmona, M.; Airoldi, C. NMR-driven identification of anti-amyloidogenic compounds in green and roasted coffee extracts. Food Chem. 2018, 252, 171−180.
(9) Zhang, Y.; Wu, K. M.; Yang, L.; Dong, Q.; Yu, J. T. Tauopathies: new perspectives and challenges. Mol. Neurodegener. 2022, 17, No. 28.
(10) Limorenko, G.; Lashuel, H. A. Revisiting the grammar of Tau aggregation and pathology formation: how new insights from brain pathology are shaping how we study and target Tauopathies. Chem. Soc. Rev. 2022, 51, 513−565.
(11) Wang, Y.; Mandelkow, E. Tau in physiology and pathology. Nat. Rev. Neurosci. 2016, 17, 5−21.
(12) Barracchia, C. G.; Tira, R.; Parolini, F.; Munari, F.; Bubacco, L.; Spyroulias, G. A.; D'Onofrio, M.; Assfalg, M. Unsaturated Fatty Acid- Induced Conformational Transitions and Aggregation of the Repeat Domain of Tau. Molecules 2020, 25, No. 2716.
(13) Ceccon, A.; D'Onofrio, M.; Zanzoni, S.; Longo, D. L.; Aime, S.; Molinari, H.; Assfalg, M. NMR investigation of the equilibrium partitioning of a water-soluble bile salt protein carrier to phospholipid vesicles. Proteins 2013, 81, 1776−1791.
(14) Munari, F.; Mollica, L.; Valente, C.; Parolini, F.; Kachoie, E. A.;

Arrigoni, G.; D'Onofrio, M.; Capaldi, S.; Assfalg, M. Structural Basis for Chaperone-Independent Ubiquitination of Tau Protein by Its E3 Ligase CHIP. Angew. Chem., Int. Ed. 2022, 61, No. e202112374.
(15) Munari, F.; Barracchia, C. G.; Franchin, C.; Parolini, F.; Capaldi, S.; Romeo, A.; Bubacco, L.; Assfalg, M.; Arrigoni, G.; D'Onofrio, M. Semisynthetic and Enzyme-Mediated Conjugate Preparations Illuminate the Ubiquitination-Dependent Aggregation of Tau Protein. Angew. Chem., Int. Ed. 2020, 59, 6607−6611.
(16) Parolini, F.; Tira, R.; Barracchia, C. G.; Munari, F.; Capaldi, S.; D'Onofrio, M.; Assfalg, M. Ubiquitination of Alzheimer′s-related Tau protein affects liquid-liquid phase separation in a site- and cofactor- dependent manner. Int. J. Biol. Macromol. 2022, 201, 173−181.
(17) Guo, J. L.; Buist, A.; Soares, A.; Callaerts, K.; Calafate, S.;
Stevenaert, F.; Daniels, J. P.; Zoll, B. E.; Crowe, A.; Brunden, K. R.; et al. The Dynamics and Turnover of Tau Aggregates in Cultured Cells: INSIGHTS INTO THERAPIES FOR TAUOPATHIES. J. Biol. Chem. 2016, 291, 13175−13193.
(18) Wei, F. F.; Furihata, K.; Hu, F. Y.; Miyakawa, T.; Tanokura, M. Complex mixture analysis of organic compounds in green coffee bean extract by two-dimensional NMR spectroscopy. Magn. Reson. Chem. 2010, 48, 857−865.
(19) D'Amelio, N.; De Angelis, E.; Navarini, L.; Schievano, E.; Mammi, S. Green coffee oil analysis by high-resolution nuclear magnetic resonance spectroscopy. Talanta 2013, 110, 118−127.
(20) Alves, R. C.; Almeida, I. M.; Casal, S.; Oliveira, M. B. Isoflavones in coffee: influence of species, roast degree, and brewing method. J. Agric. Food Chem. 2010, 58, 3002−3007.
(21) Angeloni, S.; Navarini, L.; Khamitova, G.; Maggi, F.; Sagratini, G.; Vittori, S.; Caprioli, G. A new analytical method for the simultaneous quantification of isoflavones and lignans in 25 green coffee samples by HPLC-MS/MS. Food Chem. 2020, 325, No. 126924.
(22) Fitzpatrick, A. W. P.; Falcon, B.; He, S.; Murzin, A. G.; Murshudov, G.; Garringer, H. J.; Crowther, R. A.; Ghetti, B.; Goedert, M.; Scheres, S. H. W. Cryo-EM structures of Tau filaments from Alzheimer′s disease. Nature 2017, 547, 185−190.
(23) Kumar, S.; Tepper, K.; Kaniyappan, S.; Biernat, J.; Wegmann, S.; Mandelkow, E. M.; Muller, D. J.; Mandelkow, E. Stages and conformations of the Tau repeat domain during aggregation and its effect on neuronal toxicity. J. Biol. Chem. 2014, 289, 20318−20332.
(24) Ambadipudi, S.; Biernat, J.; Riedel, D.; Mandelkow, E.; Zweckstetter, M. Liquid-liquid phase separation of the microtubule- binding repeats of the Alzheimer-related protein Tau. Nat. Commun. 2017, 8, No. 275.

(25) Mancini, R. S.; Wang, Y.; Weaver, D. F. Phenylindanes in Brewed Coffee Inhibit Amyloid-Beta and Tau Aggregation. Front. Neurosci. 2018, 12, No. 735.
(26) Yekta, R.; Sadeghi, L.; Ahmadi-Kandjani, S.; Naziri, P.; Rashidi, M. R.; Dehghan, G. The impact of caffeine on Tau-Tau interaction: LSPR detection, structural modification and molecular dynamics simulation. J. Mol. Liq. 2021, 338, No. 115914.
(27) Wegmann, S.; Eftekharzadeh, B.; Tepper, K.; Zoltowska, K. M.; Bennett, R. E.; Dujardin, S.; Laskowski, P. R.; MacKenzie, D.; Kamath, T.; Commins, C.; et al. Tau protein liquid-liquid phase separation can initiate Tau aggregation. EMBO J. 2018, 37, No. e98049.
(28) Boyko, S.; Surewicz, K.; Surewicz, W. K. Regulatory mechanisms of Tau protein fibrillation under the conditions of liquid-liquid phase separation. Proc. Natl. Acad. Sci. U.S.A. 2020, 117, 31882−31890.
(29) Uversky, V. N. Intrinsically disordered proteins in overcrowded milieu: Membrane-less organelles, phase separation, and intrinsic disorder. Curr. Opin. Struct. Biol. 2017, 44, 18−30.
(30) Alberti, S.; Gladfelter, A.; Mittag, T. Considerations and Challenges in Studying Liquid-Liquid Phase Separation and Biomolecular Condensates. Cell 2019, 176, 419−434.
(31) Shin, Y.; Brangwynne, C. P. Liquid phase condensation in cell physiology and disease. Science 2017, 357, No. eaaf4382
(32) Zhang, X.; Lin, Y.; Eschmann, N. A.; Zhou, H.; Rauch, J. N.; Hernandez, I.; Guzman, E.; Kosik, K. S.; Han, S. RNA stores Tau reversibly in complex coacervates. PLoS Biol. 2017, 15, No. e2002183.
(33) Lin, Y.; McCarty, J.; Rauch, J. N.; Delaney, K. T.; Kosik, K. S.; Fredrickson, G. H.; Shea, J. E.; Han, S. Narrow equilibrium window for complex coacervation of Tau and RNA under cellular conditions. eLife 2019, 8, No. e42571.
(34) Ukmar-Godec, T.; Hutten, S.; Grieshop, M. P.; Rezaei-Ghaleh, N.; Cima-Omori, M. S.; Biernat, J.; Mandelkow, E.; Soding, J.; Dormann, D.; Zweckstetter, M. Lysine/RNA-interactions drive and regulate biomolecular condensation. Nat. Commun. 2019, 10, No. 2909.
(35) Boyko, S.; Surewicz, W. K. Tau liquid-liquid phase separation in neurodegenerative diseases. Trends Cell Biol. 2022, 32, 611−623.
(36) Buell, A. K.; Esbjorner, E. K.; Riss, P. J.; White, D. A.; Aigbirhio, F. I.; Toth, G.; Welland, M. E.; Dobson, C. M.; Knowles, T. P. Probing small molecule binding to amyloid fibrils. Phys. Chem. Chem. Phys. 2011, 13, 20044−20052.
(37) Mayer, M.; Meyer, B. Characterization of Ligand Binding by Saturation Transfer Difference NMR Spectroscopy. Angew. Chem., Int. Ed. 1999, 38, 1784−1788.

(38) Dalvit, C.; Fogliatto, G.; Stewart, A.; Veronesi, M.; Stockman, B. WaterLOGSY as a method for primary NMR screening: practical aspects and range of applicability. J. Biomol. NMR 2001, 21, 349−359.
(39) Antanasijevic, A.; Ramirez, B.; Caffrey, M. Comparison of the sensitivities of Water-LOGSY and saturation transfer difference NMR experiments. J. Biomol. NMR 2014, 60, 37−44.
(40) Ferrari, F.; Bissaro, M.; Fabbian, S.; De Almeida Roger, J.; Mammi, S.; Moro, S.; Bellanda, M.; Sturlese, M. HT-SuMD: making molecular dynamics simulations suitable for fragment-based screen- ing. A comparative study with NMR. J. Enzyme Inhib. Med. Chem. 2021, 36, 1−14.
(41) Kayed, R.; Head, E.; Thompson, J. L.; McIntire, T. M.; Milton, S. C.; Cotman, C. W.; Glabe, C. G. Common structure of soluble amyloid oligomers implies common mechanism of pathogenesis. Science 2003, 300, 486−489.
(42) Gibbons, G. S.; Lee, V. M. Y.; Trojanowski, J. Q. Mechanisms of Cell-to-Cell Transmission of Pathological Tau: A Review. JAMA Neurol. 2019, 76, 101−108.
(43) Ghag, G.; Bhatt, N.; Cantu, D. V.; Guerrero-Munoz, M. J.; Ellsworth, A.; Sengupta, U.; Kayed, R. Soluble Tau aggregates, not large fibrils, are the toxic species that display seeding and cross- seeding behavior. Protein Sci. 2018, 27, 1901−1909.
(44) Soeda, Y.; Takashima, A. New Insights Into Drug Discovery Targeting Tau Protein. Front. Mol. Neurosci. 2020, 13, No. 590896.
(45) Hewlings, S. J.; Kalman, D. S. Curcumin: A Review of Its Effects on Human Health. Foods 2017, 6, No. 92.
(46) Nocella, C.; Cammisotto, V.; Fianchini, L.; D'Amico, A.; Novo, M.; Castellani, V.; Stefanini, L.; Violi, F.; Carnevale, R. Extra Virgin Olive Oil and Cardiovascular Diseases: Benefits for Human Health. Endocr., Metab. Immune Disord.: Drug Targets 2017, 18, 4−13.
(47) Markellos, C.; Ourailidou, M. E.; Gavriatopoulou, M.; Halvatsiotis, P.; Sergentanis, T. N.; Psaltopoulou, T. Olive oil intake and cancer risk: A systematic review and meta-analysis. PLoS One 2022, 17, No. e0261649.
(48) Hinojosa-Nogueira, D.; Perez-Burillo, S.; de la Cueva, S. P.; Rufian-Henares, J. A. Green and white teas as health-promoting foods. Food Funct. 2021, 12, 3799−3819.
(49) Ciaramelli, C.; Palmioli, A.; De Luigi, A.; Colombo, L.; Sala, G.; Salmona, M.; Airoldi, C. NMR-based Lavado cocoa chemical characterization and comparison with fermented cocoa varieties: Insights on cocoa′s anti-amyloidogenic activity. Food Chem. 2021, 341, No. 128249.

(50) Ren, B.; Liu, Y.; Zhang, Y.; Cai, Y.; Gong, X.; Chang, Y.; Xu, L.; Zheng, J. Genistein: A Dual Inhibitor of Both Amyloid beta and Human Islet Amylin Peptides. ACS Chem. Neurosci. 2018, 9, 1215− 1224.
(51) Zhang, M.; Wu, Q.; Yao, X.; Zhao, J.; Zhong, W.; Liu, Q.; Xiao, S. Xanthohumol inhibits Tau protein aggregation and protects cells against Tau aggregates. Food Funct. 2019, 10, 7865−7874.
(52) Gorantla, N. V.; Das, R.; Mulani, F. A.; Thulasiram, H. V.; Chinnathambi, S. Neem Derivatives Inhibits Tau Aggregation. J. Alzheimer Dis. Rep. 2019, 3, 169−178.
(53) Lo Cascio, F.; Puangmalai, N.; Ellsworth, A.; Bucchieri, F.; Pace, A.; Piccionello, A. P.; Kayed, R. Toxic Tau Oligomers Modulated by Novel Curcumin Derivatives. Sci. Rep. 2019, 9, No. 19011.
(54) Ross, G. W.; Abbott, R. D.; Petrovitch, H.; Morens, D. M.; Grandinetti, A.; Tung, K. H.; Tanner, C. M.; Masaki, K. H.; Blanchette, P. L.; Curb, J. D.; et al. Association of coffee and caffeine intake with the risk of Parkinson disease. JAMA 2000, 283, 2674− 2679.
(55) Tsai, T. H. Concurrent measurement of unbound genistein in the blood, brain and bile of anesthetized rats using microdialysis and its pharmacokinetic application. J. Chromatogr. A 2005, 1073, 317−
322.
(56) McCall, A. L.; Millington, W. R.; Wurtman, R. J. Blood-brain barrier transport of caffeine: dose-related restriction of adenine transport. Life Sci. 1982, 31, 2709−2715.
(57) Iqbal, K.; Liu, F.; Gong, C. X.; Grundke-Iqbal, I. Tau in Alzheimer disease and related Tauopathies. Curr. Alzheimer Res. 2010, 7, 656−664.

SUPPORTING INFORMATION

Figures S1-S12

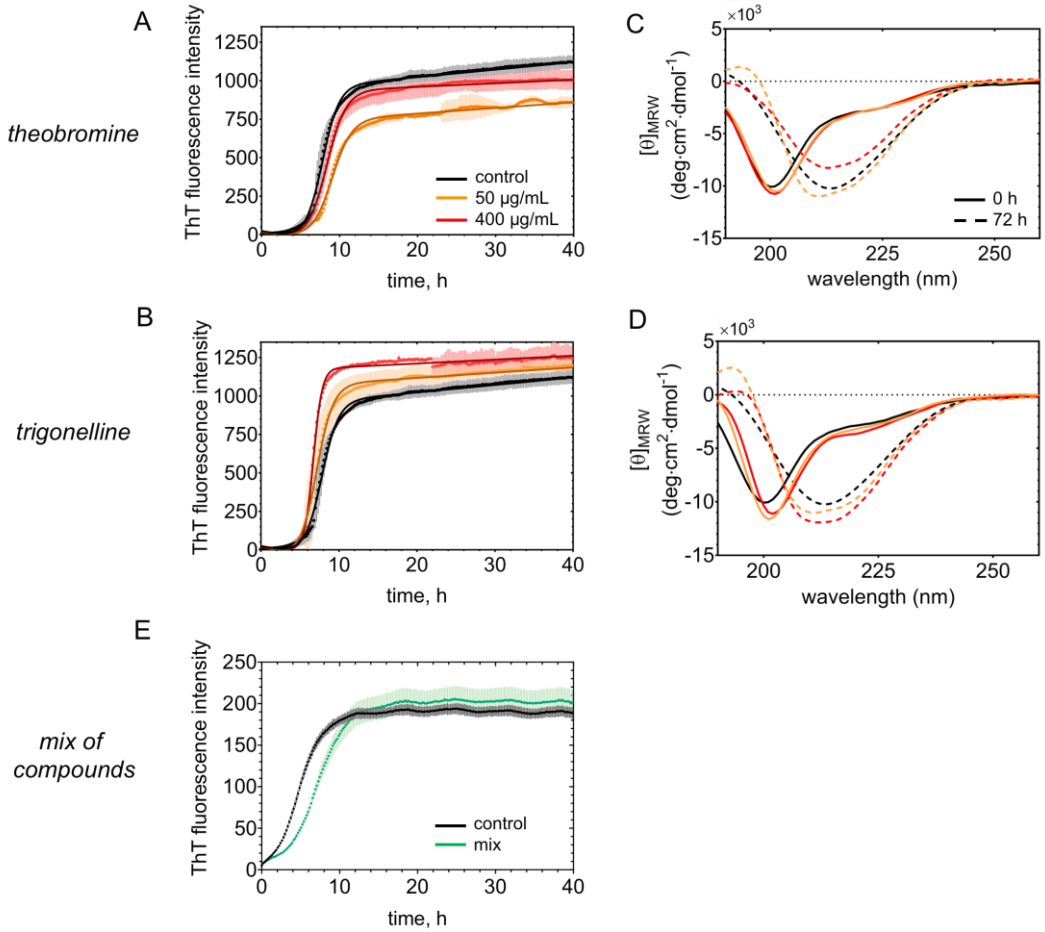

Figure S1. *Time course of Tau conformational transitions*. (A,B) ThT fluorescence-based aggregation kinetics curves measured on 50 µM Tau^{4RD} in the presence of (A) theobromine, (B) trigonelline. Compound concentrations were 0 (black), 50 (orange) or 400 (red) □g/mL. Molar concentrations of compounds were: 0.30 mM (50 □g/mL) and 2.2 mM (400 □g/mL) theobromine; 0.29 mM (50 □g/mL) and 2.3 mM (400 □g/mL) trigonelline. (E) ThT fluorescence-based aggregation kinetics curves measured on 50 □M Tau^{4RD} in the presence of a mixture of compounds prepared as follows: 10 □g/mL (50 □M) caffeine, 1 □g/mL (3.7 □M) genistein, 1 □g/mL (5.5 □M) theobromine, 5 □g/mL (36 □M) trigonelline. Measurements were carried out on four replicates and data are reported as mean ± s.d.. Solid lines correspond to the best fit curves determined using an empirical sigmoid function. (C, D) Far-UV CD spectra recorded on 6 µM Tau^{4RD} in the presence of (C) theobromine, (D) trigonelline. Measurements were performed immediately after sample preparation (continuous curves) and after 72 h (dotted curves) incubation of a concentrated stock (50 µM protein and 50 or 400 □g/mL compounds) in static conditions

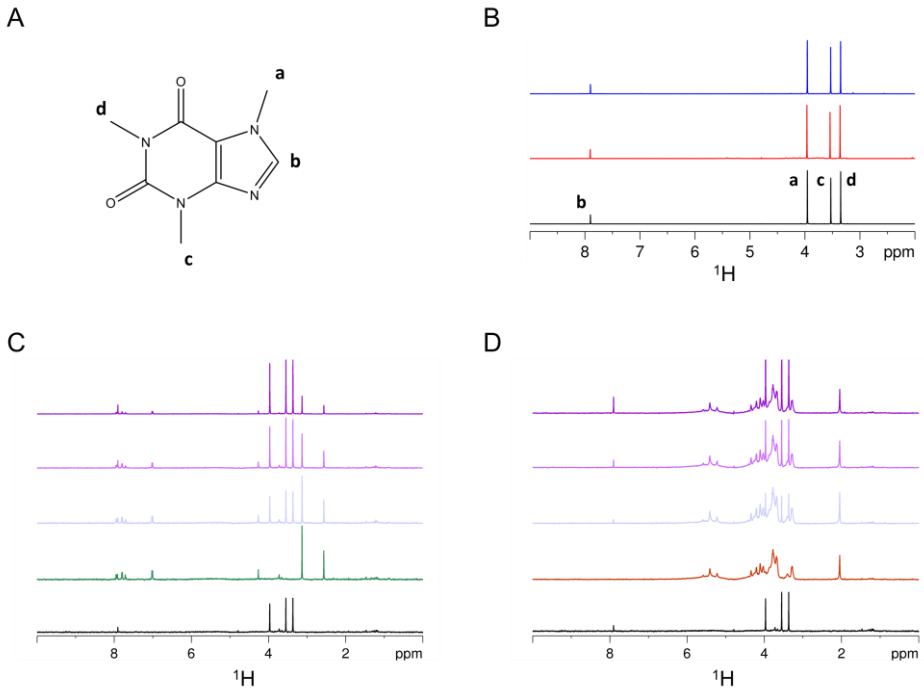

Figure S2. *Interaction of caffeine with heparin and with ThT evaluated by NMR.* (A) The chemical structure of caffeine with protons indications. (B) ^{1}H NMR spectra of 400 µg/mL (2 mM) caffeine,in the absence (black) and in the presence of 50 µM heparin (red) or 50 µM thioflavin-T (blue) (molarratios 40:1). Peaks assignments are shown. Spectra intensities have been adjusted for better visualization. (C) ^{1}H NMR titration experiments of 50 µM ThT in the absence (green) or in the presence of caffeine at concentrations of 50 µM (lavender), 100 µM (purple), and 250 µM (violet).(D) ^{1}H NMR titration experiments of 50 µM heparin in the absence (brown) or in the presence of caffeine at concentration of 50 µM (lavender), 100 µM (purple), and 250 µM (violet). The spectrumof the caffeine alone is reported as a reference (black). All the spectra were acquired at 600 MHz and25 °C

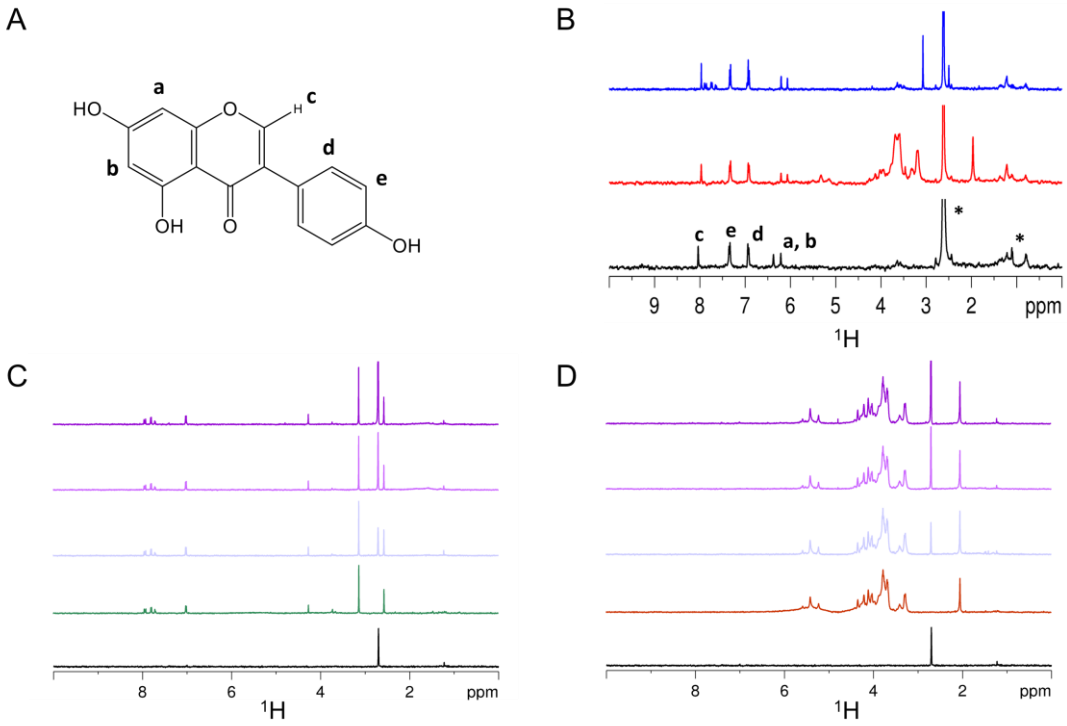

Figure S3. *Interaction of genistein with heparin and with ThT evaluated by NMR.* (A) The chemical structure of genistein with protons indications. (B) ^{1}H NMR spectra of 400 µg/mL (1.5 mM) genistein, in the absence (black) and in the presence of 50 µM heparin (red) or 50 µM thioflavin-T (blue) (molar ratios 30:1). Peaks assignments are shown, * indicates impurities. Spectra intensities have been adjusted for better visualization. (C) ^{1}H NMR titration experiments of 50 µM ThT in the absence (green) or in the presence of genistein at concentration of 50 µM (lavender), 100 µM (purple), and 250 µM (violet). (D) ^{1}H NMR titration experiments of 50 µM heparin in the absence (brown) or in the presence of genistein at concentration of 50 µM (lavender), 100 µM (purple), and 250 µM (violet). The spectrum of the genistein alone is reported as a reference (black). All the spectra were acquired at 600 MHz and 25 °C

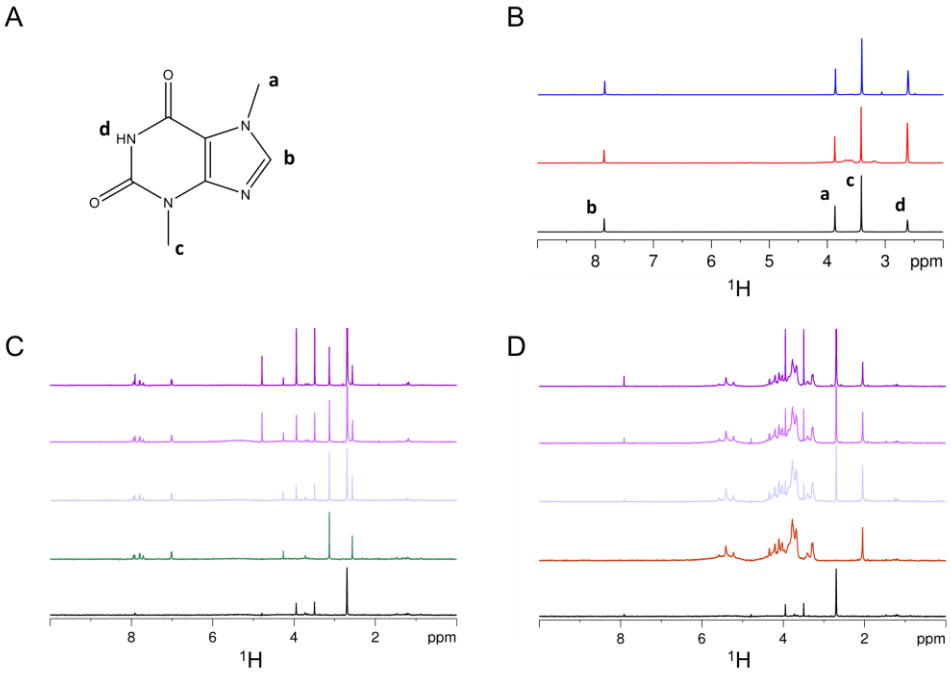

Figure S4. *Interaction of theobromine with heparin and with ThT evaluated by NMR.* (A) The chemical structure of theobromine with protons indications. **(**B) ^{1}H NMR spectra of 400 µg/mL (2.2mM) theobromine, in the absence (black) and in the presence of 50 µM heparin (red) or 50 µM thioflavin-T (blue) (molar ratios 44:1). Peaks assignments are shown. Spectra intensities have been adjusted for better visualization. (C) ^{1}H NMR titration experiments of 50 µM ThT in the absence (green) or in the presence of theobromine at concentration of 50 µM (lavender), 100 µM (purple), and 250 µM (violet). (D) ^{1}H NMR titration experiments of 50 µM heparin in the absence (brown) orin the presence of theobromine at concentration of 50 µM (lavender), 100 µM (purple), and 250 µM(violet). The spectrum of the theobromine alone is reported as a reference (black). All the spectra were acquired at 600 MHz and 25 °C.

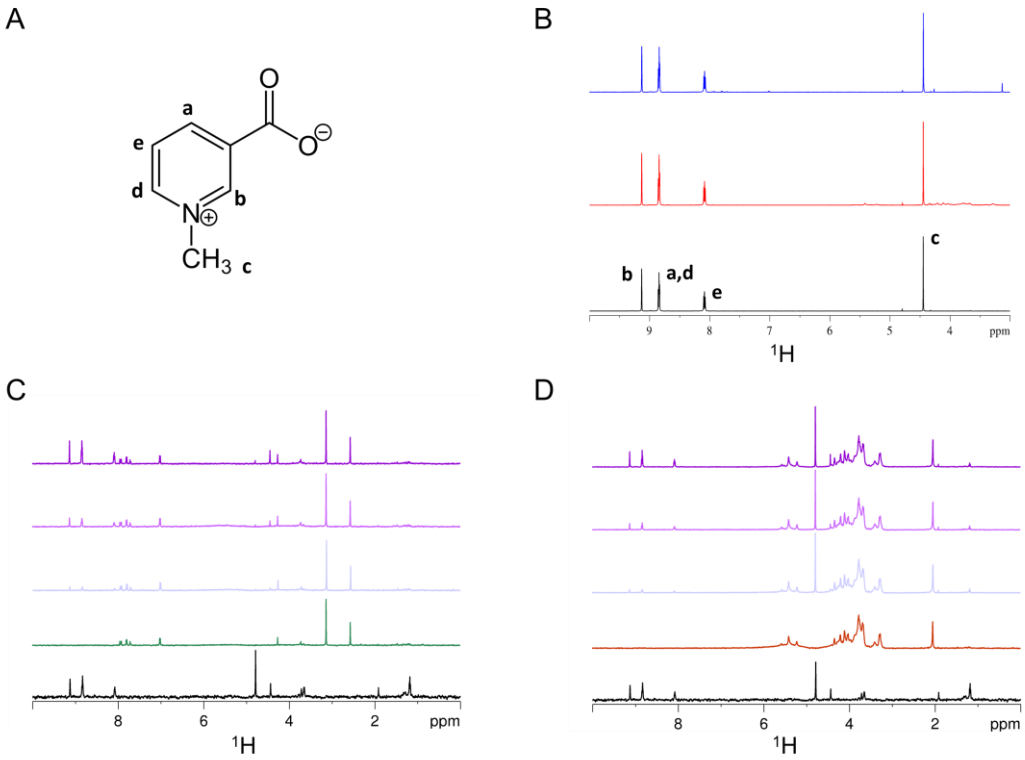

Figure S5. *Interaction of trigonelline with heparin and with ThT evaluated by NMR.* (A) The chemical structure of trigonelline with protons indications. (B) ^{1}H NMR spectra of 400 µg/mL (2.3 mM) trigonelline, in the absence (black) and in the presence of 50 µM heparin (red) or 50 µM thioflavin-T (blue) (molar ratios 46:1). Peaks assignments are shown. Spectra intensities have been adjusted for better visualization. (C) ^{1}H NMR titration experiments of 50 µM ThT in the absence (green) or in the presence of trigonelline at concentration of 50 µM (lavender), 100 µM (purple), and250 µM (violet). (D) ^{1}H NMR titration experiments of 50 µM heparin in the absence (brown) or in the presence of trigonelline at concentration of 50 µM (lavender), 100 µM (purple), and 250 µM (violet). The spectrum of the trigonelline alone is reported as a reference (black). All the spectra wereacquired at 600 MHz and 25 °C.

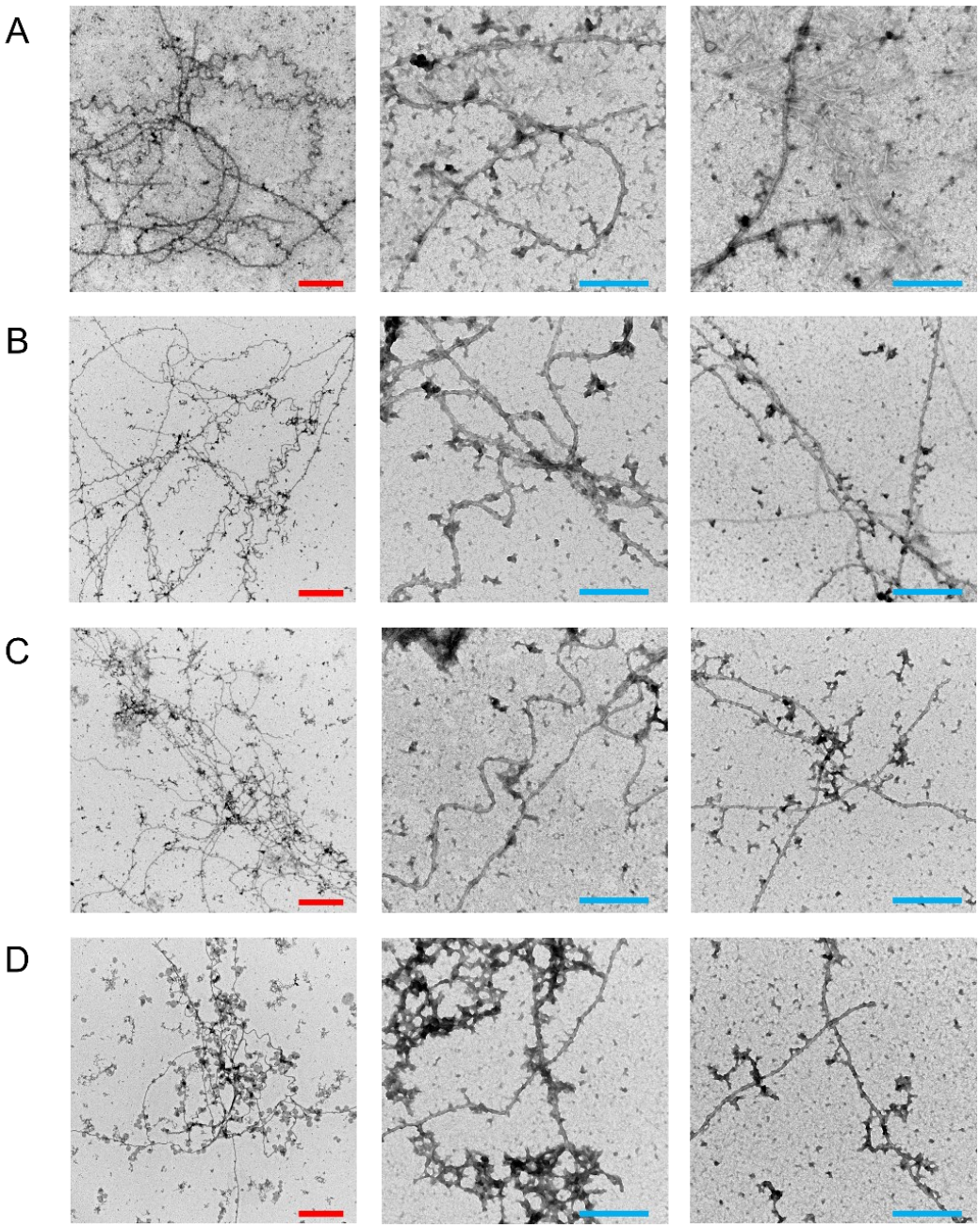

Figure S6. *Aggregates morphology evaluated by TEM*. TEM images of Tau^{4RD} filaments formed in the presence of bioactive compounds. Samples contained 50 µM Tau^{4RD} and 50 µg/mL (A) or 400 µg/mL (B) theobromine, 50 µg/mL (C), or 400 µg/mL (D) trigonelline. Samples were incubated for 48 h at 37 °C in static conditions. Scale bars are 500 nm (red) and 200 nm (light blue).

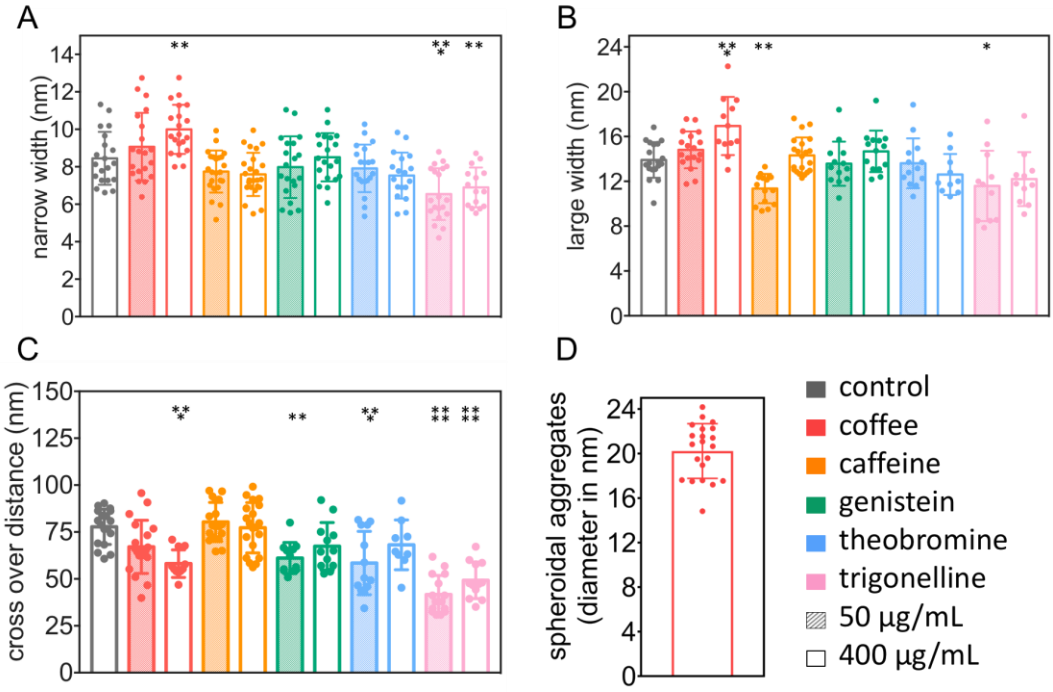

Figure S7. *Quantitative analysis of aggregates morphology*. Distributions of (A) narrow width, (B) large width, (C) crossover distance of aggregates obtained in the absence or in the presence of different bioactive molecules. (D) Diameter of the spheroidal aggregates formed in the presence of high coffee-extract concentration. Data are presented as column scatter charts, mean ± s.d. of 10-20 values for each parameter are displayed. Distributions were compared to control data by one-way ANOVA followed by Dunnett's multiple comparison test, P = * 0.01-0.05, ** 0.001-0.01, *** 0.0001-0.001, and **** < 0.0001.

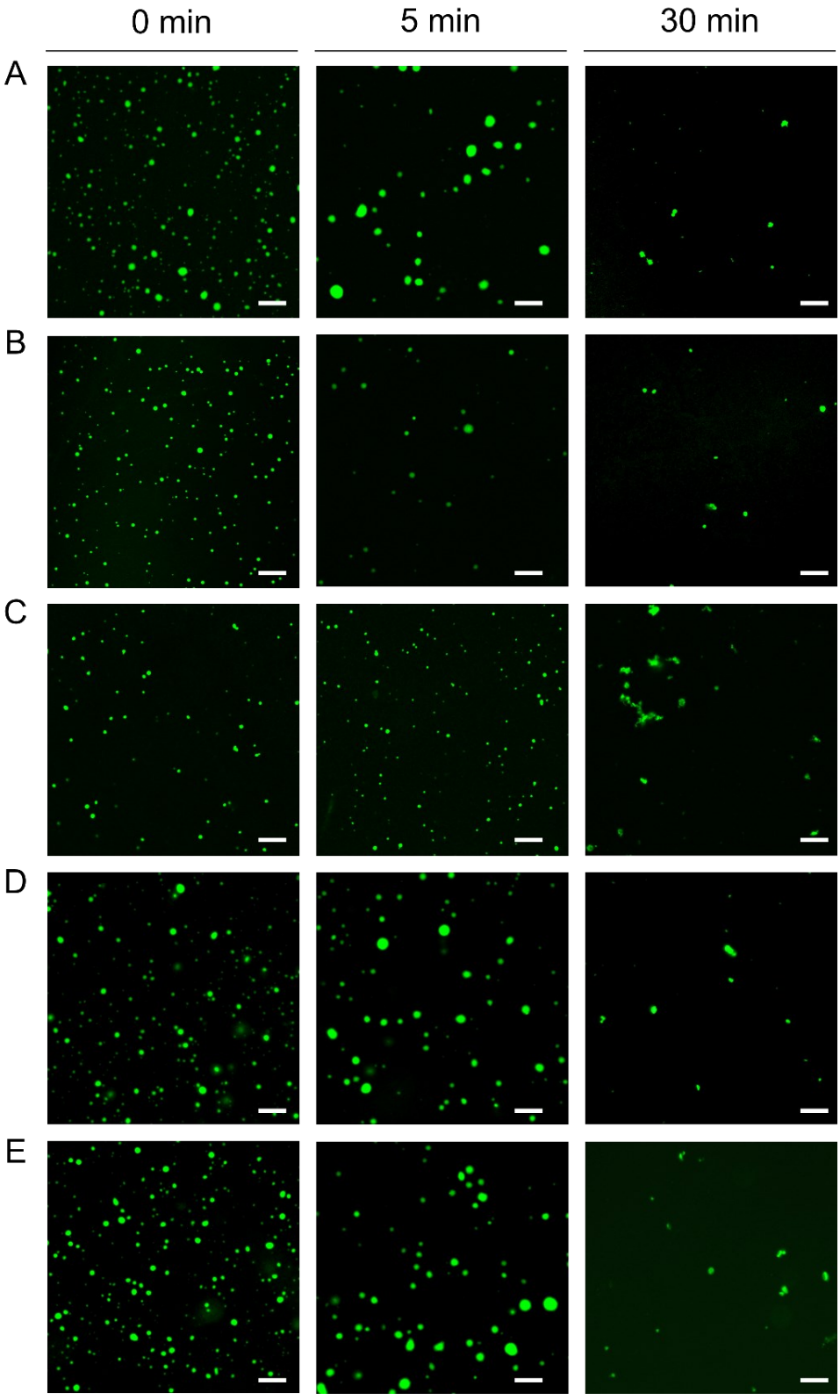

Figure S8. *Influence of coffee extract on Tau condensates*. Representative fluorescence microscopy images displaying condensates of Tau^{4RD}/heparin in simple buffer (A), in the presence of 35 µg/mL coffee extract (B), 280 µg/mL coffee extract (C), 35 µg/mL coffee extract added 5 min after mixing Tau and heparin (D), 280 µg/mL coffee extract added 5 min after mixing Tau and heparin (E). Images were acquired at 0, 5, 30 min after sample preparation. Protein was 35 µM and heparin 8.75 µM. Scale bar is 10 µm.

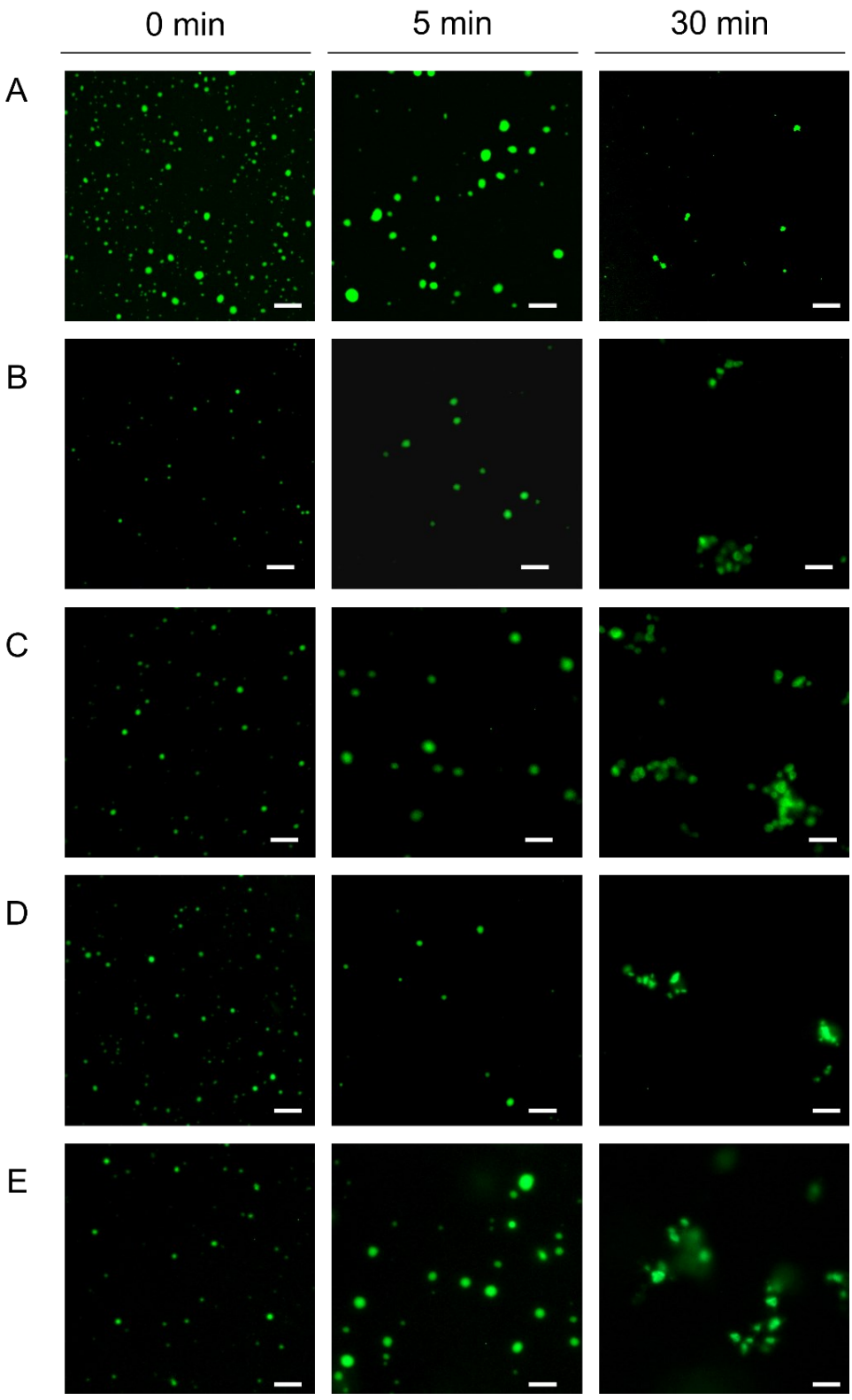

Figure S9. *Influence of caffeine on Tau condensates*. Representative fluorescence microscopy images displaying condensates of Tau^{4RD}/heparin in simple buffer (A), in the presence of 35 µg/mL (0.18 mM) caffeine (B), 280 µg/mL (1.4 mM) caffeine (C), 35 µg/mL caffeine added 5 min after mixing Tau and heparin (D), 280 µg/mL caffeine added 5 min after mixing Tau and heparin (E). Images were acquired at 0, 5, 30 min after sample preparation. Protein was 35 µM and heparin 8.75 µM. Scale baris 10 µm.

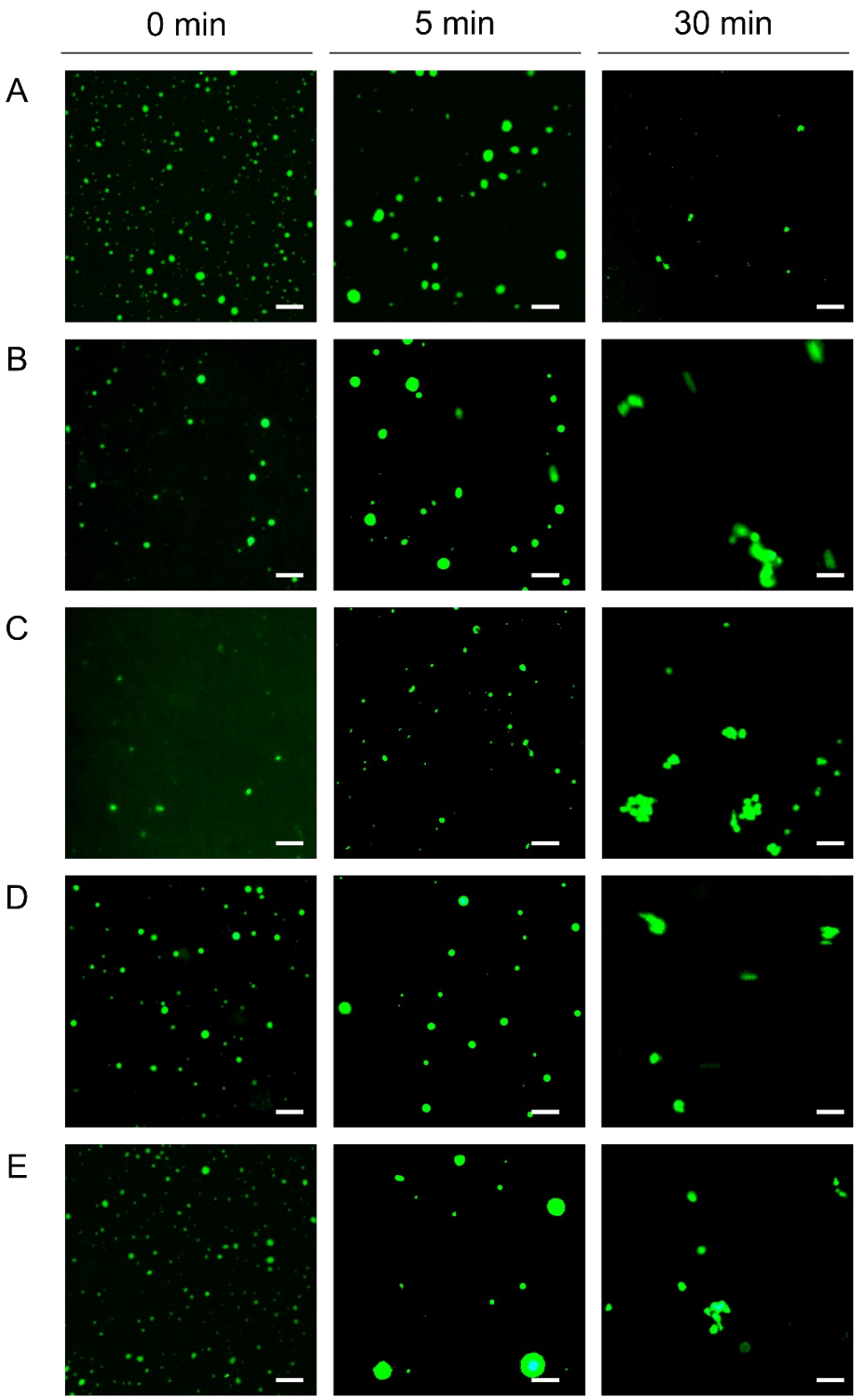

Figure S10. *Influence of genistein on Tau condensates*. Representative fluorescence microscopy images displaying condensates of Tau^{4RD}/heparin in simple buffer (A), in the presence of 35 µg/mL (0.13 mM) genistein (B), 280 µg/mL (1 mM) genistein (C), 35 µg/mL genistein added 5 min after mixing Tau and heparin (D), 280 µg/mL genistein added 5 min after mixing Tau and heparin (E). Images were acquired at 0, 5, 30 min after sample preparation. Protein was 35 µM and heparin 8.75 µM. Scale bar is 10 µm.

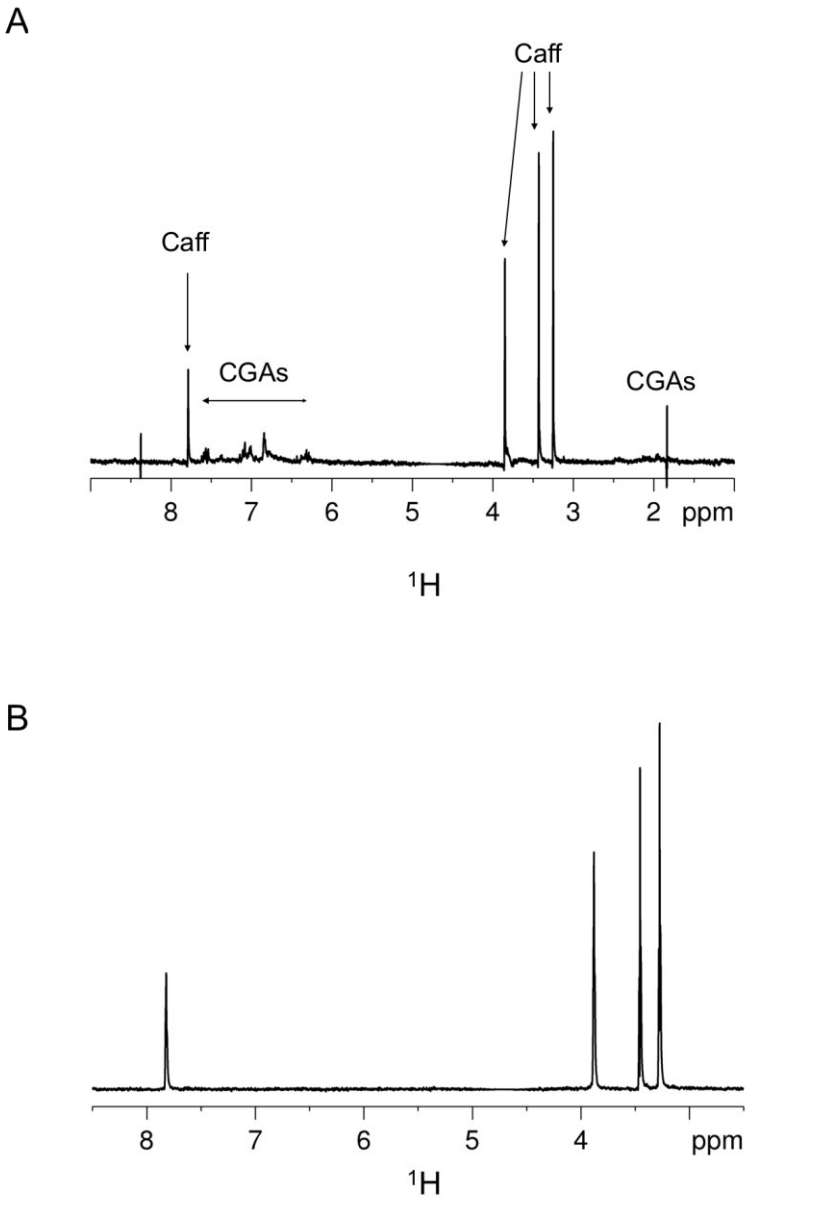

Figure S11. *Interaction of coffee compounds with Tau aggregates.* Spectra derived by subtraction of STD spectra of 5 mg/mL coffee (A) or 0.8 mg/mL caffeine (B) in the presence of fibrils from STD spectra recorded in the absence of fibrils.

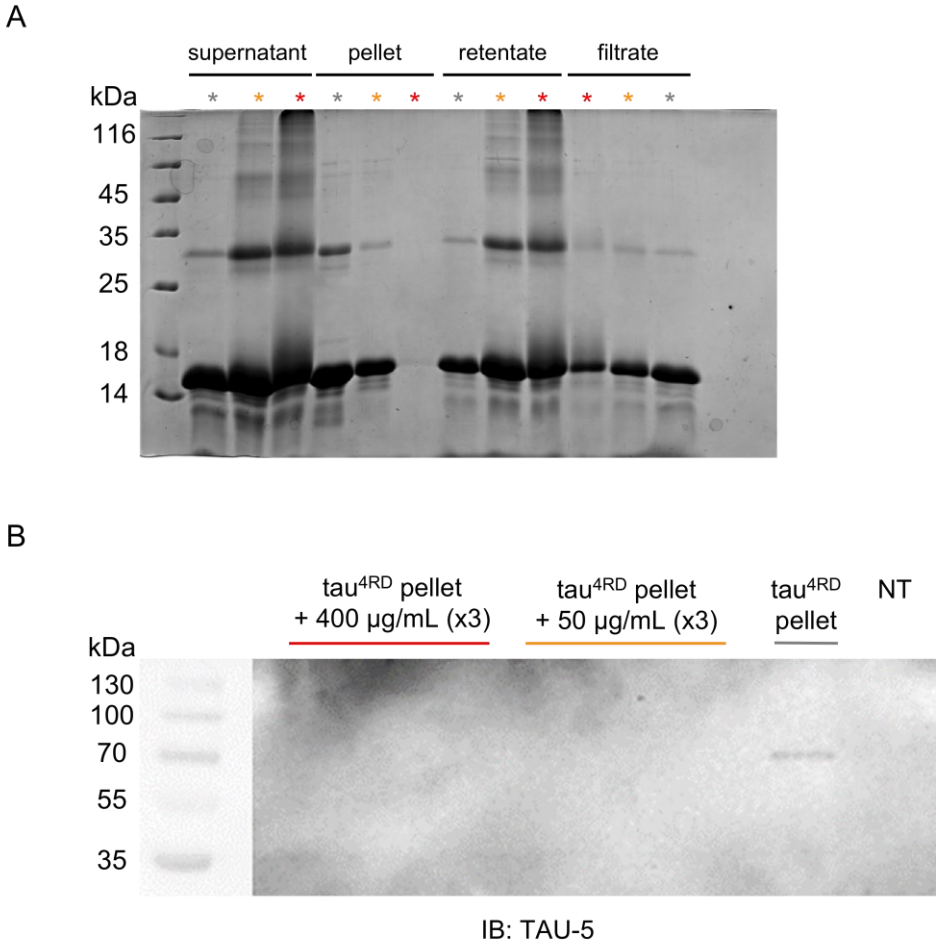

Figure S12. *SDS-PAGE and immunoblot analysis of samples of in cell experiments.* (A) SDS-PAGE analysis of samples of Tau^{4RD} aggregated in the absence (grey) or in the presence of 50 µg/mL (orange)or 400 µg/mL (red) of coffee extract, at different separation steps as depicted in Fig. 7A. (B) Immunoblot analysis of the cellular insoluble fraction after treatment with the pellets of Tau^{4RD} aggregated in buffer and in the presence of 50 µg/mL or 400 µg/mL of coffee extracts. HEK293 cellsoverexpressing Tau^{FL}/P310L-GFP, were treated with the samples for 48 h and the Triton-insoluble fractions were blotted with TAU-5 antibody. Last lane represents cells without the treatment (NT).

3.4 Published article: Tau LLPS

Ultrasmall gold nanoparticles as clients of biomolecular condensates

Giovanna Viola, Fulvio Floriani, Carlo Giorgio Barracchia, Francesca Munari, Mariapina D'Onofrio and Michael Assfalg*

Department of Biotechnology, University of Verona, 37134 Verona, Italy

* Corresponding author: Michael Assfalg
Department of Biotechnology
University of Verona
Strada Le Grazie 15
37134 Verona, Italy
Email: michael.assfalg@univr.it

Keywords: biomolecular condensates ; intrinsically disordered protein ; liquid-liquid phase separation ; multivalent interaction ; protein-nanoparticle interaction ; ultrasmall nanoparticles

ABSTRACT

Liquid-liquid phase separation (LLPS) of biopolymers to form condensates is a widespread phenomenon in living cells. Agents that target or alter condensation can help uncover elusive physiological and pathological mechanisms. Owing to their unique material properties and modes of interaction with biomolecules, nanoparticles represent attractive condensate- targeting agents.

Our work focused on elucidating the interaction between ultrasmall gold nanoparticles (usGNPs) and diverse types of condensates of Tau, a representative phase-separating protein associated with neurodegenerative disorders. usGNPs attract considerable interest in the biomedical community due to unique features, including emergent optical properties and good cell penetration. We explored the interaction of usGNPs with reconstituted self-condensates of Tau, two-component Tau/ polyanion and three-component Tau/RNA/alpha-synuclein coacervates. The usGNPs were found to concentrate into condensed liquid droplets, consistent with the formation of dynamic client (nanoparticle) - scaffold (Tau) interactions, and were observable thanks to their intrinsic luminescence. Furthermore, usGNPs were capable to promote LLPS of a protein domain which is unable to phase separate on its own. Our study demonstrates the ability of usGNPs to interact with and illuminate protein condensates. We anticipate that nano- particles will have broad applicability as nanotracers to interrogate phase separation, and as nanoactuators controlling the formation and dissolution of condensates.

Graphical abstract

Ultrasmall gold nanoparticles concentrate and distribute into biomolecular condensates. The nanoparticles establish dynamic noncovalent interactions with the scaffold protein and act as clients. They may also favor or disfavor condensate formation. The nanoparticles could be used to explore biomolecular condensates in vitro and in cellular models of pathology.

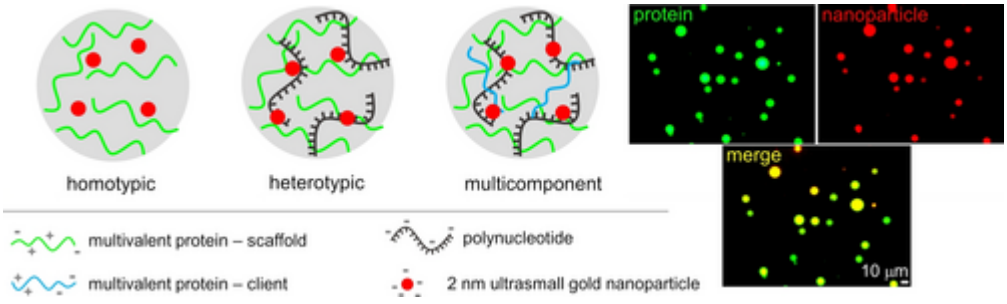
homotypic
heterotypic
multicomponent
protein
nanoparticle
merge
10 μm
multivalent protein – scaffold
multivalent protein – client
polynucleotide
2 nm ultrasmall gold nanoparticle

INTRODUCTION

Biomolecular condensation has emerged as an essential process for cellular compartmentalization, playing fundamental roles in cellular organization and physiology.[1,2] Biomolecular condensates are dynamic supramolecular assemblies that concentrate proteins and polynucleotides, acting as macromolecular reservoirs, molecular sieves, or microreactors.[3] Cellular condensates, often also termed membrane-less organelles (MLOs), are ubiquitous in eukaryotic cells and have been known for a long time, however their formation and functioning at the molecular level have begun to be understood only in recent times.[4,5] Many MLOs are now thought to form via liquid-liquid phase separation (LLPS), a thermodynamic process by which a solution spontaneously demixes into coexisting liquid phases.[3] Upon LLPS, a biopolymer-rich phase segregates from its surroundings with the formation of a boundary defined by interfacial tension. Condensates generally occur as mesoscopic liquid-like droplets possessing a high level of internal dynamics, they allow exchange of macromolecules with the external environment, and quickly adapt to internal and external stimuli.[6] Condensation, or coacervation, is driven by weak multivalent interactions, such as heterotypic electrostatic interactions between oppositely charged polyelectrolytes (e. g., mixtures of proteins and nucleic acids), or homotypic interactions involving repetitive low-complexity sequences and multiple interacting sites.[1,7] Dysregulation of LLPS may lead to maturation of liquid condensates toward gel or solid-like material states, eventually associated with protein misfolding and aggregation which often occur in age-related conditions.[6] In fact, aberrant forms of condensates are associated with many human diseases, including cancer, neurodegeneration, and infectious diseases.[8]

MLOs are often enriched in intrinsically disordered proteins (IDPs), which play an important role in driving phase separation.[9,10] IDPs are a group of proteins that do not fold into specific three-dimensional structures but exist instead as dynamic ensembles of interconverting conformers.[11] This structural plasticity allows IDPs to undergo promiscuous multi- valent homo- and heterotypic interactions. IDPs and proteins with intrinsically disordered regions (IDRs) comprise a large fraction of eukaryotic proteomes and possess a broad functional repertoire.[12–14] Beyond supporting cellular functions, numerous IDPs are associated with human disorders,

including cancer, cardiovascular disease, neurodegenerative diseases, and diabetes.[15]

With the growing awareness that LLPS of IDPs plays an important role in cellular functioning and malfunctioning, there is also growing interest in using chemical tools to study and modulate phase separation behavior, ultimately aiming at probing condensate-driven cellular processes and mitigating aberrant phase transitions associated with disease.[16–19] Many phase-separating IDPs have been recognized as therapeutic targets and LLPS provides new opportunities for modulating their activities.[20,21] The partitioning of small molecules to liquid condensates and their influence on phase separation are under scrutiny to better understand drug activity and discover new candidate drugs.[21,22] However, as both IDPs and biomolecular condensates are unconventional and challenging targets, alternative agents may prove better suited for interacting with and regulating IDPs in the condensed states. Nanoparticles (NP) have found widespread application in biomedicine, in areas ranging from imaging and diagnostics to therapeutics and regenerative medicine.[23] NPs exhibit different mechanisms of binding to biomolecules compared to small molecules. The tunable size and surface chemistry of most NP formulations allow some degree of control over their inter- actions with biological structures. Recent studies on model systems have contributed to elucidate the binding modes and driving forces that govern interactions between NPs and IDPs.[24–29] NPs have also been intensely investigated as artificial chaperones to redirect aberrant protein conformational transi- tions and mitigate the formation of toxic aggregates of IDPs associated with neurodegenerative disorders.[30,31] Finally, medium-sized (30–40 nm) or large (> 40 nm) NPs have been recently exploited for the detailed characterization of the material properties and molecular drivers of condensates,[32,33] and for the observation of their time-dependent transformation.[34]

To explore the interaction between NPs and biomolecular condensates, we focused on ultrasmall gold NPs (usGNPs) and the IDP Tau as a representative system. Ultrasmall NPs attract considerable interest in the biomedical community due to unique physicochemical features and biological behavior. Such particles generally exhibit high biocompatibility and low toxicity, efficient renal clearance, improved tumor distribution, and good cell penetration.[35–38] Moreover, on exposure to

biological media, they do not undergo hard corona formation[39–42] and could remain available for interaction with specific targets. The controllable synthesis, the facile surface functionalization, and the optical properties, make usGNPs highly attractive for diverse applications.[43,44]

Tau is an intracellular, neuron-specific protein, primarily involved in the assembly and stabilization of microtubules.[45] Under pathological conditions, Tau undergoes modifications that are thought to impair brain function and to cause neurodegeneration.[46] Intracellular aggregates of Tau are the defining feature of neurological disorders known as Tauopathies, such as Alzheimer's disease (AD).[47] Tau is present in MLOs, including the nucleolus and stress granules,[48,49] and was reported to undergo phase separation in vitro under a variety of conditions.[50–53] We have recently shown that a domain of Tau interacts with usGNPs and that usGNPs can partition into stress granules, a type of cytosolic MLO enriched for IDPs.[41] In the present study, we aimed to explore the association of NPs with in vitro reconstituted condensates of Tau to elucidate the conditions for their recruitment and their influence on Tau phase separation behavior.

RESULTS

Characteristics of nanoparticles and proteins used in the study

Ultrasmall gold nanoparticles (usGNPs) were prepared with dihydrolipoic acid (DHLA, Figure S1A) as capping agent, following a previously described procedure.[54] The conjugation of DHLA to NPs imparts excellent stability against ligand exchange due to the strong Au—S bonds. Furthermore, the ligand carboxylates stabilize the colloidal dispersion due to electro- static repulsion between the particles and confer high water solubility. In addition, carboxylates can act as reactive groups for facile functionalization. The prepared usGNPs were uniform in morphology and size (mean core diameter of ~ 1.9 nm), as determined by transmission electron microscopy (Figure S2A), and displayed negative zeta-potential in neutral solution (ζ=- 36 ± 6 mV). Consistent with their ultrasmall size, usGNPs exhibited no surface plasmon resonance band in the absorption spectrum and were fluorescent (Figure S2B). Tau protein has six isoforms in the adult human brain, the longest of which is 441 amino acids long (Tau^{FL}). This protein comprises an amino-terminal projection domain, a proline-rich region, a microtubule-binding four repeat domain (4RD), and a carboxy-terminal region (Figure S1B).[55] All four repeats are thought to interact with microtubules, assisted by abundant positive charges of basic amino acids dispersed over the sequence (Figure S1C).[56] Despite its inherent solubility, the repeat region is also involved in the formation of the core of insoluble filaments obtained in vitro and those isolated from brains of individuals with AD.[57,58] Tau^{4RD} has been frequently used for in vitro aggregation studies due to its faster aggregation compared to Tau^{FL}, generally induced by the addition of polyanionic cofactors such as heparin or arachidonic acid.[55,59] The 4RD sequence encodes a strong propensity for LLPS, and Tau^{4RD} was found to phase separate into protein/RNA coacervates.[8] Tau^{FL}, but not Tau^{4RD}, was shown to form liquid droplets in vitro, in near-physiological conditions and in the absence of cofactors.[52]

Ultrasmall gold nanoparticles partition into Tau^{4RD}/polyU coacervates

Tau^{4RD} is a polyampholyte enriched in charged amino acid residues distributed along the chain, exhibiting an excess of positive over negative charges ($f_+/f_- = 2$, Figure S1C) with no regular charge or block-charge pattern. On mixing Tau^{4RD} with

polyuridylic acid (polyU, Figure S1D) at a molar ratio corresponding to approximately overall net charge neutrality, the solution undergoes LLPS (detectable by increased sample turbidity) forming a complex coacervate (hereafter referred to as heterotypic coacervate).[59,60] We performed turbidity measurements to verify if the presence of usGNPs affected LLPS.

LLPS samples contained 25 μM protein and variable concentrations of usGNPs. Interestingly, the turbidity of the sample increased progressively with increasing usGNP concentration up to 1 μM, while higher usGNPs concentrations resulted in a decrease in turbidity until almost complete disappearance for concentrations above ~ 2 μM (Figure 1A). Since other phenomena, besides LLPS, can give rise to changes in turbidity, we investigated the formation of liquid droplets using fluorescence microscopy and Alexa^{488}-labelled Tau^{4RD} as a reporter molecule.

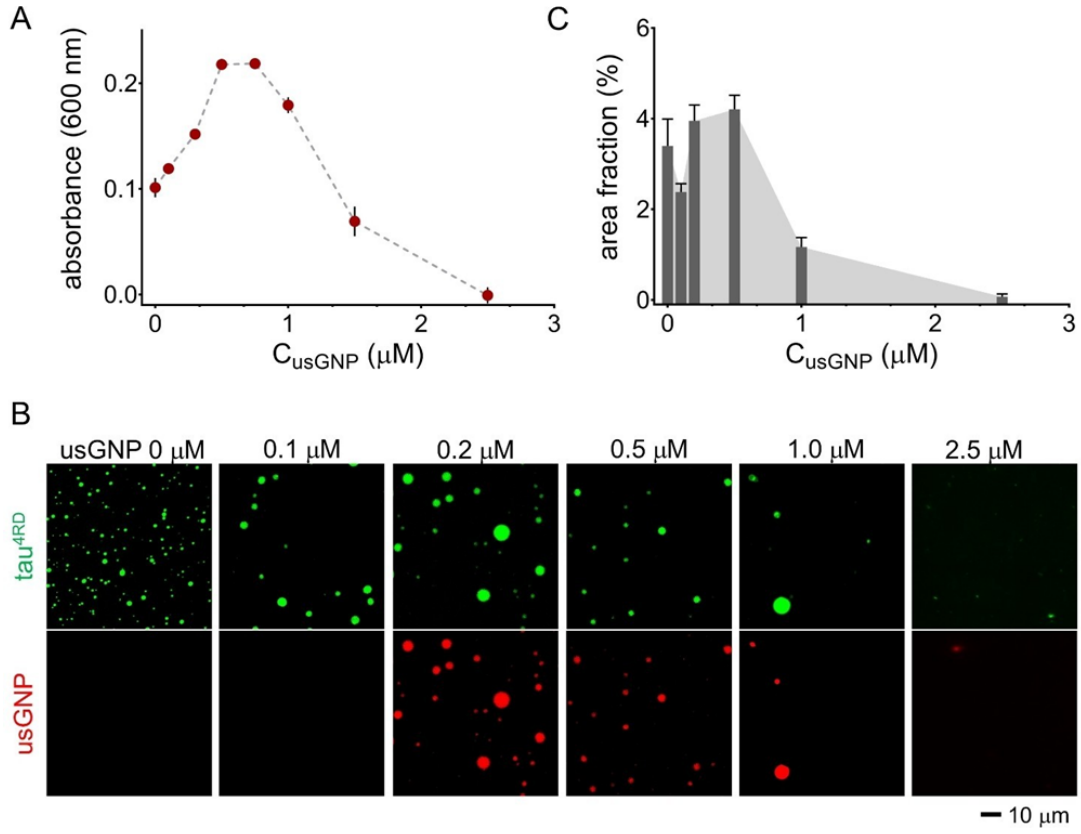

Figure 1. *Interaction of usGNP with Tau^{4RD}/polyU coacervates.* A) Turbidity measured on a solution of Tau^{4RD}/polyU in the presence of variable concentrations of usGNPs. Data are the mean s.d. from three independent measurements. B) Representative fluorescence microscopy images displaying condensates of Tau^{4RD}/ polyU in the presence of variable concentrations of usGNPs. Green: Alexa^{488}-Tau^{4RD}, red: usGNPs intrinsic emission. C) Fractional area of protein-rich phase measured from microscopy images. Data are the mean ± s.d. from five independent microscopic fields. LLPS samples contained 25 μM protein.

In the absence of NPs, fluorescence micrographs showed the formation of micron-sized spherical droplets of concentrated protein (Figure 1B). Similar images were obtained for samples containing usGNPs at concentrations up to 1 μM, however no droplets were observed in the presence of a high usGNP concentration (2.5 μM). Quantitative analysis of droplet areas indicated that the total area fraction of the dense phase was highest and similar for usGNP concentrations in the range 0–0.5 μM, and decreased on further increasing particle concentration (Figure 1C). Thus, low usGNPs concentrations were compatible with Tau^{4RD} coacervation, while higher concentrations disfavored LLPS.

The droplets obtained in the absence of NPs were found to expand over a period of 1 h after preparation (Figure S3), likely due to Ostwald ripening and coalescence. In the presence of 0.5 μM usGNPs, droplets of smaller uniform size were stabilized (Figure S3), suggesting that in these conditions usGNPs decreased the condensate interfacial tension analogously to surfactant clients described elsewhere.[61]

For usGNP concentrations between 0.2 and 1 μM, the droplets were also observed in images captured by the red channel of the microscope (Figure 1B), clearly indicating that usGNPs concentrated and distributed uniformly into the dense liquid phase, being observable due to their intrinsic red fluorescence. We conclude that, in the intermediate concentration range, usGNPs can act as fluorescent reporters for Tau^{4RD} coacervation.

It is already established that electrostatic interactions are key drivers for the coacervation of Tau^{4RD} and polyU.[8,62] Consistently, the increase in ionic strength of the solution disfavored LLPS, as shown by the dependence of sample turbidity on salt concentration (Figure 2A). A similar dependence was observed for samples containing 0.5 and 1 μM usGNPs. By contrast, in the presence of 2.5 μM usGNPs, the turbidity increased with salt concentration up to 50 mM, and then decreased at higher concentrations. The latter observation suggests that coacervation may take place at an intermediate ionic strength and, indeed, fluorescence microscopy images showed that droplets had formed in 50 mM salt, albeit very sparse (Figure 2B). Thus, high amounts of usGNPs may be compatible with LLPS under a narrow range of solution conditions.

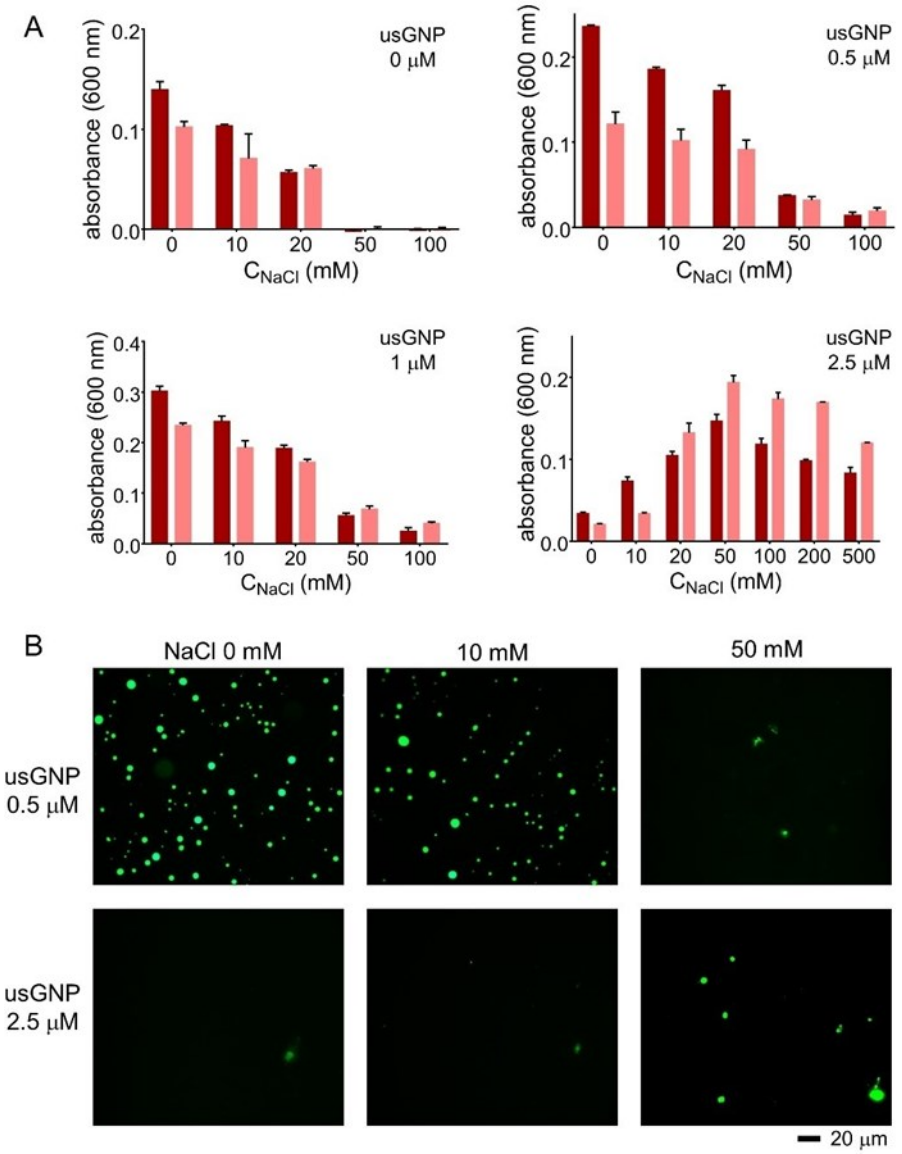

Figure 2 *Ionic strength-dependence of Tau^{4RD}/polyU coacervates in the presence of usGNPs*. A) Turbidity measured on a solution of Tau^{4RD}/polyU at increasing concentration of NaCl and at the indicated concentration of usGNPs. Data were acquired at 0 min (dark red) and 30 min (light red) from sample preparation and represent the mean±s.d. from three independent measurements. B) Representative fluorescence microscopy images displaying condensates of Tau^{4RD}/polyU at increasing concentrations of NaCl and at the indicated concentration of usGNPs. Green fluorophore: Alexa^{488}-Tau^{4RD}. Samples contained 25 μM protein.

usGNPs interact with Tau^{4RD}/heparin assemblies

Heparin (Figure S1E) is a polyanionic sulfated glycosaminoglycan that is widely used as an inducer for aggregation studies of Tau in vitro. Under specific conditions, heparin promotes LLPS of Tau^{4RD} and induces the formation of fibrillar structures

when added to Tau^{4RD} condensates.[60,63] In fact, heparin-Tau interactions are of interest as they constitute an attractive model system to explore the link between condensation and aggregation.

The mixing of Tau^{4RD} and heparin resulted in a turbid solution (Figure 3A) and small droplets appeared (Figure 3B). The droplets proved quite unstable and larger irregular assemblies were observed after 30 and 60 min of incubation. Indeed, following rapid protein aggregation, free Tau monomers are depleted and spherical liquid droplets are destabilized.[60] Next, we repeated the experiment in the presence of variable concentrations of usGNPs. We found that the solution turbidity was essentially unchanged in the presence of usGNPs in the 0.1-0.5 μM range, however it increased progressively with larger quantities of particles as observed immediately after sample preparation (Figure 3A). A low concentration of usGNPs did not prevent LLPS (although possibly perturbing the volume fractions of the phases) nor apparently modify the trans- formation of the initially formed droplets into larger assemblies (Figure 3B). By contrast, larger quantities of usGNPs affected the formation of coacervates, and larger assemblies were visible already at the start of the incubation. The latter then continued to expand over the observation period. The usGNPs were found to concentrate in the assemblies and were clearly detectable via their red fluorescence emission (Figure 3B).

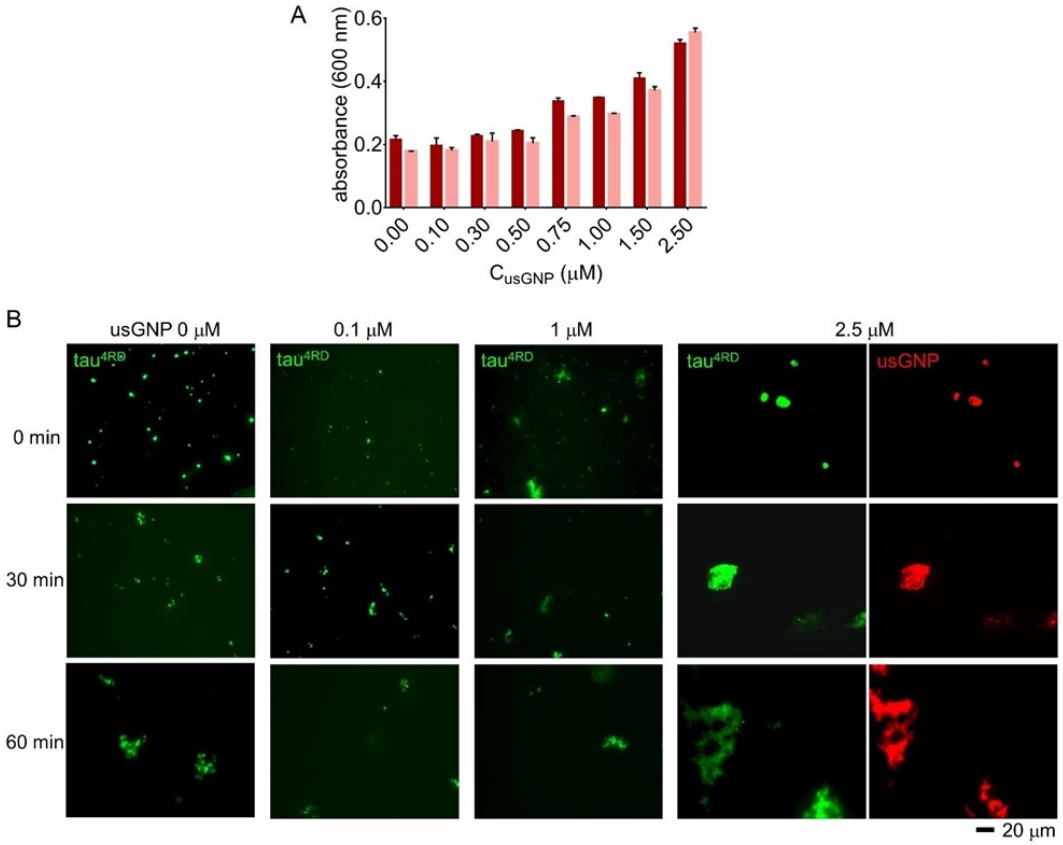

Figure 3 *Formation of Tau^{4RD}/heparin coacervates in the presence of usGNPs*. A) Turbidity measured on a solution of Tau^{4RD}/heparin in the presence of a variable concentration of usGNPs. Data were acquired at 0 min (dark red) and 30 min (light red) from sample preparation and represent the mean±s.d. from three independent measurements. B) Representative fluorescence microscopy images displaying condensates of Tau^{4RD}/heparin in the presence of a variable concentration of usGNPs. Green: Alexa^{488}-Tau^{4RD}, red: usGNPs intrinsic emission. Samples contained 25 μM protein.

Hence, usGNPs interacted with Tau^{4RD}/heparin coacervates and illuminated their transformations, however they also appeared to perturb the condensed state to an extent that depended on particle concentration, with higher particle amounts promoting larger assemblies, likely due to an increased number of available protein-NP cross-links.

Ultrasmall gold nanoparticles promote Tau^{4RD} phase separation

Despite a predicted high intrinsic propensity for phase separation, Tau^{4RD} is reported to self-assemble forming a simple coacervate (hereafter referred to as homotypic coacervate) only under non-physiological conditions such as high solution pH.[64] Indeed, the high number of positively charged amino acid residues (20 lysine

and 1 arginine) disfavors intermolecular interactions due to electrostatic repulsion. On the other hand, this region mediates the binding of Tau to microtubules, which are negatively charged, and microtubule surfaces have been proposed to facilitate the formation of Tau condensates.[65] In our study, we found that certain concentrations of usGNPs promoted the condensation of Tau^{4RD} (Figure 4), indicating that the negatively charged surfaces could engage interactions with multiple protein molecules, enabling the formation of extended protein/particle networks, perhaps involving the recently described multi-molecular assemblies as condensation nuclei.[41] Notably, the ability to induce condensation appeared to be a specific feature of usGNPs because no droplet formation was observed when using 3 nm DHLA-capped NPs, which share the same surface chemistry as usGNPs, in conditions matching the total NP area (Figure S4). By contrast, these NPs promoted the formation of sparse, irregularly shaped assemblies likely composed of NPs and protein.

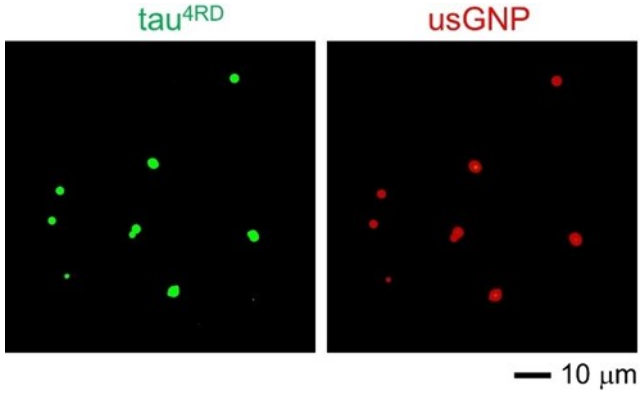

Figure 4. Representative fluorescence microscopy images displaying condensates of Tau^{4RD} induced by the presence of 2.5 µM usGNPs. Green: Alexa488-Tau^{4RD}, red: usGNPs intrinsic emission.

Coacervates of Tau^{FL} recruit usGNPs

Full-length Tau shares a highly hydrophilic character and a disordered conformation with Tau^{4RD} (apart from transient long- range interactions observed only in Tau^{FL}[66]). Residues 1–120 of the N-terminal domain bear an overall negative charge while residues 120–369, including the 4RD, are overall positively charged (Figure S1C). Tau^{FL} undergoes LLPS with lesser amount of polyU than Tau^{4RD}.[8] Here, we observed that Tau^{FL} formed spherical liquid droplets in the presence of

polyU and of 0.1 μM usGNPs (Figure 5A). Similar to what was observed with coacervates of Tau^{4RD}, usGNPs concentrated into coacervates of Tau^{FL} and were visible in the red channel due to their intrinsic luminescence. In the presence of a much higher concentration (2.5 μM) of usGNPs, phase separation did not take place, likely due to the competition between usGNPs and polyU for binding to Tau^{FL}.

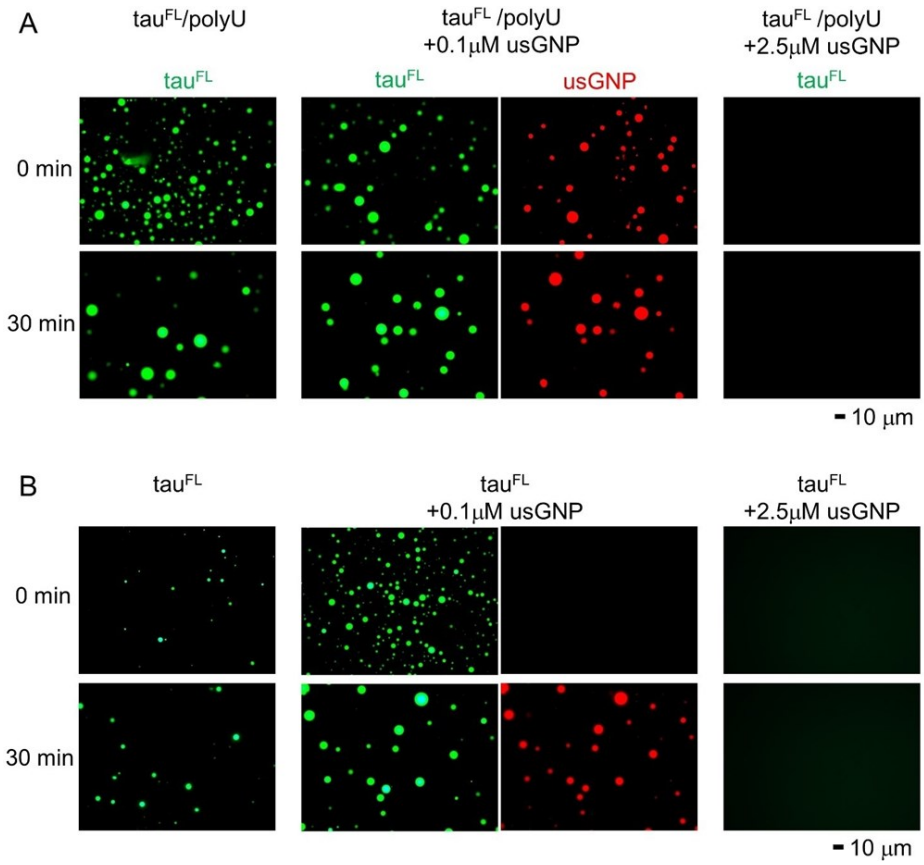

Figure 5. *Recruitment of usGNPs into condensates of Tau^{FL}*. A) Representative fluorescence microscopy images displaying condensates of Tau^{FL}/polyU in the absence or presence of usGNPs, captured at 0 min and 30 min from sample preparation. Green: $Alexa^{488}$-Tau^{4RD}, red: usGNPs intrinsic emission. B) Representative fluorescence microscopy images displaying self-condensates of Tau^{FL} in the absence or presence of usGNPs, captured at 0 min and 30 min from sample preparation. Green: $Alexa^{488}$-Tau^{4RD}, red: usGNPs intrinsic emission. Samples contained 25 μM protein.

Differently from Tau^{4RD}, Tau^{FL} can undergo phase separation in the absence of cofactors,[8,52] presumably because its ampholytic nature allows to establish intermolecular interactions between complementary chemical groups. The addition of 0.1 μM usGNPs appeared to facilitate LLPS, as deduced from the larger volume fraction of the dense phase, compared to the absence of particles (estimated from visual

analysis of the corresponding micrographs, Figure 5B). The usGNPs partitioned and distributed uniformly into phase separated droplets. The addition of 2.5 μM usGNPs once again impaired LLPS of Tau^{FL}.

usGNPs concentrate into Tau^{FL}/polyU/αSyn coacervate droplets

Recently, the interaction between the protein α-synuclein (αSyn) and Tau LLPS was investigated.[67] αSyn is another IDP associated with neurodegenerative conditions, which is believed to interact synergistically with Tau-based pathologies. αSyn has a low tendency for self-coacervation and RNA- mediated LLPS but is capable to partition into Tau^{FL}/RNA droplets, driven by electrostatic interactions between the negatively charged C-terminal domain of αSyn (Figure S1C) and the positively charged proline-rich P2 region of Tau.[67] The latter region is also involved in RNA binding, however the interaction is dynamic and the binding to αSyn and RNA is not exclusive.

We observed the partitioning of αSyn into Tau^{FL}/RNA droplets using $Alexa^{488}$-labelled αSyn (Figure 6). The presence of 0.1 μM usGNPs apparently decreased the rate of phase separation, however droplets observed after 30 min were essentially indistinguishable from those obtained in the absence of particles, and clearly showed the recruitment of usGNPs (Figure 6). A higher concentration of usGNPs disfavored condensate formation.

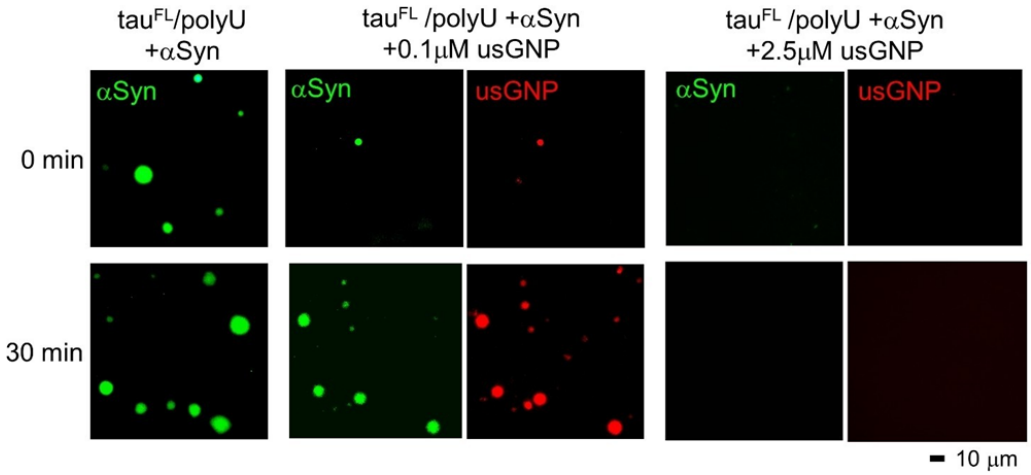

Figure 6. Representative fluorescence microscopy images displaying condensates of Tau^{FL}/polyU incorporating αSyn, in the absence or presence of usGNPs, captured at 0 min and 30 min from sample preparation. Green: $Alexa^{488}$-αSyn, red: usGNPs intrinsic emission. Samples contained 25 μM Tau^{FL} and 5 μM αSyn

DISCUSSION

Intrinsically disordered proteins are one of the main archetypes of phase-separating proteins found in cellular condensates.[2] The microtubule-binding protein Tau is an IDP that can assemble into liquid droplets by phase separation.[51] This process is thought to play a role both in normal neuronal function and in neurodegeneration, however the underlying molecular mechanisms are still far from being clarified. Our work focused on elucidating the interaction between diverse forms of Tau condensates and ultrasmall gold nanoparticles as candidate condensate-targeting agents.

The condensation of chain-like biopolymers, such as IDPs, is often described by a mean-field Flory-Huggins theory, able to provide semi-quantitative agreement with experimental phase diagrams.[7] However, differently from synthetic polymers, the phase separation behavior of IDPs remains incompletely under- stood due to complicating factors like nonuniform charge patterning and sequence specificity.[68,69] Although more advanced models have been under scrutiny,[70–72] a quantitative and general explanation of protein LLPS is still lagging behind. Here, we discuss particle interactions with coacervates in terms of the scaffold-client principle.[1] Scaffolds are (groups of) biomolecules that self-associate and drive LLPS, while clients are solutes that are unnecessary for condensate formation but are recruited into condensates on interacting with the scaffolds. Full-length Tau can act as a scaffold and phase separate on its own, likely driven by homotypic charge-charge, dipole-dipole, π-π, and cation-π intermolecular interactions involving chemically complementary regions. The protein can also form complex coacervates with polyanions like RNA, driven by electrostatic interactions involving concentrated regions of positive charges, such as the repeat domain. Both Tau and RNA act as scaffolds in such complex coacervates. The isolated RD has little propensity to phase separate on its own, due to the lack of complementary chemical groups between interacting molecules, but readily forms condensates with polyU RNA via heterotypic scaffold-scaffold interactions. Another disease associated IDP, αSyn, can concentrate into Tau/RNA coacervates by establishing electrostatic client (αSyn) - scaffold (Tau) interactions. These distinct condensates of Tau, i. e. self-condensates, Tau/RNA, Tau^{4RD}/RNA(or heparin), and Tau/RNA/αSyn, provide chemically diverse model

systems for interrogating the interaction of NPs with phase separated proteins, and could be representative of more complex cellular assemblies.

In order to target Tau and its repeat domain, we decorated usGNPs with DHLA, producing negatively charged particles. Indeed, we have previously shown that Tau^{4RD} associates with DHLA-capped usGNPs forming stable multi-molecular assemblies.[41] Moreover, we observed that DHLA-capped usGNPs were recruited by stress granules, a type of cytosolic membrane-less organelle enriched for IDPs and proteins with disordered regions.[41] Here, we found that usGNPs concentrated and distributed uniformly into Tau^{4RD}(or Tau^{FL})/polyU condensates. At low particle concentration, LLPS behavior was retained and usGNPs can be considered to act as coacervate clients, whose distribution is governed by the relative standard free energy of the particles in the different phases: $K_p \sim\approx \lambda e^{-\Delta G°/RT}$ (K_p is the partitioning coefficient and λ is a correction factor that accounts for differences in activity between both phases). ΔG° could result from multiple distinct contributions, such as $\Delta G°_{hphob}$, $\Delta G°_{charge}$, $\Delta G°_{Hbond}$, and $\Delta G°_{mesh}$.[73] Given the extensive charged regions of Tau species and the presence of net charges on usGNPs, it is expected that the charge complexation term, $\Delta G°_{charge}$, accounts for a significant part of the client (NP) -scaffold (Tau) interactions. We note that the unfavorable contribution of mesh deformation, $\Delta G°_{mesh}$, predicted for large solutes,[74] should be minimal owing to the ultrasmall size of the used particles. For example, the characteristic mesh size of liquid condensates formed by the LAF-1 protein was deter- mined to be ~ 3-8 nm,[75] thus solutes larger than this size are expected to distort a droplet mesh of that type. In the coacervate matrix, scaffold protein molecules likely dynamically switch their interaction between polyU and NPs. At high NP concentration, competition possibly resulted in a reduced density of favorable scaffold-scaffold connections in the condensed network[76] which, together with accumulation of excess negative charge, caused destabilization of the condensate. Hence, in these conditions, usGNPs affected the phase behavior of the original host, thereby acting as regulators of coacervation rather than 'inert' clients.

Although in principle similar to Tau/polyU condensation, heparin mediated LLPS exhibited different behavior. In this case, usGNPs appeared to accelerate the destabilization of initially formed droplets into large irregular assemblies. Heparin, a

sulfated glycosaminoglycan with an estimated higher charge density compared to polyU, displays strong binding affinity (sub micromolar) to Tau and promotes its conformational transition and assembly into highly ordered supramolecular filaments.[77] Protein aggregation is rapid at Tau/heparin ratios near charge neutralization, a condition that overlaps with that for LLPS. It appears that the charge imbalance introduced by the addition of usGNPs affected liquid phase separation but did not arrest the accumulation of Tau aggregates. Nonetheless, the observation of particle distribution into these assemblies indicated that scaffold-client interactions occurred in these assemblies too. Monitoring the evolution of such system could prove useful for a better understanding of the molecular mechanisms of condensation-linked protein aggregation.

The experiments on Tau^{FL}/polyU condensates incorporating αSyn demonstrated that the recruitment of usGNPs can take place within more complex condensed networks. In this case, Tau would establish dynamic interactions with either the scaffold polyU, the client αSyn, or the client usGNPs. Again, high concentrations of usGNPs destabilized liquid condensates and no phase separation was observed in that condition because of the prevalent scaffold-client(usGNPs) binding. Fur- ther studies on this multicomponent system could provide insight into the synergistic activity of αSyn and Tau in the context of neurodegeneration.

We further observed the partitioning of usGNPs into the simple condensates of Tau^{FL} formed in the absence of poly- anionic cofactors. In that case, we noted an apparent stabilization of liquid droplets at low NP concentration, possibly due to the creation of new scaffold-client-scaffold bridges that in- creased the density of connections within the condensate. Strikingly, the usGNPs were even capable to promote LLPS of Tau^{4RD}, which did not phase separate on its own, thereby acting as cofactors for its coacervation. It is noted that slightly larger NPs with the same surface functionalization as usGNPs failed to promote LLPS, indicating that NP size has an influence on the condensation process. In general, by fine tuning the concentration of usGNPs, it will be possible to shift the equilibrium between formation and dissolution of condensates.

We remark that the biomolecular composition of cellular condensates is more complex than that considered in our simplified model systems. It is well established that

on exposure to biological media, typical NPs become covered by a layer of biological macromolecules, generally referred to as the bio-molecular corona, which is known to influence the interaction of NPs with the biological system.[78] NPs in the ultrasmall scale do not appear to form stable coronas, and protein-usNP interactions are generally weak.[39] While it is possible that macromolecules encountered in the medium interact competitively with usGNPs and alter the extent and nature of the interactions between Tau and usGNPs, the multivalent binding capability and conformational plasticity of Tau represent an advantage for binding to usGNPs over most folded proteins.[41]

CONCLUSION

The present study indicates that usGNPs associate with Tau in condensates and can influence LLPS behavior. Hence, usGNPs are promising condensate-targeting agents that could be used to query protein LLPS by exploiting their intrinsic luminescence in combination with imaging technologies (nanotracers). The usGNPs could further modulate the formation, stability, and physicochemical properties of protein condensed states, allowing to control biological processes in cellular models of pathology (nanoactuators). NP-based targeting of IDPs in condensates is of extraordinary interest for the development of new therapeutic approaches against refractory diseases. The diverse surface functionalization possibilities and distinct core materials of NPs represent a vast chemical space available for designing tailored nanoobjects applied to the study of bio- molecular condensates.

MATERIALS AND METHODS

Reagents

Tetrachloroauric acid trihydrate ($HAuCl_4$), lipoic acid (LA), and sodium borohydride ($NaBH_4$) were purchased from Alfa Aesar (MA, USA). Heparin and all chemical reagents were obtained from Sigma-Aldrich (St Louis, MO, USA). Millipore system was used for high-purity deionized water production, used in all preparations.

Recombinant protein expression and purification

Recombinant Tau^{4RD} (region Q244-E372 of human full-length Tau, plus initial Met) was expressed and purified as described previously[79] with the mutations C291A and C322A to avoid unintended disulfide bond formation (hereafter referred to as Tau^{4RD} for simplicity). The protein was expressed in BL21 (DE3) cells grown at 37 °C in LB medium under shaking for 5 h, with the addition of 0.5 mM IPTG. The soluble bacterial extract was subjected to thermal treatment (80– 100 °C), and protein purification was achieved by SP-ion exchange chromatography. Purified Tau^{4RD} samples were then dialyzed in 10 mM phosphate buffer, pH 7.4.

Recombinant Tau^{FL} (also known as Tau^{441}) was expressed without tag from a pET3a vector and purified as described previously.[80] Briefly, the protein was expressed in Codon Plus E. coli cells grown in TB medium at 37 °C for 5 h, with 0.5 mM IPTG. Cells were then resuspended in 20 mM MES buffer, 0.05 M NaCl, pH 6.8, 1 Mm EGTA, complemented with 5 mM $MgCl_2$, 1 mM PMSF protease inhibitors, and 20 µg/mL DNAse, sonicated and boiled for 20 min. After cooling, 1 mM TCEP was added. The clarified supernatant was then loaded on a SP-Sepharose column, and the protein eluted with a linear 0.05–0.5 M NaCl gradient in the same buffer.

Recombinant human α-synuclein was expressed in *E. coli* BL21 (DE3) bacterial cells and purified as reported previously.[29]

Fluorescent labeling of proteins

Proteins were labeled with Alexa Fluor 488 (Thermo Fisher Scientific) by adding 10 µL of the dye in DMSO (10 mg/ml) to 100 µL of the protein (10 mg/ml) in 0.1 M sodium bicarbonate, pH 8.3, and incubating the mixture for 2 h under stirring at

room temperature. A desalting column was used to remove the excess of dye. The Alexa-conjugated protein was eluted in 20 mM sodium phosphate, pH 7.4. Labeling efficiency was estimated based on relative concentrations of the protein and the dye (the latter determined by absorbance at 488 nm).

Visualization and analysis of protein condensates

Liquid-liquid phase separation of the investigated proteins species was induced as reported.[60] Briefly, 25 μM protein was mixed with 62.5 μg/ml poly(U) RNA, 1 mM DTT in 25 mM Hepes pH 7.4, or 6.25 μM heparin, 5 mM DTT, 30 mM NaCl in 20 mM sodium phosphate, pH 6.0. The reducing agent was used only for Tau^{FL}. Images were acquired on a Leica TCS SP5 AOBS microscope to visualize the formation of droplets over time. Images analysis was performed to measure droplets size and distribution using FIJI Image H software (v2.0). The fluorescence images within a set of experiments were acquired using identical microscope setting to ensure consistency across samples and experimental runs.

Turbidimetry

LLPS was monitored by turbidity measurements (optical density at 600 nm) at 25 °C using a TECAN INFINITE M200PRO PLEX microplate reader. Experiments were carried out in 25 mM Hepes, pH 7.4. All experiments were performed at room temperature. Three spectra accumulations were averaged for each sample and the spectrum of the buffer (also containing usGNPs, where appropriate) was considered as a blank and subtracted.

Synthesis of nanoparticles

DHLA-capped gold nanoparticles were synthesized following a previously reported protocol.[81,82] Briefly, an aqueous solution of lipoic acid was dissolved with NaOH (2 M), followed by addition of $HAuCl_4$ solution (2 % by mass). $NaBH_4$ was then slowly added drop by drop, under rapid stirring. The reaction was stopped after stirring overnight. The molar ratio for the three components (DHLA:$HAuCl_4$:$NaBH_4$) was varied to synthetize 2 nm and 3 nm size AuNPs (3 : 1 : 2 and 1 : 2 : 10, respectively). Finally, the brownish solution was purified by

centrifugal filtration (Amicon Ultra 10 kDa cutoff – Merck, Millipore) and stored at 4 °C.

The NP concentration was estimated from the absorbance at 450 nm using the extinction coefficient (4.25×10^5) M^{-1} cm^{-1}, as reported by Haiss.[83] UV-vis absorption spectra were recorded with a NanoDrop™ 2000 Spectrophotometer (Thermofisher), using 1 cm path-length quartz cuvettes.

Dynamic Light Scattering (DLS)

A Zetasizer Nano ZS (Malvern Instruments, Malvern, UK) was employed to measure the hydro- dynamic diameter and ζ-potential at room temperature. For determining size distribution by DLS, measurements were recorded
in triplicate on 20 μM usGNPs in working buffer and the average of the measurements was plotted. For ζ-potential measurements, the voltage was set to 148 V and the ζ-potential values were derived from five replicates.

Fluorescence Spectroscopy

Fluorescence measurements were performed on a Jasco FP-8500 spectrofluorometer (Jasco, Easton, MD, USA) using 1 cm path-length quartz cuvettes.

Fluorescence emission spectra (range 550–750 nm) of 0.5 μM usGNPs were recorded using an excitation wavelength of 530 nm (slit width 5 nm). All experiments were performed at room temperature. Three spectra accumulations were averaged for each sample. The spectrum of the buffer was recorded as a blank.

Transmission Electron Microscopy (TEM)

TEM measurements were performed using a Tecnai G^2 (FEI) transmission electron microscope operating at 100 kV. Samples were prepared at a concentration of 0.5 μM, dissolved in mQ H_2O, then adsorbed onto holey film grids (400 mesh) and stained with uranyl acetate at 2 %. A Veleta digital camera (Olympus Soft Imaging System, Münster, Germany) and FEI TIA acquisition software were employed to capture images.

Conflict of interest

The authors declare no competing financial interest.

ACKNOWLEDGMENTS

Centro Piattaforme Tecnologiche of the University of Verona is acknowledged for providing access to the Microscopy Facility and to the DLS instrument. The University of Padova is acknowledged for providing access to the Electron Microscope (DiBio Imaging Facility).

REFERENCES

(1) S. F. Banani, H. O. Lee, A. A. Hyman, M. K. Rosen, Nat. Rev. Mol. Cell Biol. 2017, 18, 285– 298.

(2) S. Boeynaems, S. Alberti, N. L. Fawzi, T. Mittag, M. Polymenidou, F. Rousseau, J. Schymkowitz, J. Shorter, B. Wolozin, L. Van Den Bosch, P. Tompa, M. Fuxreiter, Trends Cell Biol. 2018, 28, 420–435.

(3) Y. Shin, C. P. Brangwynne, Science 2017, 357, eaaf4382.

(4) C. P. Brangwynne, C. R. Eckmann, D. S. Courson, A. Rybarska, C. Hoege, J. Gharakhani, F. Jülicher, A. A. Hyman, Science 2009, 324, 1729–1732.

(5) C. P. Brangwynne, Soft Matter 2011, 7, 3052.

(6) S. Alberti, A. Gladfelter, T. Mittag, Cell 2019, 176, 419–434.

(7) C. P. Brangwynne, P. Tompa, R. V. Pappu, Nat. Phys. 2015, 11, 899–904.

(8) T. Ukmar-Godec, S. Hutten, M. P. Grieshop, N. Rezaei-Ghaleh, M.-S. Cima- Omori, J. Biernat, E. Mandelkow, J. Söding, D. Dormann, M. Zweckstet- ter, Nat. Commun. 2019, 10, 2909.

(9) A. L. Darling, Y. Liu, C. J. Oldfield, V. N. Uversky, Proteomics 2018, 18, e1700193.

(10) V. N. Uversky, I. M. Kuznetsova, K. K. Turoverov, B. Zaslavsky, FEBS Lett. 2015, 589, 15–22.

(11) C. J. Oldfield, A. K. Dunker, Annu. Rev. Biochem. 2014, 83, 553–584.

(12) R. van der Lee, M. Buljan, B. Lang, R. J. Weatheritt, G. W. Daughdrill, A. K. Dunker, M. Fuxreiter, J. Gough, J. Gsponer, D. T. Jones, P. M. Kim, R. W. Kriwacki, C. J. Oldfield, R. V. Pappu, P. Tompa, V. N. Uversky, P. E. Wright, M. M. Babu, Chem. Rev. 2014, 114, 6589–6631.

(13) Z. Peng, J. Yan, X. Fan, M. J. Mizianty, B. Xue, K. Wang, G. Hu, V. N. Uversky, L. Kurgan, Cell. Mol. Life Sci. 2015, 72, 137–151.

(14) H. J. Dyson, P. E. Wright, Nat. Rev. Mol. Cell Biol. 2005, 6, 197–208.

(15) V. N. Uversky, C. J. Oldfield, A. K. Dunker, Annu. Rev. Biophys. 2008, 37, 215–246.

(16) J. E. Bramham, A. P. Golovanov, Nat. Commun. 2022, 13, 1767.

(17) W. M. Babinchak, B. K. Dumm, S. Venus, S. Boyko, A. A. Putnam, E. Jankowsky, W. K. Surewicz, Nat. Commun. 2020, 11, 5574.

(18) C. N. Hernández-Candia, S. Pearce, C. L. Tucker, Nat. Commun. 2021, 12, 1809.

(19)A. Mullard, Nat. Rev. Drug Discovery 2019, 10.1038/d41573-019-00069-w.

(20) M. Biesaga, M. Frigolé-Vivas, X. Salvatella, Curr. Opin. Chem. Biol. 2021, 62, 90–100.

(21) R. J. Wheeler, Emerg. Top. Life Sci. 2020, 4, 307–318.

(22) I. A. Klein, A. Boija, L. K. Afeyan, S. W. Hawken, M. Fan, A. Dall'Agnese, O. Oksuz, J. E. Henninger, K. Shrinivas, B. R. Sabari, I. Sagi, V. E. Clark, J. M. Platt, M. Kar, P. M. McCall, A. V. Zamudio, J. C. Manteiga, E. L. Coffey,
C. H. Li, N. M. Hannett, Y. E. Guo, T.-M. Decker, T. I. Lee, T. Zhang, J.-K. Weng, D. J. Taatjes, A. Chakraborty, P. A. Sharp, Y. T. Chang, A. A. Hyman, N. S. Gray, R. A. Young, Science 2020, 368, 1386–1392.
(23) S. Mitragotri, D. G. Anderson, X. Chen, E. K. Chow, D. Ho, A. V. Kabanov,
J. M. Karp, K. Kataoka, C. A. Mirkin, S. H. Petrosko, J. Shi, M. M. Stevens, S. Sun, S. Teoh, S. S. Venkatraman, Y. Xia, S. Wang, Z. Gu, C. Xu, ACS Nano 2015, 9, 6644–6654.
(24) J. A. Yang, B. J. Johnson, S. Wu, W. S. Woods, J. M. George, C. J. Murphy, Langmuir 2013, 29, 4603–4615.
(25) . Lin, T. Insley, M. D. Tuttle, L. Zhu, D. A. Berthold, P. Král, C. M. Rienstra, C. J. Murphy, J. Phys. Chem. C 2015, 119, 21035–21043.
(26)nM. Xie, A. L. Hansen, J. Yuan, R. Brüschweiler, J. Phys. Chem. C 2016, 120, 24463–24468.
(27) D.-W. Li, M. Xie, R. Brüschweiler, J. Am. Chem. Soc. 2020, 142, 10730–10738.
(28) M. Vitali, V. Rigamonti, A. Natalello, B. Colzani, S. Avvakumova, S. Brocca, C. Santambrogio, J. Narkiewicz, G. Legname, M. Colombo, D. Prosperi, R. Grandori, Biochim. Biophys. Acta BBA - Gen. Subj. 2018, 1862, 1556–1564.
(29) R. Tira, E. De Cecco, V. Rigamonti, C. Santambrogio, C. G. Barracchia, F. Munari, A. Romeo, G. Legname, D. Prosperi, R. Grandori, M. Assfalg, Int. J. Biol. Macromol. 2020, 154, 206–216.
(30) M. Mahmoudi, H. R. Kalhor, S. Laurent, I. Lynch, Nanoscale 2013, 5, 2570.
(31) M. D'Onofrio, F. Munari, M. Assfalg, Molecules 2020, 25, 5625.
(32) A. Avni, A. Joshi, A. Walimbe, S. G. Pattanashetty, S. Mukhopadhyay, Nat. Commun. 2022, 13, 4378.
(33) Q. Pan, D. Sun, J. Xue, J. Hao, H. Zhao, X. Lin, L. Yu, Y. He, ACS Nano 2021, 15, 539–549.
(34) C. G. Barracchia, F. Parolini, A. Volpe, D. Gori, F. Munari, S. Capaldi, M. D'Onofrio, M. Assfalg, Bioconjugate Chem. 2022, acs.bioconj- chem.2c00168.
(35) J. Liu, M. Yu, C. Zhou, S. Yang, X. Ning, J. Zheng, J. Am. Chem. Soc. 2013, 135, 4978–4981.
(36) C. N. Loynachan, A. P. Soleimany, J. S. Dudani, Y. Lin, A. Najer, A. Bekdemir, Q. Chen, S. N. Bhatia, M. M. Stevens, Nat. Nanotechnol. 2019, 14, 883–890.

(37) V. Sokolova, G. Nzou, S. B. van der Meer, T. Ruks, M. Heggen, K. Loza, N. Hagemann, F. Murke, B. Giebel, D. M. Hermann, A. J. Atala, M. Epple, Acta Biomater. 2020, 111, 349–362.
(38) V. Sokolova, G. Mekky, S. B. van der Meer, M. C. Seeds, A. J. Atala, M. Epple, Sci. Rep. 2020, 10, 18033.
(39) A. A. Sousa, P. Schuck, S. A. Hassan, Nanoscale Adv. 2021, 3, 2995–3027.
(40) L. Boselli, E. Polo, V. Castagnola, K. A. Dawson, Angew. Chem. Int. Ed. 2017, 56, 4215–4218.
(41) G. Viola, C. G. Barracchia, R. Tira, F. Parolini, G. Leo, M. Bellanda, F. Munari, S. Capaldi, M. D'Onofrio, M. Assfalg, Nano Lett. 2022, acs.nanolett.2c02902.
(42) M.-M. Yin, W.-Q. Chen, Y.-Q. Lu, J.-Y. Han, Y. Liu, F.-L. Jiang, Nanoscale 2020, 12, 4573–4585.
(43) B. H. Kim, M. J. Hackett, J. Park, T. Hyeon, Chem. Mater. 2014, 26, 59–71.
(44) K. Nienhaus, H. Wang, G. U. Nienhaus, Mater. Today 2020, 5, 100036.
(45) D. G. Drubin, M. W. Kirschner, J. Cell Biol. 1986, 103, 2739–2746.
(46) M. G. Spillantini, M. Goedert, Lancet Neurol. 2013, 12, 609–622.
(47) Y. Wang, E. Mandelkow, Nat. Rev. Neurosci. 2016, 17, 22–35.
(48) T. Vanderweyde, D. J. Apicco, K. Youmans-Kidder, P. E. A. Ash, C. Cook, E. Lummertz da Rocha, K. Jansen-West, A. A. Frame, A. Citro, J. D. Leszyk, P. Ivanov, J. F. Abisambra, M. Steffen, H. Li, L. Petrucelli, B. Wolozin, Cell Rep. 2016, 15, 1455–1466.
(49) M. K. Sjöberg, E. Shestakova, Z. Mansuroglu, R. B. Maccioni, E. Bonnefoy, J. Cell Sci. 2006, 119, 2025–2034.
(50) S. Wegmann, B. Eftekharzadeh, K. Tepper, K. M. Zoltowska, R. E. Bennett, S. Dujardin, P. R. Laskowski, D. MacKenzie, T. Kamath, C. Commins, C. Vanderburg, A. D. Roe, Z. Fan, A. M. Molliex, A. Hernandez-Vega, D. Muller, A. A. Hyman, E. Mandelkow, J. P. Taylor, B. T. Hyman, EMBO J. 2018, 37, e98049.
(51) T. Ukmar-Godec, S. Wegmann, M. Zweckstetter, Semin. Cell Dev. Biol. 2020, 99, 202–214.
(52) N. M. Kanaan, C. Hamel, T. Grabinski, B. Combs, Nat. Commun. 2020, 11, 2809.
(53) S. Boyko, W. K. Surewicz, Trends Cell Biol. 2022, S0962892422000265
(54) L. Shang, N. Azadfar, F. Stockmar, W. Send, V. Trouillet, M. Bruns, D. Gerthsen, G. U. Nienhaus, Small 2011, 7, 2614–2620.
(55) N. Gustke, B. Trinczek, J. Biernat, E.-M. Mandelkow, E. Mandelkow, Biochemistry 1994, 33, 9511–9522.

(56) H. Kadavath, R. V. Hofele, J. Biernat, S. Kumar, K. Tepper, H. Urlaub, E. Mandelkow, M. Zweckstetter, Proc. Nat. Acad. Sci. 2015, 112, 7501–7506.
(57) A. W. P. Fitzpatrick, B. Falcon, S. He, A. G. Murzin, G. Murshudov, H. J. Garringer, R. A. Crowther, B. Ghetti, M. Goedert, S. H. W. Scheres, Nature 2017, 547, 185–190.
(58) W. Zhang, B. Falcon, A. G. Murzin, J. Fan, R. A. Crowther, M. Goedert, S. H. Scheres, eLife 2019, 8, e43584.
(59) C. G. Barracchia, R. Tira, F. Parolini, F. Munari, L. Bubacco, G. A. Spyroulias, M. D'Onofrio, M. Assfalg, Molecules 2020, 25, 2716.
(60) F. Parolini, R. Tira, C. G. Barracchia, F. Munari, S. Capaldi, M. D'Onofrio, M. Assfalg, Int. J. Biol. Macromol. 2022, 201, 173–181.
(61) I. Sanchez-Burgos, J. A. Joseph, R. Collepardo-Guevara, J. R. Espinosa, Sci. Rep. 2021, 11, 15241.
(62) Y. Lin, Y. Fichou, Z. Zeng, N. Y. Hu, S. Han, ACS Chem. Neurosci. 2020, 11, 615–627.
(63) S. Ambadipudi, M. Zweckstetter, Expert Opin. Drug Discovery 2016, 11, 65–77.
(64) S. Ambadipudi, J. Biernat, D. Riedel, E. Mandelkow, M. Zweckstetter, Nat. Commun. 2017, 8, 275.
(65) R. Tan, A. J. Lam, T. Tan, J. Han, D. W. Nowakowski, M. Vershinin, S. Simó, K. M. Ori-McKenney, R. J. McKenney, Nat. Cell Biol. 2019, 21, 1078–1085.
(66) M. D. Mukrasch, S. Bibow, J. Korukottu, S. Jeganathan, J. Biernat, C. Griesinger, E. Mandelkow, M. Zweckstetter, PLoS Biol. 2009, 7, e1000034.
(67) A. Siegert, M. Rankovic, F. Favretto, T. Ukmar-Godec, T. Strohäker, S. Becker, M. Zweckstetter, Protein Sci. 2021, 30, 1326–1336.
(68) C. W. Pak, M. Kosno, A. S. Holehouse, S. B. Padrick, A. Mittal, R. Ali, A. A. Yunus, D. R. Liu, R. V. Pappu, M. K. Rosen, Mol. Cell 2016, 63, 72–85.
(69) L.-W. Chang, T. K. Lytle, M. Radhakrishna, J. J. Madinya, J. Vélez, C. E. Sing, S. L. Perry, Nat. Commun. 2017, 8, 1273.
(70) K. T. Delaney, G. H. Fredrickson, J. Chem. Phys. 2017, 146, 224902.
(71) C. E. Sing, Adv. Colloid Interface Sci. 2017, 239, 2–16.
(72) Y.-H. Lin, J. D. Forman-Kay, H. S. Chan, Phys. Rev. Lett. 2016, 117, 178101.
(73) Y. Guan, T. H. Lilley, M. N. Garcia-Lisbona, T. E. Treffry, Pure Appl. Chem. 1995, 67, 955–962.
(74) K. K. Nakashima, M. A. Vibhute, E. Spruijt, Front. Mol. Biosci. 2019, 6, 21.
(75) M.-T. Wei, S. Elbaum-Garfinkle, A. S. Holehouse, C. C.-H. Chen, M. Feric, C. B. Arnold, R. D. Priestley, R. V. Pappu, C. P. Brangwynne, Nat. Chem.

2017, 9, 1118–1125.
(76) J. R. Espinosa, J. A. Joseph, I. Sanchez-Burgos, A. Garaizar, D. Frenkel, R. Collepardo-Guevara, Proc. Nat. Acad. Sci. 2020, 117, 13238–13247.
(77) N. Sibille, A. Sillen, A. Leroy, J.-M. Wieruszeski, B. Mulloy, I. Landrieu, G. Lippens, Biochemistry 2006, 45, 12560–12572.
(78) M. P. Monopoli, C. Åberg, A. Salvati, K. A. Dawson, Nat. Nanotechnol. 2012, 7, 779–786.
(79) F. Munari, C. G. Barracchia, C. Franchin, F. Parolini, S. Capaldi, A. Romeo, L. Bubacco, M. Assfalg, G. Arrigoni, M. D'Onofrio, Angew. Chem. Int. Ed. 2020, 59, 6607–6611.
(80) F. Munari, L. Mollica, C. Valente, F. Parolini, E. A. Kachoie, G. Arrigoni, M. D'Onofrio, S. Capaldi, M. Assfalg, Angew. Chem. Int. Ed. 2022, anie.202112374.
(81) L. Shang, S. Brandholt, F. Stockmar, V. Trouillet, M. Bruns, G. U. Nienhaus, Small 2012, 8, 661–665.
(82) L. Shang, N. Azadfar, F. Stockmar, W. Send, V. Trouillet, M. Bruns, D. Gerthsen, G. U. Nienhaus, Small 2011, 7, 2614–2620.
(83) W. Haiss, N. T. K. Thanh, J. Aveyard, D. G. Fernig, Anal. Chem. 2007, 79, 4215–4221.

SUPPORTING INFORMATION

CONTENT

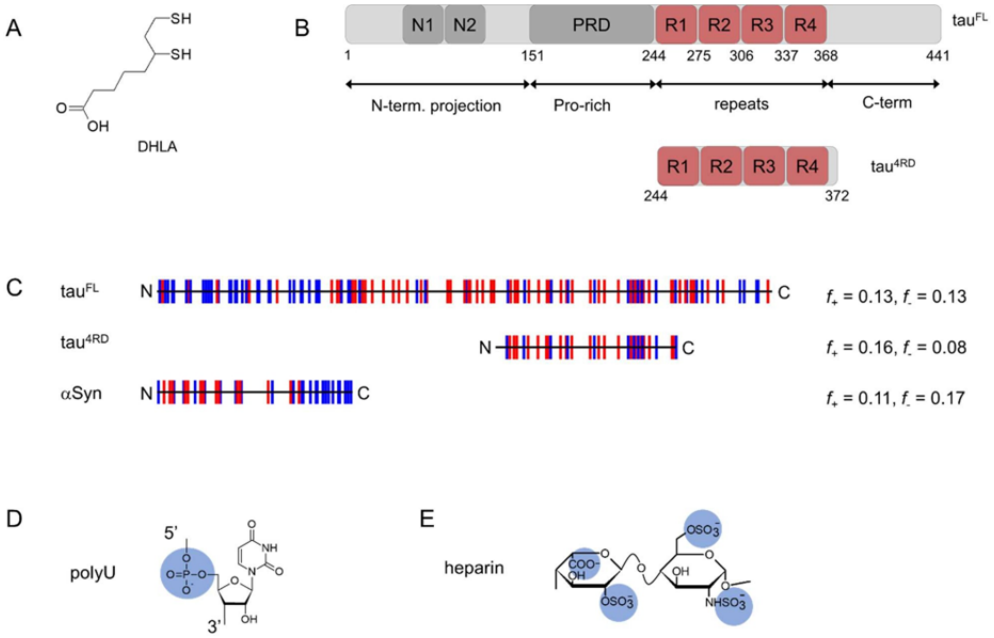

Figure S1. *Molecules used in the study*. A) Structure of dihydrolipoic acid (DHLA). B) Domain organization of Tau^{FL} and Tau^{4RD}. N1 and N2 are N-terminal inserts, R1-R4 are pseudo-repeats. C) Distribution of charged residues along the polypeptide chains of the indicated proteins. Basic (acidic) residues are coloured in red (blue). *f+* is the fraction of positive charges and *f-* is the fraction of negative charges along the chain (pH 7). D) Structure of polyU repeating unit. E) Structure of heparin repeating unit.

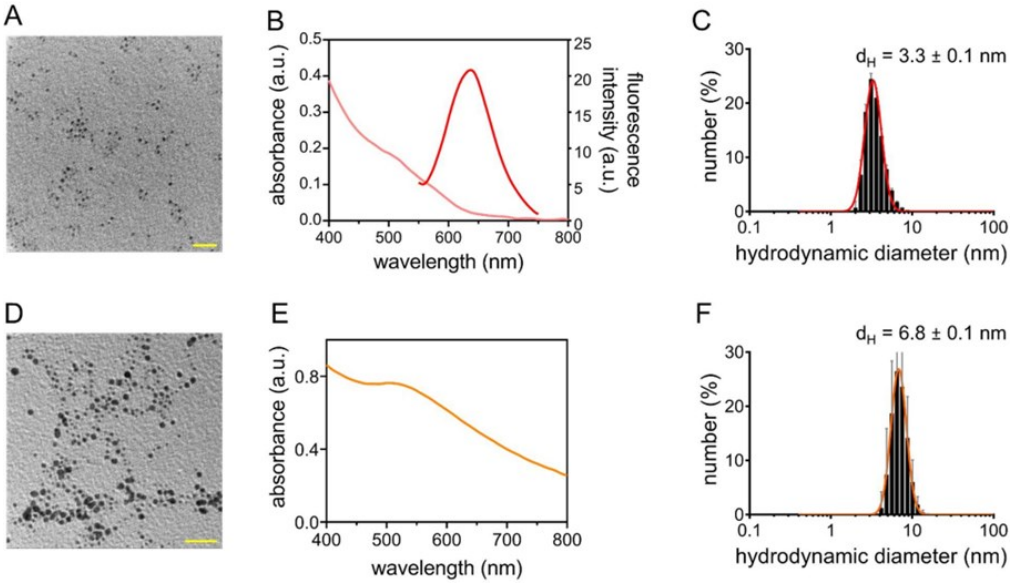

Figure S2. *Characterization of NPs*. Displayed data were obtained on usGNPs (A-C) and GNPs (D-F). A,D) Representative TEM images; scale bars are 20 nm. B) Visible light absorption spectrum (light red) and fluorescence emission spectrum (λ_{ex} = 530 nm, λ_{max} = 640 nm, red). E) Visible light absorption spectrum. C,F)Hydrodynamic diameter distribution plots as determined from dynamic light scattering; diameter distribution was essentially invariant in the 1-10 μM range; continuous lines are the best-fit Log-Gaussian curves; the mean ± s.d. values are reported.

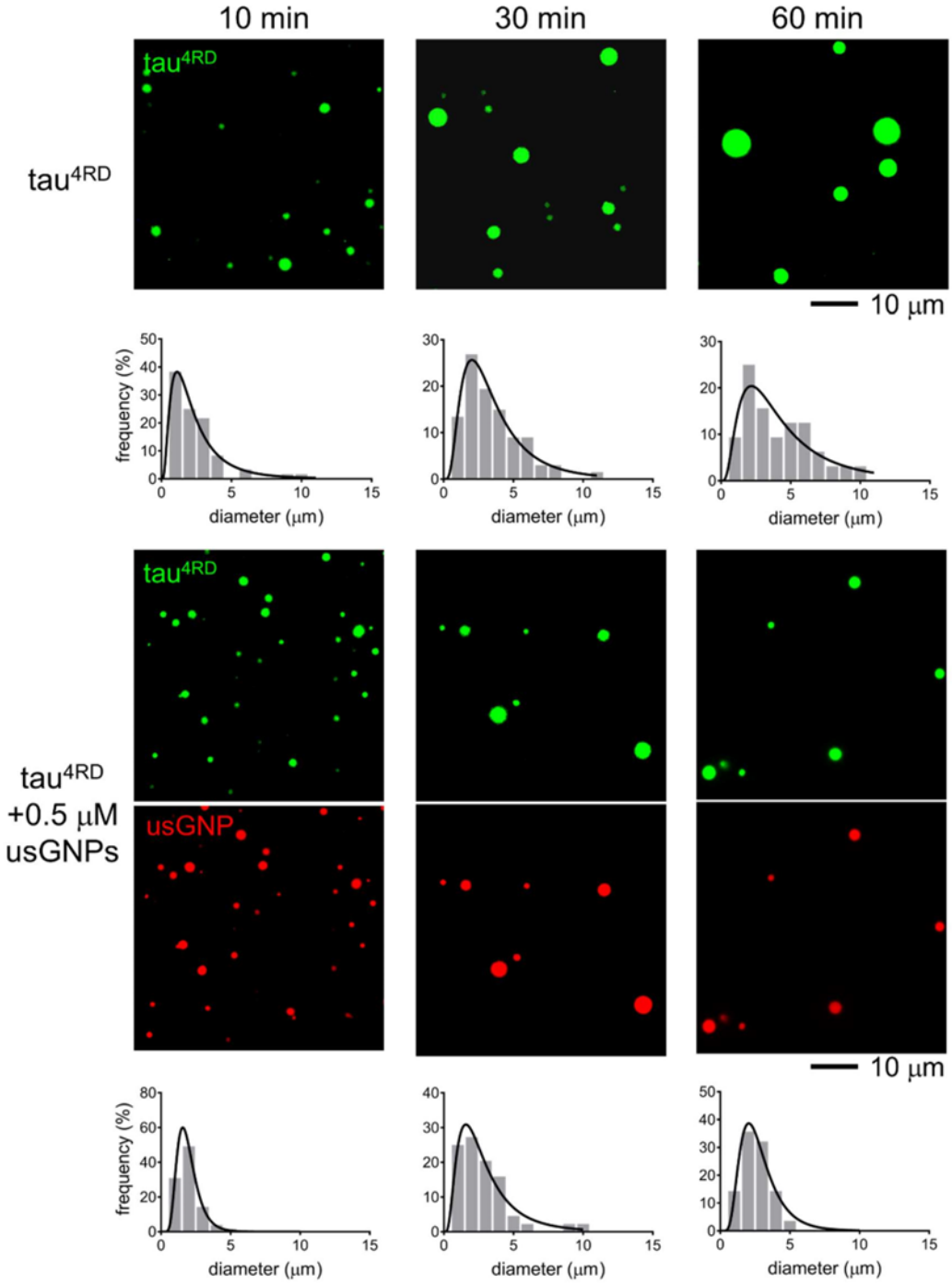

Figure S3. *Time dependence of Tau^{4RD}/polyU coacervates*. Representative fluorescence microscopy images displaying condensates of Tau^{4RD}/polyU in the absence (top) or presence (bottom) of usGNPs, captured at 10, 30, or 60 min from sample preparation. LLPS samples contained 25 μM protein. Below the micrographs, sizedistribution plots of droplet diameters are displayed, as determined from n = 100-200 droplets. Log-normalbest-fit curves are shown as black lines. Green: Alexa^{488}-Tau^{4RD}, red: usGNPs intrinsic emission.

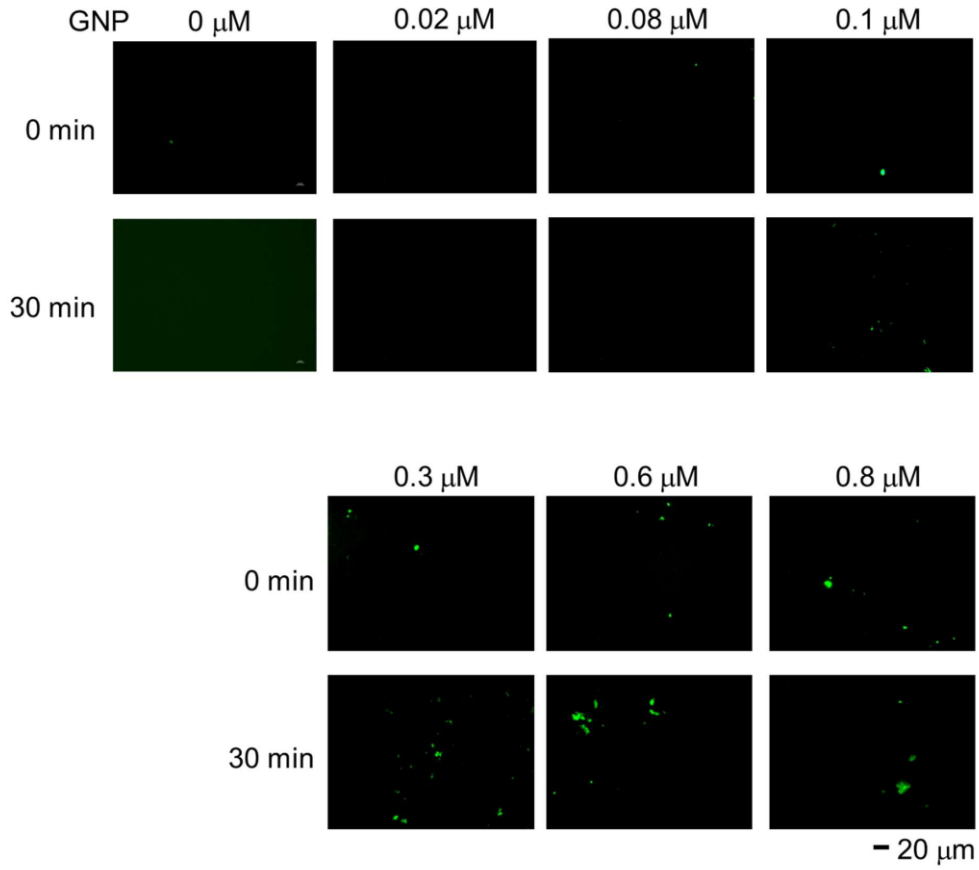

Figure S4. *Interaction of 3nm GNPs with Tau^{4RD}*. Representative fluorescence microscopy images showing the absence of condensates of Tau^{4RD} in the presence of variable concentrations of 3 nm GNPs. Sparse irregularly shaped assemblies are visible for higher GNP concentrations. Samples contained 25 μM protein. Green fluorophore: Alexa^{488}-Tau^{4RD}.

4 General conclusion

Neurodegenerative diseases affect one in ten people over the age of 65, and these numbers are growing each year. In addition to the incidence of ND, from medical level, there are currently no effective curative drugs available to make regress the disease, it is therefore necessary to gain better molecular mechanism that leads to the onset and progression of neurodegenerative diseases.

In this doctoral project I focused my attention on different modulators of aggregation and condensation propensities of Tau protein.

Ubiquitination is a post-translational modification essential in physiological conditions for eukaryotic cells as it is responsible of the degradation of proteins. [97]

Besides being one of the most important PTM in normal conditions, it is also associated with neurodegeneration, since several papers reported ubiquitinated Tau species as part of the PHFs, as revealed from i*n vitro* studies. [100,101,114]

In this thesis I exploited a new synthetic strategy to attach ubiquitin on Tau protein by a chemoselective sulfide coupling. We succeeded in the synthesis and we obtained a pure product with a good yield. The structural characterization by circular dichroism showed that Tau353Ub retained the unfolded profile typical of Tau protein. Afterwords, by following the aggregation propensity of the ubiquitinated Tau construct in comparison with Tau, a different behavior in the aggregation pathway was observed from both ThT assay and TEM images. In fact, it seems that Tau353Ub is able to form mature fibrils but less in number and with different morphology if compared with Tau itself.

Even for ADTau core the dehydroalanine reaction was successful, as demonstrated by MALDI-ToF mass spectra. Nevertheless, the reaction to obtain the ubiquitinated species should be further optimized to gain more interesting results.

Nanomaterials are widely studied for potential application in life science. The challenge to design usGNPs that target biological molecules is to deeply characterize the interactions that occur between usGNPs and the substrate. Several papers well describe the interaction mechanism between GNPs and biomolecules, which leads to the formation of an inner sphere called ‘hard corona’ and an outer one named

'soft corona'. However, the nature of the interactions of usGNPs with IDPs is still poorly investigated. [80,81]

In the present work, I optimized the synthesis of usGNPs in aqueous solution and measured their size through DLS experiment. usGNPs engage Tau protein forming stable multimolecular assemblies (Ka = ~ 10^7 M^{-1}), in contrast to what is reported in the literature about weak protein association to usGNPs. In addition, by NMR relaxation experiments it was possible to detect short-lived (τex = 1–10 ms) interactions, likely corresponding to binding events on the exterior of usGNPs/Tau complexes. The strong interaction between usGNPs and Tau protein is reflected in the aggregation assay, where a dramatically arrest in the fibrils formation, at a certain concentration of nanoparticles, is detected.

These results, in combination with the non-cytotoxic activities in neuronal cells, could find application for aggregation studies both *in vitro* and in cellular models of neurodegeneration.

The compartmentalization in living eukaryotic cells plays an import role for cell activities, like storage, RNA manipulation and controlling reactions. [115]

The findings of Tau condensation into liquid droplets *in vivo* and *in vitro* may arise questions about the initial steps of Tau aggregation into pathological amyloid fibrils. Here I investigated different conditions of LLPS formation in the presence and absence of usGNPs. The phase separation of Tau mediated by polyU, is retained in the presence of low particle concentration, and therefore usGNPs can be considered to act as coacervate clients. At high nanoparticle concentration, a possible competition between the two anionic molecules can occur, indeed the LLPS is abolished.

Although in principle similar to Tau/polyU condensation, heparin mediated LLPS exhibited different behavior because it promotes Tau conformational transition and assembly into highly ordered supramolecular filaments. In the presence of usGNPs, the net charge imbalance seems to perturb the LLPS formation, even at low nanoparticles concentration, but they are not able to arrest the fibrillization process. The same results achieved for the system Tau/polyU/usGNPs were obtained for other two systems, in particular in the case of α-synuclein/polyU and full-length Tau/polyU. In general, by fine tuning the concentration of usGNPs, it will be

possible in the future to shift the equilibrium between formation and dissolution of condensates.

In the end, promising results raised from the aggregation studies in presence of coffee extract and coffee components. Coffee is one of the most world-wide popular beverages and, thanks to its high content in polyphenols, which can cross the BBB, it is widely studied for its anti-oxidative and anti-aging properties.[86,89]

Here I explored the modulation of Tau aggregation by an Italian espresso coffee blend and some derivatives compounds. The aggregation assay revealed that in presence of coffee, Tau retained its unfolded nature without forming fibrils, even if off-pathway round-shaped aggregates were observed. Looking at the single coffee components, caffeine and genistein drove Tau fibrillization towards short and fragmented fibrils with a mixed- α-helix conformation.

The experiments performed using cellular models showed the ability of Tau aggregates formed in the presence of coffee extract, to recover H4-cell viability and demonstrated their reduced ability to induce endogenous, intracellular Tau fibrillization in HEK-293 cells with respect to canonical Tau4RD fibrils.

In summary, during my PhD project I investigated different strategies to shed light on Tau aggregation mechanism. All the results presented in this thesis converge to the idea that aberrant aggregation of amyloid protein Tau is driven by multiple factors and show how post-translational modification, bioactive molecules and nanomaterials can contribute to the design of new strategies to control odd proteins faith.

5 Experimental flow

The expression of recombinant proteins is widely used in biochemical research to achieve a high amount of protein with easy experimental steps. Bacteria are the most common organisms used for protein expression. Among the large variety of bacteria hosts, *E. coli* is the simplest recombinant protein expression system due to its short time of replication. Indeed, there is ample knowledge about its genome and its manipulation to take up the DNA sequence of interest, achieved by transformation process. The presence of specific antibiotics (normally ampicillin, kanamycin or chloramphenicol) can ensure the growth of only the positive colonies, with the exogenous inserted gene, while the rest are abated. Moreover, the cultures are not expensive since they are mainly composed of NaCl, tryptone and yeast extract. To get a good yield with high purity of the desired protein, a specific purification protocol must be optimized.

SDS-Polyacrylamide Gel Electrophoresis

The polyacrylamide gel electrophoresis is the most commonly used technique to separate protein mixtures with high resolution. Essentially, the electrophoresis separates proteins, or DNA, based on differences in mass, charge and folding. These three characteristics result in different behavior inside the gel matrix made by acrylamide polymer. To eliminate the charge and folding variables, sodium dodecyl sulphate (SDS), a surfactant, is used. SDS is capable of unfolding the proteins and imparting a negative charge to them. In this way the proteins loaded on the gel can migrate towards the anode with a different speed, depending on their mass. SDS-PAGE provides preliminary information on the mass and purity of the proteins. For a more complete characterization we need to use other biophysical techniques.

Matrix-Assisted Laser Desorption/Ionization spectroscopy

MALDI is a soft ionization that involves a laser striking a matrix of molecules to vaporise the sample without fragmentation or decomposition. In this PhD thesis, I conducted several chemical and semisynthetic reactions to bind Tau and ubiquitin. The easiest method to assess the success of a reaction is to acquire a mass spectrum

and to compare the calculated mass values with the experimental ones. The only precaution is to dialyse the protein in an aqueous solution, as the presence of salt can generate adducts that can affect the mass values determined by mass spectrometry analysis.

Circular Dichroism spectroscopy

The amino acid sequence of proteins is built up of chiral subunits, that give chirality to the entire structure. When a protein is irradiated by circularly-polarised light in the near-infrared (NIR) or far-ultraviolet (far-UV) wavelength ranges, the amide and carbonyl groups of the polypeptide backbones, undergo to $n \rightarrow \pi^*$ and $\pi \rightarrow \pi^*$ transitions, centred at 210 and 190 nm respectively . The differential absorption of left- and right-circularly polarised light by such chromophores, is strictly dependent on the protein secondary structure. Indeed, specific profiles are associated with α-helix, β-sheet, or random coil structures.

Since Tau is an intrinsically disordered protein, its CD spectrum is represented by a random coil profile. However, when it interacts with other molecules, such as nanoparticles (NPs) or natural compounds, variation in the secondary structure can occur, making CD spectroscopy the best way to monitor these variations. The concentration typically used is around 6 μM to avoid the detector overflow. Moreover, a phosphate buffer at physiological pH, is used since the pH can affect the structure variations.

Isothermal Titration Calorimetry assay

ITC is a powerful technique for determining thermodynamic information of biological processes. Several parameters can be extracted by ITC titration; the number of binding sites, directly related to the stoichiometry of the reaction, the affinity between the ligand and the substrate, described by the Gibbs free energy (or K_a) and the variation of enthalpy (ΔH) and entropy (ΔS).

The ITC instrument operates according to the power compensation principle, whereby it calculates the power necessary to maintain the temperature of the system constant, with respect to a reference cell. Each injection of the ~~syringe~~ solution (containing the ligand L) leads to the formation of a complex with the substrate M,

through an endo or exothermic reaction. The fitting of the resulting titration curves provides all the thermodynamic information. In our case, it was possible to determine the strong affinity between Tau and usGNPs, under different ionic strength conditions.

ThT assay

Thioflavin-T (ThT) is a benzothiazole dye commonly used to monitor fibrillation kinetics of amyloidogenic proteins. When ThT is free in an aqueous environment, it exhibits weak fluorescence, while upon binding to β-sheet structures, a fluorescence enhancement is detectable with excitation and emission maxima at 440 and 490 nm respectively.

In vitro, fibrils formation of tau protein is typically triggered by the polyanion called heparin, which is normally used in a molar ratio of 1:1 or 1:4 with the protein, while the ThT should be used in a large excess compared to the protein concentration.

Although the ThT assay is largely used for aggregation studies, in crowded environments, it may be hindered from binding to β-sheet structures due to competitor molecules. For this reason the ThT fluorescence assay is complemented with analysis of images of the fibrils acquired using transmission electron microscopy (TEM).

Transmission electron microscopy

TEM is a technique that can lead to detailed images of samples, since it can achieve high resolution until 20 nm. TEM images are formed by the interaction of an electron beam with the matter. The biological media are usually stained by a negative staining like uranyl acetate that interacts with the electrons beam.

In this PhD thesis, TEM was used to visualize the morphology of Tau fibrils, and morphological analysis were conducted by measuring the narrow width, large width and cross over length of fibrils.

Additionally, TEM was used to confirm the usGNPs size. In this case, since the nanoparticles have a metal core, the staining is not mandatory.

Dynamic light scattering

(Dynamic light scattering) DLS is used to measure the average size of molecules in solution. This technique is based on the light scattering mediated by the sample, after irradiation with a light source. The scattered light is then converted in size values using the Stoke-Einstein equation. In our case, the metal core of the nanoparticles make them excellent candidates for this measurement.

In the case of usGNPs, DLS measurements present a limitation due to the size of the nanoparticles which is close to the detection limit of the instrument, therefore, many sample replicates must be averaged to get the correct information.

Nuclear Magnetic Resonance

Nuclear Magnetic Resonance (NMR) spectroscopy is a powerful technique used in biological studies to elucidate the structure, dynamics, and interactions at atomic level.

The determination of protein three-dimensional structure is possible by labelling the proteins with ^{13}C and ^{15}N nuclei, given the low natural abundant of these isotopes. Once the ^{1}H-^{15}N HSQC spectrum with the assignment of the amino acid sequence is obtained, it is possible to investigate protein-protein, protein-ligand, and protein-nucleic acid interactions, by observing changes in NMR signals. The two variables usually detected are the intensity variation, strictly linked to alterations in relaxation time that influence the peak width, and chemical shift perturbation which reflects differences in chemical environment. Thus, it is possible to map binding interfaces and characterize the binding kinetics and thermodynamics.

NMR can also probe protein dynamics, providing information about motions ranging from picoseconds to milliseconds. This information is crucial for understanding protein function, as proteins are not static structures but rather undergo conformational changes essential for their biological activity.

Concerning Tau-NP interaction a strong affinity was observed, therefore R_2 measurements and the analysis of the different relaxation times were employed to describe the nature and the amino acids involved in the interaction.

Moreover, ligand based experiments as the STD and Water-LOGSY, can be used to characterize interactions between small molecules and proteins. Both types of experiments are based on intermolecular NOEs to the transiently bound ligand ^{1}H. In this thesis work these experiments were employed to identify molecules of a coffee extract able to interact with preformed fibrils.

Overall, NMR spectroscopy is a versatile and indispensable tool in the study of biomolecules, providing valuable insights into the structure, dynamics, and interactions of proteins.

6 References

1. Forman, M. S., Trojanowski, J. Q. & Lee, V. M.-Y. Neurodegenerative diseases: a decade of discoveries paves the way for therapeutic breakthroughs. *Nature Medicine* **10**, 1055–1063 (2004).
2. Sweeney, P. *et al.* Protein misfolding in neurodegenerative diseases: implications and strategies. *Translational Neurodegeneration* **6**, 6 (2017).
3. Checkoway, H., Lundin, J. I. & Kelada, S. N. Neurodegenerative diseases. *IARC Sci Publ* 407–419 (2011).
4. Glenner, G. G. & Wong, C. W. Alzheimer's disease: Initial report of the purification and characterization of a novel cerebrovascular amyloid protein. *Biochemical and Biophysical Research Communications* **120**, 885–890 (1984).
5. Masters, C. L. *et al.* Neuronal origin of a cerebral amyloid: neurofibrillary tangles of Alzheimer's disease contain the same protein as the amyloid of plaque cores and blood vessels. *The EMBO journal* **4**, 2757–2763 (1985).
6. KoSIK, K. S., Joachim, C. L. & Selkoe, D. J. Microtubule-associated protein Tau (Tau) is a major antigenic component of paired helical filaments in Alzheimer disease. *Proceedings of the National Academy of Sciences* **83**, 4044–4048 (1986).
7. Selkoe, D. J. & Hardy, J. The amyloid hypothesis of Alzheimer's disease at 25 years. *EMBO molecular medicine* **8**, 595–608 (2016).
8. Cummings, A. C. *et al.* Galactic cosmic rays in the local interstellar medium: Voyager 1 observations and model results. *The Astrophysical Journal* **831**, 18 (2016).
9. Devi, G. The Tauopathies. *Handb Clin Neurol* **196**, 251–265 (2023).
10. Kovacs, G. G. Chapter 21 - Concepts and classification of neurodegenerative diseases. in *Handbook of Clinical Neurology* (eds. Kovacs, G. G. & Alafuzoff, I.) vol. 145 301–307 (Elsevier, 2018).

11. Arendt, T., Stieler, J. T. & Holzer, M. Tau and Tauopathies. *Brain research bulletin* **126**, 238–292 (2016).

12. Iqbal, K. *et al.* Tau pathology in Alzheimer disease and other Tauopathies. *Biochimica et Biophysica Acta (BBA)-Molecular Basis of Disease* **1739**, 198–210 (2005).

13. Rösler, T. W. *et al.* Four-repeat Tauopathies. *Progress in Neurobiology* **180**, 101644 (2019).

14. Gast, K. *et al.* Prothymosin. alpha.: A biologically active protein with random coil conformation. *Biochemistry* **34**, 13211–13218 (1995).

15. Weinreb, P. H., Zhen, W., Poon, A. W., Conway, K. A. & Lansbury, P. T. NACP, a protein implicated in Alzheimer's disease and learning, is natively unfolded. *Biochemistry* **35**, 13709–13715 (1996).

16. Hemmings, H. C., Nairn, A. C., Aswad, D. W. & Greengard, P. DARPP-32, a dopamine-and adenosine 3': 5'-monophosphate-regulated phosphoprotein enriched in dopamine-innervated brain regions. II. Purification and characterization of the phosphoprotein from bovine caudate nucleus. *Journal of Neuroscience* **4**, 99–110 (1984).

17. Uversky, V. N. *Introduction to intrinsically disordered proteins (IDPs)*. *Chemical reviews* vol. 114 6557–6560 (ACS Publications, 2014).

18. Tompa, P. Intrinsically disordered proteins: a 10-year recap. *Trends in Biochemical Sciences* **37**, 509–516 (2012).

19. Oldfield, C. J. & Dunker, A. K. Intrinsically Disordered Proteins and Intrinsically Disordered Protein Regions. *Annual Review of Biochemistry* **83**, 553–584 (2014).

20. Wright, P. E. & Dyson, H. J. Linking folding and binding. *Current opinion in structural biology* **19**, 31–38 (2009).

21. Ban, D., Iconaru, L. I., Ramanathan, A., Zuo, J. & Kriwacki, R. W. A small molecule causes a population shift in the conformational landscape of an intrinsically disordered protein. *Journal of the American Chemical Society* **139**, 13692–13700 (2017).

22. Malagrinò, F. *et al.* Unveiling induced folding of intrinsically disordered proteins–Protein engineering, frustration and emerging themes. *Current Opinion in Structural Biology* **72**, 153–160 (2022).

23. Toto, A. *et al.* Templated folding of intrinsically disordered proteins. *Journal of Biological Chemistry* **295**, 6586–6593 (2020).

24. Bah, A. *et al.* Folding of an intrinsically disordered protein by phosphorylation as a regulatory switch. *Nature* **519**, 106–109 (2015).

25. Pufall, M. A. *et al.* Variable control of Ets-1 DNA binding by multiple phosphates in an unstructured region. *science* **309**, 142–145 (2005).

26. Jensen, M. R., Zweckstetter, M., Huang, J. & Blackledge, M. Exploring free-energy landscapes of intrinsically disordered proteins at atomic resolution using NMR spectroscopy. *Chemical reviews* **114**, 6632–6660 (2014).

27. Kikhney, A. G. & Svergun, D. I. A practical guide to small angle X-ray scattering (SAXS) of flexible and intrinsically disordered proteins. *FEBS letters* **589**, 2570–2577 (2015).

28. Chemes, L. B., Alonso, L. G., Noval, M. G. & de Prat-Gay, G. Circular dichroism techniques for the analysis of intrinsically disordered proteins and domains. *Intrinsically Disordered Protein Analysis: Volume 1, Methods and Experimental Tools* 387–404 (2012).

29. Jones, E. M. *et al.* Interaction of Tau protein with model lipid membranes induces Tau structural compaction and membrane disruption. *Biochemistry* **51**, 2539–2550 (2012).

30. Best, R. B. Computational and theoretical advances in studies of intrinsically disordered proteins. *Current opinion in structural biology* **42**, 147–154 (2017).

31. Gustke, N., Trinczek, B., Biernat, J., Mandelkow, E.-M. & Mandelkow, E. Domains of Tau protein and interactions with microtubules. *Biochemistry* **33**, 9511–9522 (1994).

32. Mandelkow, E.-M. & Mandelkow, E. Tau in Alzheimer's disease. *Trends in cell biology* **8**, 425–427 (1998).

33. Wang, Y. & Mandelkow, E. Tau in physiology and pathology. *Nature reviews neuroscience* **17**, 22–35 (2016).

34. Congdon, E. E. & Sigurdsson, E. M. Tau-targeting therapies for Alzheimer disease. *Nature Reviews Neurology* **14**, 399–415 (2018).

35. Morris, M., Maeda, S., Vossel, K. & Mucke, L. The many faces of Tau. *Neuron* **70**, 410–426 (2011).

36. Chen, X. & Jiang, H. Tau as a potential therapeutic target for ischemic stroke. *Aging (albany NY)* **11**, 12827 (2019).

37. Trojanowski, J. Q., Schuck, T., Schmidt, M. L. & Lee, V. M. Distribution of Tau proteins in the normal human central and peripheral nervous system. *Journal of Histochemistry & Cytochemistry* **37**, 209–215 (1989).

38. Hasegawa, M., Smith, M. J. & Goedert, M. Tau proteins with FTDP-17 mutations have a reduced ability to promote microtubule assembly. *FEBS letters* **437**, 207–210 (1998).

39. Martin, L., Latypova, X. & Terro, F. Post-translational modifications of Tau protein: implications for Alzheimer's disease. *Neurochemistry international* **58**, 458–471 (2011).

40. Huang, H.-C. & Jiang, Z.-F. Accumulated amyloid-β peptide and hyperphosphorylated Tau protein: relationship and links in Alzheimer's disease. *Journal of Alzheimer's disease* **16**, 15–27 (2009).

41. Von Bergen, M. *et al.* Assembly of τ protein into Alzheimer paired helical filaments depends on a local sequence motif (306VQIVYK311) forming β structure. *Proceedings of the National Academy of Sciences* **97**, 5129–5134 (2000).

42. Shi, Y. *et al.* Cryo-EM structures of Tau filaments from Alzheimer's disease with PET ligand APN-1607. *Acta neuropathologica* **141**, 697–708 (2021).

43. Fitzpatrick, A. W. P. *et al.* Cryo-EM structures of Tau filaments from Alzheimer's disease. *Nature* **547**, 185–190 (2017).

44. Falcon, B. *et al.* Tau filaments from multiple cases of sporadic and inherited Alzheimer's disease adopt a common fold. *Acta Neuropathol* **136**, 699–708 (2018).

45. Arakhamia, T. *et al.* Posttranslational modifications mediate the structural diversity of Tauopathy strains. *Cell* **180**, 633-644. e12 (2020).

46. Shammas, S. L. *et al. A mechanistic model of Tau amyloid aggregation based on direct observation of oligomers. Nat Commun 6: 7025*. (2015).

47. Wegmann, S. *et al.* Tau protein liquid-liquid phase separation can initiate Tau aggregation. *EMBO J* **37**, (2018).

48. Fan, T.-S., Liu, S. C.-H. & Wu, R.-M. Alpha-synuclein and cognitive decline in Parkinson disease. *Life* **11**, 1239 (2021).

49. Emanuele, M. & Chieregatti, E. Mechanisms of alpha-synuclein action on neurotransmission: cell-autonomous and non-cell autonomous role. *Biomolecules* **5**, 865–892 (2015).

50. Lashuel, H. A., Overk, C. R., Oueslati, A. & Masliah, E. The many faces of α-synuclein: from structure and toxicity to therapeutic target. *Nat Rev Neurosci* **14**, 38–48 (2013).

51. Spillantini, M. G. *et al.* α-Synuclein in Lewy bodies. *Nature* **388**, 839–840 (1997).

52. Aebersold, R. *et al.* How many human proteoforms are there? *Nature Chemical Biology* **14**, 206–214 (2018).

53. Soria, P. S., McGary, K. L. & Rokas, A. Functional Divergence for Every Paralog. *Molecular Biology and Evolution* **31**, 984–992 (2014).

54. Cripps, D. *et al.* Alzheimer disease-specific conformation of hyperphosphorylated paired helical filament-Tau is polyubiquitinated through Lys-48, Lys-11, and Lys-6 ubiquitin conjugation. *Journal of Biological Chemistry* **281**, 10825–10838 (2006).

55. Tapia-Rojas, C. *et al.* It's all about Tau. *Progress in neurobiology* **175**, 54–76 (2019).

56. Hanger, D. P., Anderton, B. H. & Noble, W. Tau phosphorylation: the therapeutic challenge for neurodegenerative disease. *Trends in molecular medicine* **15**, 112–119 (2009).

57. Luna-Muñoz, J. *et al.* Phosphorylation of Tau protein associated as a protective mechanism in the presence of toxic, C-terminally truncated Tau in Alzheimer's disease. *Understanding Alzheimer's Disease* **89**, (2013).

58. Lee, M. J., Lee, J. H. & Rubinsztein, D. C. Tau degradation: The ubiquitin–proteasome system versus the autophagy-lysosome system. *Progress in Neurobiology* **105**, 49–59 (2013).

59. Kleiger, G. & Mayor, T. Perilous journey: a tour of the ubiquitin–proteasome system. *Trends in Cell Biology* **24**, 352–359 (2014).

60. von Mikecz, A. The nuclear ubiquitin-proteasome system. *Journal of Cell Science* **119**, 1977–1984 (2006).

61. Komander, D. The emerging complexity of protein ubiquitination. *Biochemical Society Transactions* **37**, 937–953 (2009).

62. Üstün, S. & Börnke, F. Interactions of Xanthomonas type-III effector proteins with the plant ubiquitin and ubiquitin-like pathways. *Frontiers in Plant Science* **5**, (2014).

63. Wesseling, H. *et al.* Tau PTM profiles identify patient heterogeneity and stages of Alzheimer's disease. *Cell* **183**, 1699-1713. e13 (2020).

64. Morishima-Kawashima, M. *et al.* Ubiquitin is conjugated with amino-terminally processed Tau in paired helical filaments. *Neuron* **10**, 1151–1160 (1993).

65. Ochtrop, P. & Hackenberger, C. P. R. Recent advances of thiol-selective bioconjugation reactions. *Current Opinion in Chemical Biology* **58**, 28–36 (2020).

66. Blennow, K., de Leon, M. J. & Zetterberg, H. Alzheimer's disease. *The Lancet* **368**, 387–403 (2006).

67. Bates, G. P. & Benn, C. 14 The polyglutamine diseases. *Huntington's disease* 429 (2002).

68. Dauer, W. & Przedborski, S. Parkinson's disease: mechanisms and models. *Neuron* **39**, 889–909 (2003).

69. Prusiner, S. B. Molecular biology of prion diseases. *Science* **252**, 1515–1522 (1991).

70. Morris, A. M., Watzky, M. A. & Finke, R. G. Protein aggregation kinetics, mechanism, and curve-fitting: a review of the literature. *Biochimica et Biophysica Acta (BBA)-Proteins and Proteomics* **1794**, 375–397 (2009).

71. Chiti, F. & Dobson, C. M. Protein misfolding, functional amyloid, and human disease. *Annu. Rev. Biochem.* **75**, 333–366 (2006).

72. Sabaté, R., Gallardo, M. & Estelrich, J. An autocatalytic reaction as a model for the kinetics of the aggregation of β-amyloid. *Peptide Science* **71**, 190–195 (2003).

73. Nielsen, L. *et al.* Effect of environmental factors on the kinetics of insulin fibril formation: elucidation of the molecular mechanism. *Biochemistry* **40**, 6036–6046 (2001).

74. Auer, S. & Kashchiev, D. Insight into the correlation between lag time and aggregation rate in the kinetics of protein aggregation. *Proteins: Structure, Function, and Bioinformatics* **78**, 2412–2416 (2010).

75. Invernizzi, G., Papaleo, E., Sabate, R. & Ventura, S. Protein aggregation: Mechanisms and functional consequences. *The International Journal of Biochemistry & Cell Biology* **44**, 1541–1554 (2012).

76. Singh, S. K., Kumar, A., Singh, R. B., Ghosh, P. & Bajad, N. G. Recent Applications of Bioinformatics in Target Identification and Drug Discovery for Alzheimer's Disease. *Current Topics in Medicinal Chemistry* **22**, 2153–2175 (2022).

77. Eftekhari, A. *et al.* The use of nanomaterials in tissue engineering for cartilage regeneration; current approaches and future perspectives. *International journal of molecular sciences* **21**, 536 (2020).

78. Caracciolo, G., Vali, H., Moore, A. & Mahmoudi, M. Challenges in molecular diagnostic research in cancer nanotechnology. *Nano Today* **27**, 6–10 (2019).

79. Jazayeri, M. H., Amani, H., Pourfatollah, A. A., Pazoki-Toroudi, H. & Sedighimoghaddam, B. Various methods of gold nanoparticles (GNPs) conjugation to antibodies. *Sensing and bio-sensing research* **9**, 17–22 (2016).

80. Sarkar, A. *et al.* Nanoparticles as a carrier system for drug delivery across blood brain barrier. *Current drug metabolism* **18**, 129–137 (2017).

81. Asefy, Z., Hoseinnejhad, S. & Ceferov, Z. Nanoparticles approaches in neurodegenerative diseases diagnosis and treatment. *Neurological Sciences* **42**, 2653–2660 (2021).

82. Zheng, Y., Lai, L., Liu, W., Jiang, H. & Wang, X. Recent advances in biomedical applications of fluorescent gold nanoclusters. *Advances in Colloid and Interface Science* **242**, 1–16 (2017).

83. Nair, L. V., Nair, R. V., Shenoy, S. J., Thekkuveettil, A. & Jayasree, R. S. Blood brain barrier permeable gold nanocluster for targeted brain imaging and therapy: an in vitro and in vivo study. *Journal of Materials Chemistry B* **5**, 8314–8321 (2017).

84. Orhan, I. E. *et al.* Flavonoids and dementia: an update. *Current medicinal chemistry* **22**, 1004–1015 (2015).

85. Pathak, L., Agrawal, Y. & Dhir, A. Natural polyphenols in the management of major depression. *Expert opinion on investigational drugs* **22**, 863–880 (2013).

86. Larsson, S. C. Coffee, tea, and cocoa and risk of stroke. *Stroke* **45**, 309–314 (2014).

87. Travassos, M. *et al.* Does caffeine consumption modify cerebrospinal fluid amyloid-β levels in patients with Alzheimer's disease? *Journal of Alzheimer's Disease* **47**, 1069–1078 (2015).

88. Ciaramelli, C. *et al.* NMR-driven identification of anti-amyloidogenic compounds in green and roasted coffee extracts. *Food Chemistry* **252**, 171–180 (2018).

89. Mancini, R. S., Wang, Y. & Weaver, D. F. Phenylindanes in brewed coffee inhibit amyloid-beta and Tau aggregation. *Frontiers in neuroscience* 735 (2018).

90. Banani, S. F., Lee, H. O., Hyman, A. A. & Rosen, M. K. Biomolecular condensates: organizers of cellular biochemistry. *Nature reviews Molecular cell biology* **18**, 285–298 (2017).

91. Boeynaems, S. *et al.* Protein phase separation: a new phase in cell biology. *Trends in cell biology* **28**, 420–435 (2018).

92. Brangwynne, C. P., Tompa, P. & Pappu, R. V. Polymer physics of intracellular phase transitions. *Nature Physics* **11**, 899–904 (2015).

93. Alberti, S., Gladfelter, A. & Mittag, T. Considerations and challenges in studying liquid-liquid phase separation and biomolecular condensates. *Cell* **176**, 419–434 (2019).

94. Ross, C. A. & Poirier, M. A. Protein aggregation and neurodegenerative disease. *Nature medicine* **10**, S10–S17 (2004).

95. Lee, V. M., Goedert, M. & Trojanowski, J. Q. Neurodegenerative Tauopathies. *Annual review of neuroscience* **24**, 1121–1159 (2001).

96. Min, S.-W. *et al.* Acetylation of Tau inhibits its degradation and contributes to Tauopathy. *Neuron* **67**, 953–966 (2010).

97. Komander, D. & Rape, M. The ubiquitin code. *Annual review of biochemistry* **81**, 203–229 (2012).

98. Petrucelli, L. *et al.* CHIP and Hsp70 regulate Tau ubiquitination, degradation and aggregation. *Human molecular genetics* **13**, 703–714 (2004).

99. Abreha, M. H. *et al.* Quantitative analysis of the brain ubiquitylome in Alzheimer's disease. *Proteomics* **18**, 1800108 (2018).

100. Munari, F. *et al.* Semisynthetic and Enzyme-Mediated Conjugate Preparations Illuminate the Ubiquitination-Dependent Aggregation of Tau Protein. *Angewandte Chemie* **132**, 6669–6673 (2020).

101. Munari, F. *et al.* Semisynthetic modification of Tau protein with di-ubiquitin chains for aggregation studies. *International journal of molecular sciences* **21**, 4400 (2020).

102. Parolini, F. *et al.* Ubiquitination of Alzheimer's-related Tau protein affects liquid-liquid phase separation in a site-and cofactor-dependent manner. *International Journal of Biological Macromolecules* **201**, 173–181 (2022).

103. Chatterjee, C., McGinty, R. K., Fierz, B. & Muir, T. W. Disulfide-directed histone ubiquitylation reveals plasticity in hDot1L activation. *Nature chemical biology* **6**, 267–269 (2010).

104. Chen, J., Ai, Y., Wang, J., Haracska, L. & Zhuang, Z. Chemically ubiquitylated PCNA as a probe for eukaryotic translesion DNA synthesis. *Nature chemical biology* **6**, 270–272 (2010).

105. Dadova, J., Galan, S. R. & Davis, B. G. Synthesis of modified proteins via functionalization of dehydroalanine. *Current opinion in chemical biology* **46**, 71–81 (2018).

106. Chalker, J. M. *et al.* Methods for converting cysteine to dehydroalanine on peptides and proteins. *Chemical Science* **2**, 1666–1676 (2011).

107. Lindstedt, P. R., Taylor, R. J., Bernardes, G. J. & Vendruscolo, M. Facile installation of post-translational modifications on the Tau protein via chemical mutagenesis. *ACS Chemical Neuroscience* **12**, 557–561 (2021).

108. Muir, T. W., Sondhi, D. & Cole, P. A. Expressed protein ligation: a general method for protein engineering. *Proceedings of the National Academy of Sciences* **95**, 6705–6710 (1998).

109. Mukrasch, M. D. *et al.* Structural polymorphism of 441-residue Tau at single residue resolution. *PLoS biology* **7**, e1000034 (2009).

110. Munari, F., D'Onofrio, M. & Assfalg, M. Solution NMR insights into dynamic supramolecular assemblies of disordered amyloidogenic proteins. *Archives of biochemistry and biophysics* **683**, 108304 (2020).

111. Barracchia, C. G. *et al.* Unsaturated fatty acid-induced conformational transitions and aggregation of the repeat domain of Tau. *Molecules* **25**, 2716 (2020).

112. Biancalana, M. & Koide, S. Molecular mechanism of Thioflavin-T binding to amyloid fibrils. *Biochimica et Biophysica Acta (BBA)-Proteins and Proteomics* **1804**, 1405–1412 (2010).

113. Lövestam, S. *et al.* Assembly of recombinant Tau into filaments identical to those of Alzheimer's disease and chronic traumatic encephalopathy. *Elife* **11**, e76494 (2022).

114. Trivellato, D. *et al.* Site-directed double monoubiquitination of the repeat domain of the amyloid-forming protein Tau impairs self-assembly and coacervation. *Bioorganic Chemistry* 106347 (2023).

115. Shin, Y. & Brangwynne, C. P. Liquid phase condensation in cell physiology and disease. *Science* **357**, eaaf4382 (2017).